The muscle-type nicotinic acetylcholine receptor function in health and disease

Hakan Cetin, MD

A thesis submitted to the University of Oxford for the degree of Doctor of Philosophy in Clinical Neurosciences

Somerville College
University of Oxford
Hilary Term 2019



The muscle-type nicotinic acetylcholine receptor function in health and disease

Hakan Cetin, MD, Somerville College, University of Oxford

A thesis submitted for the degree of Doctor of Philosophy in Clinical Neurosciences, Hilary term 2019

Abstract

Myasthenic syndromes are characterised by weakness and increased fatigability due to an impairment of neuromuscular transmission. Autoimmune or genetic factors compromise the function of muscle-type nicotinic acetylcholine receptors (AChRs), which have two isoforms composed of five subunits in muscle – fetal AChRs have a γ- and adult AChRs have an ε-subunit. Rapsyn is another key component of the postsynaptic molecular machinery required for neuromuscular transmission. It directly interacts with AChRs and is required for AChR clustering at the neuromuscular junction (NMJ).

The NMJ is one of the most widely studied synapses but there are still aspects of normal NMJ development and function that need to be better understood. In this work, patch clamp experiments on muscle (TE671/CN21) and non-muscle cells (HEK293) were performed to elucidate AChR function under different physiological and pathological conditions. The adult AChR isoform recovered faster from desensitisation compared to the fetal AChR. Rapsyn was shown to induce AChR aggregation in TE671/CN21 and HEK293 cells and facilitated recovery kinetics in both fetal and adult AChRs in the muscle cell line. Rapsyn also increased the

sensitivity for myasthenia gravis (MG) sera to inhibit adult AChR currents, and confined current inhibition to sera with AChR autoantibodies only. Finally, the novel αL251R mutation found in a patient with congenital myasthenic syndrome (CMS) was shown to be associated with a voltage-dependent conversion of AChR ion selectivity from cationic to anionic, transforming the receptor into an inhibitory channel.

This work provides an evaluation of the functional impact of rapsyn on AChRs and helps to understand better the significance of the developmental switch from the fetal to the adult isoform. The data suggest that rapsyn is important for the analysis of the functional effect of MG sera on AChRs, and show novel functional effects of a new CMS mutation that sheds light on AChR function.

Acknowledgements

I would like to begin by thanking my supervisors Prof. Angela Vincent, Dr. Richard Webster and Prof. David Beeson for the chance to work with and learn from them, and for their constant and generous support.

I am tremendously grateful to Prof. Angela Vincent, who helped me to get funding and supported my aims to extend my stay in Oxford. It was an exceptional chance to learn from her technical and academic experience. During the DPhil course, she gave me guidance but also great freedom in the choice and performance of experiments. The scientific discussions with her and her enthusiasm for science were a source of inspiration and encouragement.

This work would not have been possible without the enormous help of Dr. Richard Webster. As a supervisor he taught me the patch clamp technique and helped me to design electrophysiological experiments, and as a friend he introduced me into British life and culture. I am extremely grateful for his support, his patience and his healthy common sense, which significantly contributed to the progress and success of my studies.

I am also extremely grateful to Prof. David Beeson for allowing me to work with him alongside a number of excellent scientists in his group. He generously supported me when I planned to extend my stay in Oxford and get funding. His tremendous experience in genetics and congenital myasthenic syndromes was inspiring and undoubtedly contributed to the success of this work.

I would also like to thank

Dr. Judith Cossins and Dr. Wei Liu for teaching me the techniques in molecular biology required for the construction of the chimeric AChR constructs,

Prof. Lucia Sivilotti and Dr. Remigijus Lape for their generous advice on patch clamp methods and data interpretation,

Prof. Stephan Traynelis for providing ChannelLab (Synaptosoft Inc.) and for helpful discussions,

Susan Maxwell for providing technical help in fluorescence microscopy and everyday technical advice,

Dr. Akiko Nagaishi for testing myasthenia gravis sera by cell-based assays,

Max Epstein and Prof. Philip Biggin for their collaboration and providing structural data that helped to understand the underlying pathomechanism of the αL251R mutation,

Dr. An Vanhaesebrouck, Dr. Pedro Rodriguez-Cruz, Dr. Michelangelo Cao, Dr. Jonathan Cheung for helpful discussions and everyday technical and experimental advice,

David Parr and Martin Brydson for their help with orders for the laboratory,

Prof. Kevin Talbot for giving me the chance to visit the Amyotrophic Lateral Sclerosis Clinic at the John Radcliffe Hospital and to learn from his enormous clinical experience,

Prof. David Hilton-Jones for giving me the chance to visit the Neuromuscular Clinic at the John Radcliffe Hospital and teaching me the management and the various phenotypes of myopathies and muscular dystrophies,

Prof. Fritz Zimprich for introducing me to myasthenia gravis research, and who together with Prof. Karl Vass and Prof. Eduard Auff supported my aims to get funding and come to Oxford,

the Kluzek and Hesketh families for their warm friendship, and Stefan Kluzek for the refreshing runs through Oxford and the inspiring discussions,

My brothers and parents for their love, support and encouragement, particularly my parents for their hard work to enable me an academic career,

My daughter Elin and my son Timi for being both inspiration and motivation, and my wife Conny for her love, support and unwavering belief in me,

The Austrian Science Fund (Fonds zur Förderung der wissenschaftlichen Forschung, FWF) and the Nuffield Department of Clinical Neurosciences (NDCN) for providing me with fellowships that funded my stay in Oxford,

And finally, I am grateful to have had the privilege of attending the prestigious University of Oxford, where I worked with some of the best and brightest. Thank you for this opportunity.

Contents

Abstract i

Acknowledgements iii

Contents vii

List of Figures xv

List of Tables xxii

Abbreviations xxiv

Chapter 1 Introduction 1

1.1 The neuromuscular junction from a historical viewpoint 2

1.2 Physiology of the neuromuscular junction 4

1.3 The AChR clustering pathway 6

1.4 The exchange of AChR isoforms during NMJ development 9

1.5 Autoimmune myasthenia gravis 11

1.5.1 Clinical classification 11

1.5.2 Serological classification 12

1.5.2.1 AChR antibodies 12

1.5.2.2 Clustered AChR antibodies 16

1.5.2.3 MuSK antibodies 17

1.5.2.4 LRP4 antibodies 18

1.5.2.5 Seronegative myasthenia gravis 19

1.6 Congenital myasthenic syndromes 20

1.6.1 Congenital myasthenic syndromes due to kinetic abnormalities of the AChR 20
1.6.1.1 Slow-channel syndromes 22
1.6.1.2 Fast-channel syndromes 23
1.6.1.3 CMS due to reduced AChR conductance 23
1.7 The nicotinic AChR in muscle 23
1.7.1 The agonist-binding site 29
1.7.2 The gating mechanism 32
1.7.3 Charge selectivity 33
1.7.4 Structural determinants of desensitisation 34
1.8 Open questions and thesis aims 36

Chapter 2 Materials and methods 38
2.1 DNA methods 38
2.1.1 PCR reactions 38
2.1.2 Molecular cloning 38
2.1.3 Bacterial transformation 39
2.1.4 Agarose gel electrophoresis 39
2.2 Cell cultures 41
2.3 Plasmids and constructs 42
2.4 Transfections 42
2.5 Fluorescence and confocal microscopy 44
2.6 Analysis of AChR expression by fluorescence-activated cell scanning 45

2.7 Analysis of AChR expression by the cell-surface ^{125}I-α-bungarotoxin binding assay 45
2.8 Electrophysiology 46
2.8.1 Whole-cell patch clamping 46
2.8.2 The perforated patch method 47
2.8.3 Single-channel recordings 48
2.8.4 The patch clamp fast perfusion system 48
2.8.4.1 The perfusion setup 48
2.8.4.2 The perfusion setup for serum application 50
2.8.4.3 Cell perfusion and solution exchange 50
2.8.5 Analysis of desensitisation and recovery from desensitisation 52
2.9 Calculation of AChR transitions between different conformational states in a computer simulation of the AChR kinetic model 54
2.10 Preparation of sera 54
2.10.1 Ethical statement 55
2.11 Randomisation, blinding and statistical analysis 55

Chapter 3 Functional differences between fetal and adult AChRs 56
3.1 Introduction 56
3.2 Aims 57
3.3 The acetylcholine application protocol 57
3.4 The influence of methodological factors on AChR desensitisation and recovery from desensitisation 59
3.4.1 Estimation of solution application times 59

3.4.2 Computer simulation of AChR desensitisation and recovery from desensitisation 64
3.4.2.1 Simulation of acetylcholine concentration changes 64
3.4.2.2 Simulation of AChR transitions upon acetylcholine application 66
3.4.2.3 Dependence of desensitisation and recovery from desensitisation on acetylcholine concentration and its rise time 71
3.4.3 Series resistance compensation in whole-cell patch clamp experiments 74
3.4.4 Spatial aspects of voltage inhomogeneity 79
3.5 Desensitisation is similar between fetal and adult AChRs 81
3.6 Adult AChRs recover faster from desensitisation compared to fetal AChRs 84
3.7 Characterisation of electrophysiological differences between cell cultures thawed from different stocks of the same cell line 87
3.8 Analysis of AChR desensitisation and recovery from desensitisation by the perforated patch method 87
3.9 The impact of the voltage error correction method on desensitisation and recovery measurements 89
3.10 The impact of the fetal and adult AChR isoform specific M3-M4 cytoplasmic loop on desensitisation and recovery from desensitisation 91
3.10.1 Construction of plasmids containing cDNA of chimeric γ- and ε-subunits with exchanged M3-M4 loops 94

3.10.2 Recovery kinetics is determined by the AChR isoform specific cytoplasmic M3-M4 loop....107
3.11 Salbutamol facilitates recovery from desensitisation in the adult but not fetal AChR isoform....107
3.12 Discussion....111
3.12.1 Dependence of desensitisation and recovery from desensitisation on methodological parameters....111
3.12.2 Differential modification of recovery kinetics in fetal and adult AChRs by intracellular factors....115
3.12.3 Physiological implications of fast recovery from desensitisation in adult AChRs....117

Chapter 4 Modification of AChR function by rapsyn....119
4.1 Introduction....119
4.2 Aims....122
4.3 Rapsyn improves AChR aggregation in HEK293 and TE671/CN21 cells....122
4.4 Influence of rapsyn on AChR surface expression....123
4.4.1 Estimation of AChR surface expression by the measurement of peak current amplitudes....127
4.4.2 Estimation of AChR surface expression using a cell-surface ^{125}I-BTX binding assay....127
4.4.3 Estimation of AChR surface expression using FACS....129

4.5 The impact of rapsyn on AChR desensitisation and recovery from desensitisation 136
4.5.1 The acetylcholine application protocol 136
4.5.2 The impact of rapsyn on AChR desensitisation and recovery from desensitisation in TE671/CN21 cells 136
4.5.3 The impact of rapsyn on AChR desensitisation and recovery from desensitisation in HEK293 cells 137
4.6 Rapsyn can facilitate recovery kinetics in an AChR mutant that prevents receptor clustering in C2C12 myotubes 142
4.6.1 The δR375H prevents AChR clustering in C2C12 myotubes 142
4.6.2 Rapsyn does not affect current decay but facilitates recovery kinetics in fetal $AChR_{\delta R375H}$ 145
4.6.3 Rapsyn colocalises with $AChR_{\delta R375H}$ in HEK293-γ cells 145
4.7 Discussion 148
4.7.1 The impact of rapsyn on AChR distribution on the cell surface 150
4.7.2 The effect of rapsyn on AChR function 151

Chapter 5 Inhibition of AChR function by myasthenia gravis sera 153
5.1 Introduction 153
5.2 Aims 155
5.3 The acetylcholine application protocol 155
5.4 Serum samples 157
5.5 Testing of the effect of MG sera on AChR peak current amplitudes, desensitisation and recovery from desensitisation 157

5.6 The effect of control agents on AChR whole-cell currents 158
5.6.1 The effect of control agents on AChR peak current amplitudes.....159
5.6.2 The effect of control agents on AChR desensitisation 160
5.6.3 The effect of control agents on AChR recovery from desensitisation.....160
5.7 AMC sera inhibit fetal AChR function only.....164
5.8 AChR current inhibition by MG sera depends on receptor clustering.....164
5.9 Discussion.....170
5.9.1 The effect of AChR-Ab and clustered AChR-Ab positive sera on AChR function.....170
5.9.2 The effect of AMC sera on AChR function.....171
5.9.3 Clinical relevance of current inhibition by AChR-Ab and clustered AChR-Ab positive sera 172
5.9.4 The effect of AChR-Ab negative MG sera on AChR function 172

Chapter 6 Functional characterisation of the αL251R mutation found in a patient with congenital myasthenic syndrome.....175
6.1 Introduction.....175
6.2 Aims.....176
6.3 Transfection of HEK293 cells for the expression of wild-type and mutant AChRs.....177
6.4 The acetylcholine application protocol.....177
6.5 Surface expression of mutant AChRs is reduced.....179
6.6 No single-channel currents can be recorded in $AChR_{\alpha L251R}$ 181

6.7 Whole-cell current amplitude, desensitisation and deactivation are altered in $AChR_{\alpha L251R}$ 181

6.8 In $HEK293_{\alpha L251R}$, the mutation is associated with a change of rectification from linear to outward 184

6.9 In $AChR_{\alpha L251R}$, current characteristics are not chloride-dependent at a holding potential of –60 mV 186

6.10 In $AChR_{\alpha L251R}$, the mutation is associated with a conversion from cationic to anionic selectivity at positive holding potentials 191

6.11 In $AChR_{\alpha L251R}$, sodium conductance is severely reduced but prevails at negative holding potentials 191

6.12 Discussion 195

6.12.1 Unravelling the pathomechanism of the αL251R mutation by whole-cell patch clamp experiments 197

6.12.2 Data from computational modelling reveals the introduction of an energetic reward for chloride by both arginine residues 200

6.12.3 Pathophysiological implications of CMS due to the αL251R mutation 204

Chapter 7 Concluding remarks and future directions 205

Bibliography 214

List of Figures

Figure 1-1	Organisation of the neuromuscular junction
Figure 1-2	Structure of the main AChR clustering molecules
Figure 1-3	Pentameric structure of the AChR in muscle
Figure 1-4	Structure of AChR subunits
Figure 1-5	Structural model of the AChR from the Torpedo electric organ
Figure 1-6	The principal and complementary components of the agonist-binding site
Figure 2-1	The perfusion setup
Figure 2-2	The perfusion setup for serum application
Figure 3-1	Acetylcholine application protocol for the measurement of AChR desensitisation and recovery from desensitisation
Figure 3-2	Open pipette junction current changes
Figure 3-3	10-90% current rise times in TE671/CN21 and HEK293 cells
Figure 3-4	Linear AChR kinetic scheme
Figure 3-5	Sigmoidal curve fitting to the open pipette junction current changes
Figure 3-6	AChR transition states upon stimulation with 1 mM ACh
Figure 3-7	The influence of AChR numbers on AChR desensitisation and recovery from desensitisation

Figure 3-8 The influence of ACh concentration on AChR desensitisation and recovery from desensitisation

Figure 3-9 The influence of the ACh concentration rise time on AChR desensitisation and recovery from desensitisation

Figure 3-10 Series resistance in the whole-cell patch clamp configuration

Figure 3-11 The impact of series resistance error on current decay and recovery time constants

Figure 3-12 Comparison of cell capacitance as a proxy for the cell size in non-muscle and muscle cell lines expressing fetal and adult AChRs

Figure 3-13 Desensitised current fractions in fetal and adult AChRs

Figure 3-14 Current decay time constants in muscle and non-muscle cell lines

Figure 3-15 Recovered current fractions in fetal and adult AChRs

Figure 3-16 Recovery time constants in muscle and non-muscle cell lines

Figure 3-17 Electrophysiological differences between cell cultures thawed from different stocks of the same cell line

Figure 3-18 Current decay and recovery from desensitisation assessed in HEK293 cells by the perforated patch method

Figure 3-19 Current decay time constants in fetal and adult AChRs after voltage error correction by hardware and software based methods

Figure 3-20 Recovery time constants in fetal and adult AChRs after voltage error correction by hardware and software based methods

Figure 3-21 Screening for *Age*I and *BsrG*I restriction sites in pcDNA3.1-γ and pcDNA3.1-ε

Figure 3-22 Cloning of restriction sites into the 5'- and 3'-end of the γ- and ε-M3-M4 loop cDNA region

Figure 3-23 Screening for *Age*I and *BsrG*I restriction sites in pcDNA3.1-γ and pcDNA3.1-ε after mutagenesis

Figure 3-24 Exchange of the M3-M4 loops between CHRNG and CHRNE

Figure 3-25 Back-mutation of the *BsrG*I and *Age*I restriction sites in chimeric CHRNG and CHRNE with exchanged M3-M4 loop cDNA

Figure 3-26 Sequence of the chimeric γ-subunit with the ε-M3-M4 loop

Figure 3-27 Sequence of the chimeric ε-subunit with the γ-M3-M4 loop

Figure 3-28 Chimeric AChRs with exchanged M3-M4 cytoplasmic loops between the γ- and ε-subunit

Figure 3-29 Desensitisation and recovery from desensitisation in chimeric AChRs with exchanged M3-M4 cytoplasmic loops between the γ- and ε-subunit

Figure 3-30 Effect of the PKA activating drug salbutamol on fetal and adult AChR desensitisation and recovery from desensitisation

Figure 3-31 Cyclic kinetic scheme with five different desensitised states

Figure 4-1 The functional domains of rapsyn

Figure 4-2 Effect of rapsyn on surface AChR expression and distribution in HEK293 cells

Figure 4-3 Effect of rapsyn on surface AChR expression and distribution in TE671/CN21 cells

Figure 4-4 Effect of rapsyn on surface AChR expression and distribution in TE671/CN21 cells after co-transfection with fetal and adult AChR subunit cDNA

Figure 4-5 Impact of rapsyn on peak current amplitudes in HEK293-γ and HEK293-ε

Figure 4-6 Estimation of AChR surface expression in HEK293T-γ and HEK293T-ε using a cell-surface ^{125}I-BTX binding assay

Figure 4-7 Estimation of AChR surface expression in HEK293-γ and HEK293-ε using FACS

Figure 4-8 Mean EGFP and AF594 fluorescence intensities in HEK293-γ and HEK293-ε co-transfected with pEGFP-N1 and pIRES2-RAPSN-EGFP

Figure 4-9 Estimation of AChR surface expression in HEK293-γ and HEK293-ε with low EGFP fluorescence intensities using FACS

Figure 4-10 Comparison of AF594 fluorescence intensities in HEK293-γ and HEK293-ε with low EGFP fluorescence intensities

Figure 4-11 The effect of rapsyn on current decay time constants in AChRs expressed in TE671 and CN21 cells

Figure 4-12 The effect of rapsyn on recovery time constants in AChRs expressed in TE671 and CN21 cells

Figure 4-13 The effect of rapsyn on current decay time constants in AChRs expressed in HEK293-γ and HEK293-ε cells

Figure 4-14 The effect of rapsyn on recovery time constants in AChRs expressed in HEK293-γ and HEK293-ε cells

Figure 4-15 The δR375H mutation prevents agrin stimulated clustering of AChRs in C2C12 myotubes

Figure 4-16 The δR375H mutation prevents agrin stimulated clustering of AChRs in C2C12 myotubes

Figure 4-17 The effect of rapsyn on current decay time constants in AChRs expressed in HEK293-γ cells bearing the wild-type or mutant δ-subunit

Figure 4-18 Rapsyn facilitates recovery from desensitisation in mutant AChRs bearing the δR375H mutation

Figure 4-19 The effect of rapsyn on the surface distribution of $AChR_{\delta WT}$ and $AChR_{\delta R375H}$ expressed in HEK293-γ cells

Figure 5-1 Acetylcholine application protocol to test inhibition of AChR currents by MG sera

Figure 5-2 The effect of control agents on AChR whole-cell currents

Figure 5-3 The effect of control agents on AChR desensitisation

Figure 5-4 The effect of control agents on AChR recovery from desensitisation

Figure 5-5 Fetal and adult AChR current inhibition by AMC sera

Figure 5-6 AChR whole-cell current inhibition by different MG sera

Figure 5-7 The effect of three sera on AChR whole-cell currents

Figure 5-8 AChR current inhibition by AChR-Ab and clustered AChR-Ab positive sera in dependence of receptor clustering

Figure 6-1 Different AChR subunit stoichiometries resulting from the heterozygous αL251R status of the CMS patient

Figure 6-2 Acetylcholine application protocols

Figure 6-3 The influence of the αL251R mutation on AChR surface expression

Figure 6-4 Single-channel recordings of wild-type and mutant AChRs

Figure 6-5 Current characteristics of wild-type and mutant AChRs expressed in HEK293 cells

Figure 6-6 Peak currents, desensitisation and deactivation in $HEK293_{\alpha WT}$, $HEK293_{\alpha L251R}$ and $HEK293_{\alpha WT/\alpha L251R_Mix}$

Figure 6-7 The I-V relationship in $HEK293_{\alpha WT}$, $HEK293_{\alpha L251R}$ and $HEK293_{\alpha WT/\alpha L251R_Mix}$

Figure 6-8 Peak currents, desensitisation and deactivation in $AChR_{\alpha WT}$ and $AChR_{\alpha L251R}$ after substitution of intracellular or extracellular Cl^- by SO_4^{2-}

Figure 6-9 The I-V relationship in $AChR_{\alpha WT}$ was independent of the intracellular and extracellular Cl^- concentration

Figure 6-10 The I-V relationship in $AChR_{\alpha L251R}$ in dependence of the intracellular and extracellular Cl^- concentration

Figure 6-11 The I-V relationship in $AChR_{\alpha WT}$ and $AChR_{\alpha L251R}$ after substitution of extracellular NaCl by glucose

Figure 6-12 Mutations of the charge selectivity filter in Cys-loop ligand-gated ion channels published in the literature

Figure 6-13 Analysis of Na^+ and Cl^- passage through the transmembrane pore in wild-type and mutant AChRs by calculations of the potential of mean force profiles

Figure 6-14 Solvation shells of Na^+ and Cl^- ions as a function of their position along the reaction coordinate

List of Tables

Table 1-1	Functional differences between the fetal and adult AChR isoform
Table 1-2	Antibody characteristics in myasthenia gravis
Table 1-3	Genes underlying congenital myasthenic syndromes
Table 1-4	Studies on the AChR structure
Table 1-5	Loop structure of the agonist-binding site
Table 2-1	Parameters used for PCR reactions
Table 2-2	Transformation conditions for competent bacterial cells
Table 2-3	DNA plasmids that were available in the laboratory and used in experiments
Table 3-1	Extracellular and pipette solution composition
Table 3-2	Sequences of primers used for cloning of *BsrG*I and *Age*I restriction sites into CHRNG and CHRNE cDNA
Table 3-3	Sequences of primers used for back-mutation of the *BsrG*I and *Age*I restriction sites into the wild-type sequence in CHRNG and CHRNE cDNA
Table 3-4	Sequencing primers used to confirm the exchange of the M3-M4 loops between the γ- and ε-subunit
Table 3-5	The influence of methodological factors on desensitisation and recovery from desensitisation

Table 6-1 Extracellular and pipette solution composition for the substitution of intracellular Cl^- by SO_4^{2-} to a final Cl^- concentration of 10 mM (i.e. 10 mM Cl^-_{IN})

Table 6-2 Extracellular and pipette solution composition for the substitution of extracellular Cl^- by SO_4^{2-} to a final Cl^- concentration of 10 mM (i.e. 10 mM Cl^-_{EX})

Table 6-3 Extracellular and pipette solution composition for the substitution of extracellular NaCl by glucose to a final NaCl concentration of 20 mM

Abbreviations

Ab	Autoantibodies
ACh	Acetylcholine
AChE	Acetylcholine esterase
AChR	Muscle-type nicotinic acetylcholine receptor
AChR-Ab	Acetylcholine receptor antibodies
AChR-MG	Acetylcholine receptor antibody positive myasthenia gravis
AF594	Alexa Fluor® 594
AMC	Arthrogryposis multiplex congenita
BSA	Bovine serum albumin
BTX	α-bungarotoxin
CBA	Cell-based assay
Cdk5	Cyclin-dependent kinase 5
CMS	Congenital myasthenic syndrome
ColQ	Collagen Q
cpm	Counts per minute
DMEM	Dulbecco-modified essential medium
Dok7	Downstream of kinase 7
ECD	Extracellular domain
E. coli	Escherichia coli
EDTA	Ethylenediaminetetraacetic acid

EGFP	Enhanced green fluorescent protein
EPP	Endplate potential
FACS	Fluorescence-activated cell scanning
FCS	Fetal calf serum
HC	Healthy controls
HEPES	4-(2-hydroxyethyl)piperazine-1-ethanesulphonic acid
^{125}I-BTX	I^{125}-radiolabelled α-bungarotoxin
I-V	Current-voltage
LRP4	Low-density lipoprotein receptor-related protein 4
LRP4-Ab	Low-density lipoprotein receptor-related protein 4 antibodies
mAb	Monoclonal antibody
MEPP	Miniature endplate potential
MG	Myasthenia gravis
MuSK	Muscle specific kinase
MuSK-Ab	Muscle specific kinase antibodies
MuSK-MG	Muscle specific kinase antibody positive myasthenia gravis
NMJ	Neuromuscular junction
N-Myr	N-myristoylation
PEI	Polyethylenimine
PKA	Protein kinase A
PMF	Potential of mean force
Rapsyn	43 kDa receptor-associated protein of the synapse
RI	Rectification index
RIA	Radioimmunoprecipitation assay

SNMG	Seronegative myasthenia gravis
SR	Series resistance
TMD	Transmembrane domain
TPR	Tetratricopeptide
VGCC	Voltage-gated calcium channel
VGSC	Voltage-gated sodium channel

Chapter 1

Introduction

Synapses are the points of structural contact between neurons and their targets and enable the transmission of signals from one cell to the next. At electrical synapses, nerve impulses are transmitted directly by the flow of current between cells. At chemical synapses, the action potential arriving at the presynaptic nerve terminal triggers the release of neurotransmitter, which diffuses within the synaptic cleft and binds to its receptor on the postsynaptic cell membrane. Binding of neurotransmitter to some postsynaptic receptors leads to modulation of second messengers inside the postsynaptic cell and initiate a molecular information cascade (i.e. metabotropic receptor). Other receptors form ion channels that open upon binding of neurotransmitter and allow ions to pass into the postsynaptic cell and change the transmembrane potential (i.e. ionotropic receptors or ligand-gated ion channels). The muscle-type nicotinic acetylcholine receptor (AChR) is one of the best-studied ligand-gated ion channels. It is located at the postsynaptic membrane of the neuromuscular junction (NMJ), a highly specialised chemical synapse between motor neurons and muscle fibres, the study of which has helped to elucidate some very important general mechanisms underlying synaptic transmission.

This introduction gives an overview of several structural and functional aspects of the NMJ in health and disease. Autoimmune and congenital myasthenic syndromes (CMS) based on a defective NMJ will be addressed, with a focus on the

AChR as the main antigenic target in autoimmune myasthenia and involved in the majority of CMS. The introduction also includes a comprehensive discussion of molecular details linking AChR structure with functional characteristics. Open questions regarding developmental, physiological and pathophysiological aspects of AChRs will be raised leading to the aims of the work described in this thesis.

1.1 The neuromuscular junction from a historical viewpoint

The NMJ is one of the most widely studied synapses and has served as a prototype for our understanding of neurotransmission. In their pivotal studies on frog nerve-muscle preparations, Claude Bernard (Bernard, 1856) and his pupil Alfred Vulpian (Vulpian, 1866) first postulated the idea of the NMJ as a specific structure on which curare acts (Cousin, 2013). A more precise concept of the NMJ was hypothesised later by demonstrating that chemical compounds released by the nerve ending transmitted across the NMJ to act on the muscle cell and cause contraction (Langley, 1905; Loewi, 1921). Acetylcholine (ACh) was shown to be released from autonomic ganglia upon nerve stimulation and was ultimately identified to act as a transmitter at the NMJ (Feldberg and Gaddum, 1934; Dale et al., 1936). Using intracellular voltage recordings, the electrical response of ACh in the muscle cell could be isolated by the application of curare to reduce the amplitude of the end-plate potential (EPP) below the threshold for action potentials (Fatt and Katz, 1951). It was observed that the synaptic potential was largest at the endplate region and decreased progressively with increasing distance from the endplate region. It was concluded that ACh-activated ion channels must be confined to the endplate region and opposite the nerve terminal from where ACh was released. In their intracellular recordings from

frog nerve-muscle preparations, Paul Fatt and Bernard Katz also noticed spontaneous postsynaptic potentials characterised by large amplitudes at the endplate region that decreased with distance (Fatt and Katz, 1952). These depolarisations of the postsynaptic membrane, termed as miniature endplate potentials (MEPP), led to the description of the quantal nature of presynaptic ACh release, i.e. the release of ACh in "packets" rather than single molecules, which depolarise the postsynaptic membrane (Katz and Miledi, 1965). With the isolation of AChRs from the electric organ of Gymnotus (Changeux et al., 1970) or Torpedo fish (Miledi et al., 1971), it became possible to characterise the receptor showing that it was an intrinsic membrane protein. Jean-Pierre Changeux and collaborates were also among the first who described the structure of the protein (Devillers-Thiery et al., 1983; Hucho and Changeux, 1973), and elucidated the different signalling pathways involved in the concentration of AChRs at the postsynaptic region. This was shown to result from inhibition of gene transcription in nuclei outside the synaptic region and stimulation of gene transcription in subsynaptic nuclei (Betz and Changeux, 1979; Fontaine et al., 1987; Klarsfeld and Changeux, 1985). By the application of the patch clamp technique, Erwin Neher and Bert Sakmann were the first to successfully obtain recordings of single AChRs (Neher and Sakmann, 1976). They found small rectangular currents corresponding to channel openings and closings in a stochastic manner, and subsequently, two isoforms could be discerned electrophysiologically differing in current amplitudes and mean open times (Mishina et al., 1986). The AChR was soon found to be the site of autoimmune myasthenia (Patrick and Lindstrom, 1973) and CMS (Engel et al., 1977; Vincent et al., 1981), the

characterisation of which coincided with the elucidation of the structural and functional properties of the NMJ and the AChR.

1.2. Physiology of the neuromuscular junction

This section is largely taken from my published review (Cetin and Vincent, 2018). The NMJ is a highly specialised synapse enabling the functional communication between motor neurons and muscle fibres. Each NMJ comprises an unmyelinated motor nerve terminal separated from the postsynaptic muscle membrane by the synaptic cleft. A basal lamina within the synaptic cleft is important for the structural integrity of the NMJ. Together with a set of pre- and postsynaptic molecular machineries, the NMJ forms a functional unit ensuring the quick and reliable transmission of electrical information (Figure 1-1).

Neuromuscular transmission at vertebrate voluntary striated muscle depends on the release of ACh and its binding to postsynaptic AChRs. Action potentials arriving at the presynaptic nerve terminal activate P/Q-type voltage-gated calcium channels (VGCC) located within active zones, which are essentially small arrays of structural proteins that promote exocytosis. In human muscle, the influx of calcium results in the release of about 20-30 vesicles containing ACh (Slater et al., 1992). The postsynaptic membrane is characterised by deep invaginations, at the crest of which AChRs are clustered at very high densities reaching 10,000 per μm^2 (Matthews-Bellinger and Salpeter, 1983). Each AChR binds up to two molecules of ACh, opens and becomes permeable to cations (mainly sodium and potassium). This generates the EPP, which usually exceeds the threshold potential of –50 mV required for the activation of $Na_V1.4$ voltage-gated sodium channels (VGSCs), which are

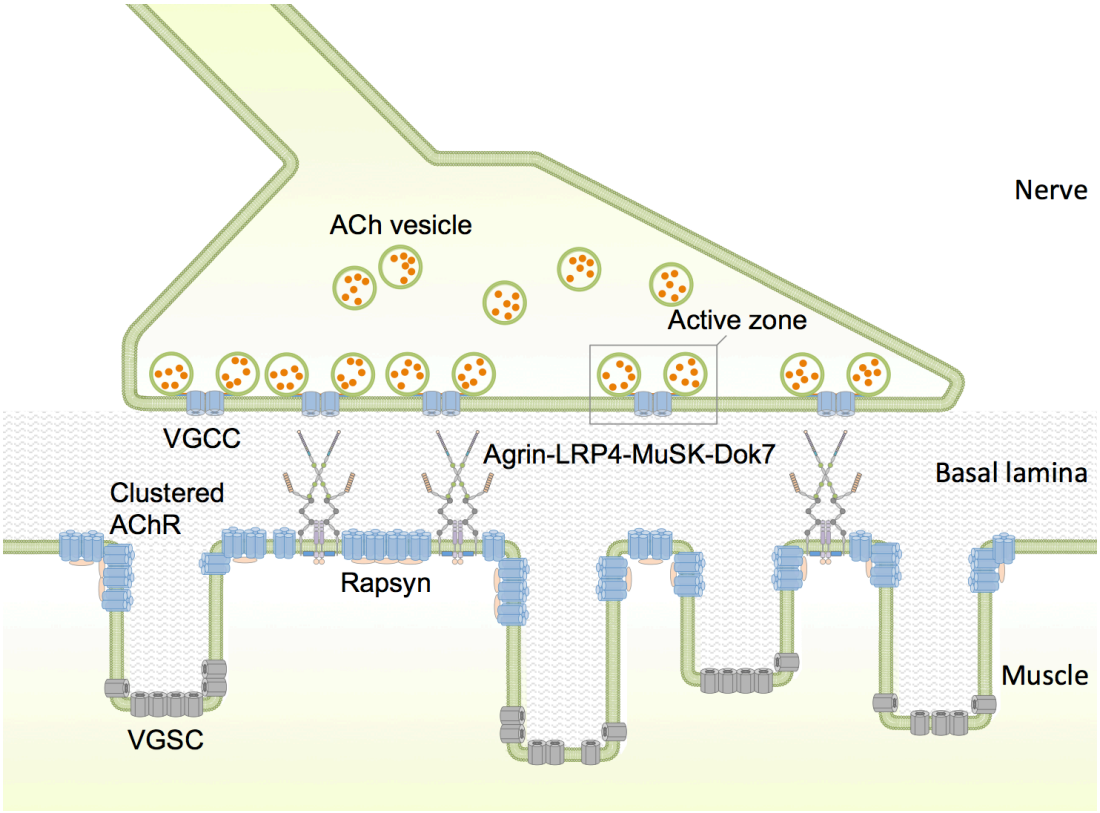


Figure 1-1 Organisation of the neuromuscular junction
The NMJ is a highly organised functional unit ensuring the reliable transmission of electrical information from nerve to muscle. Agrin-LRP4-MuSK-Dok7 complexes mediate AChR clustering on the crest of the postsynaptic folds, where they can be activated by ACh within the fraction of a millisecond. Voltage gated sodium channels are located at the bottom of the folds. Voltage-gated calcium channels are located within active zones on the presynaptic nerve terminal and induce vesicle release by increasing the intracellular Ca^{2+} concentration upon activation. The basal lamina contains some of the key molecules crucial for the structural and functional NMJ integrity. This figure was taken from my published review (Cetin and Vincent, 2018).

concentrated at the bottom of the postsynaptic folds. This results in an action potential that propagates along the muscle fibre and triggers muscle contraction by the release of calcium from the sarcoplasmic reticulum and the polarised movement of myosin molecules along actin filaments.

The extent to which the EPP exceeds the electrical threshold necessary to initiate an action potential in the muscle fibre is called the safety factor. The excess of presynaptic vesicles released by each nerve action potential together with high AChR and VGSC densities at the postsynaptic membrane are key elements underlying the safety factor.

1.3 The AChR clustering pathway

The very high density of AChRs at the NMJ that has been shown by many studies (Albuquerque et al., 1974; Barnard et al., 1975) is achieved during development and maintained at the mature NMJ by a complex clustering pathway (Huh and Fuhrer, 2002). Neural agrin, a basal lamina proteoglycan secreted from the motor nerve terminal, interacts with low-density lipoprotein receptor-related protein 4 (LRP4) on the postsynaptic muscle membrane (the muscle isoform of agrin lacks a specific alternative splicing sequence and is incapable of inducing AChR clusters (Hoch et al., 1993)). Neural agrin-LRP4 heterodimers aggregate into tetrameric agrin-LRP4 complexes that enhance the interaction between LRP4 and muscle specific kinase (MuSK), resulting in activation and autophosphorylation of MuSK (Zong and Jin, 2013). Via its intracellular phosphotyrosine binding domain, MuSK recruits downstream of tyrosine kinase 7 (Dok7) creating a tetramer, in which a Dok7 dimer

crosslinks two MuSK monomers. Further phosphorylation of MuSK releases auto-inhibition and increases its catalytic activity. An intracellular kinase cascade then leads to AChR subunit phosphorylation (Wallace et al., 1991; Friese et al., 2007) and, as a consequence, a 43 kDa receptor-associated protein of the synapse (rapsyn) is recruited and stabilises AChRs in clusters (Figure 1-2).

It is important to appreciate that, in contrast to the agrin-LRP4-MuSK-Dok7 signalling pathway that promotes AChR clustering, ACh itself disperses AChR clusters by activation of a pathway involving calpain and cyclin-dependent kinase 5 (Cdk5). Calpain activity in the muscle cell is increased upon cholinergic stimulation and activates Cdk5, a cytoplasmic serine/threonine kinase that mediates AChR dispersion (Chen et al., 2007). Rapsyn has been shown to interact with calpain in an agrin-dependent manner and inhibit its activity, thereby stabilising AChR clusters. Excessive use of acetylcholine esterase (AChE) inhibitors, which will increase the level and duration of ACh in the synaptic cleft, can be associated with loss of postsynaptic AChRs (Chang et al., 1973; Engel et al., 1973), probably as a result of AChR dispersion. It is important to note, however, that these details of neuromuscular transmission have been identified over the last three decades in parallel with an equally informative understanding of myasthenic syndromes that affect the NMJ, which will be discussed later in this chapter.

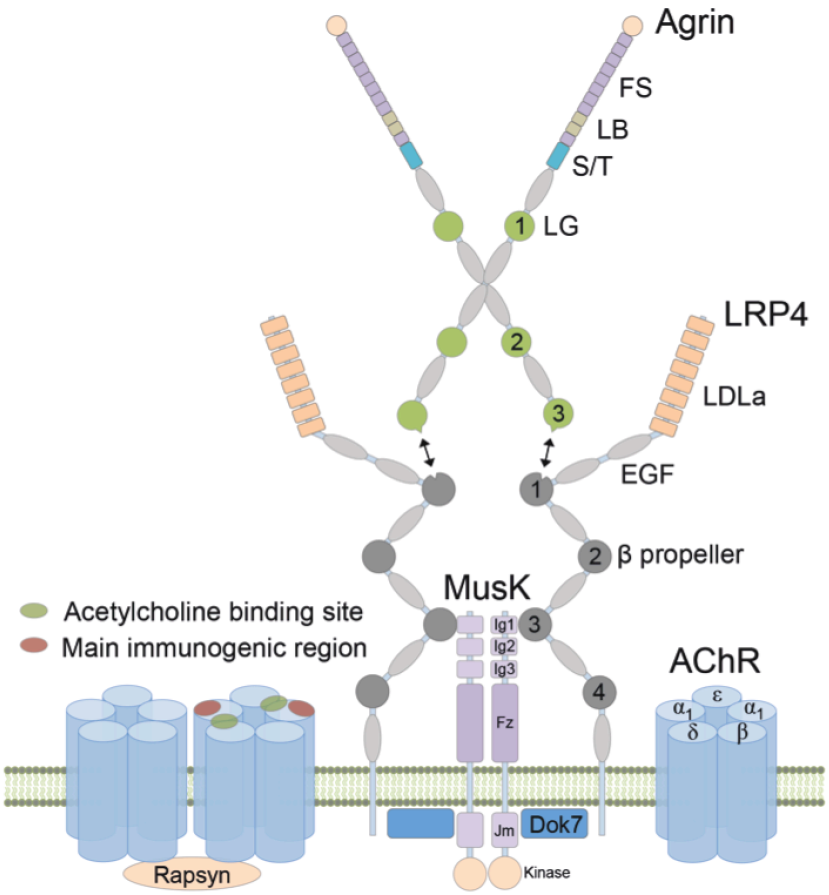


Figure 1-2 Structure of the main AChR clustering molecules

A complex signalling cascade is involved in AChR clustering. Neural agrin secreted from the motor nerve terminal binds to the LRP4 β1-propeller domain through a neuron-specific z8 insert within its LG3 domain (indicated by the bulge). After reorganisation of the agrin-LRP4 interaction sites, two binary agrin-LRP4 complexes aggregate into tetrameric agrin-LRP4 supercomplexes that are necessary to activate MuSK. The LRP4-MuSK interaction occurs between the LRP4 β3-propeller domain and the Ig-like 1 (and part of Ig-like 2) domain of MuSK. This induces MuSK dimerisation, which activates its kinase domain. Dok7 is recruited, which subsequently activates an intracellular kinase cascade resulting in AChR phosphorylation and clustering by rapsyn.

Jm: juxtamembrane region; Fz: Frizzled domain; Ig1-3: Immunoglobulin-like domain 1-3; EGF: epidermal growth factor-like domain; LDLa: low-density lipoprotein-like domain class A; Fs: follistatin-like repeat; LB: laminin-B-like domain; S/T: serine/threonine glycosylation site; LG: laminin-G-like domain. This figure was taken from my published review (Cetin and Vincent, 2018).

1.4 The exchange of AChR isoforms during NMJ development

The AChR is composed of two α-, one β-, one δ- and one γ-subunit in fetal muscle, which is replaced by one ε-subunit in adult muscle. Fetal AChRs are aggregated in pre-clusters along the muscle fibre before innervation but, on innervation, become clustered at the postsynaptic membrane (Braithwaite and Harris, 1979) dependent on the agrin-LRP4-MuSK-Dok7-rapsyn pathway (Tintignac et al., 2015). At the same time, γ-subunit mRNA is repressed and replaced by ε-subunit mRNA transcribed from subsynaptic nuclei (Brenner et al., 1990; Croxen et al., 2001). In human muscle, the switch from fetal to adult AChRs is largely completed in the third trimester of gestation (Hesselmans et al., 1993), but fetal AChRs continue to be expressed at low levels in adult muscle (MacLennan et al., 1997). In mice, by contrast, the switch from fetal to adult AChR mRNA expression takes place postnatally and appears to be complete within two weeks with no easily detectable γ-subunit expression in adult muscle (Sakmann and Brenner, 1978).

Fetal and adult AChR differ in various functional aspects (Table 1-1). It is already known that the fetal isoform has a longer mean open time and a lower conductance compared to the adult receptor (Mishina et al., 1986), and that agonist affinities are higher in fetal AChRs (Nayak et al., 2014). It has been suggested that the higher affinity of the fetal AChR for choline, together with the longer mean open time, results in substantially larger responses of fetal AChRs in prenatal stages, when choline is present at higher serum concentration levels than in adults (Nayak et al., 2014). However, the full significance of the developmental switch from fetal to adult AChRs remains elusive.

Table 1-1 Functional differences between the fetal and adult AChR isoform

	Fetal AChR	Adult AChR	
Subunits	$\alpha_2\beta\delta\gamma$	$\alpha_2\beta\delta\varepsilon$	
Time of occurrence	Man: up to 31st prenatal week; Rodents: up to 2nd postnatal week	Thereafter	Sakmann and Brenner, 1978; Hesselmans et al., 1993
Location in muscle	Extrajunctional	Junctional	Berg et al., 1972; Gu and Hall, 1988; Brenner et al., 1990
Conductance	40 pS	60 pS	Mishina et al., 1986
Open time	7.2 ms	2.3 ms	Mishina et al., 1986
Ca^{2+} permeability	Lower	Higher	Villarroel and Sakmann, 1996; Fucile et al., 2006
Affinity to ACh	7.1 kcal/mol	5.1 kcal/mol	Nayak et al., 2014
Affinity to choline	4.5 kcal/mol	2.7 kcal/mol	Nayak et al., 2014
Affinity to α-bungarotoxin, k_D	4.2 x 10^{-11} M	10.0 x 10^{-11} M	Vincent et al., 1998

1.5 Autoimmune myasthenia gravis

Myasthenia gravis (MG) is a relatively rare neurological disease characterised by exertional fatigability and muscle weakness due to autoantibodies directed against the AChR or associated proteins at the postsynaptic membrane. In 1672, Thomas Willis probably published what is considered to be the first clinical description of MG, reporting the case of a woman with fatigable weakness of the limbs and bulbar symptoms (Willis, 1672). Near the end of the 19th century, Wilhelm Erb (Erb, 1879) and Samuel Goldflam (Goldflam, 1893) described the clinical features of MG in more detail emphasising the fluctuating occurrence of weakness. For many years, MG was referred to as Erb-Goldflam disease, until Friedrich Jolly established the term "myasthenia gravis pseudoparalytica" (Jolly, 1895). He was the first who hypothesised an impairment of neuromuscular transmission as the underlying cause of MG by demonstrating that repeated nerve stimulations resulted in decreased muscle contractions (Jolly, 1895). Intensive research on MG throughout the 20th century successfully unravelled the underlying disease mechanisms and helped to develop effective therapies (Vincent, 2002). Disease mechanisms and clinical correlations will be discussed in more detail in the following sections.

1.5.1 Clinical classification

Differences in disease onset, the distribution of affected muscles, thymus pathology and disease severity contribute to a heterogeneous phenotype in MG. In early-onset MG, patients become symptomatic before the age of 50 years. There is a female preponderance in this age group and thymic follicular hyperplasia and other

autoimmune diseases are more frequent (Matsui et al., 2009). Late-onset MG is often defined by initial symptomatology after the age of 50 years. The patients are usually seropositive for AChR antibodies and males predominate. Late-onset MG has been shown to be an independent risk factor for exacerbations within three years after disease onset (de Meel et al., 2015). Another important prognostic factor is the distribution of affected muscles. Diplopia and ptosis are frequent at disease onset with a high conversion rate into generalised MG within the first two years. Patients with pure ocular symptoms after two years are classified as ocular MG. The other major subgroup is defined by patients with thymomas who usually have generalised, and often severe, disease.

1.5.2 Serological classification

MG autoantibodies are directed against different proteins of the postsynaptic membrane and are accepted as important MG biomarkers associated with specific MG phenotypes (Table 1-2). The classification of MG patients according to antibody status is an important step in the diagnostic process and can help to guide further therapeutic decision-making.

1.5.2.1 AChR antibodies

Antibodies against AChRs can be detected in about 80% of generalised MG and 50% of ocular MG patients using routine assays (Lindstrom et al., 1976; Kawanami et al., 1984; Vincent and Newsom-Davis, 1985). The radioimmunoprecipitation assay (RIA) is the most commonly used test for the detection of AChR antibodies and

Table 1-2 Antibody characteristics in myasthenia gravis

	Ig subclass	Pathomechanism
AChR antibodies	IgG1, IgG3	• Complement activation • AChR crosslinking and internalisation • Functional blocking
Clustered AChR antibodies	IgG1	• Complement activation
MuSK antibodies	IgG4 > IgG1-3	• Disruption of MuSK-LRP4 interaction • Disruption of MuSK-ColQ interaction
LRP4 antibodies	IgG1 > IgG2/3	• Complement activation • Disruption of agrin-LRP4 interaction

utilises the specific binding of the ^{125}I-radiolabelled snake toxin α-bungarotoxin (^{125}I-BTX) to the AChR (reviewed in Leite et al., 2010; Zisimopoulou et al., 2013). As a quantitative method, RIA allows the accurate estimation of antibody titres by the immunoprecipitation of ^{125}I-BTX-labelled AChRs by patient antibodies. AChR antibodies are found to be polyclonal IgG binding to different epitopes on the extracellular domains of AChR subunits (Tzartos et al., 1998; Vincent, 2002). Many antibodies bind to one epitope on each of the two α-subunits called the main immunogenic region (Tzartos et al., 1982; Tzartos et al., 1998) and are likely to increase the degradation rate by AChR crosslinking (Drachman et al., 1978). By contrast, antibodies against the ACh binding site are characterised by their ability to block the binding of ^{125}I-BTX to AChRs and their potential inhibition of AChR function (Lang et al., 1988; Burges et al., 1990; Bufler et al., 1996b), although they are rare and their symptomatic contribution remains uncertain in most patients (Drachman et al., 1982; Vernet-der Garabedian et al., 1986; Lennon and Griesmann, 1989).

AChR antibodies are typically of the IgG1, and variably IgG3, subclasses that activate complement and lead to lysis of the postsynaptic membrane. The associated simplification of postsynaptic folds affects NMJ physiology in three ways: i) the loss of AChRs at the crest of postsynaptic folds decreases the sensitivity of the postsynaptic membrane to ACh, ii) the loss of VGSCs at the depths of the postsynaptic folds increases the threshold depolarisation necessary to generate an action potential in the muscle fibre (Ruff and Lennon, 2008), and iii) the loss of postsynaptic folds also reduces the EPP. It was estimated that the postsynaptic folds contribute to an approximately tenfold increase of the effective input resistance at the

postsynaptic region (Martin, 1994), the loss of which would thus generate a smaller depolarisation by an equivalent flow of current via AChRs (Ruff, 2011). All three mechanisms result in a reduction of the safety factor.

Pre- and postsynaptic compensatory mechanisms have been described in AChR-antibody positive MG (AChR-MG) (Verschuuren et al., 2013). In muscle, the mRNA expression level of AChR subunits was increased in severely affected patients (Guyon et al., 1994; Guyon et al., 1998). Other experiments based on experimental autoimmune MG revealed that mRNA levels of various AChR subunits, as well as of myogenic factors, were increased (Asher et al., 1993). Presynaptic compensatory changes include an increased activity of choline acetyltransferase (Molenaar et al., 1981) as well as a rise in the number of vesicles released from the nerve terminal (i.e. quantal content) (Molenaar et al., 1979; Cull-Candy et al., 1980; Plomp et al., 1995). The presynaptic compensatory changes in MG are of particular interest because they are most likely caused by a reduced number of functional postsynaptic AChRs (Miledi et al., 1978). Thus, a retrograde signal from the postsynaptic compartment to the presynaptic nerve terminal appears to be involved in compensating for the loss of functional AChRs. LRP4 is one possible candidate for this important role in presynaptic differentiation and plasticity (Wu et al., 2012; Yumoto et al., 2012).

Most antibodies bind to both fetal and adult AChRs by virtue of the shared α-subunits. A rare but interesting condition is when a mother has antibodies that bind to the extracellular domain of the γ-subunit specific for the fetal AChR and cause a condition called arthrogryposis multiplex congenita (AMC) (Vincent et al., 1995). In this situation, the antibodies cross the placenta during pregnancy and paralyse the

infant by inhibiting the function of fetal AChRs (Riemersma et al., 1996). AMC is characterised by multiple joint contractures, lung hypoplasia and neonatal or prenatal death. Mothers of affected infants can have MG, have very atypical MG or be completely normal because the adult NMJ depends on the adult AChR, which is not targeted by the γ-specific AChR autoantibodies.

1.5.2.2 Clustered AChR antibodies

The cell-based assay (CBA) provides a high-sensitivity method for the detection of AChR antibodies. It is based on cultured cell lines co-transfected with rapsyn in order to cluster AChRs on the cell surface. The CBA allowed the identification of AChR antibodies, which have now been reported to be present in 20-60% of patients in whom antibodies cannot be detected using RIA or ELISA (Leite et al., 2008; Jacob et al., 2012; Devic et al., 2014; Rodriguez Cruz et al., 2015c). One probable explanation for the improved sensitivity of the CBA is that the antibodies have low affinities for AChR epitopes and that crosslinking the tightly clustered AChRs enables them to bind divalently (Rodriguez Cruz et al., 2015a), though this has not been shown formally. Clustered AChR antibodies are mainly of the IgG1 subclass and activate complement (Leite et al., 2008). They were shown to transfer disease to mice with reduction of MEPP amplitudes indicating the loss of postsynaptic AChRs (Jacob et al., 2012). The results were similar to those found in experiments using typical RIA-positive AChR antibodies, although less severe.

1.5.2.3 MuSK antibodies

MuSK antibodies can be found in up to 70% of patients with undetectable AChR antibodies in routine assays (Hoch et al., 2001). The CBA again provides a more sensitive method and can detect MuSK antibodies also in 8% of MG sera negative for both AChR and MuSK RIAs or clustered AChR CBAs (Huda et al., 2017). MuSK antibodies are predominantly, but not exclusively, of the IgG4 subclass and characterised by unique properties (Huijbers et al., 2015). IgG4 antibodies can undergo Fab arm exchange (i.e. the exchange of half-antibodies with other IgG4) resulting in hybrid antibodies, which are bispecific and thus do not crosslink identical antigens (Koneczny et al., 2017) or activate complement.

The extracellular MuSK domain consists of three Ig-like domains and a Frizzled-like domain (Figure 1-2). The first Ig-like domain is essential for the interaction with LRP4 (Zhang et al., 2011). MuSK antibodies bind to an epitope within the first Ig-like MuSK domain and prevent its interaction with LRP4 (Huijbers et al., 2013; Koneczny et al., 2013), which is a crucial step in the AChR clustering pathway. As a result, AChR clustering is significantly impaired (Koneczny et al., 2013). MuSK also interacts with collagen Q (ColQ), a collagen-like protein that anchors AChE to the basal lamina in the synaptic cleft. Passive transfer studies in mice revealed that MuSK IgG exerts a dose-dependent block of MuSK binding to ColQ (Kawakami et al., 2011). It was hypothesised that this would abolish AChE localisation in the synaptic cleft, but this could not be confirmed in patient intercostal muscle sections by the same group (Kawakami et al., 2011).

It is a matter of debate how a reduction of AChR clustering contributes to the phenotype of MuSK-antibody positive MG (MuSK-MG), which is generally more

severe than in AChR-MG. As shown in mice injected with MuSK-IgG, impaired clustering seems to be associated with reduced postsynaptic AChR densities (Cole et al., 2008; Cole et al., 2010). However, quantitative analyses of patient limb muscle tissue did not reveal reduced AChR numbers although this might be because the most affected muscles were not sampled (Shiraishi et al., 2005). The pathogenicity of MuSK specific IgG1-3 subclasses, which are present at lower concentrations in MuSK patients compared to IgG4, is less clear. They were found to reduce AChR clusters in cultured myotubes (Koneczny et al., 2013) but very small amounts did not induce weakness when injected into immunodeficient mice (Klooster et al., 2012). One plausible explanation for the severe phenotype of MuSK-MG is that the presynaptic compensatory mechanism that can be observed in AChR-MG is absent in animal models of MuSK-MG (Mori et al., 2012; Morsch et al., 2012; Viegas et al., 2012). The mechanism of this presynaptic defect is unknown but may involve the retrograde signalling by LRP4 mentioned above (Yumoto et al., 2012).

1.5.2.4 LRP4 antibodies

LRP4 antibodies are usually detected by CBAs and have been reported in highly varying frequencies ranging from 2% to 54% in double-seronegative MG patients (i.e. negative for AChR and MuSK antibodies) (Higuchi et al., 2011; Pevzner et al., 2012; Zhang et al., 2012). Methodological differences (e.g. using live cells versus fixed or unfixed permeabilised cells in CBAs) have been discussed to account for these differences (Rodriguez Cruz et al., 2015a).

LRP4 antibodies were classified to be predominantly of the IgG1 subclass and seem to inhibit the agrin-LRP4 interaction (Higuchi et al., 2011; Pevzner et al.,

2012). The pathogenicity of LRP4 antibodies was demonstrated in LRP4-immunised mice (Shen et al., 2013). The experimentally induced antibodies fragmented mice NMJs with decreased LRP4 levels and inhibition of agrin-induced MuSK activation and AChR clustering leading to an impairment of neuromuscular transmission and muscle weakness. Quantal content was reduced due to the lack of presynaptic compensatory mechanisms as described in MuSK-MG. In myotubes, the addition of mouse serum decreased cell surface LRP4 levels, inhibited agrin-induced MuSK phosphorylation and AChR clustering and activated complement. The passive transfer of IgG from LRP4-immunised rabbits into mice also caused MG-like symptoms, but there have been no reports of passive transfer of human LRP4 antibodies. Moreover, some laboratories find LRP4 antibodies in AChR- and MuSK-MG (Zisimopoulou et al., 2014) as well as in a significant proportion of other neurological diseases including amyotrophic lateral sclerosis (Tzartos et al., 2014; Rivner et al., 2017) and neuromyelitis optica (Zhang et al., 2012). Future studies need to optimise the assays and determine the relevance of LRP4 antibodies in different conditions.

1.5.2.5 Seronegative myasthenia gravis

Seronegative myasthenia (SNMG) refers to MG patients, in whom autoantibodies cannot be detected using routine assays. SNMG accounts for up to 10% of MG cases (Kerty et al., 2014; Vincent et al., 2018). It is possible that at presentation, these patients have serum concentrations of AChR antibodies that are below the assay sensitivity because of the sequestration of the antibodies at the NMJ. They may also be of lower affinity early in the disease course. In a proportion of SNMG sera,

antibodies directed against other antigens have been reported including agrin (Cossins et al., 2012; Gasperi et al., 2014; Zhang et al., 2014) and cortactin (Gallardo et al., 2014; Cortes-Vicente et al., 2016) but they often coexist with AChR- or MuSK antibodies (Cossins et al., 2012).

1.6 Congenital myasthenic syndromes

CMS are a rare group of genetic disorders characterised by a malfunction of the NMJ. Currently, over 30 different genes have been ascribed to CMS (Table 1-3) (Rodriguez Cruz et al., 2018). According to the location of the molecular defect, CMS can be grouped into presynaptic, synaptic and postsynaptic forms, with a new category of CMS due to defects of ubiquitously expressed proteins. This genetic variety contributes to a highly heterogeneous clinical presentation. Although all CMS share the common feature of fatigable muscle weakness, disease onset and distribution of affected muscles, the response to treatment and systemic manifestations vary according to the underlying genetic defect (Rodriguez Cruz et al., 2018).

1.6.1 Congenital myasthenic syndromes due to kinetic abnormalities of the AChR

Mutations in any of the AChR subunits have been associated with kinetic abnormalities of the receptor, although mutations in CHRNA1 and CHRNE are the most frequent representing about 15% of total CMS cases in the UK (Rodriguez Cruz et al., 2018). Mutations can be located in the agonist-binding site, the coupling

Table 1-3 Genes underlying congenital myasthenic syndromes

Presynaptic CMS syndromes
• Choline-O-acetyltransferase (CHAT) • Unconventional myosin 9 (MYO9A) • PREPL • Vesicular ACh transporter (SLC18A3) • High-affinity ACh transporter 1 (SLC5A7) • Synaptosome associated protein 25 (SNAP25) • Synaptotagmin 2 (SNT2) • MUNC13-1 (UNC13-1) • Synaptobrevin 1 (VAMP1)
Synaptic CMS syndromes
• Collagen type XIII α1chain (COL13A1) • Endplate AChE deficiency (COLQ) • Laminin α5 deficiency (LAMA5) • Laminin β2 deficiency (LAMB2)
Postsynaptic CMS syndromes
• Neural agrin (AGRN) • Primary AChR deficiency (CHRNA, CHRNB, CHRND, CHRNE) • Slow/fast channel syndromes (CHRNA, CHRNB, CHRND, CHRNE) • Low conductance syndrome (CHRNE) • Escobar syndrome (CHRNG) • DOK7 • LRP4 • MuSK (MUSK) • Plectin deficiency (PLEC1) • Rapsyn (RAPSN) • Sodium channel myasthenia (SCN4A)
CMS syndromes due to ubiquitously expressed proteins
• ALG2 • ALG14 • DPAGT1 • GFPT1 • GMPPB • SLC25A1

PREPL: prolyl-endopeptidase-like gene, ALG2: α-1,3/1,6-mannosyltransferase; ALG14: UDP-N-acetylglucosaminyltransferase subunit; DPAGT1: dolichyl-phosphate N-acetylglucosaminephosphotransferase 1, GFPT1: glutamine-fructose-6-phosphate transaminase 1, GMPBB: GDP-mannose pyrophosphorylase B; SLC25A1: solute carrier family 25 member 1. Adapted from Rodriguez Cruz et al., 2018.

region, the pore-forming domains and the M3-M4 cytoplasmic loop (Engel et al., 2015), and the resulting defects are grouped in slow-channel syndromes characterised by prolonged channel openings and fast-channel syndromes with abnormally brief channel openings (Engel et al., 2015; Rodriguez Cruz et al., 2015b).

1.6.1.1 Slow-channel syndromes

Mutations underlying slow-channel syndromes are of dominant inheritance and occur in different functional domains (Croxen et al., 1997), although they are most common in the M2 transmembrane domain (Engel et al., 1996). Mutations affecting the agonist-binding domain enhance affinity for ACh and impair its dissociation from the binding site, and mutations in the channel pore enhance receptor activation after agonist binding. Both mechanisms are associated with prolonged channel openings in single channel recordings (Engel et al., 2015). As a result, excess calcium entry can reach toxic intracellular concentrations and activate various enzymatic pathways leading to degradation of muscle cells (Engel et al., 1982; Ohno et al., 1995). This can lead to endplate myopathy associated with an impairment of neuromuscular transmission through decay of the postsynaptic folds and loss of AChRs (Engel et al., 2015). Neuromuscular transmission can also be compromised by facilitated desensitisation at physiological stimulation rates (Elenes et al., 2006) or a depolarisation block of the VGSCs (Engel et al., 2015).

1.6.1.2 Fast-channel syndromes

Fast-channel syndromes are caused by recessive mutations in one allele of an AChR subunit and often a null or low-expressor mutation (or rarely another fast-channel mutation) in the other allele (Engel et al., 2015). Shortened channel openings and reduced (miniature) endplate potentials are characteristic for fast-channel syndromes. Different mechanisms have been reported to underlie the disorder, including mutations in the extracellular domain of the receptor decreasing affinity for ACh (Ohno et al., 1996; Shen et al., 2012b), decoupling agonist binding from channel opening (Shen et al., 2003; Shen et al., 2008; Shen et al., 2012a) or decreasing gating efficiency (Wang et al., 1999a).

1.6.1.3 CMS due to reduced AChR conductance

The loss of residue F266 within the M2 transmembrane domain of the ε-subunit was associated with reduced AChR conductance and reported to represent another abnormal kinetic mechanism in CMS (Webster et al., 2012).

1.7 The nicotinic AChR in muscle

As mentioned above, the AChR plays a crucial role in autoimmune and genetic disorders of the NMJ. It belongs to the excitatory, cation-selective ligand-gated ion channels (Albuquerque et al., 2009). As a heteropentameric receptor it is composed of two α1-, one β1-, one δ- and one γ-subunit in the fetal isoform or one ε-subunit in the adult isoform that are arranged around a central pore (Figure 1-3). Together with the excitatory 5-hydroxytryptamine receptor and the inhibitory glycine and GABAA

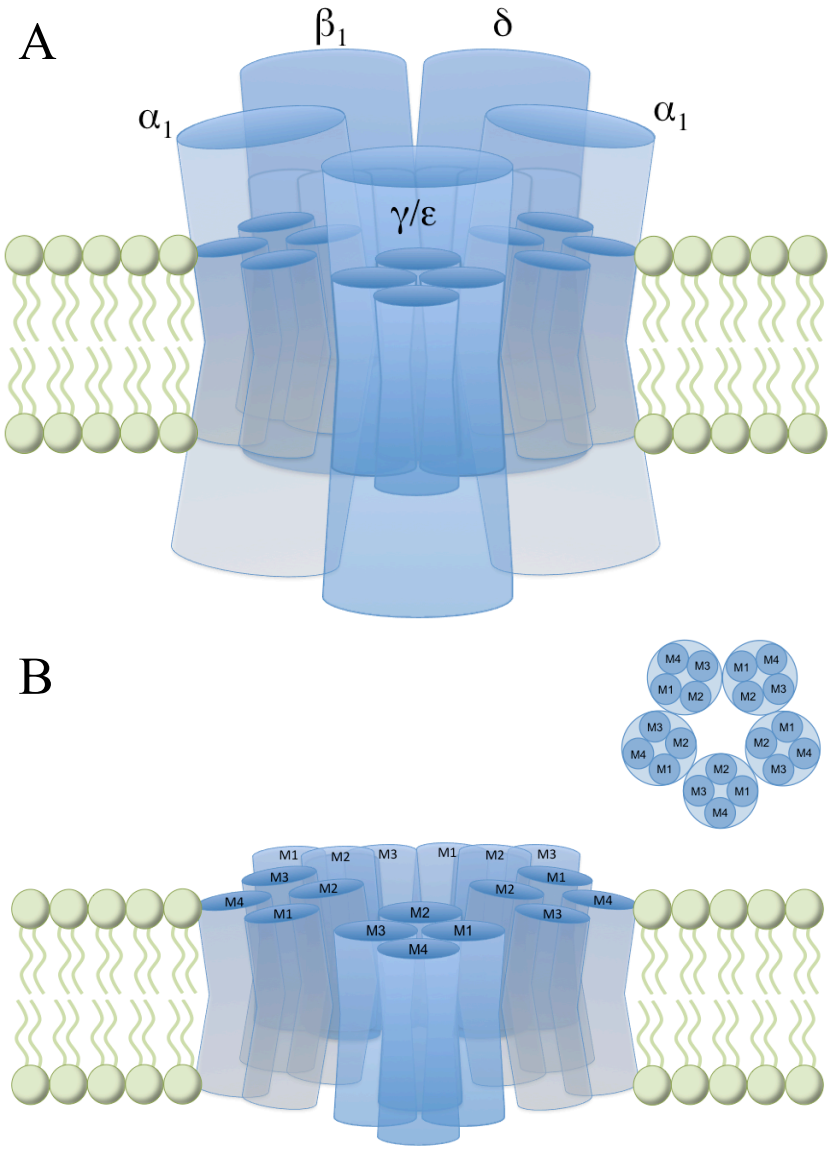


Figure 1-3 Pentameric structure of the AChR in muscle
In AChRs, two α1- and three non-α-subunits encompass a central pore (A). Each subunit is characterised by the transmembrane domains M1-M4 with the M2 domain forming the channel pore (B). The transmembrane domain M4 is most interactive with the lipid bilayer (Baenziger et al., 2015).

receptors, the AChR is characterised by a signature sequence of 13 residues flanked by cysteines, which form a disulfide-bond near the N-terminal extracellular domain (i.e. Cys-loop ligand-gated ion channel superfamily) (Sine and Engel, 2006).

The determination of the molecular AChR structure was enabled by the discovery of the water-soluble acetylcholine binding protein (AChBP) in the freshwater snail *Lymnaea stagnalis* (Smit et al., 2001), which is generally released by glial cells of molluscs into cholinergic synapses, where it modulates transmission by binding ACh. Sequence alignment revealed high similarity with the N-terminal extracellular region of nicotinic AChRs. Subsequently, the structures of the AChBP, the Torpedo AChR and the human neuronal AChR were resolved by X-ray crystallography and cryo-electron microscopy (Table 1-4).

All AChR subunits have a large extracellular N-terminal domain, four transmembrane domains (M1-M4) and a cytoplasmic loop domain of variable size and amino acid sequence between the M3 and M4 transmembrane helices (Figure 1-4). The extracellular domain is predominantly composed of β-strands grouped into an inner (β-strands 1, 2, 3, 5, 5', 6, 6' and 8) and outer sheet (β-strands 4, 7, 9 and 10) that form a β-sandwich (Unwin, 2005). The disulphide-bond of the Cys-loop (C128-C142) links together the inner and outer β-sheets and stabilises the three-dimensional fold (Brejc et al., 2001; Unwin et al., 2002). The transmembrane domains M1-M4 are α-helices that traverse the lipid bilayer and extend beyond the extracellular membrane surface (Unwin, 1998, 2005) (Figure 1-5). The cytoplasmic domain is depicted as an α-helix in the Torpedo AChR subunits in Figure 1-5 (Unwin, 2005), but it is rather composed of a mix of α-helical and β-strand structures in other cytoplasmic loop domains (Albuquerque et al., 2009).

Table 1-4 Studies on the AChR structure

Receptor type	Species	Method, resolution
AChBP	*Lymnaea stagnalis*	X-ray crystallography, 2.7Å (Brejc et al., 2001; Smit et al., 2006)
AChBP	*Aplysia californica*	X-ray crystallography, 1.96-3.4Å (Hansen et al., 2005; Ulens et al., 2006)
AChBP	*Bulinus truncatus*	X-ray crystallography, 2.0Å (Celie et al., 2005b; Celie et al., 2005a)
Muscle AChR	*Torpedo marmorata*	Cryo-EM, 4.6Å (Miyazawa et al., 1999)
Muscle AChR	*Torpedo marmorata*	Cryo-EM, 4.0Å (Unwin, 2005)
Neuronal AChR, α4β2	Human	X-ray crystallography, 3.9Å (Morales-Perez et al., 2018)
Neuronal AChR, α4β2	Human	Cryo-EM, 3.5Å (Walsh et al., 2018)
Neuronal, $AChR_{ECD}$, α2	Human	X-ray crystallography, 3.2Å (Kouvatsos et al., 2016)

AChBP: acetylcholine binding protein, $AChR_{ECD}$: extracellular domain of the AChR, cryo-EM: cryo-electron microscopy.

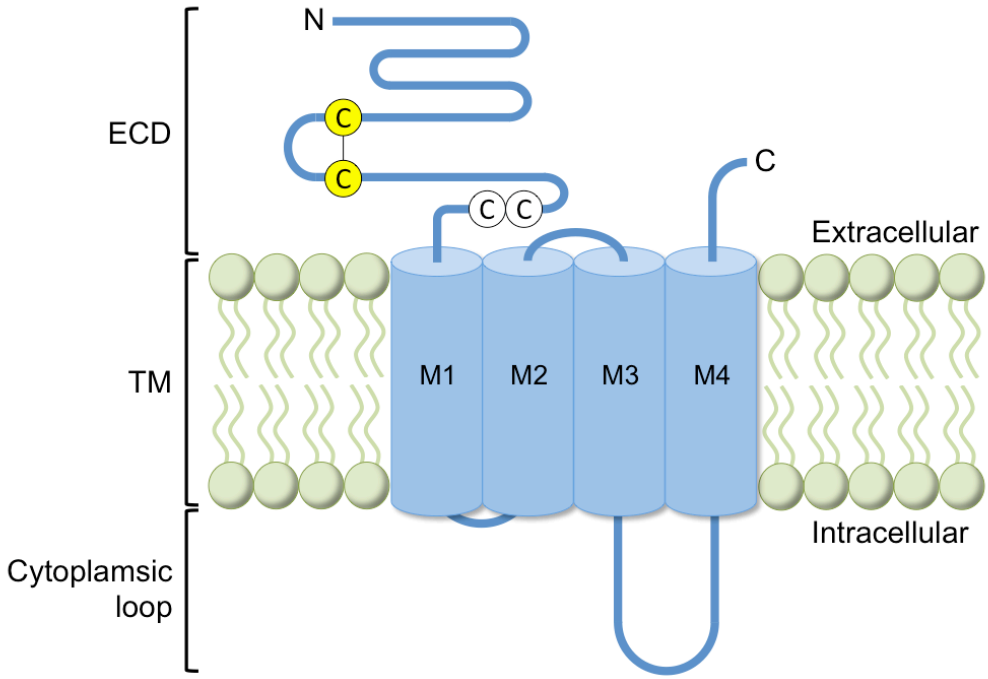


Figure 1-4 Structure of AChR subunits
Each AChR subunit consists of a N-terminal extracellular domain (ECD) with the disulfide bond (yellow circles), four transmembrane (TM) domains M1-M4 and an intracellular cytoplasmic loop. A Cys-Cys pair close to the extracellular end of M1 (white circles, C192 and C193 in the human α1-subunit) is present in the α-subunit only and was shown to be required for agonist binding (Karlin et al., 1986).

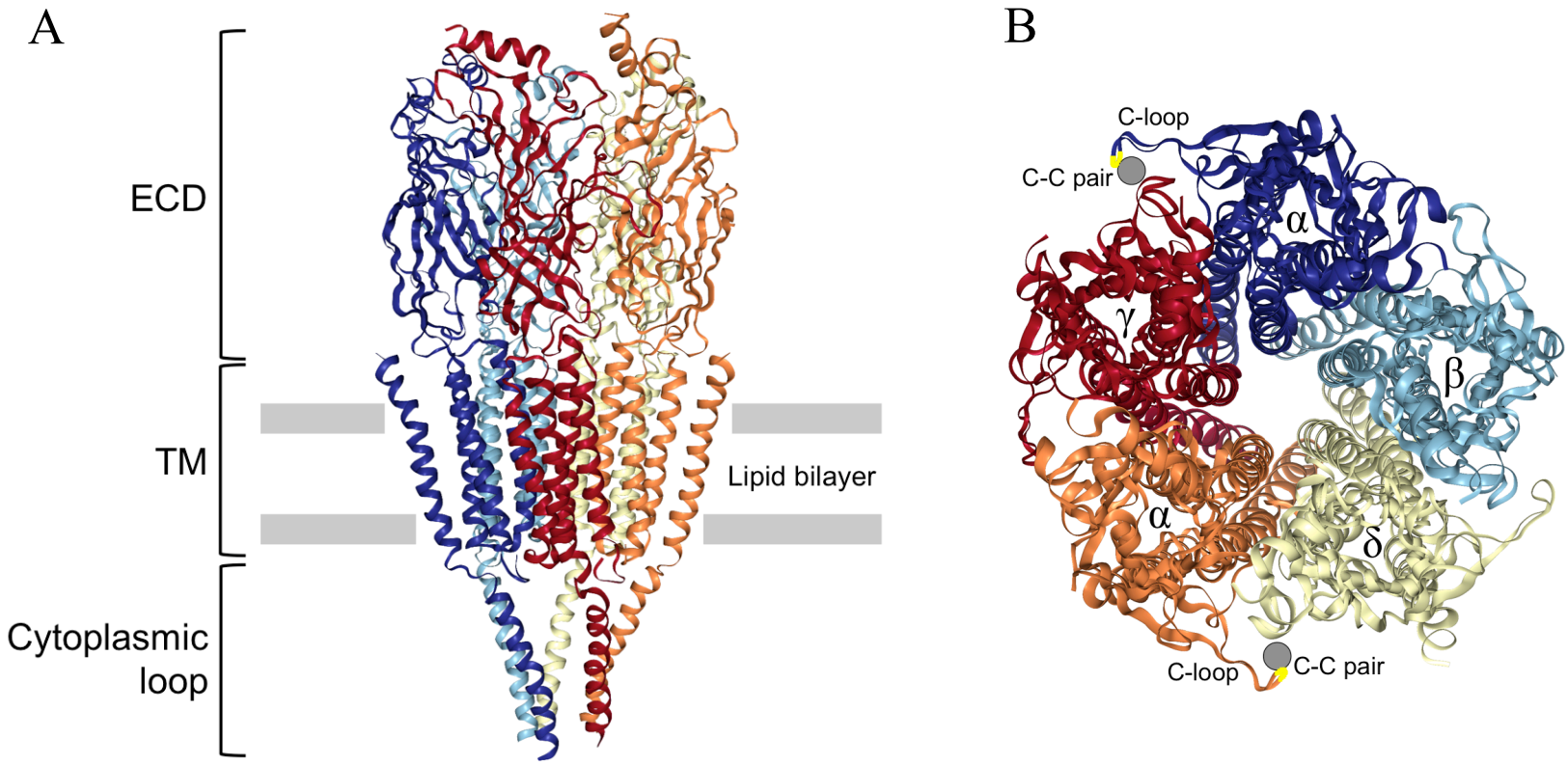


Figure 1-5 Structural model oft the AChR from the Torpedo electric organ
Ribbon representation of the AChR as viewed from the side (A) and from the synaptic cleft (B) was generated using coordinates deposited in the Protein Data Bank (code 2BG9) (Unwin, 2005). In the α-subunit, a loop (C-loop) extends counterclockwise to the neighbouring subunit. At its apex, it contains the Cys-Cys pair (C192 and C193, yellow sequence) and is part of the "hydrophobic pocket" of the agonist-binding site (gray circle). ECD, extracellular domain; TM, transmembrane domain.

1.7.1 The agonist-binding site

The agonist-binding site is a hydrophobic pocket at the interface between an α-subunit and the adjacent γ-/ε- or δ-subunit (Figure 1-5B) (Albuquerque et al., 2009). According to the strength of interaction with agonists, the α-subunit is referred to as a "principal component" and the non-α-subunit as a "complementary component" of the agonist-binding site (Corringer et al., 1995). The principal component contributes three loops from discontinuous sections of the primary sequence (loops A, B and C), whereas the complementary component contributes four discontinuous sections (loops D, E, F and G) (Sine and Engel, 2006; Sine, 2012) (Figure 1-6 and Table 1-5). On the principal component, the hydrophobic aromatic amino acids Y93, W149, Y190, Y198 and the Cys-pair (C192 and C193) were shown to be important for agonist binding (Karlin et al., 1986; Dennis et al., 1988; Galzi et al., 1990). On the complementary component, a number of hydrophobic aromatic (W55 in loop D, (Corringer et al., 1995)) but also negatively charged amino acids on the various loops have been reported to be required for robust agonist binding (Grutter and Changeux, 2001; Sine, 2012). In general, residues on the principal component determine agonist affinity, whereas residues on the complementary component determine ligand selectivity (Albuquerque et al., 2009).

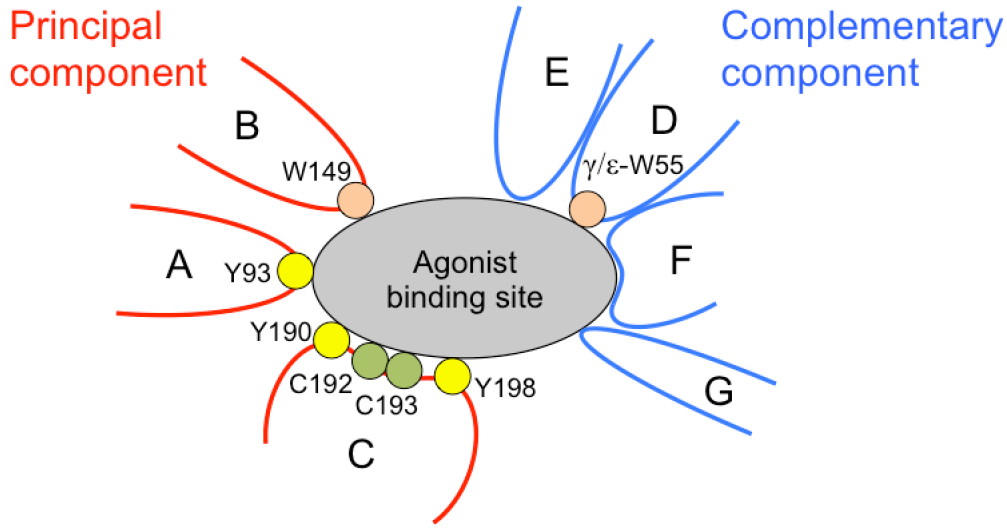


Figure 1-6 The principal and complementary components of the agonist-binding site

The principal and complementary components comprise three (A, B and C) and four loops (D, E, F and G), respectively. The principal component loops are far apart in the closed AChR conformation, but rearrange close to the binding site upon agonist binding including the closure of the C-loop around the bound acetylcholine (Unwin. 2005). Amino acids are identified using the human subunit numbering system (Beeson et al., 1993).

Table 1-5 Loop structure of the agonist-binding site

Loop	Residue span	Secondary structure
A	α93-97	β4-β5 linker
B	α148-153	β7-β8 linker
C	α189-200	β9-β10 linker
D	ε55-59 δ57-61	β2 strand
E	ε109-119 δ111-121	β5'-β6 strands
F	ε161-183 δ163-187	β8-β9 linker
G	ε29-45 δ31-47	β1 strand

Table was adapted from (Sine, 2012). Loops of the principal component are red, and loops of the complementary component are blue. Residue positions correspond to the human AChR (Beeson et al., 1993).

1.7.2 The gating mechanism

Early experiments used affinity labelling and site-directed mutagenesis to determine the molecular basis of the ACh binding site and the gating mechanism (Changeux et al., 1992; Corringer et al., 1998). However, a more detailed picture of the relationship of the AChR structure and several functional aspects including the gating mechanism was generated by three-dimensional structural models using X-ray crystallography and molecular dynamics simulations (Miyazawa et al., 2003; Unwin, 2005).

Agonist binding is converted into channel opening within microseconds by a conformational change involving the fine-tuned interaction of amino acid residues in the coupling region located in the interface between the extracellular and the transmembrane domains (i.e. the ECD-TMD interface) (Miyazawa et al., 2003; Unwin, 2005; Albuquerque et al., 2009). Upon stabilisation of the agonist by the Cys-pair in the apex of the C-loop, which caps the agonist in the hydrophobic pocket (Bourne et al., 2005; Gao et al., 2005; Hansen et al., 2005; Unwin, 2005), torque is generated in the extracellular domain resulting in rotation and the relocation of residues critical to channel gating (Albuquerque et al., 2009). The rotation includes the docking of V46 into the hydrophobic gap between S269 and P272 in the M2-M3 linker domain (Miyazawa et al., 2003; Albuquerque et al., 2009), and a second interaction between E45 and R209 (Lee and Sine, 2005), with both interactions highly conserved in nicotinic acetylcholine receptors and Cys-loop receptors, respectively (Albuquerque et al., 2009). Another interaction between the Cys-loop and the M2-M3 linker region is crucial for the conformational coupling between the agonist-binding site and the pore forming domains and plays a central role in

accelerating the kinetics of activation (Grutter et al., 2005; Grutter et al., 2006). Together, these interactions result in a ~15° clockwise rotation of the M2 transmembrane domains that moves away the pore lining hydrophobic residues L251 and V255, and towards the pore the polar residues S248 and S252 (Unwin, 1995; Unwin et al., 2002; Miyazawa et al., 2003; Unwin, 2003; Albuquerque et al., 2009). The pore widens to a diameter of ~8Å (Unwin, 2003, 2005; Albuquerque et al., 2009), which is similar to the diameter of a sodium or potassium ion surrounded by its first solvation shell (Unwin, 2005).

1.7.3 Charge selectivity

The AChR channel selects for cations according to size (Adams et al., 1980). Cation selectivity is determined by the charge distribution along the ion permeation pathway (Sine et al., 2010). The intracellular and extracellular vestibules of the receptor adjacent to the transmembrane pore are electronegative (D238, E241 and E262) and provide an environment to stabilise cations and increase their local concentration (Imoto et al., 1988; Corringer et al., 1999; Unwin, 2005; Ivanov et al., 2007). The upper portion of the pore is lined with hydrophobic residues restricting water occupancy and, as a result, preventing the passage of ions in the closed state (i.e. the hydrophobic gating mechanism) (Corry, 2006; Song and Corry, 2009). At receptor activation, the pore widens due to a displacement of M2 and the pore-lining hydrophobic residues L251 and V255 (Unwin et al., 2002; Miyazawa et al., 2003; Unwin, 2003, 2005). This relieves the hydrophobic gate and allows the hydration of the pore and, consecutively, the conduction of cations (Miyazawa et al., 2003; Unwin and Fujiyoshi, 2012). Within the pore, cations are further stabilised by interactions

with ionised side chains in the first turn of the M2 α-helices (Cymes and Grosman, 2016). However, it is not the mere presence of charged residues in a pore-lining AChR region that stabilises ions and ensures charge selectivity but also the rotameric conformation of the charged side chains (Harpole and Grosman, 2014; Cymes and Grosman, 2016).

1.7.4 Structural determinants of desensitisation

Desensitisation is a general term referring to the decrease or loss of response following prolonged receptor stimulation (Ochoa et al., 1989). For the muscle AChR, desensitisation was first described by Katz and Thesleff in 1957 (Katz and Thesleff, 1957) and can be observed as a time- and concentration-dependent decline of the macroscopic current during continuous exposure to agonists (Quick and Lester, 2002), corresponding to an accumulation of receptors in agonist-bound but non-conducting conformational states (Sakmann et al., 1980; Colquhoun and Ogden, 1988). Desensitisation is potentially reversible, although a long-lasting accumulation of receptors in deep desensitised states may occur (Feltz and Trautmann, 1982; Simasko et al., 1986; Boyd, 1987). Up to five conformational states could be distinguished in single-channel analyses of desensitisation (Elenes and Auerbach, 2002), and time-resolved affinity labelling revealed that fast- and slow desensitisation states are structurally distinct (Yamodo et al., 2010).

Desensitisation is mediated by global conformational changes involving the extracellular, transmembrane and cytoplasmic domains (Keramidas and Lynch, 2013). Evidence for a desensitisation state distinct from a diliganded/shut resting state derives from structural as well as functional studies (Keramidas and Lynch,

2013; Nemecz et al., 2016). Using cryo-electron microscopy, the muscle AChR was shown to be characterised by distinct resting, open and desensitised conformations (Unwin et al., 1988; Unwin, 1995). In muscle AChR, evidence for two distinct gates corresponding to the resting and desensitised state, respectively, derived from single-channel analyses (Auerbach and Akk, 1998; Purohit and Grosman, 2006) and from a systematic mutagenesis study (Wilson and Karlin, 2001). Despite an overlap between the resting gate (located between G240 and T244 in the M1-M2 loop and the adjacent M2 domain) and the desensitised gate region (located between G240 and L251), there was sufficient difference to ascribe desensitisation to unique structural rearrangements (Wilson and Karlin, 2001). The X-ray structure of desensitised neuronal AChRs (Morales-Perez et al., 2016), however, revealed that the narrowest point in the pore was defined by glutamate at the –1' position in the M1-M2 loop (with the numbering according to the consensus system of Miller, in which position 1' refers to the cytoplasmic end of the M2 domain (Miller, 1989)). Similar results were obtained for the GABAA receptor, in which the desensitisation gate was also located in the M1-M2 loop with the narrowest point in the pore defined by alanine at the –2' position (Miller and Aricescu, 2014). Following desensitisation-specific conformational changes at the ECD-TMD interface of the α4β2 neuronal AChR (Morales-Perez et al., 2016) and the glycine receptor (Wang and Lynch, 2011), the ECD-TMD interface was reported to play a major role in desensitisation (Nemecz et al., 2016). As for the α4β2 neuronal AChR, the structural displacements required for desensitisation were shown to be generated by a 15° intra-subunit rotation around an axis passing through the Cys-loop (Morales-Perez et al., 2016). The rearrangement of

the ECD-TMD interface was also proposed to contribute to the increased affinity for agonist in the desensitised state (Morales-Perez et al., 2016; Nemecz et al., 2016).

1.8 Open questions and thesis aims

As outlined above, there are aspects of normal NMJ development and function that need to be better understood. In particular, there are still questions regarding the implications of the developmental switch from fetal to adult AChRs and how their functions might be modified by rapsyn that clusters the AChRs. The physiological role of desensitisation and recovery from desensitisation is still poorly understood, and their dependence on clustering has never been examined. An impact of clustering on desensitisation and recovery from desensitisation could reveal novel insights into the pathomechanism of disorders of the NMJ, in which AChR clustering is often impaired. Moreover, the underlying pathomechanism of many AChR mutations in CMS patients are unresolved. The study of these mutations can help to optimise patient care and also to better understand aspects of AChR function. The main hypotheses of this thesis were:

i) Rapsyn not only mediates AChR clustering but also alters AChR function

ii) The M3-M4 cytoplasmic loop is involved in the modification in AChR function by rapsyn

iii) Rapsyn affects the binding of autoantibodies directed against the AChR commonly detected in sera from MG patients

Thus, the following aims were intended to throw light on some of the open questions:

i) To investigate potential differences in desensitisation and recovery from desensitisation between fetal and adult AChRs.

ii) To assess the impact of AChR clustering by rapsyn on desensitisation and recovery from desensitisation.

iii) To determine the effect of various MG sera on unclustered and clustered AChR function.

iv) To reveal the pathomechanism of the novel αL251R mutation found in a CMS patient.

Chapter 2

Materials and methods

2.1 DNA methods

All chemicals were purchased by Sigma-Aldrich (Sigma). Sanger DNA sequencing of plasmid DNA or PCR products was performed by the in-house facility provided by the Weatherall Institute of Molecular Medicine (WIMM).

2.1.1 PCR reactions

The thermostable *PfuTurbo* DNA polymerase (Agilent Technologies) characterised by a high fidelity DNA synthesis was used for PCR reactions in mutagenesis experiments. Following the manufacturer's protocol, a 25 µl PCR reaction mix contained 1 µl *PfuTurbo* DNA polymerase, 1 µl of DNA template (100 ng/µl), 2 µl of primer mix (1 µl each of 100 ng/µl), 1 µl of dNTP mix, 2.5 µl of 10x QuickChange Multi reaction buffer and 17.5 µl distilled water. The cycling parameters for the PCR *PfuTurbo* DNA polymerase were also set according to the manufacturer's protocol and are shown in Table 2-1.

2.1.2 Molecular cloning

Restriction enzymes were purchased from New England Biolabs (NEB) and used according to the manufacturer's protocol. DNA ligations were performed using the

T4 DNA ligase (Invitrogen) in a reaction mixture at room temperature for 2 hours. A 7:1 molar ratio of insert to vector was used for ligation reactions.

2.1.3 Bacterial transformation

The chemically competent *Escherichia coli* (*E. coli*) strains JM109 (NEB) and 10-beta (NEB) were used to replicate plasmid DNA. Cells were cultured in LB-agar plates (15g agar/l LB). Between 1 ng to 100 ng of DNA was transformed into the bacterial strains by heat shock methods according to the manufacturer's protocol (Table 2-2). After the heat shock process, 400 µl of LB was added to the transformation mixture and the cells were incubated at 37°C for 1 hour in a shaking incubator. About 100 µl was then spread onto LB-agar selection plates containing 100 µg/ml ampicillin, which were incubated at 37°C overnight. Plasmid DNA was purified from bacterial cultures using the QIAprep spin miniprep kit (Qiagen, for the purification of up to 20 µg plasmid DNA) or the PureLink HiPure plasmid filter maxiprep kit (Invitrogen, for the purification of up to 1000 µg plasmid DNA) following the manufacturer's protocol.

2.1.4 Agarose gel electrophoresis

Agarose gel electrophoresis was used to resolve DNA fragments (0.7% agarose dissolved in 1x TBE buffer consisting of 90 mM Trizma base, 90 mM boric acid and 2 mM EDTA). Ethidium bromide (0.5 µg/ml) was added to visualise DNA. DNA samples were prepared in a mixture with loading buffer (4 mM bromophenol blue, 0.35 M EDTA, 30% glycerol) and ran in 1x TBE at 60-100 V. Analysis was

Table 2-1 Parameters used for PCR reactions

Number of cycles	Temperature	Duration
	Step 1	
1	95°C	1 minute
	Step 2	
30	95°C	1 minute
	55°C	1 minute
	65°C	12 minutes (2 minute/kb plasmid length)
	Step 3	
1	4°C	Up to the next day

Table 2-2 Transformation conditions for competent bacterial cells

	JM109	10-beta
Ice	10 minutes	30 minutes
Heat shock	42°C for 45 s	42°C for 30 s
Ice	2 minutes	5 minutes

performed using a UV transilluminator. If necessary, DNA bands in agarose gels were excised and purified using the QIAquick gel extraction kit (Qiagen) following the manufacturer's protocol.

2.2 Cell cultures

TE671 is a rhabdomyosarcoma cell line with muscle-like properties (Stratton et al., 1989). CN21 cells derive from the TE671 cell line and have been stably transfected with the cDNA of the human AChR ε-subunit, so that the adult AChR isoform is expressed in high numbers with only a remaining small fraction of fetal AChRs (Beeson et al., 1996). TE671 and CN21 cells were cultured at 37°C and 5% CO_2 in Dulbecco-modified essential medium (DMEM) (Sigma-Aldrich) supplemented with 10% fetal calf serum (FCS) and 1% antibiotics/antimycotics (i.e. penicillin G, streptomycin and amphotericin B, PSA) (Invitrogen). HEK293 cells (or HEK293T cells that were only used in the cell-surface ^{125}I-BTX binding assay as described below) were maintained at 37°C and 5% CO_2 in DMEM supplemented with 10% FCS and 1% PSA. HEK293T cells derive from the HEK293 cell line and have been stably transfected with the SV40 large T antigen, which can bind to transfected plasmid cDNA carrying the SV40 origin of replication. This results in increased protein production from the plasmid (Pear et al., 1993).

Two different cell lines were used to account for cell specific differences in post-translational AChR modification, which could have contributed to alterations of AChR function. TE671/CN21 cells as a muscle cell line endogenously expressing AChRs were used to ensure a more physiological intracellular environment for AChRs. The application of HEK293 cells as a non-muscle cell line is well

established in patch clamp experiments (Hu et al., 2018). They can easily be transfected with wild-type and mutant AChR subunits and were used in contrast to TE671/CN21 cells to elucidate the role of cell specific intracellular factors on AChR function. For electrophysiological studies, both TE671/CN21 and HEK293 cells were derived from frozen stocks and maintained in culture for up to 20 passages in order to reduce phenotypic heterogeneity (Ponce et al., 2018).

2.3 Plasmids and constructs

A list of the plasmids used in this thesis is shown in Table 2-3.

2.4 Transfections

To express AChR isoforms in the HEK293 (or HEK293T) cell line, cells were seeded at 10^6 cells per well in 6-well plates. At a 60-80% confluence on the following day, cells were exposed to a mix of 3 μg cDNA, 20% glucose and polyethylenimine (PEI) in 2 ml of growth medium. Human muscle AChR α-, β-, δ- and either γ-subunit cDNA were used for fetal AChR expression or ε-subunit cDNA for adult AChR expression. Cells were co-transfected with pEGFP-N1 (Invitrogen), pEGFP-N1-RAPSN or pIRES2-RAPSN-EGFP. After 5–7 h of exposure, HEK293 cells were detached from the plates using trypsin/EDTA, centrifuged at 1200 g for 4 min, resuspended in growth medium and plated onto poly-L-lysine coated glass coverslips.

To express rapsyn in the TE671/CN21 cell line, cells were seeded at 2 x 10^5 cells per well in 6-well plates. On the following day, cells were detached from the

Table 2-3 DNA plasmids that were available in the laboratory and used in experiments

Plasmid	Description
pcDNA3.1-α	Expression plasmid that encodes full-length CHRNA1
pcDNA3.1-β	Expression plasmid that encodes full-length CHRNB1
pcDNA3.1-δ	Expression plasmid that encodes full-length CHRND
pcDNA3.1-γ	Expression plasmid that encodes full-length CHRNG
pcDNA3.1-ε	Expression plasmid that encodes full-length CHRNE
pcDNA3.1-α_{L251R}	Expression plasmid that encodes full-length CHRNA1 bearing the L251R mutation
pcDNA3.1-δ_{R375H}	Expression plasmid that encodes full-length CHRND bearing the R375H mutation
pEGFP-N1	Expression plasmid that encodes the fluorescent marker enhanced green fluorescent protein (EGFP)
pEGFP-N1-RAPSN	Expression plasmid that encodes EGFP-tagged human rapsyn
pIRES2-EGFP	IRES-containing bicistronic vector that encodes EGFP
pIRES2-RAPSN-EGFP	IRES-containing bicistronic vector that encodes human rapsyn and EGFP

plates using trypsin/EDTA, centrifuged at 1200 g for 4 min and resuspended in pre-warmed growth medium without PSA. A corresponding amount of the cell suspension containing 1.25 x 10^6 cells was again centrifuged at 1200 g for 5 min and resuspended in 250 µl resuspension buffer R (Invitrogen) containing 20 µg of DNA at a concentration of 1 µg/µl. Cells were electroporated with either pIRES2-EGFP or pIRES2-RAPSN-EGFP at a voltage of 1100 V and a pulse width of 30 ms using the NEON transfection system (Invitrogen, MPK 5000). In order to increase AChR expression levels, another group of TE671 and CN21 was additionally transfected with cDNA encoding fetal and adult AChR subunits, respectively. Immediately after electroporation, cells were resuspended in pre-warmed growth medium without PSA and plated onto poly-L-lysine coated glass coverslips. The medium was replaced by growth medium with PSA the following day.

2.5 Fluorescence and confocal microscopy

Microscopy was performed on a Zeiss LSM 880 confocal microscope. Between two or three days after transfection, cells were incubated with the C7 monoclonal antibody (mAb), which was shown to be highly specific to the extracellular domain of the AChR δ-subunit (Whiting et al., 1986; Jacobson et al., 1999), 1:1000 in staining medium (DMEM containing 20 mM HEPES and 1% bovine serum albumin, BSA) for 1 h at room temperature, before being washed 3x with staining medium. (In contrast to fluorescent α-bungarotoxin conjugates, the use of the C7 mAb in an indirect immunofluorescence assay was expected to give an amplified signal due to the binding of several secondary antibodies to the primary antibody and was thus used commonly in the host laboratory). Cells were fixed with 3% paraformaldehyde

at room temperature for 10 min, washed 3x with PBS and incubated with secondary antibody Alexa Fluor® 594 (AF594) goat anti-mouse IgG (H+L) (Invitrogen) diluted 1:750 in staining medium for 1 h. Cells were washed 3x in PBS and mounted in fluorescence mounting medium (Dako Cytomation). Images were captured by using the ZEN System imaging software.

2.6 Analysis of AChR expression by fluorescence-activated cell scanning

HEK293 cells were transfected with cDNA encoding fetal or adult AChR subunits. To compare the expression of fetal and adult AChRs in the presence or absence of rapsyn, each group was additionally co-transfected with either pIRES2-RAPSN-EGFP or pEGFP-N1, and cells were seeded in 6-well plates. Between two or three days after transfection, cells were incubated with a 1:1000 dilution of the C7 mAb in staining medium (DMEM supplemented with 1% BSA and 20 mM HEPES) for 45 min at 4°C, before being washed 3x with staining medium. Cells were fixed with 3% paraformaldehyde for 5 min at 4°C, washed 3x with PBS and incubated with secondary antibody AF594 goat anti-mouse IgG (H+L) (Invitrogen) diluted 1:750 in staining medium for 1 h. Cells were again washed 3x in PBS with 5 mM EDTA, then resuspended in PBS with 5 mM EDTA and analysed with a BD FACS Aria Fusion cytometer.

2.7 Analysis of AChR expression by the cell-surface ^{125}I-α-bungarotoxin binding assay

AChR levels on the surface of cells cultured in 6-well plates were measured by the

^{125}I-BTX binding assay. The assay was performed on HEK293T cells 48 hours post-transfection (the HEK293T cell line was used in order to enable higher AChR surface expression in order to increase the sensitivity of the assay). To ensure the reproducibility of results, each assay analysed triplicate wells of cells for each condition. Each well of cells was washed 3x with PBS, followed by incubations with 500 µl of ^{125}I-BTX at 10^6 cpm/ml diluted in blocking solution (DMEM containing 20 mM HEPES and 1% BSA) for 1 h at room temperature with gentle rocking. Subsequently, the cells were washed 3x for 5 min each with 1 ml of PBS and then dissolved in 500 µl of protein extraction buffer. The cell extracts were transferred to Eppendorf tubes and the amounts of ^{125}I-BTX bound were quantified by a gamma-counter. Untransfected HEK293T cells were used for the estimation of the background radioactivity level, which was subtracted from the cell-surface ^{125}I-BTX binding in transfected cells to calculate AChR expression levels.

2.8 Electrophysiology

2.8.1 Whole-cell patch clamping

Both TE671/CN21 and HEK293 cells were patched between two or three days after transfection. Cells were chosen according to the fluorescence intensity of EGFP under the microscope with a preference for the least green cells, which tended to give more stable currents that were lower in amplitude. All experiments were performed at room temperature using the whole-cell patch clamp configuration. Recording pipettes were made of thin-walled borosilicate glass (GC150TF-10, Harvard Apparatus) using a micropipette puller (P-97 Flaming/Brown Micropipette Puller,

Sutter Instruments). Pipette tips were fire-polished to a final resistance of ~3 MΩ (MF-900 Microforge, Narishige). All measurements were performed at a holding potential of –60 mV. Currents were amplified using an Axopatch-1D amplifier (Molecular Devices) and, after filtering at 5 kHz, sampled to hard disk at 25 kHz. Series resistance was either corrected by using the amplifier-based compensation circuit during the recording or a posteriori by the software-based algorithm as implemented in ChannelLab (Synaptosoft Inc.) (Traynelis, 1998). Residual holding potential errors were <2 mV.

2.8.2 The perforated patch method

The transition to whole-cell configuration was usually achieved by the application of a quick suction. Perforated patch configurations, by contrast, were accomplished by using nystatin (200 µg/ml) (N6261, Sigma Aldrich) in the pipette solution. The presence of nystatin in the pipette tip during the establishment of the membrane seal, however, was reported to diminish the likelihood of successful recordings (Horn and Marty, 1988). Here, pipette tips were therefore filled in a two stage process in order to facilitate sealing: for a distance of ~400 µm, pipette tips were first filled with a nystatin-free pipette solution by dipping the pipette tip into extracellular solution, before backfilling with nystatin containing pipette solution. The whole-cell mode was usually attained within 15 min due to diffusion of nystatin to the pipette tip after the establishment of the membrane seal. Access resistances varied from cell to cell and usually ranged between 20 and 50 MΩ. The stock of the nystatin containing pipette solution was light protected and kept for a maximum of 3 h.

2.8.3 Single-channel recordings

Single channel currents were recorded in the cell-attached configuration of the patch clamp technique and were amplified with an Axopatch 200B amplifier (Molecular devices), filtered at 5 kHz (–3 dB, Bessel filter) and sampled to hard disk at 100 kHz. The resolution was set to 50 μs. Channel transitions were detected by 50% amplitude threshold crossing (pClamp 10).

2.8.4 The patch clamp fast perfusion system

2.8.4.1 The perfusion setup

A Perspex® cell chamber filled with ~2 ml of extracellular solution contained AChR-expressing cells adhered to a coverglass (Figure 2-1). The perfusion pipette was constructed by pulling two-barrel borosilicate glass capillaries (Septum Theta, TST150-6, World Precision Instruments) using a vertical puller (Narishige). The tip of the perfusion pipette was cut with a diamond cutter and sanded to a final diameter of approximately 300 μm (Figure 2-1A). Polyimide-coated silica tubes with an inner diameter of 100 μm (MicroFil, MF28G-5, World Precision Instruments) were introduced in each barrel of the perfusion pipette (red and green tubes in Figure 2-1A). Each barrel was then back-filled with instant glue up to the tip of the silica tubes without sealing their opening. Bath inflow and outflow pipettes (Figure 2-1C and E) made of thin-walled borosilicate glass (GC150TF-10, Harvard Apparatus) were used for continuous perfusion of the cell chamber with extracellular solution during recordings.

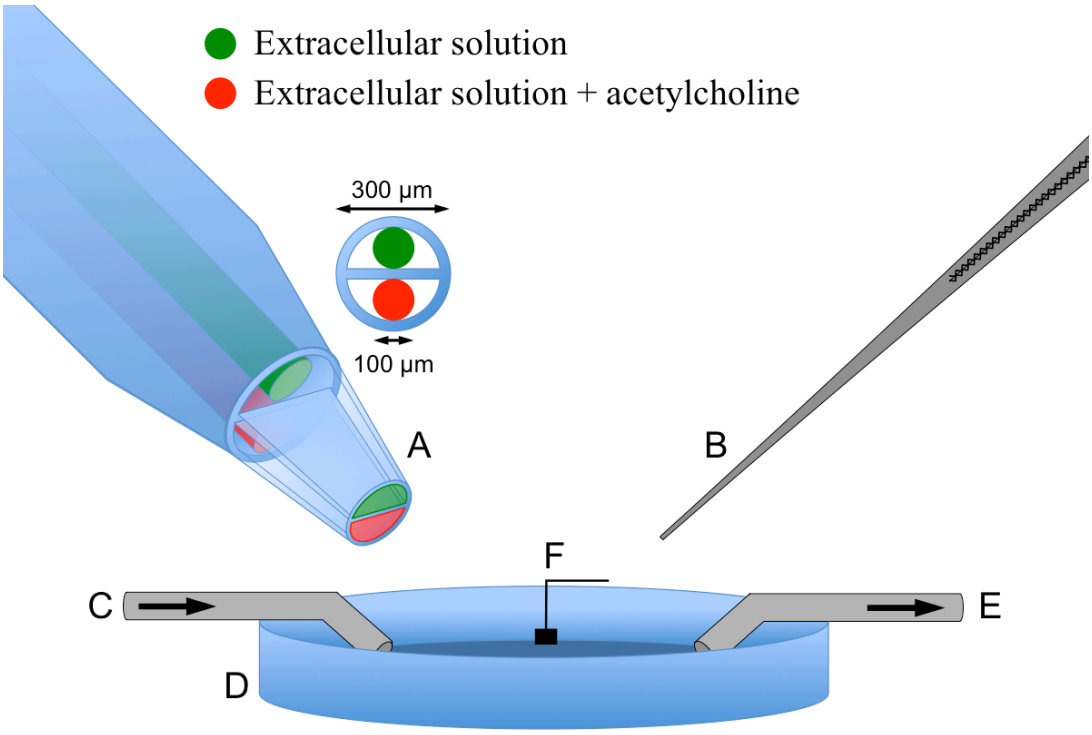


Figure 2-1 The perfusion setup
(A) Perfusion pipette with two tubes, (B) electrode, (C) bath inflow pipette, (D) Perspex® cell chamber, (E) bath outflow pipette, (F) bath electrode.

2.8.4.2 The perfusion setup for serum application

A modified version of the perfusion pipette was used for experiments that required the transient perfusion of cells with serum (for experiments as outlined in Chapter 5). After the construction of the perfusion pipette as described above, two polyimide-coated silica tubes with an inner diameter of 100 μm (MicroFil, MF28G-5, World Precision Instruments) were introduced in each barrel of the perfusion pipette (solid green, solid red, striped green/orange and striped red/orange tubes in Figure 2-2A). Each barrel of the perfusion pipette was then back-filled with instant glue up to the tip of the silica tubes without sealing their opening.

2.8.4.3 Cell perfusion and solution exchange

Fast solution exchange was accomplished using the gravity driven HSSE-2/3 application system (ALA Scientific Instruments) with a digitally controlled pinch valve enabling rapid changes between the two tubes in Figure 2-1 or the four tubes in Figure 2-2. Patched cells were continuously perfused with extracellular solution (through the green tube in Figure 2-1 and the solid green or striped green/orange tube in Figure 2-2) to prevent AChR stimulation by residual ACh in the cell chamber.

In addition to solution application by the perfusion pipette, the bath inflow pipette perfused the cell chamber with extracellular solution at a speed of ~1 ml/min. This continuous perfusion contributed to dilution of the ACh concentration in the cell chamber and helped to prevent AChR stimulation in between ACh applications through the perfusion pipette. The bath outflow pipette was connected to a pump (EP-1 Econo Pump, Bio-Rad) removing the solution from the cell chamber at a speed

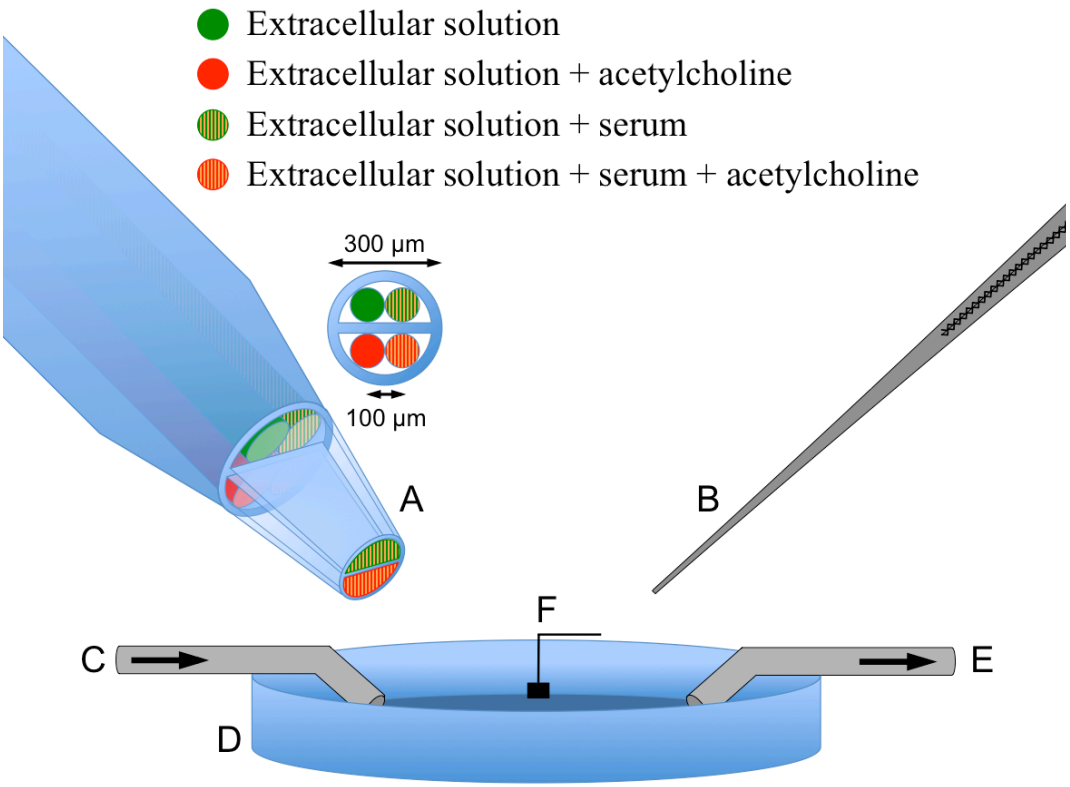


Figure 2-2 The perfusion setup for serum application
(A) Perfusion pipette with four tubes, (B) electrode, (C) bath inflow pipette, (D) Perspex® cell chamber, (E) bath outflow pipette, (F) bath electrode.

of ~2 ml/min.

2.8.5 Analysis of desensitisation and recovery from desensitisation

Receptor stimulation protocols included ten sweeps of 25 s duration, each of which consisted of two consecutive ACh pulses. A “desensitising” pulse of 3 s duration was followed by a 50 ms “test” pulse. The interval between pulses increased with each sweep from 300 ms to 7 s until full recovery from desensitisation. Desensitisation was analysed by fitting one or two exponential components to the current decay phase during the application of the desensitising pulse. For better comparison of desensitisation between groups, weighted current decay time constants were calculated according to Equation 2-1. Recovery from desensitisation was analysed as the ratio between peak current amplitudes of the test and desensitising pulse in ten sweeps plotted against the interval between the desensitising and test pulse. Recovery time constants were determined by fitting one or two exponential components to the data points. Peak current amplitudes, desensitisation and recovery from desensitisation were measured at a holding potential of –60 mV. Clampfit 10.5 or GraphPad Prism v7.0a were used for exponential curve fitting and current decay or recovery time constant calculation, respectively.

$$\tau_W = (\tau_1 A_1 + \tau_2 A_2)/(A_1 + A_2) \qquad \text{Equation 2-1}$$

τ_W: Weighted current decay time constant, τ_X: Current decay time constant for the x-th component of the curve, A_X: Current amplitude of the x-th component of the curve.

2.9 Calculation of AChR transitions between different conformational states in a computer simulation of the AChR kinetic model

The computer simulation of AChR transitions between different conformational states based on a simple linear kinetic scheme as proposed by del Castillo and Katz (Del Castillo and Katz, 1957), with all rates and constants taken from (Franke et al., 1993). The functions of ACh concentration changes were derived from measurements of open pipette junction potential changes by curve fitting using a sigmoidal function. The time course of the distribution of AChRs in various conformational states upon ACh concentration jumps was described by the sum of multiple exponential functions (Colquhoun and Hawkes, 1995). The total amount of AChRs in the simulation was set to 2000. The conductance of a single AChR was set to 40 pS corresponding to the conductance of the fetal AChR isoform. All simulations were carried out using Microsoft Excel and graphed using GraphPad Prism.

2.10 Preparation of sera

All sera used in this thesis were heated to 56°C for 30 min to inactivate complement, centrifuged at 13,000 g for 5 min at room temperature, dialysed against extracellular solution (Slide-A-Lyzer™ MINI Dialysis Device, 20K MWCO, Thermo Fisher Scientific), filter sterilised (Corning® 0.2 μm syringe filters, Sigma-Aldrich) and diluted 1:20 in extracellular solution before use.

2.10.1 Ethical statement

All experiments on serological samples were conducted at the University of Oxford with the approval of the local committees Oxfordshire REC A 07/Q1604/28 and Oxfordshire REC C 09/H0606/74.

2.11 Randomisation, blinding and statistical analysis

In electrophysiological experiments on cell cultures comparing two (or more than two) different treatments (e.g. fetal AChR versus adult AChR or wild-type AChR versus mutant AChR), randomisation was achieved by the order of experiments on different groups, i.e. experiments were performed alternately on cells from different groups rather than testing each group in a block. Blinding was not feasible as all experiments and analyses were performed by the same person. However, the effect of a potential bias was reduced by defining strict methodological inclusion criteria (e.g. residual holding potential errors of <2 mV, see Chapter 2.8.1) and by the application of automated algorithms for data analyses as implemented in Clampfit 10.5.

All data were analysed using GraphPad Prism 7.0a. The statistical tests used in this thesis are described in the figure legends of respective experiments. Tests in all experiments were two-tailed and a p-value <0.05 was considered significant. Error bars represent standard error of the mean, unless otherwise stated in the figure legends.

Chapter 3

Functional differences between fetal and adult AChRs

3.1 Introduction

The AChR is counted among the best-studied ligand-gated ion channels, but there are still questions regarding the implications of the developmental switch from the fetal to the adult isoform. Differences in desensitisation and recovery from desensitisation between fetal and adult AChRs are poorly understood, and a better characterisation could help to elucidate the physiological role of both isoforms. Previous data on desensitisation and recovery from desensitisation show that both isoforms depend on phosphorylation of the M3-M4 cytoplasmic loop of various AChR subunits (Huganir et al., 1986; Middleton et al., 1986; Hopfield et al., 1988; Paradiso and Brehm, 1998), but there is no clear explanation for a difference between the two isoforms in the literature. Experiments using outside-out patches on frog AChRs revealed recovery time constants around several seconds that were similar between the fetal and adult isoform but recovery appeared to be highly variable between patches ranging from 4-63% after a 1 s interval (Paradiso and Brehm, 1998). Other experiments using outside-out patches on mouse AChRs found recovery time constants ranging between 400 and 600 ms (Franke et al., 1992; Krampfl et al., 2002). There was no obvious difference between the two AChR isoforms, but they were not compared directly and agonist concentration was 10-times higher in experiments on adult AChRs (Krampfl et al., 2002). The comparison

of data between studies may thus be limited not only by the use of AChRs from different species with potentially different recovery kinetics but also by methodological differences. It is possible that different cellular expression systems and the application of cell-attached or outside-out patches, which alter the intracellular milieu, were associated with different posttranslational modifications of the AChR and are responsible for varying results.

3.2 Aims

This chapter aimed to assess and reveal potential differences in desensitisation and recovery from desensitisation between fetal and adult AChRs expressed in muscle and non-muscle cell lines. The application of the whole-cell patch clamp technique enabled the assessment of AChR function in a physiological intracellular environment that might be crucial for the elucidation of true biological effects. The role of the cytoplasmic M3-M4 domain on desensitisation and recovery from desensitisation was addressed by the use of chimeric AChRs with exchanged M3-M4 loops.

3.3 The acetylcholine application protocol

The AChR stimulation protocol included ten sweeps of 25 s duration, each of which consisted of two consecutive ACh pulses. A “desensitising” pulse of 3 s duration was followed by a 50 ms “test” pulse. The interval between pulses increased with each sweep from 300 ms to 7 s until full recovery from desensitisation (Figure 3-1). The extracellular solution contained (in mM): NaCl 150, KCl 2.8, HEPES 10, $MgCl_2$ 2,

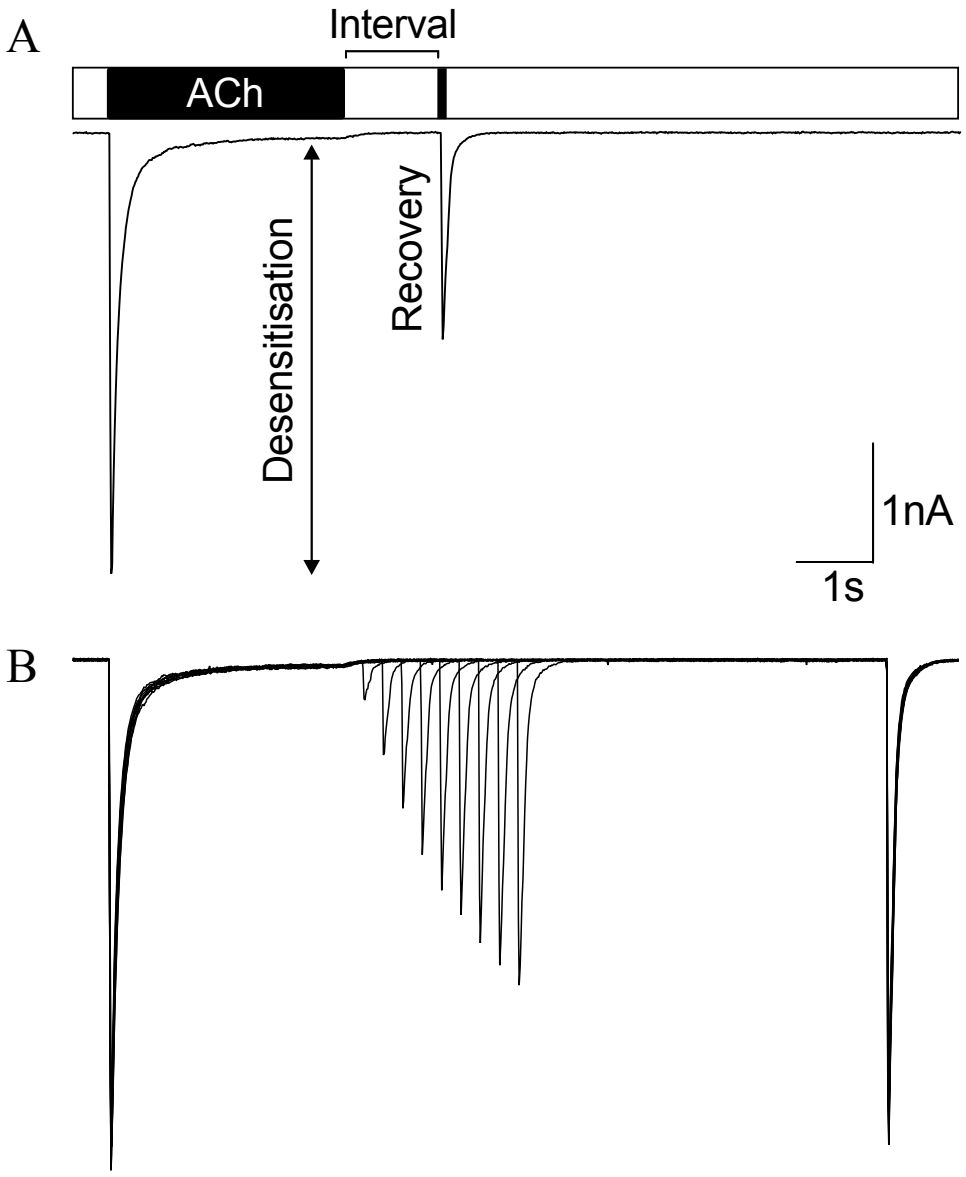


Figure 3-1 Acetylcholine application protocol for the measurement of AChR desensitisation and recovery from desensitisation
The trace was recorded from a HEK293 cell expressing fetal AChRs. The 5th sweep is displayed in (A) with designation of desensitised and recovered current fractions. Ten sweeps are overlaid in (B) to visualise increasing recovery from desensitisation with longer intervals between the desensitising and test pulse.

$CaCl_2$ 2 and glucose 10 with pH adjusted to 7.4 using NaOH. The pipette solution contained (in mM): NaCl 4, KCl 144, HEPES 10, $MgCl_2$ 2, Mg-ATP 2 and EGTA 10 with pH adjusted to 7.2 using KOH (Table 3-1). Osmolarity of pipette solution was calculated to be ~10 mOsm/l lower than extracellular solution to facilitate sealing.

3.4 The influence of methodological factors on AChR desensitisation and recovery from desensitisation

Measurements of desensitisation and recovery from desensitisation depend on various methodological factors. In patch clamp experiments, desensitisation is a function of agonist concentration of the solution to which the cell is exposed (Dilger and Liu, 1992; Quick and Lester, 2002), and solution application times are determined by the perfusion system. Insufficient series resistance compensation in whole-cell patch clamp experiments results in voltage errors (Traynelis, 1998) and voltage inhomogeneity across the cytoplasm, which both can also affect desensitisation and recovery from desensitisation. In order to understand these correlations better, the influence of methodological factors on desensitisation and recovery from desensitisation was assessed by measurements of solution application times and computer simulations as outlined in the following sections.

3.4.1 Estimation of solution application times

Fast ACh application is essential in order to achieve simultaneous activation of AChRs, so that their single channel currents can summate into a whole cell

Table 3-1 Extracellular and pipette solution composition

	Extracellular solution (mM)	Pipette solution (mM)
NaCl	150	4
KCl	2.8	144
HEPES	10	10
$MgCl_2$	2	2
$CaCl_2$	2	-
Glucose	10	-
Mg-ATP	-	2
EGTA	-	10
pH	7.4	7.2

current. An established method to evaluate the quality of the perfusion system is to measure the time course of the current shift induced by the switch between two solutions with different ionic concentrations by an open pipette electrode (Brett et al., 1986; Maconochie and Steinbach, 1998). In this work, a switch from 75 mM to 150 mM NaCl resulted in a mean 10-90% current rise time of 519±21 μs (n=20) and a shift from 150 mM back to 75 mM NaCl resulted in a mean 10-90% current decay time of 601±19 μs (n=20) (Figure 3-2).

The open pipette method, however, underestimates the time needed for concentration changes across an outside-out or cell-attached patch because the unstirred layer of solution adjacent to the surface of the cell membrane presents an additional diffusion barrier (Liu and Dilger, 1991). The use of saturating agonist concentrations can help to reduce current onset times, but very high agonist concentrations might also cause channel block and reduce current amplitudes (Maconochie and Steinbach, 1998). In this project, a 1 mM ACh concentration was used for AChR stimulation. This represents the physiological ACh concentration estimated at the region of postsynaptic membrane opposite to the presynaptic release site at the NMJ (Fertuck and Salpeter, 1976; Matthews-Bellinger and Salpeter, 1978; Kleinle et al., 1996; Smart and McCammon, 1998) and has been shown to result in insignificant channel block in outside-out configuration experiments (Maconochie and Steinbach, 1998). Solution exchange in the whole-cell configuration was assessed by measurements of 10-90% current rise times, which were <10 ms and not different between TE671/CN21 and HEK293-γ/HEK293-ε cells (Figure 3-3).

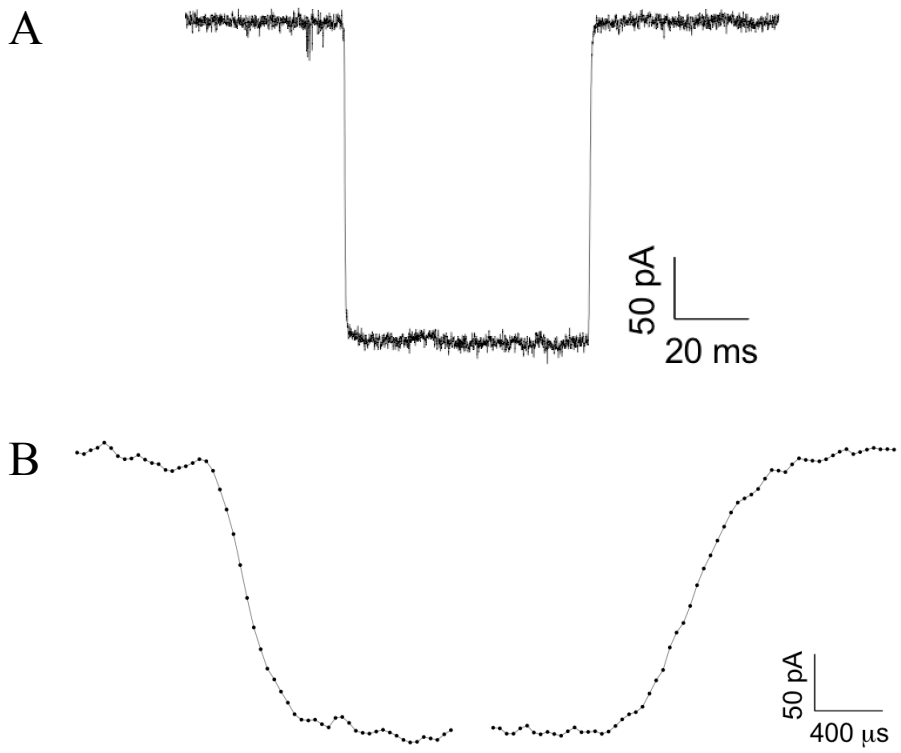


Figure 3-2 Open pipette junction current changes
(A) shows the junction current at a 10 MΩ pipette filled with 150 mM KCl, which was followed as the external NaCl concentration was increased from 75 mM to 150 mM. The duration of the step is 50 ms. (B) shows the leading and trailing edge of the same trace in more detail.

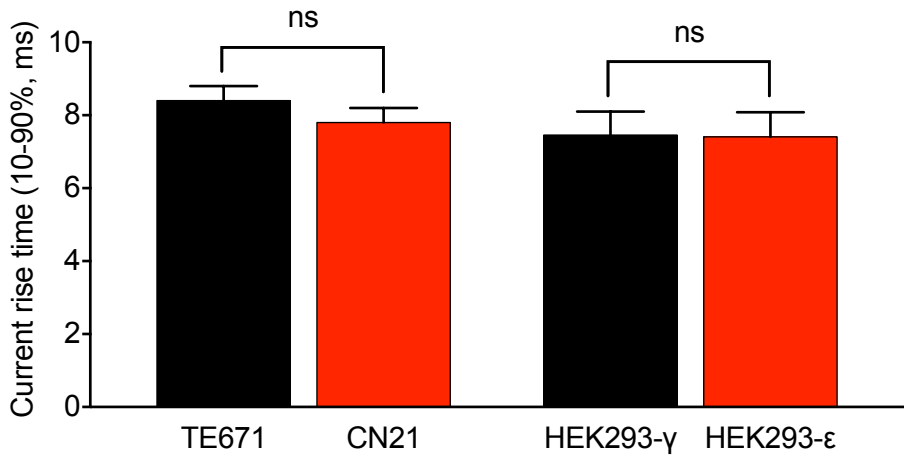


Figure 3-3 10-90% current rise times in TE671/CN21 and HEK293 cells
Mean 10-90% current rise times were <10 ms in the whole-cell configuration and not significantly different between TE671/CN21 and HEK293-γ/HEK293-ε cells (n=10 per group). Unpaired t-test.

3.4.2 Computer simulation of AChR desensitisation and recovery from desensitisation

The AChR oscillates between different closed and open transition states depending on agonist concentration. As one of these transition states, desensitisation is an intrinsic mechanism of the AChR with bound agonist defined by the transition into a closed state from where the receptor can be activated again after agonist removal (i.e. recovery from desensitisation). The time course of desensitisation and recovery from desensitisation can be estimated by simulation of AChR kinetic models. Here, a simple linear kinetic scheme based on the model of del Castillo & Katz was used for computer simulation of current responses (Figure 3-4) (Del Castillo and Katz, 1957; Franke et al., 1993). All rates and constants were derived from a comprehensive study on outside-out patches of mouse-muscle membrane expressing fetal AChRs (Franke et al., 1993). This allowed the evaluation of the impact of AChR numbers, ACh concentration and the rise time of ACh concentration on desensitisation and recovery from desensitisation. However, a direct comparison of the calculated desensitisation and recovery time constants in the computer simulation (based on rate constants derived from mouse AChRs) with data obtained by whole-cell patch clamp experiments on human AChRs in this thesis might be limited.

3.4.2.1 Simulation of acetylcholine concentration changes

The functions for changes of ACh concentration were derived from the open pipette junction potential changes by curve fitting using a sigmoidal function (Equation 3-1). A separate function was used to simulate ACh application resulting in a

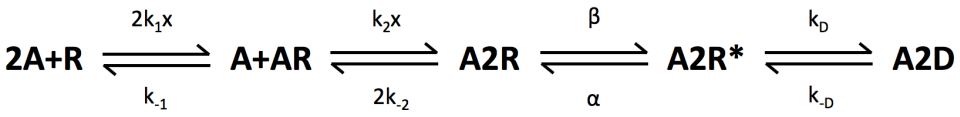


Figure 3-4 Linear AChR kinetic scheme
R: AChR, A: ACh, x: ACh concentration, R*: open AChR conformation, D: desensitised AChR conformation, $k_1/k_{-1}/k_2/k_{-2}$: acetylcholine binding and unbinding rate constants, β: AChR opening rate constant, α: AChR closing rate constants, k_D/k_{-D}: forward and backward rate constants for desensitisation. All rates and constants were taken from (Franke et al., 1993) and defined as $k_1=k_2=1.5x10^8$ $M^{-1}s^{-1}$, $k_{-1}=k_{-2}=8000$ s^{-1}, $\beta=30000$ s^{-1}, $\alpha=700$ s^{-1}, $k_D=20$ s^{-1} and $k_{-D}=2$ s^{-1}.

concentration rise and ACh removal resulting in a concentration decline. In open pipette experiments, the junction potential fall corresponded to ACh application and the junction potential rise to ACh removal (Figure 3-5).

3.4.2.2 Simulation of AChR transitions upon acetylcholine application

The generation of current simulations as described by Colquhoun and Hawkes for the calculation of the AChR open probability as a function of time using the rate constants of a kinetic scheme relies on constant ACh concentration (Colquhoun and Hawkes, 1977). This approach is unsuitable for the simulation of AChR desensitisation and recovery kinetics resulting from changes in ACh concentrations (Maconochie and Steinbach, 1998). The time course of the distribution of AChRs in various conformational states upon an ACh concentration jump can instead be described by the sum of multiple exponential functions (Colquhoun and Hawkes, 1995). For unidirectional transitions from a state ***A*** to a state ***B***, the number of receptors in state ***A*** decreases and, at the same time, the number of receptors in state ***B*** increases according to Equations 3-2 and 3-3.

Upon ACh concentration jumps, AChR transitions usually occur between all conformational states in a kinetic scheme, and the AChRs distribute to a new equilibrium between conformational states. For a given time t, the number of AChRs in state ***B*** depends on the rate constants to and from neighbouring states, that the AChRs can flip to from state ***B***, and the time interval. The new equilibrium for state ***B*** after time ***dt*** can be calculated by a sum of exponentials according to Equation 3-4.

All simulations were carried out using Microsoft Excel and graphed using GraphPad Prism. All calculations were performed separately for each line in the

$$Y = \text{Bottom} + \frac{(Top - Bottom)}{1 + 10^{(Log t_{0.5} - X)\ Slope\ factor}} \qquad \text{Equation 3-1}$$

Bottom: Y value at the bottom plateau, Top: Y value at the top plateau, Log $t_{0.5}$: X value when the response is halfway between Bottom and Top, Slope factor describes the steepness of the curve.

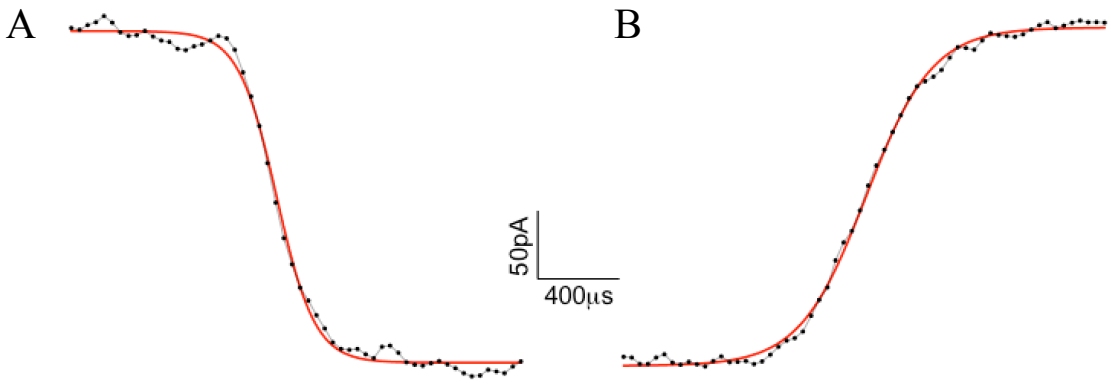


Figure 3-5 Sigmoidal curve fitting to the open pipette junction current changes
Calculations were performed by the application of Equation 3-1. Curve fitting to the junction potential fall (A) revealed a Log $t_{0.5}$ of 1.69 ms and a Slope factor of –4535. Curve fitting to the junction potential rise (B) revealed a Log $t_{0.5}$ of 1.59 ms and a Slope factor of 2664. Top corresponded to the maximum ACh concentration used for AChR stimulation (i.e. 1 mM ACh) and Bottom corresponded to extracellular solution without ACh (i.e. 0 mM ACh).

$$\boldsymbol{A \xrightarrow{ab} B}$$

$$A(t) = A(t - dt)\, e^{-(ab\ dt)} \qquad \text{Equation 3-2}$$

$$B(t) = B(t - dt) + \left(A(t - dt)\left(1 - e^{-(ab\ dt)}\right)\right) \qquad \text{Equation 3-3}$$

A(t): Number of AChR in state $\boldsymbol{A}$ at time t, B(t): Number of AChR in state $\boldsymbol{B}$ at time t, A(t-dt): Number of AChR in state $\boldsymbol{A}$ at time t-dt, B(t-dt): Number of AChR in state $\boldsymbol{B}$ at time t-dt, e: Euler's number, ab: rate constant for the transition from state $\boldsymbol{A}$ to state $\boldsymbol{B}$, dt: Time interval.

$$\boldsymbol{A \underset{ba}{\overset{ab}{\rightleftharpoons}} B \underset{cb}{\overset{bc}{\rightleftharpoons}} C \underset{dc}{\overset{cd}{\rightleftharpoons}} \dots}$$

$$B(t) = B(t - dt)e^{-\left((ba+bc)\, dt\right)} \qquad \dots \boldsymbol{A \underset{ba}{\overset{bc}{\leftarrow\ B\ \rightarrow}} C}$$

Equation 3-4

$$+\left(A(t - dt)\left(1 - e^{-(ab\ dt)}\right)\right) \qquad \dots \boldsymbol{A \overset{ab}{\rightarrow} B}$$

$$+\left(\frac{cb}{cb+cd}\right)\left(C(t - dt)\left(1 - e^{-\left((cb+cd)\, dt\right)}\right)\right) \qquad \dots \boldsymbol{B \underset{cb}{\overset{}{\leftarrow}} C}$$

B(t): Number of AChR in state $\boldsymbol{B}$ at time t, A(t-dt): Number of AChR in state $\boldsymbol{A}$ at time t-dt, B(t-dt): Number of AChR in state $\boldsymbol{B}$ at time t-dt, C(t-dt): Number of AChR in state $\boldsymbol{C}$ at time t-dt, e: Euler's number, ab/ba/bc/cb/cd: Rate constant for the transition between corresponding states, dt: Time interval. The transitions from state $\boldsymbol{B}$ to state $\boldsymbol{A}$ and $\boldsymbol{C}$ correlate to the exponential in the upper line of the equation (red), the transitions from state $\boldsymbol{A}$ to state $\boldsymbol{B}$ correlate to the exponential in the middle line of the equation (blue), and the transitions from state $\boldsymbol{C}$ to state $\boldsymbol{B}$ correlate to the exponential in the lower line of the equation (green).

simulation table with each line equivalent to the time interval of 40 μs (corresponding to a sampling rate of 25 kHz in patch clamp experiments). The AChR distribution in several conformational states calculated for each line in the simulation table was used for the calculation in the next line for a time interval of 40 μs. The duration of the whole simulation was 2.4 s with the ACh application period lasting for 0.9 s and the period after ACh removal lasting for 1.5 s. These simulation periods were long enough to reach steady state conditions between the conformational states (Figure 3-6).

Upon ACh application, the conformational states prior to the open A2R* state are passed through quickly so that the majority of the total AChR population (i.e. 94%) accumulates in the peak at 1.9 ms (Figure 3-6). Desensitisation, by contrast, evolves gradually with only 0.8% of the AChR population residing in the desensitised A2D state at peak current. Thereafter, open AChRs pass through into desensitisation with equal fractions in the open and desensitised state at 37.8 ms with each fraction accounting for 48.7% of the total AChR population. Upon ACh removal, open AChRs quickly close and enter the resting 2A+R state with a deactivation time constant of 4.0 ms. Recovery from desensitisation is an order of magnitude slower than desensitisation and determined by the rate constants k_D/k_{-D} with AChR transitions from the desensitised state into the resting 2A+R state passing quickly through the states A2R*, A2R and A+AR.

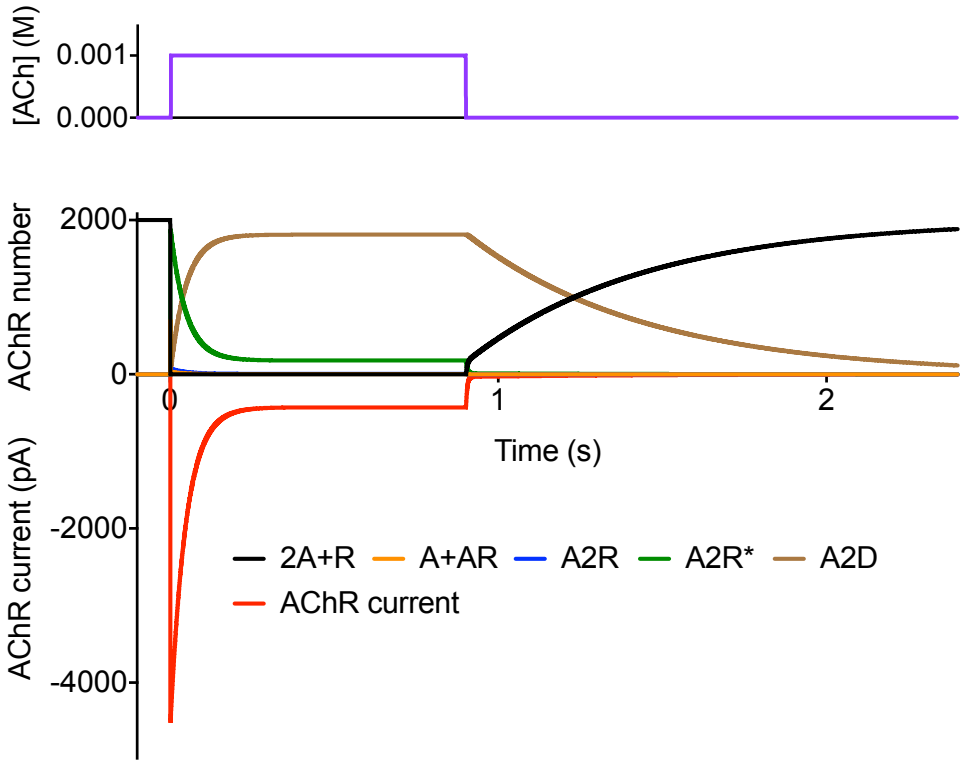


Figure 3-6 AChR transition states upon stimulation with 1 mM ACh
Different fractions of a given AChR population occupy each conformational state outlined in Figure 3-4. The total amount of AChRs in the simulation was set to 2000. The conductance of a single AChR was 40 pS (corresponding to the conductance of the fetal AChR isoform) and the potential difference was –60 mV. The time resolution of the simulation was set to 40 µs corresponding to the sampling rate in patch clamp recordings (i.e. 25 kHz).

3.4.2.3 Dependence of desensitisation and recovery from desensitisation on acetylcholine concentration and its rise time

Variations of cell perfusion parameters could have contributed to differences found in patch clamp recordings. The computer simulation of AChR conformational transitions was used to assess the potential impact of extrinsic factors on desensitisation and recovery from desensitisation. Extrinsic factors included AChR numbers as a measure of AChR cell surface expression, ACh concentration and the rise time of ACh concentration as a measure of the perfusion system quality. Desensitisation time constants were measured by exponential curve fitting to the current decay phase of the AChR current upon ACh stimulation, and recovery from desensitisation was measured by exponential curve fitting to the redistribution of AChRs into resting and activatable states following ACh removal (i.e. 2A+R, A+AR and A2R). AChR numbers had no impact on desensitisation and recovery from desensitisation (Figure 3-7) and there was a linear relationship between AChR numbers and current amplitudes.

Low ACh concentrations were associated with prolonged desensitisation time constants. From an ACh concentration of 100 μM, desensitisation time constants levelled at about 50 ms and remained constant at higher ACh concentrations up to 1 M (Figure 3-8A). Recovery time constant, by contrast, was not influenced by ACh concentration (Figure 3-8B, C). This differential impact of ACh concentration on desensitisation and recovery from desensitisation was due to the correlation of the forward rate constants $2k_1x$ and k_2x with ACh concentration, whereas the backward rate constants α and k_{-D} were independent of ACh concentration.

The influence of the ACh concentration rise time on desensitisation was less

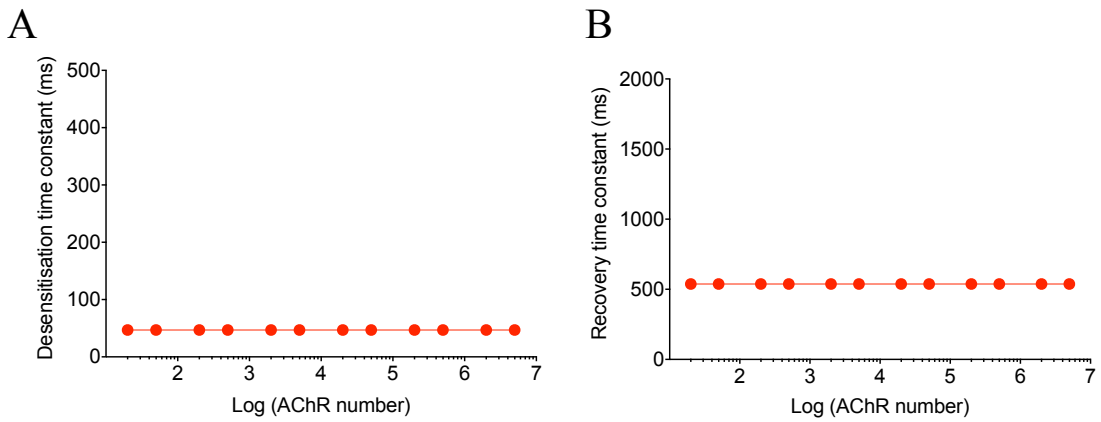


Figure 3-7 The influence of AChR numbers on AChR desensitisation and recovery from desensitisation

With other parameters held constant, AChR number had no influence on desensitisation (A) and recovery time constants (B).

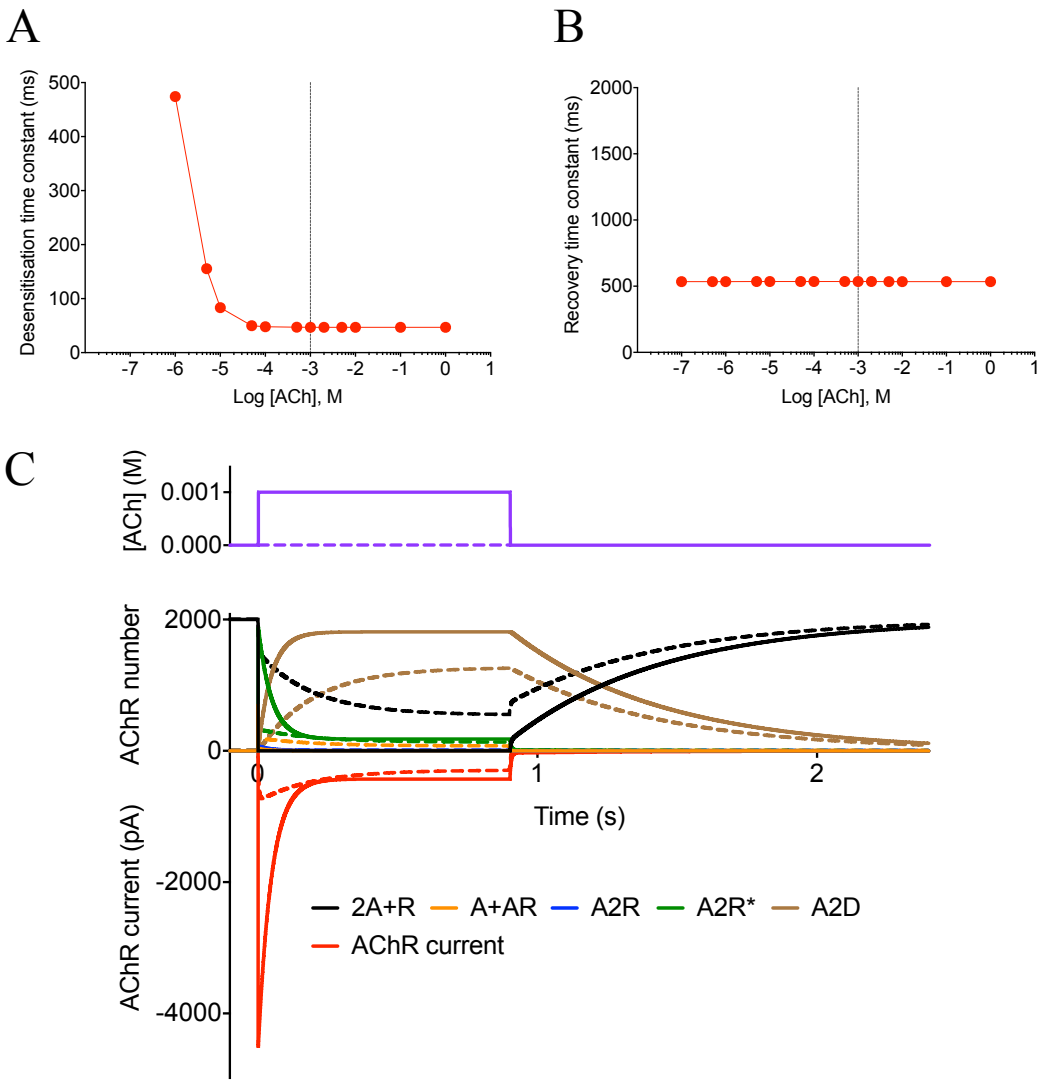


Figure 3-8 The influence of ACh concentration on AChR desensitisation and recovery from desensitisation

With other parameters held constant, low ACh concentrations were associated with prolonged desensitisation time constants (A), whereas recovery time constants remained unaffected (B). Two computer simulations at different ACh concentrations (solid line 1 mM ACh, dashed line 5 µM ACh) are overlaid to emphasise differences of the AChR distribution (C). At an ACh concentration of 5 µM, the forward rate constants $2k_1x$ and k_2x became limiting and prevented AChRs from accumulating in sufficiently high numbers in the open (A2R*) state. This resulted in a significantly reduced peak current amplitude. The AChRs slowly entered A2R* and passed through gradually accumulating in the desensitised state A2D. The vertical dashed lines in (A) and (B) represent the condition in the experiments in this thesis.

significant compared to the influence of ACh concentration and only present at very slow ACh concentration rise times in the range of several seconds (Figure 3-9A, C). This was due to the failure to reach sufficiently high ACh concentrations necessary for quick AChR transitions into the desensitised state. Recovery from desensitisation was not affected by ACh concentration rise times within the range from about 100 µs to 35 s (Figure 3-9B, C).

3.4.3 Series resistance compensation in whole-cell patch clamp experiments

Series resistance (SR) refers to the resistance across the pipette tip, which is usually enhanced from cell debris that becomes attached to the pipette tip upon seal formation and membrane breakthrough. This resistance in the pipette tip is in series with the membrane resistance and therefore implements a voltage divider (Traynelis, 1998). As a result, there is a voltage drop across the SR (i.e. voltage error or SR error) and a second voltage drop across the membrane resistance, and together both voltage drops correspond to the holding potential (Figure 3-10). The voltage drop across the SR and membrane resistance can be calculated according to Equations 3-5 and 3-6.

The membrane resistance is usually two to four orders of magnitude higher than the SR, and the voltage drop across the pipette tip is therefore negligible. Upon agonist application and receptor activation, however, the membrane resistance decreases to levels comparable to the SR resulting in a significant voltage drop across the pipette tip. The voltage error can be calculated according to Equation 3-7. Insufficient SR correction can alter current recordings and bias desensitisation and recovery from desensitisation (Figure 3-11). The SR error can be corrected actively

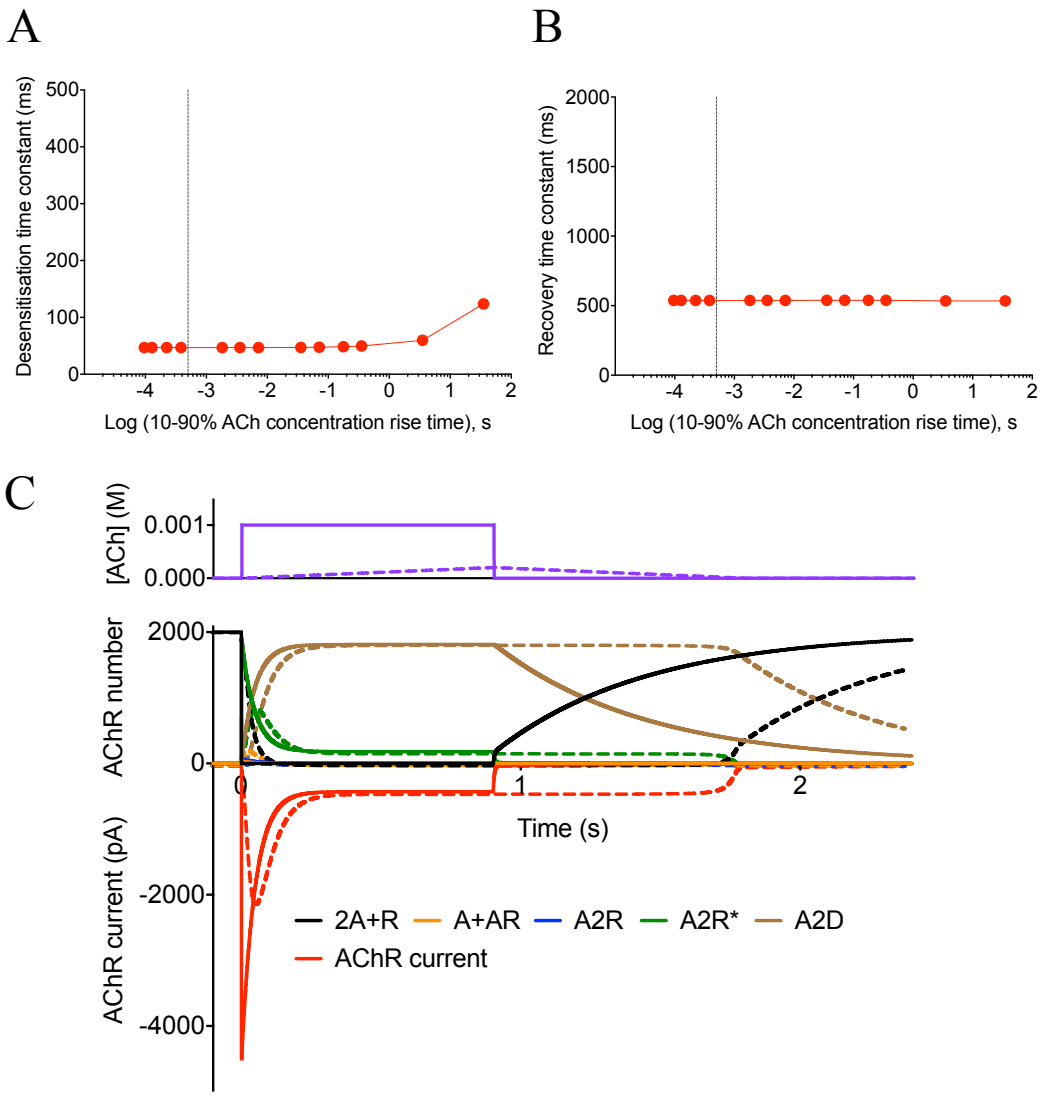


Figure 3-9 The influence of the ACh concentration rise time on AChR desensitisation and recovery from desensitisation

With other parameters held constant, very long ACh concentration rise times in the range of several seconds were associated with prolonged desensitisation time constants (A), whereas recovery time constants remained unaffected (B). Two computer simulations at different 10-90% rise times of ACh concentration (solid line 500 µs, dashed line 3.5 s) are overlaid to emphasise differences of the AChR distribution (C). Due to the failure to quickly reach sufficient ACh concentrations the forward rate constants $2k_1x$ and k_2x became limiting the AChR transition rate into the desensitised state. The vertical dashed lines in (A) and (B) represent the condition in the experiments in this thesis.

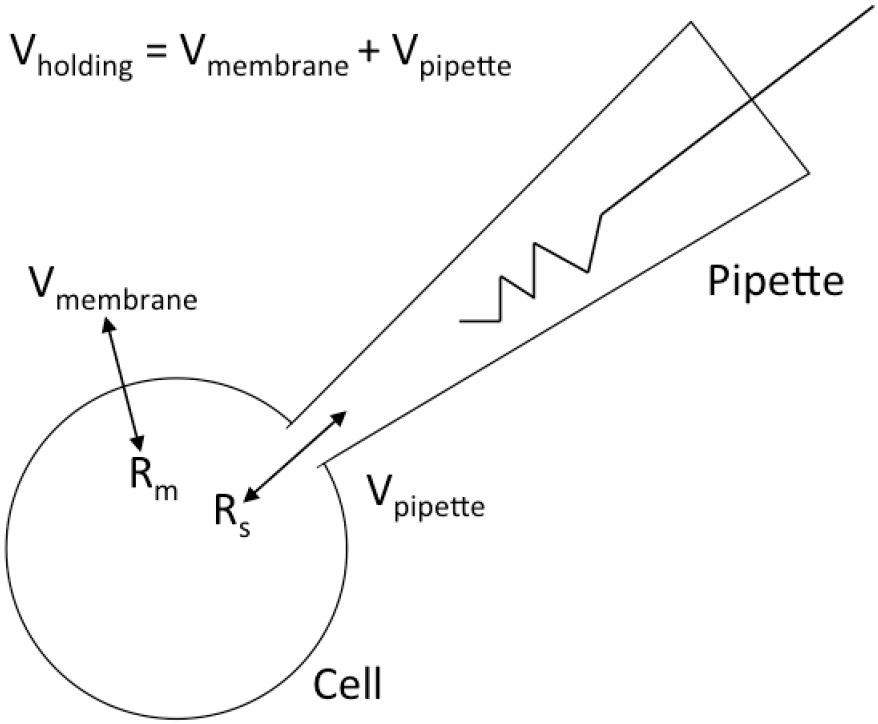


Figure 3-10 Series resistance in the whole-cell patch clamp configuration
In the whole-cell patch clamp configuration, series resistance refers to the resistance across the pipette tip. There is a voltage drop across the series resistance resulting in a reduction (depolarisation) of the membrane potential.

$$V_{PIPETTE} = V_{HOLD}[R_S/(R_S + R_M)] \quad \text{Equation 3-5}$$

$$V_{MEMBRANE} = V_{HOLD}[R_M/(R_S + R_M)] \quad \text{Equation 3-6}$$

$V_{PIPETTE}$: Voltage drop across the pipette, $V_{MEMBRANE}$: Voltage drop across the membrane, V_{HOLD}: Holding potential, R_S: Series resistance, R_M: Membrane resistance.

$$V_{PIPETTE} = IR_S \quad \text{Equation 3-7}$$

$V_{PIPETTE}$: Voltage drop across the pipette, I: Current that flows across the pipette, R_S: Series resistance.

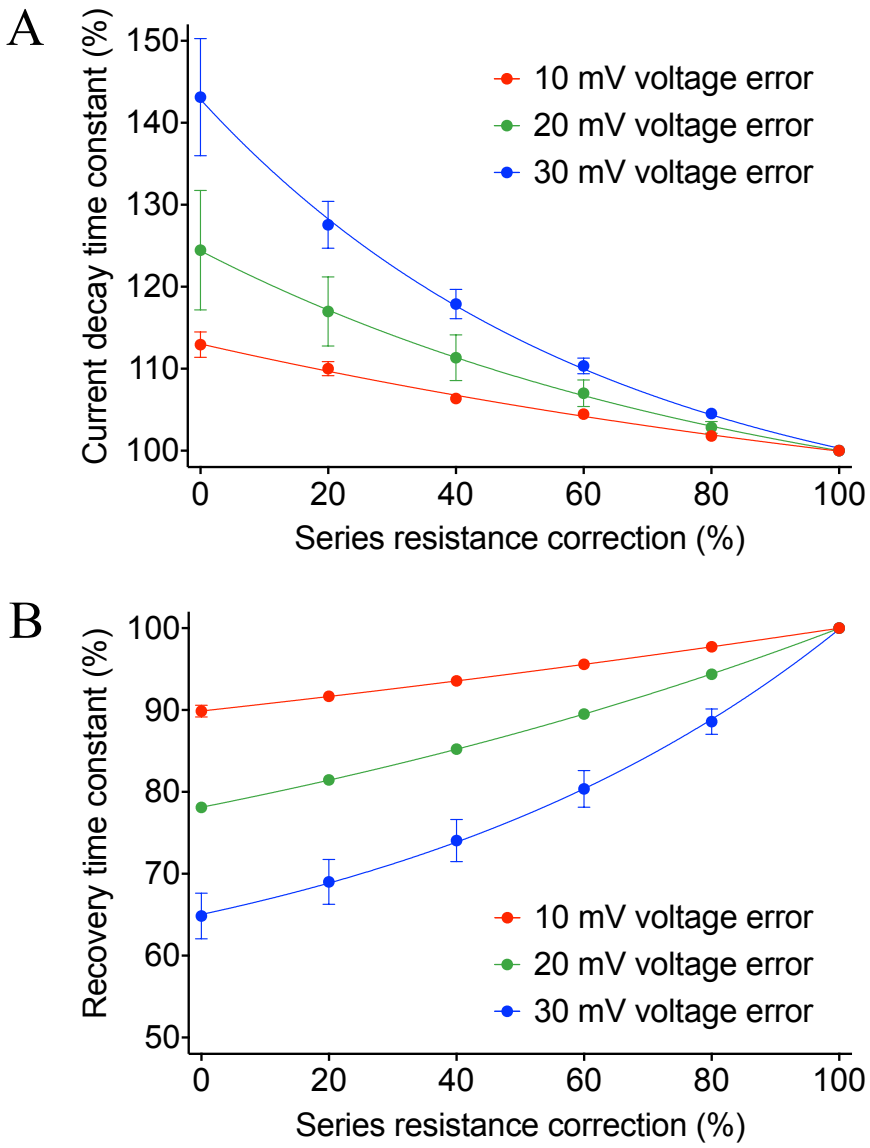


Figure 3-11 The impact of series resistance error on current decay and recovery time constants

Series resistance correction was applied to recordings from cells with 10 mV (n=3), 20 mV (n=3) or 30 mV (n=3) voltage error and a holding potential of –60 mV using the software-based algorithm as implemented in ChannelLab (Synaptosoft Inc.). Insufficient series resistance correction was associated with overestimation of current decay time constants (A) and underestimation of recovery time constants (B).

by SR compensation on most commercially available amplifiers. However, SR compensation is based on a positive feedback element that adds noise to the current signal and is prone to oscillations (i.e. ringing). Especially at high current amplitude recordings or in high SR patches these downside factors limit sufficient SR compensation. A software-based algorithm designed to operate on data that are already recorded has thus been proposed for SR correction in order to overcome these limitations (Traynelis, 1998).

3.4.4 Spatial aspects of voltage inhomogeneity

In voltage clamp experiments, insufficient SR compensation results in the failure to hold membrane potential constant. Such membrane potential changes distribute along the cytoplasm with the length constant according to Equation 3-8, and the fall of voltage from the pipette tip along the cell length is described by Equation 3-9.

When membrane resistance is large, the fall in voltage can be negligible in small cells. During the flow of large currents across the cell membrane, λ significantly decreases and the voltage at the cell edge is not the same as that at the pipette tip. Voltage inhomogeneity across the cytoplasm can be reduced by SR compensation and by choosing small and spherical cells with small currents for patch clamp experiments. Voltage error correction by the software-based algorithm as implemented in ChannelLab (Synaptosoft Inc.) does not account for intracellular voltage inhomogeneity. It is thus crucial to compare cells of similar shape and size when applying the software-based voltage correction method. In this thesis, cell size in different cell lines was analysed by the calculation of cell capacitance upon application of a 10 mV voltage step according to Equations 3-10, 3-11 and 3-12

$$\lambda = \sqrt{\frac{r_m}{r_i}}$$ Equation 3-8

λ: Length constant, *rm:* Membrane resistance, *ri*: Axial resistance of cytoplasm.

$$V(x) = V_0\ (e^{-x/\lambda})$$ Equation 3-9

V(x): Voltage at distance x from the pipette tip, V_0: Voltage at the pipette tip, *x*: Distance from the pipette tip.

$$R_S = V_{Step}/I_{Peak}$$ Equation 3-10

$$R_P = V_{Step}/I_{SS} - R_S$$ Equation 3-11

$$C_P = \tau\ (1/R_S + 1/R_P)$$ Equation 3-12

R_S: Series resistance, V_{Step}: Amplitude of the voltage step, I_{Peak}: Peak amplitude of the current transient upon application of the voltage step, R_P: Membrane resistance, I_{SS}: Steady-state current, C_P: Membrane capacitance, τ: Decay time constant of the current.

as outlined in (Gentet et al., 2000). Cell surface area was deduced from cell capacitance and the specific membrane capacitance that was shown to range from 0.9-1.0 μF/cm^2 (Sukhorukov et al., 1993; Gentet et al., 2000). In the experiments performed, cell capacitance was comparable between HEK293 cells expressing fetal and adult AChRs (25.7±3.1 pF in HEK293-γ [n=20] and 23.8±3.1 pF in HEK293-ε [n=20], ns) and between TE671 and CN21 cells (30.6±3.0 pF in TE671 [n=20] and 29.3±2.3 pF in CN21 [n=20], ns) (Figure 3-12).

3.5 Desensitisation is similar between fetal and adult AChRs

Desensitisation and recovery from desensitisation were compared between fetal and adult AChRs in a muscle and a non-muscle cell line in order to reveal cell-specific differences, potentially deriving from differences in posttranslational AChR modification or the interaction of AChRs with other proteins (Burden et al., 2018) in the two cell types. Current traces displayed a fast current rise, a peak and a current decay (Figure 3-1). Desensitisation was assessed by the calculation of current decay time constants during a 3 s pulse of 1 mM ACh, a period sufficient to enable almost complete desensitisation. Desensitised current fractions were 93.0±1.3% in TE671 cells (n=20), 93.1±1.8% in CN21 cells (n=20), 94.4±1.2% in HEK293-γ cells (n=30) and 93.0±1.4% in HEK293-ε cells (n=30) (Figure 3-13). Current decay time constants were not significantly different between fetal and adult AChRs in the muscle-cell line (407±62 ms in TE671 cells [n=20] and 299±52 ms in CN21 cells [n=20], ns) and in the non-muscle cell line (248±33 ms in HEK293-γ [n=30] and 240±31 ms in HEK293-ε cells [n=30], ns) (Figure 3-14). Current decay time constants were in general faster in the non-muscle cell line compared to the muscle

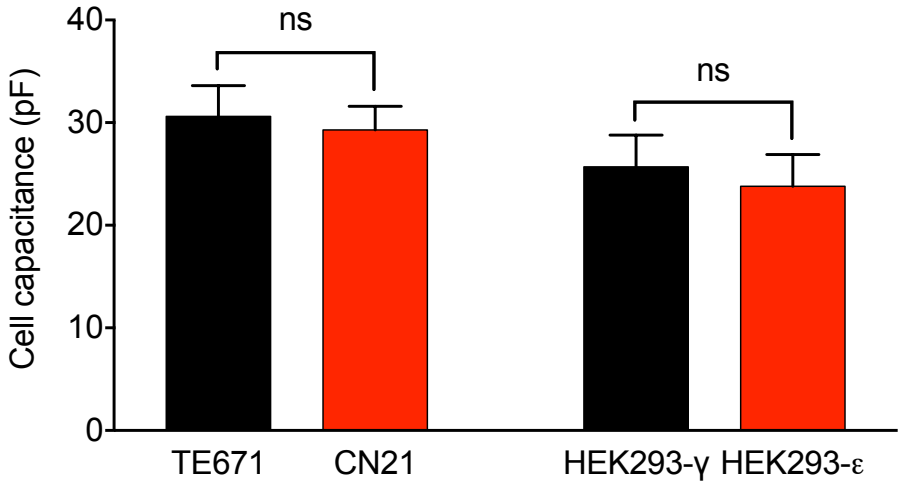


Figure 3-12 Comparison of cell capacitance as a proxy for the cell size in non-muscle and muscle cell lines expressing fetal and adult AChRs
In both the non-muscle and muscle cell lines, cell capacitance was comparable between cells expressing either fetal or adult AChRs. Unpaired t-test.

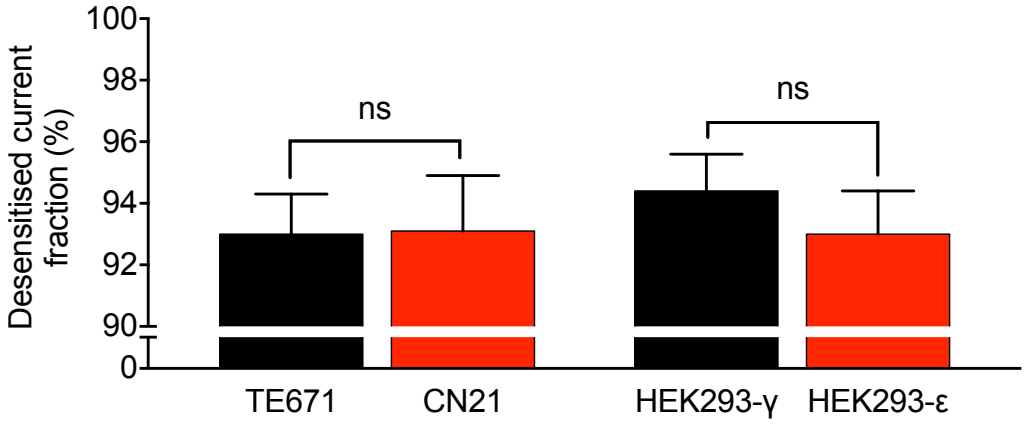


Figure 3-13 Desensitised current fractions in fetal and adult AChRs
Desensitisation was almost complete in both fetal and adult AChRs expressed in muscle and non-muscle cells after stimulation with 1 mM ACh for 3 s. Unpaired t-test.

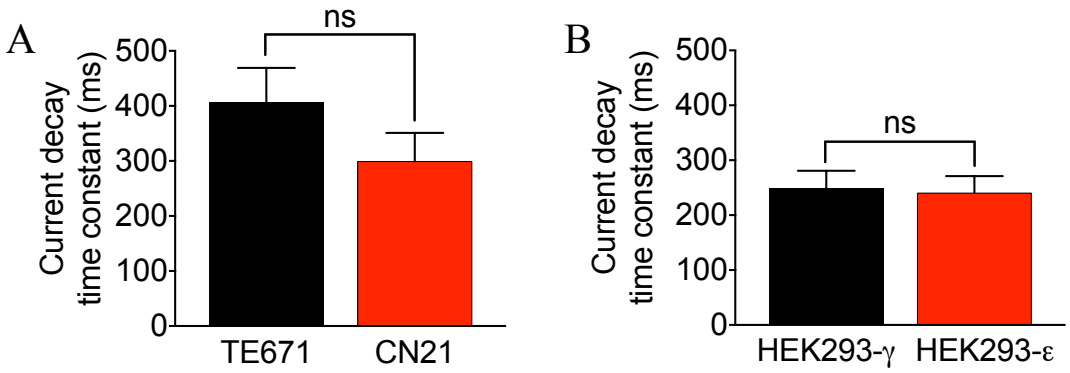


Figure 3-14 Current decay time constants in muscle and non-muscle cell lines

Current decay time constants were not different between fetal and adult AChRs expressed in a muscle (A) and a non-muscle cell line (B). Unpaired t-test.

cell line with a significant difference for the fetal AChR isoform (407±62 ms in TE671 cells [n=20] and 248±33 ms in HEK293-γ [n=30], p=0.0176). The difference of current decay time constants in adult AChRs between both cell lines was not significant.

3.6 Adult AChRs recover faster from desensitisation compared to fetal AChRs

Recovery from desensitisation was measured as the ratio between peak current amplitudes of the test and desensitising pulse in ten sweeps with increasing intervals ranging from 300 ms to 7 s, a period after which the majority of receptors had recovered from desensitisation (87.7±1.2% in TE671 [n=20], 93.4±0.7% in CN21 [n=20], 91.6±0.8 in HEK293-γ [n=30] and 93.1±0.7 in HEK293-ε [n=30]) (Figure 3-15). After an interval of 22 s, i.e. the end of each sweep, recovery from desensitisation was complete. Recovery ratio plots could be fitted best by a single exponential that resulted in shorter recovery time constants in adult compared to fetal AChRs in the muscle cell line (2297±197 ms in TE671 cells [n=20] and 1417±93 ms in CN21 cells [n=20], p=0.0003) and in the non-muscle cell line (2093±142 ms in HEK293-γ cells [n=30] and 1097±88 ms in HEK293-ε [n=30], p<0.0001) (Figure 3-16). Recovery time constants tended to be faster in the non-muscle cell line compared to the muscle cell line, with a significant difference for adult AChRs only (1417±93 ms in CN21 cells [n=20] and 1097±88 ms in HEK293-ε [n=30], p=0.0191).

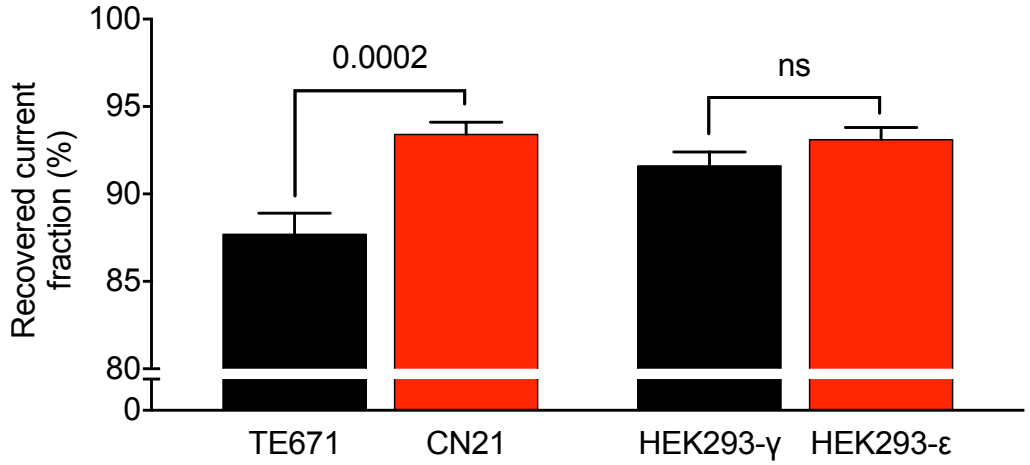


Figure 3-15 Recovered current fractions in fetal and adult AChRs
Current fractions were largely recovered at an interval of 7 s after stimulation with 1 mM ACh for 3 s. In the muscle cell line, current recovery was significantly larger in CN21 cells expressing adult AChRs, whereas in HEK293 cells the difference was not significant. Unpaired t-test.

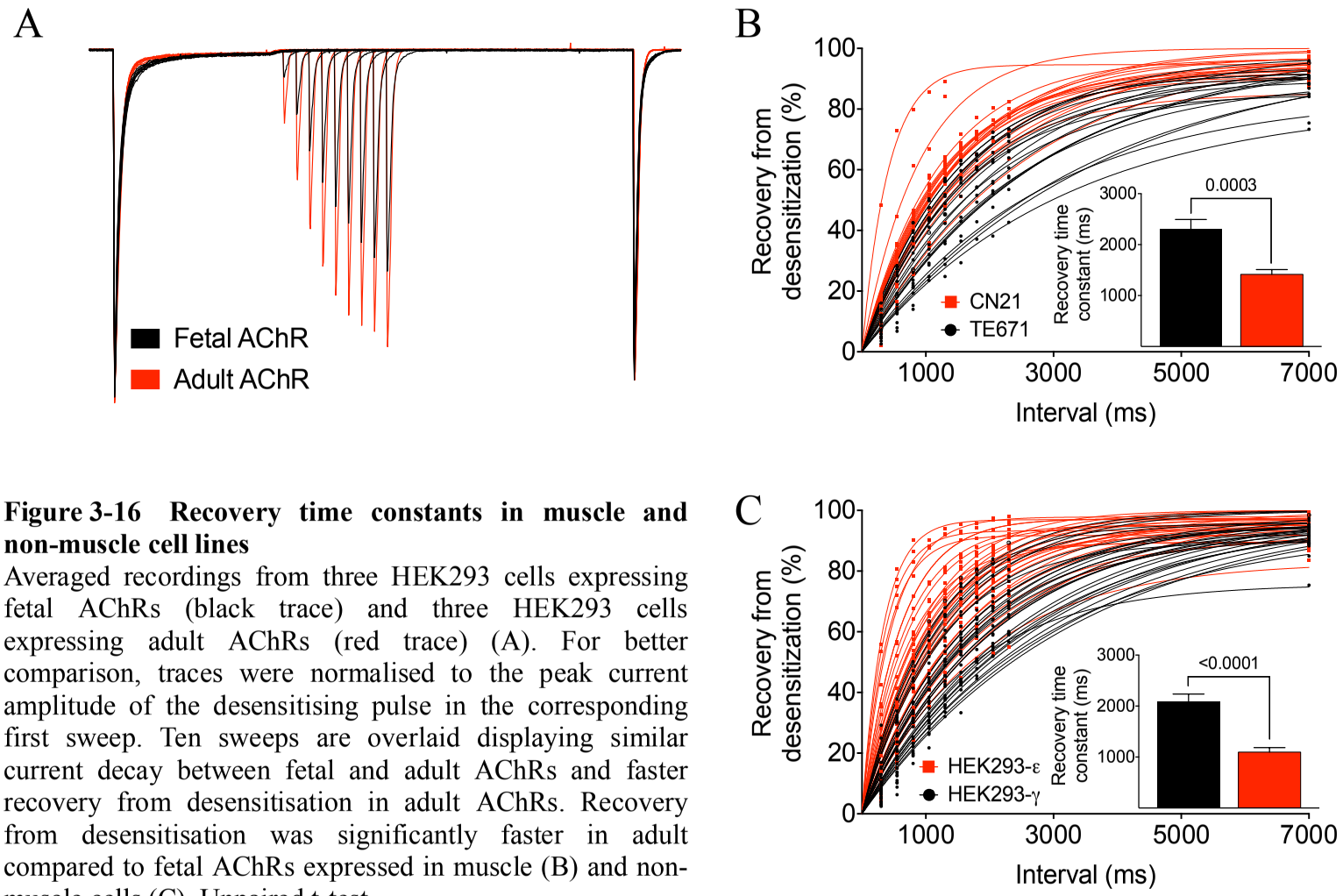


Figure 3-16 Recovery time constants in muscle and non-muscle cell lines

Averaged recordings from three HEK293 cells expressing fetal AChRs (black trace) and three HEK293 cells expressing adult AChRs (red trace) (A). For better comparison, traces were normalised to the peak current amplitude of the desensitising pulse in the corresponding first sweep. Ten sweeps are overlaid displaying similar current decay between fetal and adult AChRs and faster recovery from desensitisation in adult AChRs. Recovery from desensitisation was significantly faster in adult compared to fetal AChRs expressed in muscle (B) and non-muscle cells (C). Unpaired t-test.

3.7 Characterisation of electrophysiological differences between cell cultures thawed from different stocks of the same cell line

Peak current amplitudes and current decay as well as recovery time constants were compared between cell cultures thawed from different stocks of the same cell line in order to determine electrophysiological differences. Peak current amplitudes were similar between two stocks of TE671 cells (–1299±173 pA [n=10] and –1113±289 pA [n=10], ns, unpaired t-test), but differed significantly between two stocks of CN21 cells (–5006±980 pA [n=10] and –9703±1727 pA [n=10], p=0.0295, unpaired t-test), three stocks of HEK293-γ cells (one-way ANOVA: $F_{(2,27)}$=7.2, p=0.0032) and three stocks of HEK293-ε cells (one-way ANOVA: $F_{(2,27)}$=22.9, p<0.0001) (Figure 3-17A). Current decay time constants between different stocks of the same cell line also varied significantly (two-way ANOVA: $F_{(4,90)}$=27.0, p<0.0001) with no difference between fetal and adult AChRs (two-way ANOVA: $F_{(1,90)}$=1.6, ns) (Figure 3-17B). Recovery from desensitisation, by contrast, did not vary significantly between different stocks (two-way ANOVA: $F_{(4,90)}$=1.3, ns), but recovery time constants were consistently shorter in adult compared to fetal AChRs in each of the cell cultures thawed from a different stock (two-way ANOVA: $F_{(1,90)}$=49.3, p<0.0001) (Figure 3-17C).

3.8 Analysis of AChR desensitisation and recovery from desensitisation by the perforated patch method

In the whole-cell configuration there is an electrical and chemical pathway from the pipette to the interior of the cell with a very high volume ratio between both (~10 µl

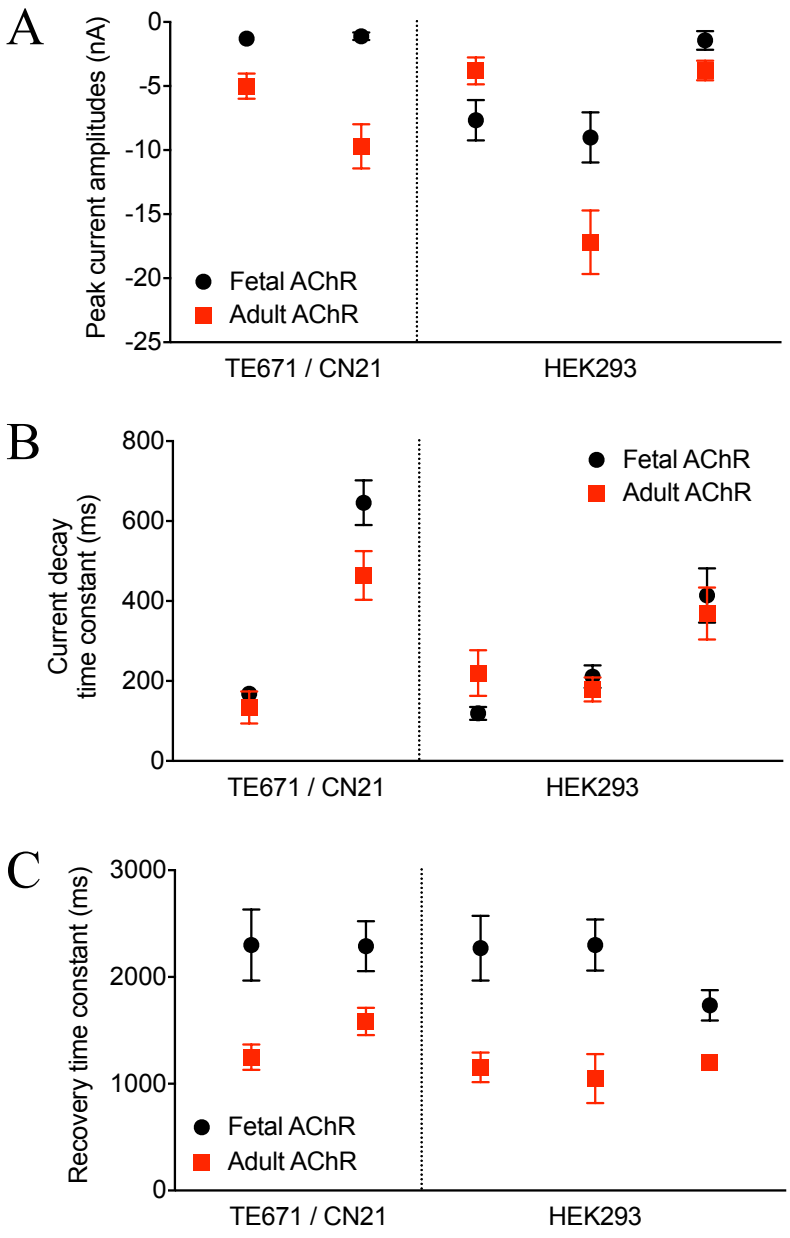


Figure 3-17 Electrophysiological differences between cell cultures thawed from different stocks of the same cell line

Peak current amplitudes and current decay time constants varied significantly between different stocks of the same cell line (A). Current decay time constants varied significantly between different cell cultures of the same cell line (B). Recovery from desensitisation was similar between different stocks and consistently faster in adult compared to fetal AChRs in each of the cell cultures thawed from a different stock (C).

pipette and ~1 pl cell). Thus, the pipette solution eventually dictates the concentration of all molecules and diffusible cellular compartments. The perforated patch configuration allows an electrical pathway from the pipette to the cell (permeable mainly for Na^+, K^+ and Cl^-) without a chemical connection. This ensures a more physiological intracellular environment that is not diluted by the pipette solution during the experiment.

The application of the perforated patch method on HEK293 cells expressing either fetal or adult AChRs revealed no difference in current decay time constants (373±174 ms in HEK293-γ cells [n=5] and 374±76 ms in HEK293-ε [n=5], ns), but consistent with experiments in the whole-cell configuration, recovery from desensitisation was significantly faster in adult AChRs (1314±358 ms in HEK293-γ cells [n=5] and 437±103 ms in HEK293-ε [n=5], p=0.0463) (Figure 3-18). Compared to experiments in the whole-cell configuration, recovery time constants were significantly shorter in the perforated patch method (1314±358 ms vs. 2093±142 ms for the fetal AChR isoform [p=0.0467] and 437±103 ms vs. 1097±88 ms for the adult AChR isoform [p=0.0054]). Current decay time constants were not significantly different between both methods.

3.9 The impact of the voltage error correction method on desensitisation and recovery measurements

Voltage errors deriving from insufficient SR compensation can alter current recordings and bias desensitisation and recovery from desensitisation as described above. Voltage error is usually corrected by SR compensation using a positive feedback element in most commercially available patch clamp amplifiers. This

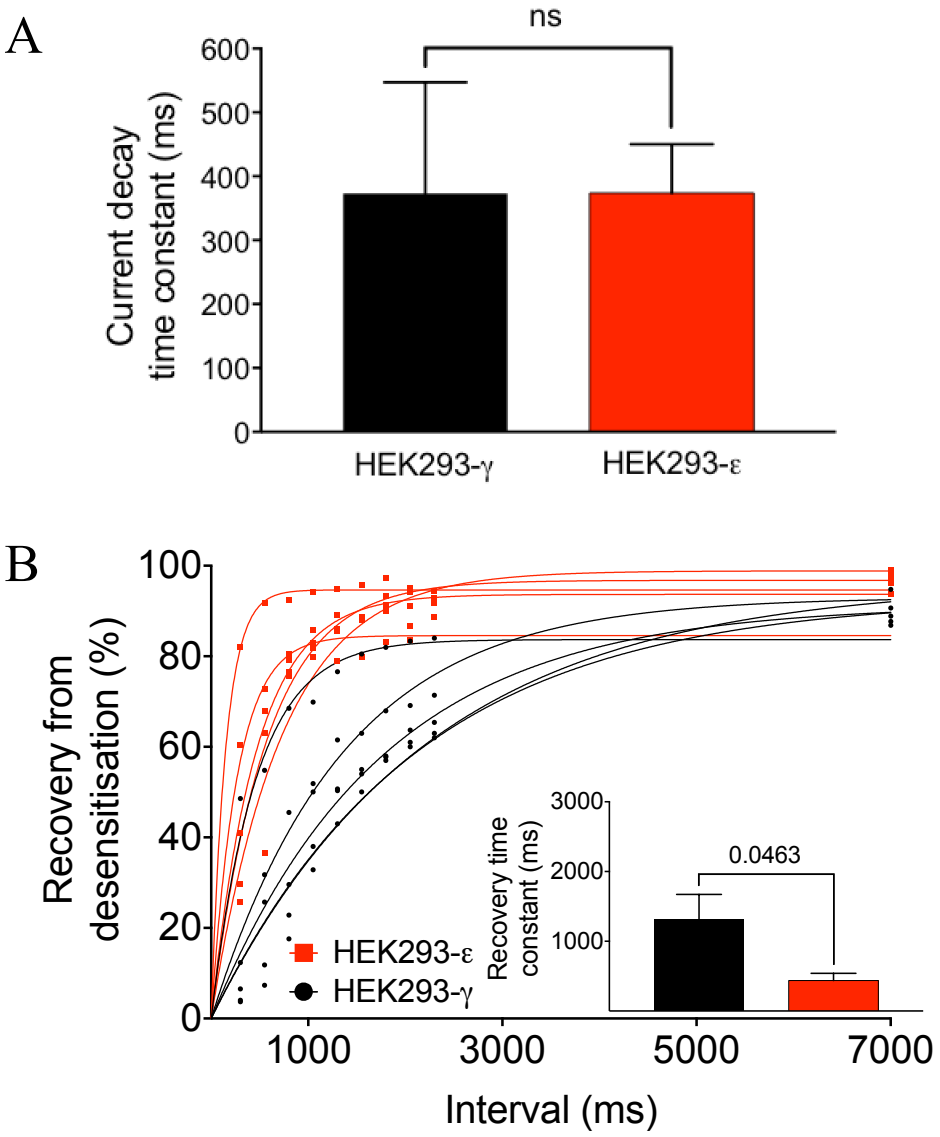


Figure 3-18 Current decay and recovery from desensitisation assessed in HEK293 cells by the perforated patch method

Current decay time constants were not different between fetal and adult AChRs (A), but recovery from desensitisation was faster in adult compared to fetal AChRs (B). Unpaired t-test.

element, however, adds noise to the current signal and is prone to oscillations especially in high current recordings and in high SR patches. Alternatively, a software-based algorithm can be operated on data that is already recorded to correct voltage error (Traynelis, 1998). The algorithm can also correct for capacitative filtering deriving from time-dependent capacitative currents that get induced by intracellular potential changes as a result of the voltage error.

To reveal any differential influence of the applied method on current recordings, desensitisation and recovery from desensitisation were assessed in HEK293-γ and HEK293-ε by the application of both voltage error correction methods in two different experiments. Current decay time constants were similar in fetal and adult AChRs using both methods (414±68 ms in HEK293-γ [n=10] and 369±65 ms in HEK293-ε [n=10] using SR compensation and 119±16 ms in HEK293-γ [n=10] and 220±57 ms in HEK293-ε [n=10] using the software based voltage error correction method) (Figure 3-19). Recovery time constants were faster in adult compared to fetal AChRs using both voltage error correction methods (2270±303 ms in HEK293-γ [n=10] and 1154±138 ms in HEK293-ε [n=10] using SR compensation and 2299±239 ms in HEK293-γ [n=10] and 1049±229 ms in HEK293-ε [n=10] using software based voltage error correction) (Figure 3-20).

3.10 The impact of the fetal and adult AChR isoform specific M3-M4 cytoplasmic loop on desensitisation and recovery from desensitisation

The M3-M4 cytoplasmic loops of various AChR subunits were shown to play an important role for desensitisation and recovery from desensitisation (Huganir et al., 1986; Middleton et al., 1986; Hopfield et al., 1988; Paradiso and Brehm, 1998).

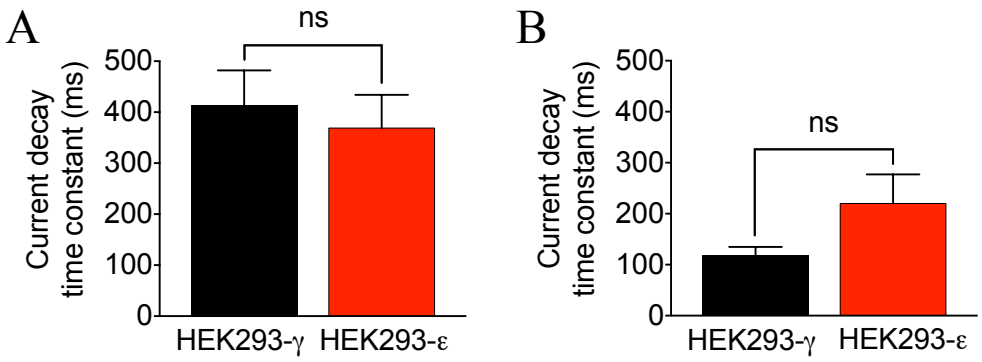


Figure 3-19 Current decay time constants in fetal and adult AChRs after voltage error correction by hardware and software based methods
The application of both voltage error correction methods resulted in comparable current decay time constants between fetal and adult AChRs expressed in HEK293 cells. Current decay was measured after series resistance compensation in (A). The mean voltage error was 10.7±2.0 mV, n=10 (according to a mean series resistance of 3.0±0.3 MΩ and a mean peak current amplitude of –3524±734 pA). Mean series resistance compensation was 88% resulting in a residual mean voltage error of 1.3±0.3 mV. Current decay was measured without series resistance compensation but voltage error correction using a computational algorithm as implemented in ChannelLab (Synaptosoft Inc.) in (B). The mean voltage error was 14.1±3.0 mV, n=10 (according to a mean series resistance of 5.4±0.6 MΩ and a mean peak current of –2600±595 pA). Voltage error was corrected for 100% using ChannelLab. Both methods revealed no significant difference of current decay time constants between fetal and adult AChRs. Current decay time constants, however, were shorter using ChannelLab, but cells used in both experiments derived from different cell cultures (thawed from different stocks). A direct comparison, therefore, might be limited because current decay time constants varied significantly between cell cultures (see Chapter 3.7). Unpaired t-test.

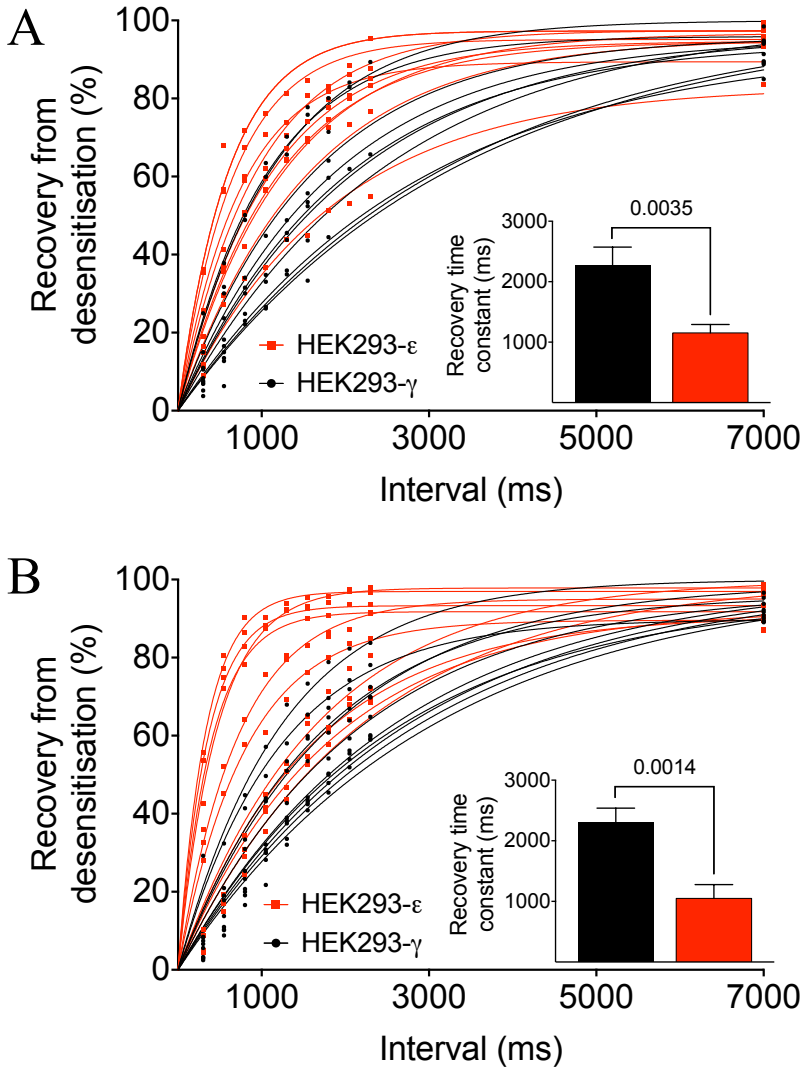


Figure 3-20 Recovery time constants in fetal and adult AChRs after voltage error correction by hardware and software based methods
Current decay and recovery from desensitisation was analysed from the same recordings. The application of both voltage error correction methods revealed shorter recovery time constants in adult compared to fetal AChRs. Recovery from desensitisation was measured after series resistance compensation in (A), and after voltage error correction using a computational algorithm as implemented in ChannelLab (Synaptosoft Inc.) in (B). For mean voltage errors see Figure 3-19. Unpaired t-test.

Differences in recovery from desensitisation between the fetal and adult AChR isoform as observed in this thesis could have been determined by the respective M3-M4 cytoplasmic loops of the γ- and ε-subunit. To address this question, chimeric AChRs with exchanged M3-M4 cytoplasmic loops between the γ- and ε-subunit were constructed and tested by whole-cell patch clamp experiments. As outlined in detail in the following section, this was achieved by cloning different restriction sites at both ends of the M3-M4 loops in the respective plasmids containing γ- and ε-subunit cDNA. After digestion and separation by electrophoresis, the γ-M3-M4 loop cDNA (γ-insert) was ligated into the ε-construct and the ε-M3-M4 loop cDNA (ε-insert) was ligated into the γ-construct. Finally, the restriction sites were back-mutated again.

3.10.1 Construction of plasmids containing cDNA of chimeric γ- and ε-subunits with exchanged M3-M4 loops

The plasmids pcDNA3.1-γ (γ-subunit cDNA cloned into pcDNA3.1-hygro) and pcDNA3.1-ε (ε-subunit cDNA cloned into pcDNA3.1-hygro) do not contain *BsrG*I and *Age*I restriction sites, which was confirmed by agarose gel electrophoresis (Figure 3-21). In order to exchange the M3-M4 loops between the γ- and ε-subunit, restriction sites had to be cloned into the 5'- and 3'-end of the γ- and ε-M3-M4 loop cDNA, respectively. A *BsrG*I restriction site was cloned into the 5'-end of both the γ- and ε-M3-M4 loop cDNA, and an *Age*I restriction site was cloned into the 3'-end of both the γ- and ε-M3-M4 loop cDNA region (Figure 3-22). Cloning was performed using the QuickChange multi site-directed mutagenesis kit (Agilent Technologies) following the manufacturer's protocol. This system allows

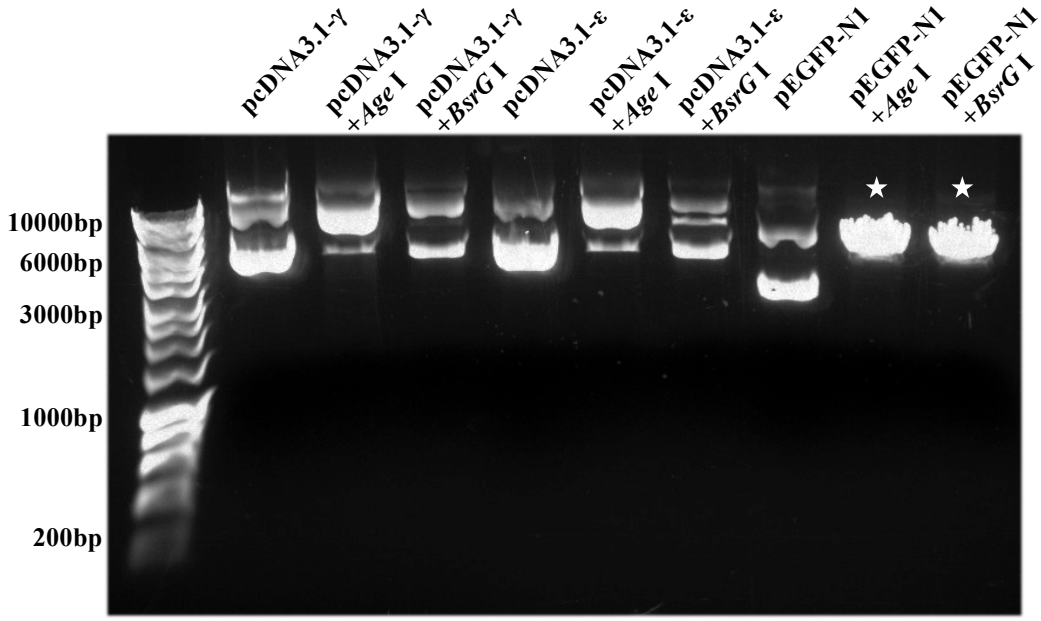


Figure 3-21 Screening for *Age*I and *BsrG*I restriction sites in pcDNA3.1-γ and pcDNA3.1-ε

The digestion of plasmids by the restriction endonucleases *Age*I and *BsrG*I was performed following the manufacturer's protocol. The plasmids pcDNA3.1-γ and pcDNA3.1-ε were left untreated or were treated with *Age*I or *BsrG*I. The plasmid pEGFP-N1 was used as a positive control due to its known restriction sites for both *Age*I and *BsrG*I, and was also used untreated or treated with *Age*I or *BsrG*I. All plasmids were resolved in 0.7% agarose gel to check for a single band product. Multiple bands of pcDNA3.1-γ and pcDNA3.1-ε could be detected for each treatment group, and for untreated pEGFP-N1, suggesting the presence of covalently closed circular or open-circular plasmid DNA (Aaij & Borst, 1972; Meyers et al., 1976) and, thus, the lack of restriction endonuclease digestion. A single lane of pEGFP-N1 was only detected after treatment with *Age*I or *BsrG*I, indicating the digestion of pEGFP-N1 by *Age*I and *BsrG*I, as expected, into linearised DNA (white stars).

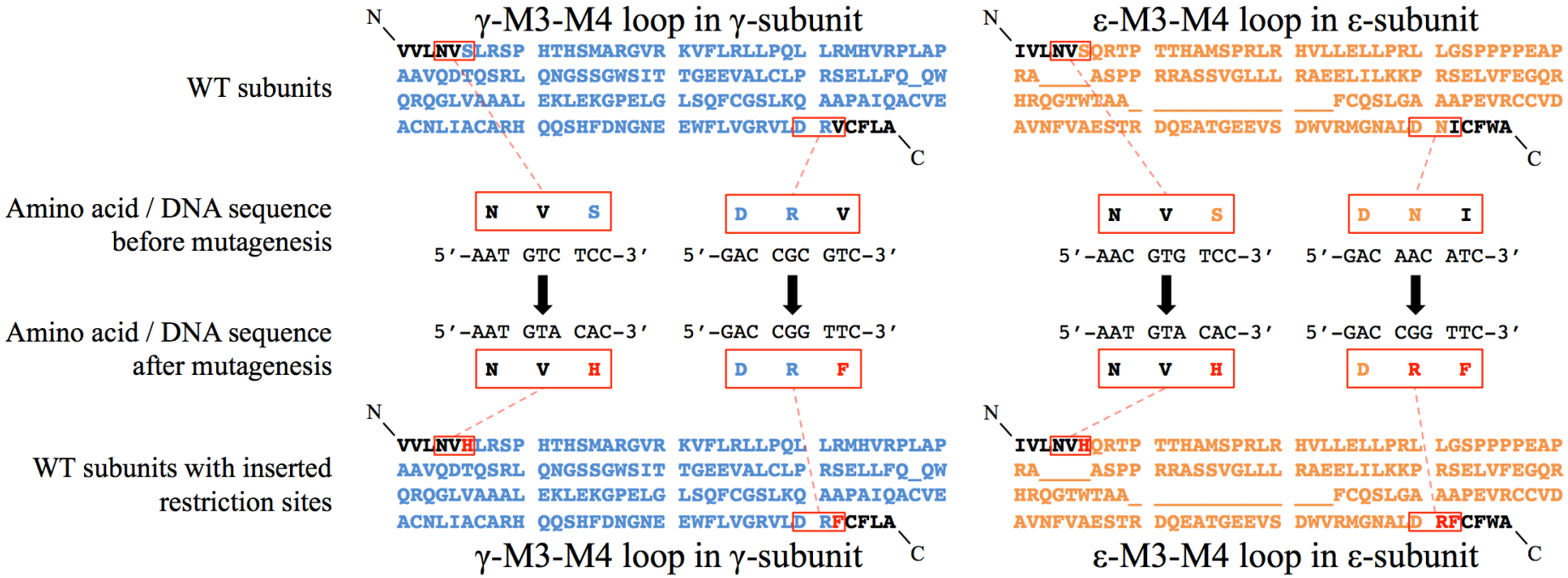


Figure 3-22 Cloning of restriction sites into the 5'- and 3'-end of the γ- and ε-M3-M4 loop cDNA region
Restriction sites had to be cloned into the 5'- and 3'-end of the γ- (blue) and ε-M3-M4 loop cDNA (orange) region, respectively, in order to cut and exchange the M3-M4 loop cDNA regions between CHRNG and CHRNE.

mutagenesis at multiple sites in a single thermal cycling reaction with *PfuTurbo* DNA polymerase and generates plasmid DNA with one strand containing the mutation. Specifically designed primers were used for each mutation (synthesised by Invitrogen), harbouring the mutation centrally within the primer (Table 3-2). Subsequently, the thermal cycling reaction products were treated with the restriction endonuclease *Dpn*I, which is specific for methylated and hemimethylated DNA and thus digested the parental DNA template only. This was due to the use of dam^+ *E. coli* strains for the generation of the parental template plasmids, causing the templates to become methylated and susceptible to *Dpn*I digestion. The *Dpn*I–treated DNA was then transformed in 10-beta *E. coli* competent cells, and the transformed cells cultured in LB-agar containing appropriate selection antibiotics. Plasmid DNA was extracted from bacterial cultures and purified using the QIAprep spin miniprep kit (Qiagen) following the manufacturer's protocol. The insertion of the restriction sites into pcDNA3.1-γ and pcDNA3.1-ε was confirmed by agarose gel electrophoresis after treatment with the restriction endonucleases *BsrG*I and *Age*I (Figure 3-23), and also by sequencing. After digestion and electrophoresis, the separated PCR products were excised from the agarose gel and purified using the QIAquick gel extraction kit (Qiagen) following the manufacturer's protocol. The γ-M3-M4 loop cDNA (γ-insert) was then ligated into the ε-construct and the ε-M3-M4 loop cDNA (ε-insert) was ligated into the γ-construct (Figure 3-24), with following confirmation by sequencing. Finally, the restriction sites were mutated back to the wild-type sequence in chimeric CHRNG and CHRNE using the QuickChange multi site-directed mutagenesis kit (Agilent Technologies) and specifically designed primers (Invitrogen) harbouring the wild-type sequence centrally (Table 3-3 and

Figure 3-25). The exchange of the M3-M4 loop cDNA regions between CHRNG and CHRNE and the back-mutation of the *BsrG*I and *Age*I restriction sites were confirmed by gene sequencing (Table 3-4, Figure 3-26, 3-27 and 3-28).

Table 3-2 Sequences of primers used for cloning of *BsrG*I and *Age*I restriction sites into CHRNG and CHRNE cDNA

Primer	Mutation	Primer sequence (5' to 3')
CHRNG_5'	c.987_989delinsACA	TGTGGTTGTGCTCAATGTACACT TGCGGTCTCCACAC
CHRNG_3'	c.1422_1423delinsGT	GGGCCGAGTGCTGGACCGGTTC TGCTTCCTGGCCATG
CHRNE_5'	c.981C>T c.984_986delinsACA	GCGTCATCGTGCTCAATGTACA CCAGCGGACGCCCAC
CHRNE_3'	c.1366_1369delinsCGGT	TGGGGAATGCCCTTGACCGGTT CTGCTTCTGGGCCGC

Primers CHRNG_5' and CHRNE_5' bind at the 5'-end of the γ- and ε-M3-M4 loop cDNA, respectively, and contain the *BsrG*I restriction site (red). Primers CHRNG_3' and CHRNE_3' bind at the 3'-end of the γ- and ε-M3-M4 loop cDNA region, respectively, and contain the *Age*I restriction site (blue). The mutated nucleotides are highlighted in yellow.

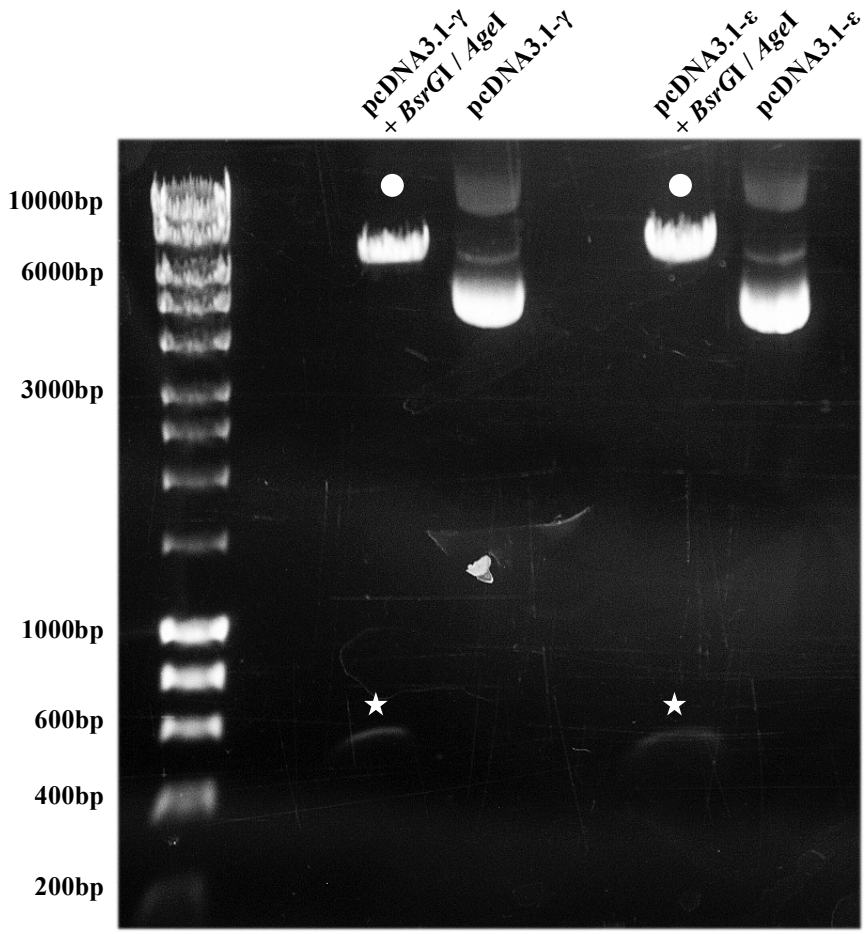


Figure 3-23 Screening for *Age*I and *BsrG*I restriction sites in pcDNA3.1-γ and pcDNA3.1-ε after mutagenesis

After mutagenesis, the PCR products were resolved in 0.7% agarose gel and separated by electrophoresis. Two bands could be detected after digestion of pcDNA3.1-γ and pcDNA3.1-ε with *BsrG*I and *Age*I, suggesting the successful insertion of the restriction sites into CHRNG and CHRNE. After digestion with *BsrG*I and *Age*I, the length of pcDNA3.1-γ (i.e. γ-construct) and pcDNA3.1-ε (i.e. ε-construct) was calculated to be ~6.6 kb (white circles). The length of the γ-M3-M4 loop cDNA (i.e. γ-insert) and ε-M3-M4 loop cDNA (i.e. ε-insert) (white stars) was calculated to be 145 amino acids/435bp and 128 amino acids/384bp, respectively.

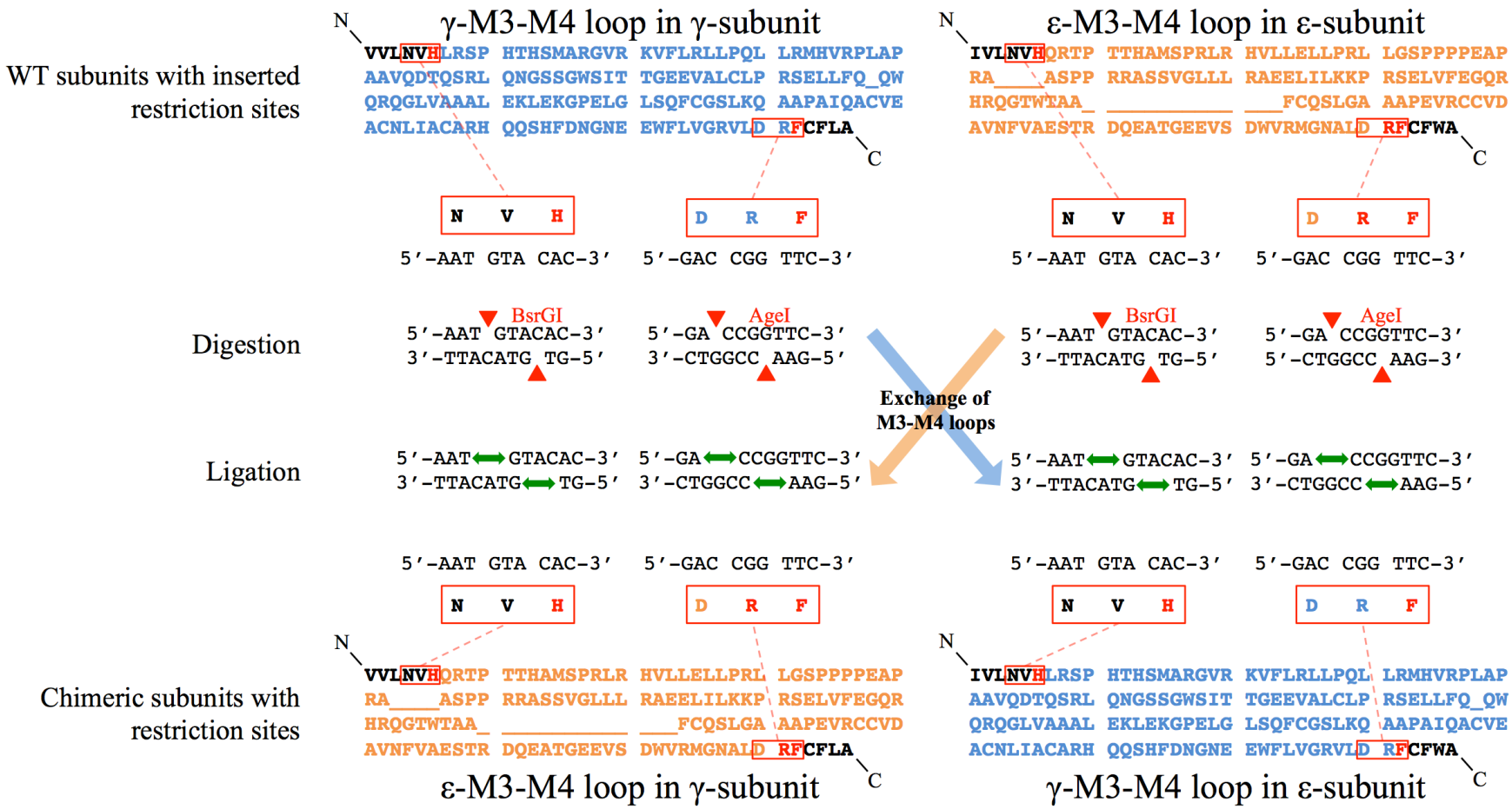


Figure 3-24 Exchange of the M3-M4 loops between CHRNG and CHRNE
After digestion and electrophoresis, the γ-M3-M4 loop cDNA (γ-insert, blue) was inserted into the ε-construct and the ε-M3-M4 loop cDNA (ε-insert, orange) was ligated into the γ-construct.

Table 3-3 Sequences of primers used for back-mutation of the *BsrG*I and *Age*I restriction sites into the wild-type sequence in CHRNG and CHRNE cDNA

Primer	Primer sequence (5' to 3')
CHRNE_5'_WT	CTGTGGTTGTGCTCAATGTCTCCCAGCGGACGCCCAC
CHRNE_3'_WT	GGGAATGCCCTTGACAACGTCTGCTTCCTGGCCATGC
CHRNG_5'_WT	TGCGTCATCGTGCTCAACGTGTCCTTGCGGTCTCCAC
CHRNG_3'_WT	GGCCGAGTGCTGGACCGCATCTGCTTCTGGGCCGCTC

Primers CHRNE_5'_WT and CHRNG_5'_WT bind at the 5'-end of the ε-M3-M4 loop cDNA (in the γ-construct) and γ-M3-M4 loop cDNA (in the ε-construct), respectively, and contain the wild-type sequence (red). Primers CHRNE_3'_WT and CHRNG_3'_WT bind at the 3'-end of the ε-M3-M4 loop cDNA (in the γ-construct) and γ-M3-M4 loop cDNA (in the ε-construct), respectively, and also contain the wild-type sequence (blue). The mutated nucleotides are highlighted in yellow.

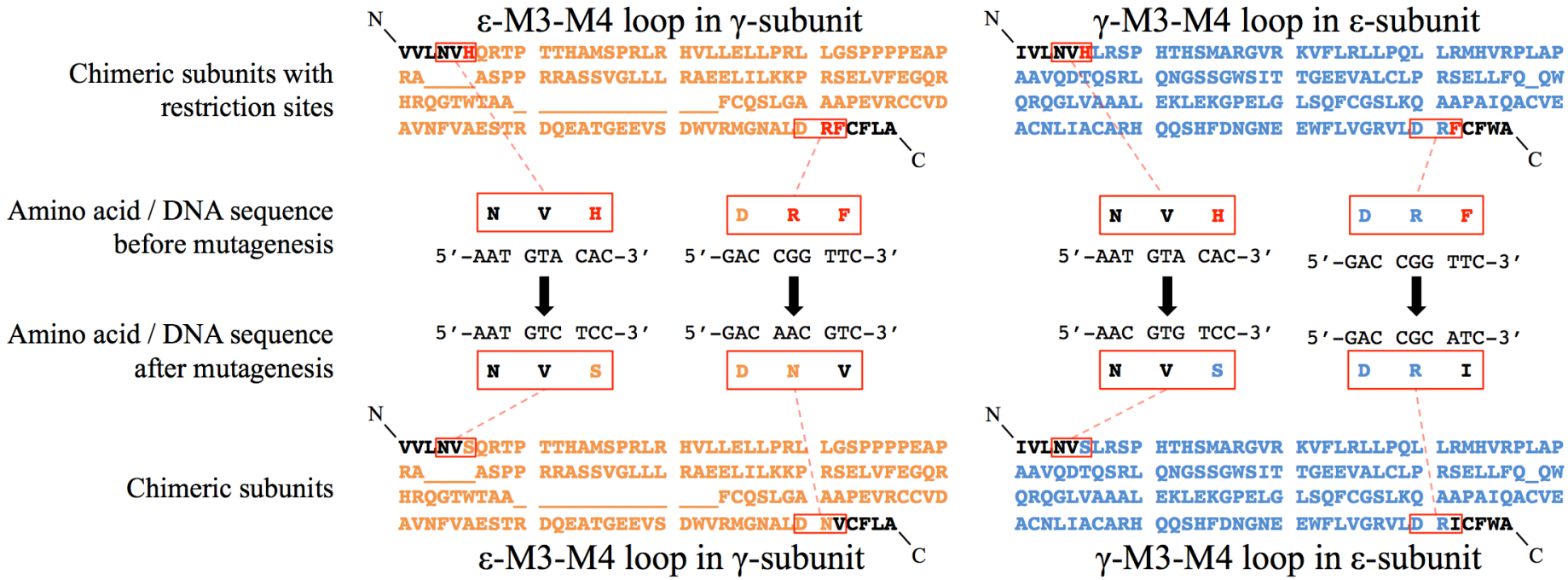


Figure 3-25 Back-mutation of the *BsrG*I and *Age*I restriction sites in chimeric CHRNG and CHRNE with exchanged M3-M4 loop cDNA

After back-mutation of the *BsrG*I and *Age*I restriction sites, the chimeric CHRNG contained the ε-M3-M4 loop cDNA and the chimeric CHRNE contained the γ-M3-M4 loop cDNA. On translational level, this resulted in a chimeric γ-subunit with the ε-M3-M4-loop (orange) and a chimeric ε-subunit with the γ-M3-M4-loop (blue).

Table 3-4 Sequencing primers used to confirm the exchange of the M3-M4 loops between the γ- and ε-subunit

Primer	Primer sequence (5' to 3')
CHRNG_Exon7	GTCGCCATCCTCATCCACTTCC
CHRNE_Exon8	GTCTCCATCAACGTCCTGCTCG

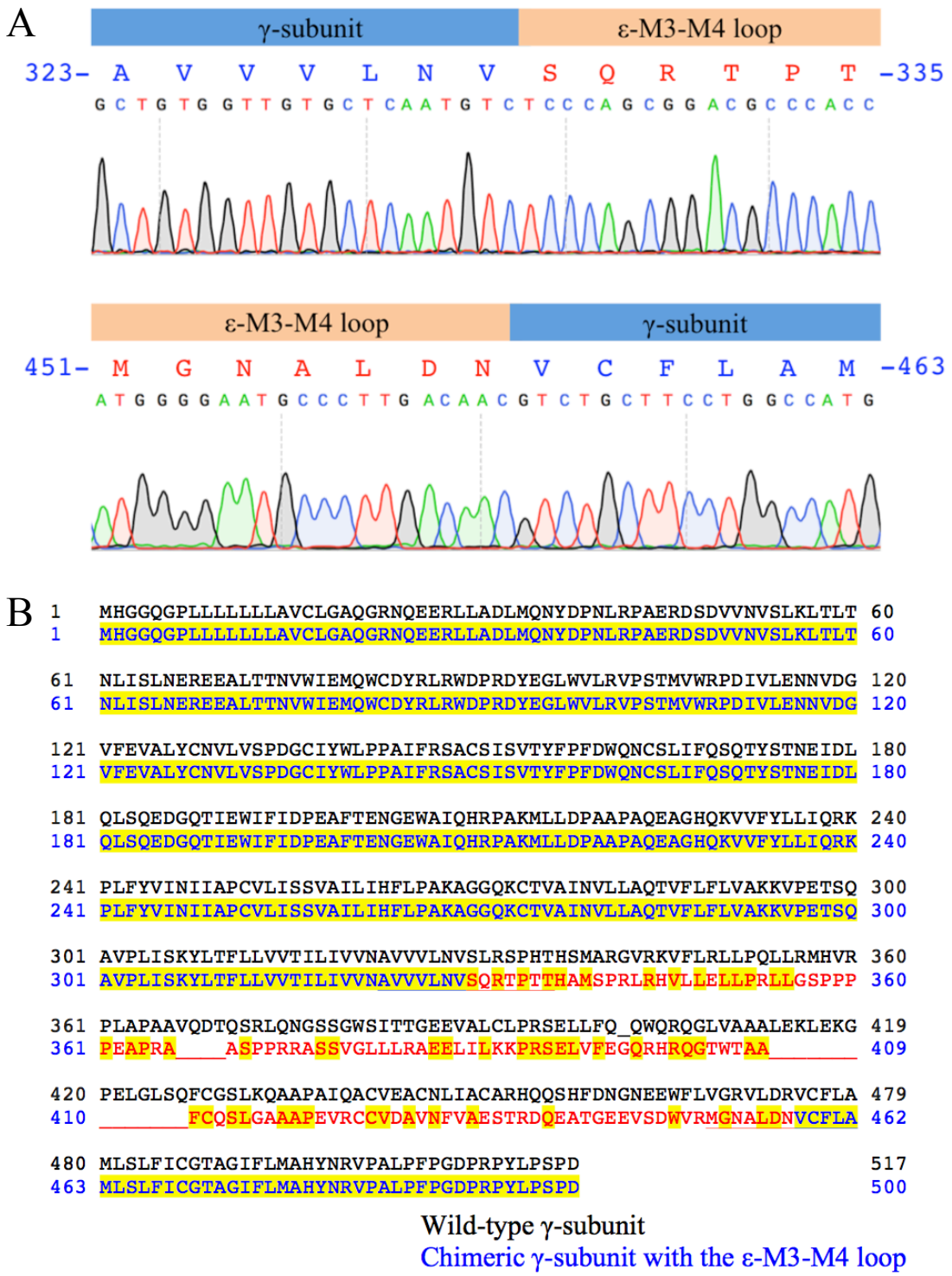


Figure 3-26 Sequence of the chimeric γ-subunit with the ε-M3-M4 loop
(A) The insertion of the ε-M3-M4 loop into the γ-subunit was confirmed by sequencing. (B) Amino acid sequence of the wild type (black) and chimeric γ-subunit (blue) with the inserted ε-M3-M4 loop (red). The conserved amino acids between both forms are highlighted in yellow. The underlined amino acid sequences correspond to the sequences in (A).

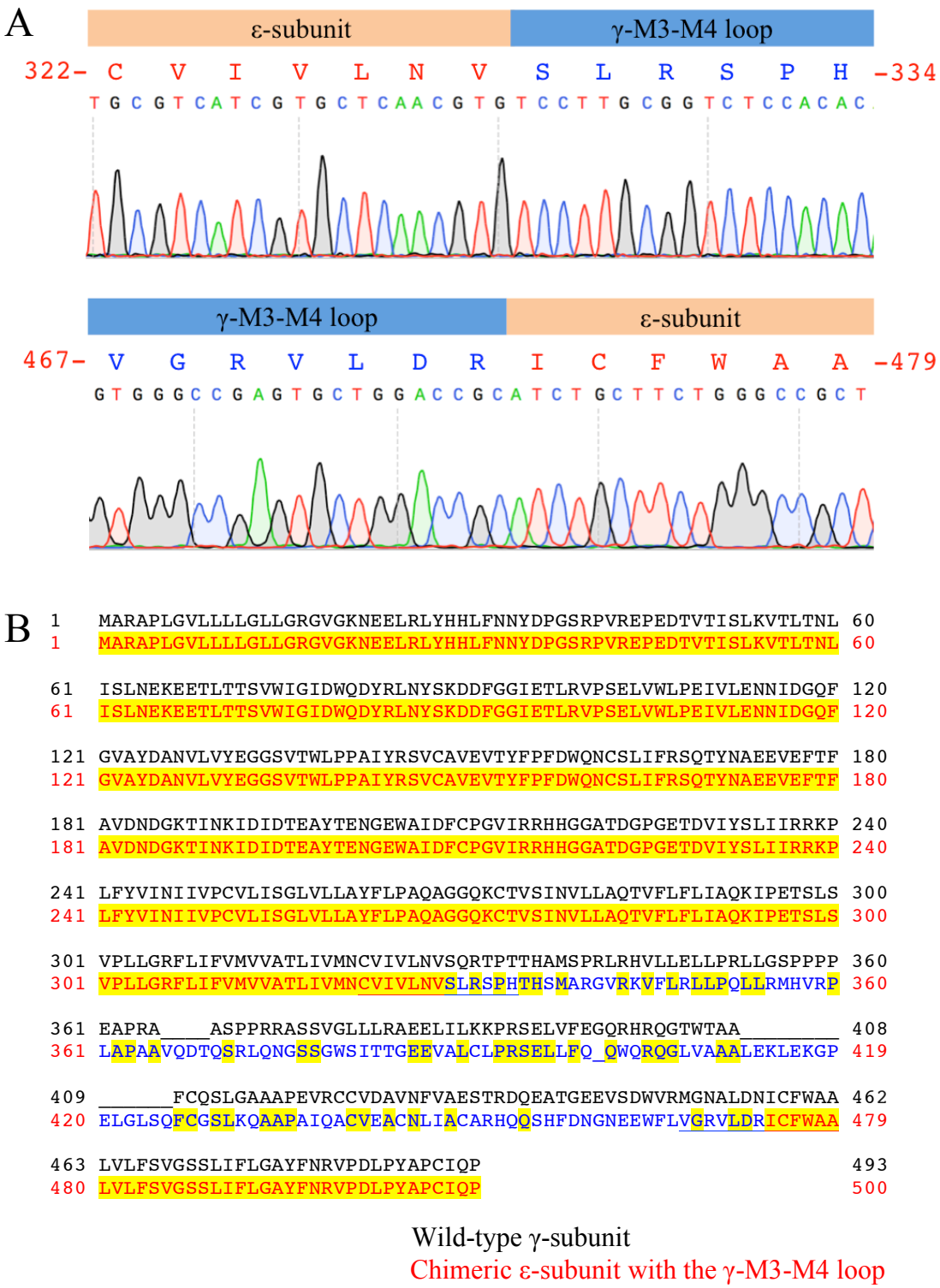


Figure 3-27 Sequence of the chimeric ε-subunit with the γ-M3-M4 loop
(A) The insertion of the γ-M3-M4 loop into the ε-subunit was confirmed by sequencing. (B) Amino acid sequence of the wild type (black) and chimeric ε-subunit (red) with the inserted γ-M3-M4 loop (blue). The conserved amino acids between both forms are highlighted in yellow. The underlined amino acid sequences correspond to the sequences in (A).

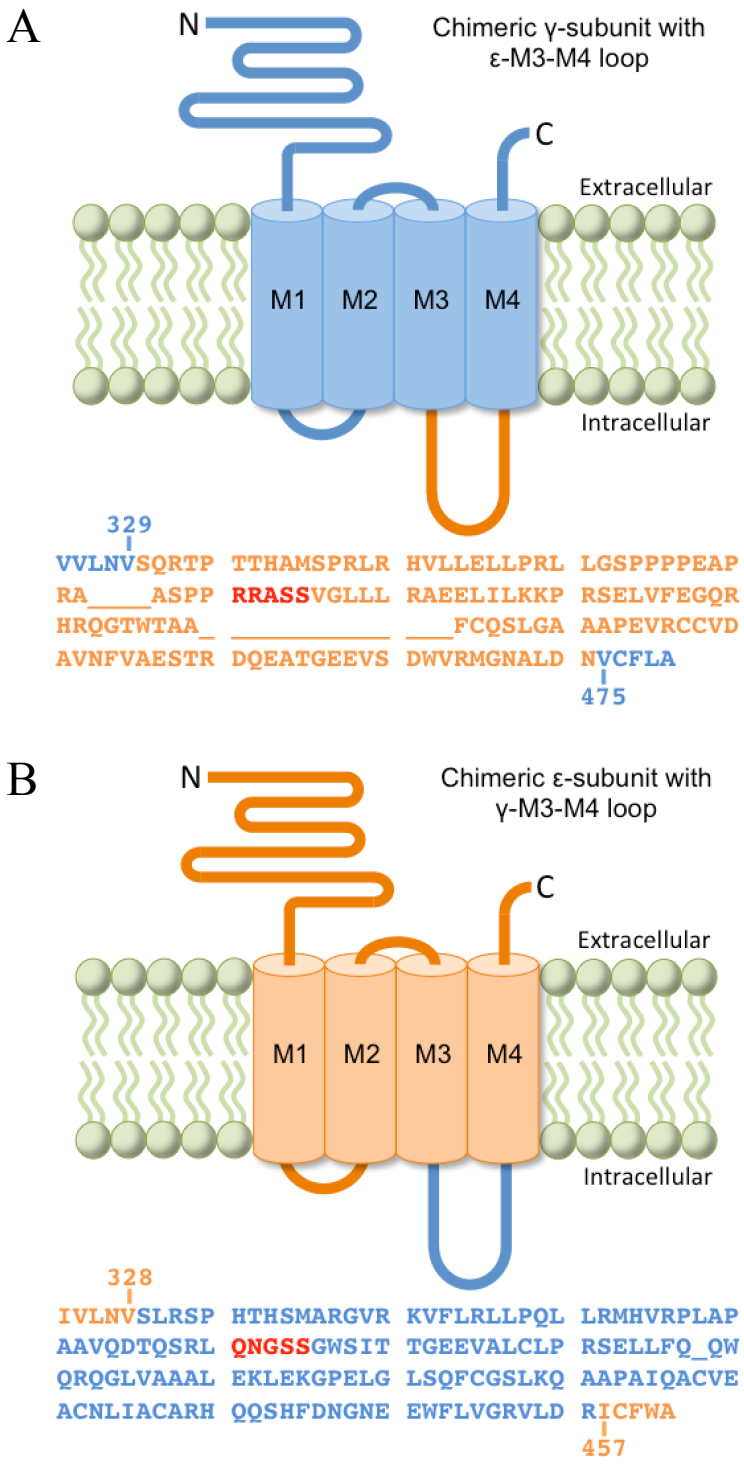


Figure 3-28 Chimeric AChRs with exchanged M3-M4 cytoplasmic loops between the γ- and ε-subunit
Chimeric γ-subunit (blue) with the ε-M3-M4 cytoplasmic loop (orange) (A) and chimeric ε-subunit (orange) with the γ-M3-M4 cytoplasmic loop (blue) (B). A consensus sequence for phosphorylation by protein kinase A is only present in the adult M3-M4 loop (RRXSX, where X is any amino acid, red).

3.10.2 Recovery kinetics is determined by the AChR isoform specific cytoplasmic M3-M4 loop

The cytoplasmic loop between the M3 and M4 transmembrane segment of the γ- and ε-subunit (differing at 94/146 positions) could have contributed to the reported difference in recovery kinetics between the fetal and adult AChR isoform. As outlined in detail above, this question was addressed by whole-cell patch clamp experiments performed on HEK293 cells transfected with chimeric fetal (chimeric-γ) or chimeric adult AChRs (chimeric-ε). Current decay time constants were not different between the two chimeric receptors (265±72 ms in the chimeric-γ [n=10] and 237±23 ms in the chimeric-ε AChR [n=10], ns) (Figure 3-29A), but recovery from desensitisation was faster in chimeric-γ AChRs with the ε-M3-M4 cytoplasmic loop compared to chimeric-ε AChRs with the γ-M3-M4 loop (recovery time constant of 1419±174 ms in the chimeric-γ [n=10] and 2022±188 ms in the chimeric-ε AChR [n=10], p=0.0301) (figure 3-29B). It was concluded that the ε-M3-M4 loop transferred fast recovery to the fetal AChR and the γ-M3-M4 loop transferred slow recovery to the adult AChR.

3.11 Salbutamol facilitates recovery from desensitisation in the adult but not fetal AChR isoform

Differential modifications of the M3-M4 loop in fetal and adult AChRs by intracellular factors could have contributed to faster recovery kinetics observed in the adult AChR isoform. As one of those potential intracellular factors, protein kinase A (PKA) was shown to alter AChR desensitisation and recovery from desensitisation

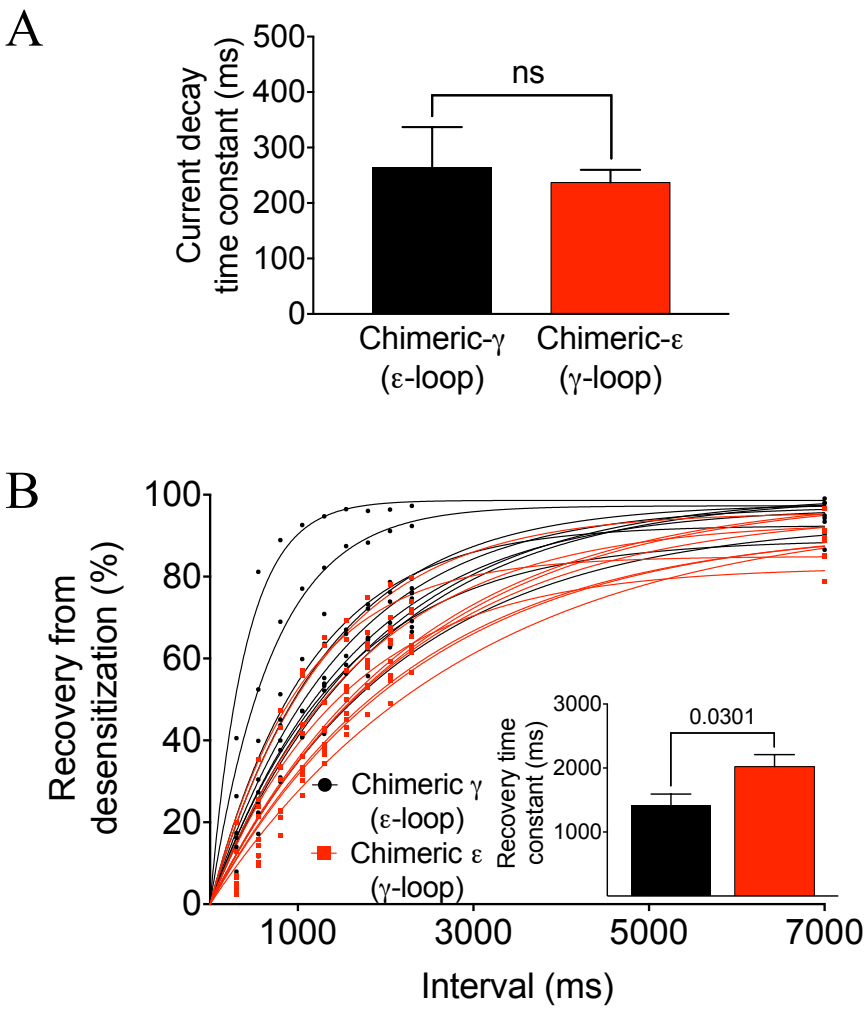


Figure 3-29 Desensitisation and recovery from desensitisation in chimeric AChRs with exchanged M3-M4 cytoplasmic loops between the γ- and ε-subunit

Current decay time constants were not different between chimeric-γ and chimeric-ε AChRs (A), but recovery from desensitisation was faster in adult compared to fetal AChRs (B). Unpaired t-test.

by phosphorylation of consensus sequences within the M3-M4 loop of various AChR subunits (Huganir et al., 1986; Hoffman et al., 1994; Paradiso and Brehm, 1998). In human AChRs, a PKA consensus sequence is present in the M3-M4 loop of the ε-subunit only without any corresponding sequence in the γ-subunit (residues 370-374 in the ε-subunit, i.e. RRASS) (Figure 3-28A). Salbutamol is a β_2-agonist that acts through the G-protein second messenger pathway inducing an increase in intracellular cAMP and, subsequently, activating PKA (Lynch and Ryall, 2008). It was found to have a beneficial effect in CMS patients (Burke et al., 2013; Rodriguez Cruz et al., 2015b), although the underlying mechanism is poorly understood. The effect of salbutamol on desensitisation and recovery from desensitisation in fetal and adult AChRs was examined in order to understand the underlying mechanism better.

Whole-cell patch clamp experiments were performed on TE671/CN21 cells after incubation in growth medium containing 1 μM salbutamol for at least 30 min. This corresponded to an approximately 10x higher concentration compared to serum levels usually obtained after oral administration of salbutamol in patients ranging around 15 ng/ml (Kurosawa et al., 1993). There was no effect on desensitisation in either TE671 cells (mean weighted current decay time constant of 473±62 ms without salbutamol [n=8] and 479±107 ms with salbutamol [n=8], ns) or CN21 cells (mean weighted current decay time constant of 429±55 ms without salbutamol [n=8] and 505±140 ms with salbutamol [n=8], ns) (Figure 3-30A, B). Recovery from desensitisation, however, was faster in CN21 cells after salbutamol exposure (mean recovery time constant of 1616±67 ms without salbutamol [n=8] and 1336±46 ms with salbutamol [n=8], p=0.0038), but there was no effect in TE671 cells (mean recovery time constant of 2064±81 ms without salbutamol [n=8] and 2353±332 ms

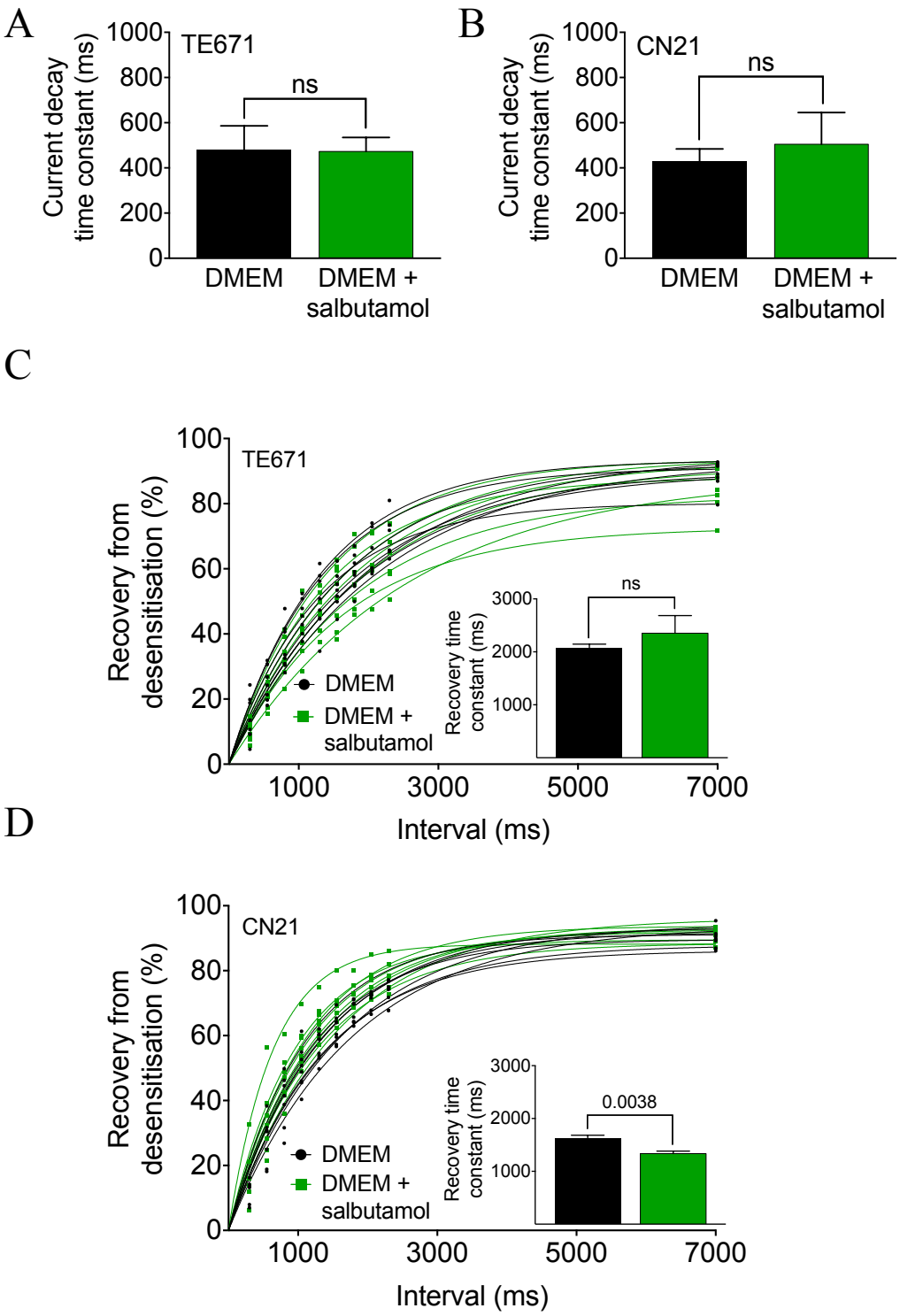


Figure 3-30 Effect of the PKA activating drug salbutamol on fetal and adult AChR desensitisation and recovery from desensitisation

The incubation of TE671 and CN21 cells in growth medium containing 1 µM salbutamol for at least 30 minutes had no effect on current decay in both cell lines (A, B). Recovery from desensitisation (C, D) was only faster in CN21 cells after salbutamol exposure. Unpaired t-test.

with salbutamol [n=8], ns) (Figure 3-30C, D). These results suggest the possibility that only adult AChRs harbouring a PKA consensus sequence in the ε-M3-M4 loop are modulated by salbutamol as an activator of PKA.

3.12 Discussion

This chapter assessed desensitisation and recovery from desensitisation in fetal and adult AChRs expressed in non-muscle and muscle cells, revealing faster recovery from desensitisation in the adult isoform. In experiments using chimeric AChRs with exchanged M3-M4 loops, recovery kinetics was determined by the AChR isoform specific cytoplasmic M3-M4 loop. Salbutamol, an activator of PKA, further facilitated recovery from desensitisation in the adult AChR isoform only, which in contrast to the fetal AChR isoform harbours a PKA consensus sequence. Intracellular factors might thus play an important role for fast recovery from desensitisation in adult AChRs.

3.12.1 Dependence of desensitisation and recovery from desensitisation on methodological parameters

Desensitisation and recovery from desensitisation depend on various methodological parameters and can be altered by experimental manipulation (Table 3-5). Desensitisation of the muscle-type AChR has been shown to depend on agonist concentration (Dilger and Liu, 1992), temperature (Magazanik and Vyskocil, 1975) and membrane potential (Magazanik and Vyskocil, 1970; Fiekers et al., 1980). Data on the dependence of recovery from desensitisation on methodological factors, by

Table 3-5 The influence of methodological factors on desensitisation and recovery from desensitisation

	Current decay time constant	Recovery time constant
Agonist concentration (Dilger et al., 1992)	↓	No effect
Agonist concentration rise time	↑	No effect
Series resistance	↑	↓
Temperature (Magazanik and Vyskocil, 1975)	↓	↓
Membrane potential (depolarisation) (Magazanik and Vyskocil, 1970; Fiekers et al., 1980)	↑	Not tested

contrast, is sparse, with evidence for the influence of temperature on recovery kinetics only (Magazanik and Vyskocil, 1975). In this project, agonist concentration, temperature and membrane potential were kept constant and are thus unlikely to have confounded the findings. The relationship between agonist application and AChR kinetics was analysed by computer simulation and revealed that only low ACh concentrations and very slow ACh concentration rise times are associated with prolonged desensitisation time constants, but recovery from desensitisation remained unaffected. The computer simulation was based on a simple linear kinetic scheme with a single desensitised state. More complex models assume a set of non-conducting desensitised states (Quick and Lester, 2002; Elenes et al., 2006; Sine, 2012). As one of those models, a cyclic kinetic reaction scheme was shown to provide a better description of experimental data obtained by outside-out patch clamp experiments on BC3H-1 cells expressing mouse fetal AChRs (Dilger and Liu, 1992) (Figure 3-31). By that model, recovery from desensitisation was also shown to be independent of agonist concentration (Dilger and Liu, 1992).

SR compensation is crucial for the analysis of desensitisation and recovery from desensitisation. The exact relationship between SR and desensitisation and recovery from desensitisation was assessed by the calculation of current decay and recovery time constants at different SR compensation levels. Insufficient SR compensation was associated with an overestimation of current decay time constants and an underestimation of recovery time constants. A maximum voltage error of 2 mV was therefore tolerated in all experiments (corresponding to 3.3% of the holding potential), and the main findings were confirmed by the application of two different voltage error correction methods, both of which revealed faster recovery time

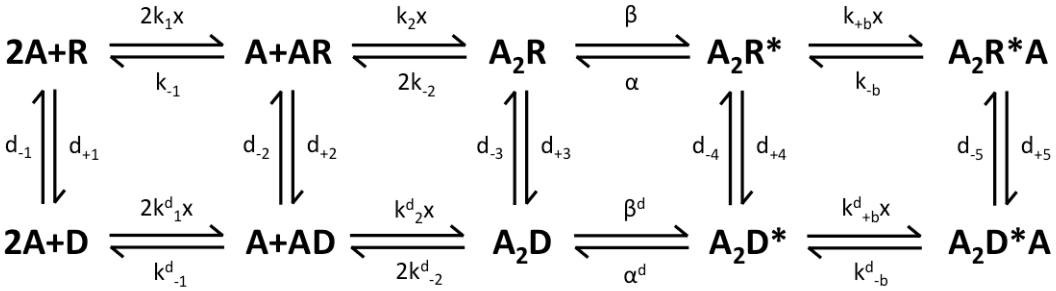


Figure 3-31 Cyclic kinetic scheme with five different desensitised states
R: AChR, A: ACh, x: ACh concentration, R*: open AChR conformation, D/D*: desensitised AChR conformation, $k_1/k_{-1}/k_2/k_{-2}/k^d_1/k^d_{-1}/k^d_2/k^d_{-2}$: acetylcholine binding and unbinding rate constants, β: AChR opening rate constant, α: AChR closing rate constants, β^d/α^d: rate constants from/to A_2D and A_2D^* corresponding to β and α, $k_{+b}/k_{-b}/k^d_{+b}/k^d_{-b}$: blocking and unblocking rate constants. The rates d_n (n=1–5) and d_{-n} refer to transitions from active states to desensitised states and vice versa. In this scheme, each state is considered to have a desensitised counterpart. The rate-limiting step for recovery from desensitisation after removal of agonist was described by the rate constants d_1/d_{-1} and is thus independent of agonist concentration (Dilger and Liu, 1992).

constants in adult AChRs. Cell size was shown to be comparable between groups, which is an important requirement for the software-based voltage error correction method, where currents are recorded without SR compensation resulting in an unpredictable intracellular voltage inhomogeneity.

3.12.2 Differential modification of recovery kinetics in fetal and adult AChRs by intracellular factors

Desensitisation of the nicotinic AChR at the NMJ was described over sixty years ago and shown to occur within seconds of agonist application and recover within seconds of agonist removal (Katz and Thesleff, 1957). More recent studies subsequently characterised desensitisation in fetal and adult AChRs with time constants ranging from tens of milliseconds (Paradiso and Brehm, 1998; Jahn et al., 2001; Krampfl et al., 2002) to several seconds (Hopfield et al., 1988; Wagoner and Pallotta, 1988) or even minutes (Chesnut, 1983). Desensitisation is a function of agonist concentration (Dilger and Liu, 1992) and these differences may have resulted from varying agonist concentrations used in different studies. But it has also been suggested that different factors of posttranslational AChR modification influencing desensitisation or different applications of the patch clamp technique could have contributed to the differences (Auerbach and Akk, 1998). Solution exchange times can be very fast in outside-out patches, which is important to resolve accurately the time course of desensitisation and recovery from desensitisation, but, contrasting with cell-attached patches, outside-out patches lack the physiological intracellular compartment with potential modifying factors.

In this work, desensitisation and recovery kinetics were compared between fetal and adult AChRs expressed in two different cell lines using whole-cell patches and an optimised perfusion system. There was no difference in desensitisation between the fetal and adult isoform as reported by others (Auerbach and Akk, 1998; Jahn et al., 2001), but recovery from desensitisation was significantly faster in adult AChRs in both the muscle and non-muscle cell line. Current decay and recovery time constants were generally faster in the non-muscle cell line. As stated above, this could have derived from differences in posttranslational AChR modification or the interaction of AChRs with other proteins (Burden et al., 2018) differently expressed in the two cell lines. This is further supported by experiments using cell cultures that derived from different frozen stocks of the same cell line, revealing significantly different current decay time constants between different stocks. This could have resulted from a phenotypic heterogeneity due to varying protein expression profiles in the cell cultures after thawing that could have lead to different AChR modifications.

It is likely that the isoform specific M3-M4 cytoplasmic loop is essential for the observed difference in recovery kinetics between both AChR isoforms. In experiments on chimeric γ- and ε-subunits with exchanged M3-M4 cytoplasmic loops, fast recovery from desensitisation depended on the ε-loop and slow recovery from desensitisation on the γ-loop. Intracellular factors could have modified the γ- and ε-subunit posttranslationally and influenced recovery kinetics differently in both isoforms. This hypothesis is supported by experiments after incubation of cells with salbutamol, an activator of PKA that has been shown to stimulate phosphorylation at consensus sequences on the M3-M4 cytoplasmic loops of various AChR subunits

(Huganir et al., 1986; Hoffman et al., 1994; Paradiso and Brehm, 1998). Recovery from desensitisation was significantly faster only in adult AChRs upon salbutamol exposure. This is not unexpected considering that the consensus sequence for PKA phosphorylation (i.e. RRXSX, where X is any amino acid, (Hoffman et al., 1994)) is present in the ε- but not in the γ-M3-M4 loop in humans. In CMS patients, however, the therapeutic relevance of this finding is unclear. Salbutamol is also effective in CMS with ε-subunit mutations, where neuromuscular transmission depends on the fetal AChR isoform without the PKA consensus sequence. Other mechanisms are thus likely to underlie the beneficial effect of salbutamol in these patients.

Together, the findings in this chapter suggest that the evaluation of fetal and adult AChR function in a physiological intracellular environment might be crucial for the elucidation of true biological effects. The use of the outside-out configuration in former reports on AChR recovery kinetics could have prevented such modifications and obscured differences between the fetal and adult AChR isoform.

3.12.3 Physiological implications of fast recovery from desensitisation in adult AChRs

The physiological significance of desensitisation and recovery from desensitisation at the NMJ is disputed in literature (Giniatullin et al., 2005). Desensitisation is a slow process compared to the lifetime of ACh in the synaptic cleft that ranges between 200-500 μs (Smart and McCammon, 1998). Therefore, desensitisation might not have a significant impact on shaping endplate currents in muscle. It has been shown, however, that desensitisation might become relevant under certain physiological conditions at highly active synapses. ACh concentration at the postsynaptic

membrane is a function of its release from the presynaptic nerve terminal and its clearance from the synaptic cleft by AChE. High motor neuron firing rates can overcome the catalytic AChE capacity and increase the lifetime of ACh in the synaptic cleft sufficiently to desensitise AChRs (Magleby and Pallotta, 1981; Ruzzier and Scuka, 1986; Giniatullin et al., 1993; Giniatullin et al., 1997). As a result, an increasing fraction of desensitised receptors after each nerve stimulus can decrease endplate currents over time. AChRs with fast recovery kinetics could counteract this and help to maintain a sufficient number of activatable receptors between stimuli even at high frequent firing rates.

Experiments in mice revealed that up to the first postnatal week, when muscle fibres are multiply innervated, motor neuron firing rates are extremely low ranging around 0.5 Hz. From the second week there is an increase of motor neuron firing frequencies to levels usually found in adult mice (around 9-12 Hz) (Vrbova et al., 1985; Personius and Balice-Gordon, 2001). These changes happen around the same time of the AChR isoform change. In this context, the developmental switch to the ε-subunit with faster recovery kinetics could provide an adaptation to increasing motor neuron firing rates after birth, facilitating the robust and reproducible high-frequent neuromuscular transmission in adult muscle.

Chapter 4

Modification of AChR function by rapsyn

4.1 Introduction

Rapsyn is a 43 kDa membrane-associated cytoplasmic protein colocalised with AChRs in the postsynaptic membrane. It is 412 amino acids long and has been predicted to possess four distinct functional domains including a N-myristoylation (N-Myr) signal required for targeting rapsyn at the postsynaptic muscle membrane (Frail et al., 1988), seven tetratricopeptide (TPR) repeats for rapsyn self-association (Ramarao et al., 2001), a coiled-coil domain for the association of rapsyn with AChRs (Ramarao and Cohen, 1998; Ramarao et al., 2001) and a RING-H2 domain that interacts with β-dystroglycan and anchors rapsyn at the cell membrane (Bartoli et al., 2001) but was also shown to contain E3 ligase activity and catalyse AChR neddylation (Figure 4-1). Due to difficulties in isolating purified, well-folded rapsyn there are no crystallographic data available on the protein structure. The predicted functional domains of rapsyn are thus based on deletion studies highlighting the role of the deleted region only. The functional role of other regions cannot be deduced from such studies.

Rapsyn connects AChRs by up to three bridges, which is the minimum number required to form a two-dimensional network (Zuber and Unwin, 2013), and was shown to interact with all individual AChR subunits when overexpressed in

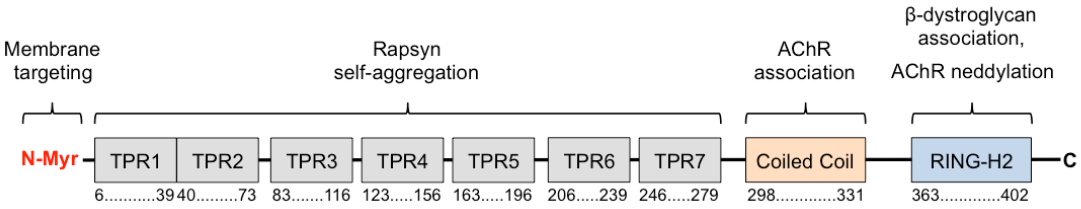


Figure 4-1 The functional domains of rapsyn
Rapsyn was reported to possess eight TPRs (amino acids 6-319) instead of seven (Ramarao et al., 1998), but the eight TPR overlaps with the coiled-coil domain and was shown to be required for the interaction of rapsyn with the AChR and not for rapsyn self-association (Ramarao et al., 1998; Ramarao et al., 2001). The thirty-four amino acid TPR repeats form super-helical structures, the shape of which depends on residues interposed between adjacent TPR repeats. Self-association or association with other TPR domain containing proteins is mediated by dimerisation or oligomerisation (Zeytuni and Zarivach, 2012).

heterologous cells. The interaction depends on the M3-M4 cytoplasmic loop of the receptor subunits (Maimone and Merlie, 1993; Maimone and Enigk, 1999; Huebsch and Maimone, 2003). Studies on chimeric membrane proteins containing various cytoplasmic domains of the AChR subunits identified an α-helical motif in the C-terminal region of the M3-M4 cytoplasmic loop that was shown to interact with rapsyn. Rapsyn co-clustered with membrane proteins harbouring the α-, β- or ε-subunit loops but not the δ-subunit loop (Lee et al., 2009). Correspondingly, the approximately forty amino acid α-helical motif was predicted in the C-terminal region of the α-, β- or ε-subunit loop only (Le Novere et al., 1999). The δ-subunit loop, by contrast, was predicted to contain a shorter helix (Ito et al., 1997; Lee et al., 2009).

Rapsyn was shown to facilitate phosphorylation of the Y390 residue within the β-subunit cytoplasmic loop and stabilise AChR clusters by activating Src-family kinases (Mohamed and Swope, 1999; Lee et al., 2008), and agrin-stimulated β^{Y390} phosphorylation was found to be directly related to rapsyn binding, AChR clustering (Borges et al., 2008) and an increase of the half-life of AChRs in myotubes (Rudell and Ferns, 2013). Preventing the phosphorylation of β^{Y390} impairs but does not block AChR clustering (Friese et al., 2007), thus indicating that β^{Y390} phosphorylation stabilises but is not crucial for AChR clustering. The coiled-coil domain of rapsyn, by contrast, was shown to be crucial for AChR clustering and hypothesised to interact with the receptor (Ramarao and Cohen, 1998), but the exact molecular mechanism by which rapsyn interacts with various M3-M4 loops remains unknown. Recently, the RING-H2 domain containing E3 ligase activity was demonstrated to catalyse AChR neddylation, which was also shown to be required for AChR

clustering and NMJ assembly (Li et al., 2016). However, the interaction of rapsyn with AChRs seems not necessarily to be associated with AChR clustering. Rapsyn can associate with unclustered AChRs suggesting that rapsyn recruitment on its own is insufficient to mediate AChR clustering (Friese et al., 2007). It has therefore been hypothesised that agrin-stimulation alters rapsyn or rapsyn associated proteins enabling pre-bound rapsyn to act as an anchoring protein (Burden et al., 2018).

4.2 Aims

All experiments in Chapter 3 had been performed on cells in which AChRs were not clustered. At the NMJ, AChR clustering is established by rapsyn that interacts with the M3-M4 cytoplasmic loops of the receptor subunits and clusters AChRs in a two-dimensional network on the cell surface. The impact of this interaction between rapsyn and AChRs on receptor function is unknown. This chapter aims to analyse whether the transfection of cells with rapsyn is sufficient to redistribute AChRs in clusters and whether rapsyn affects desensitisation and recovery from desensitisation in fetal and adult AChRs expressed in both muscle and non-muscle cell lines.

4.3 Rapsyn improves AChR aggregation in HEK293 and TE671/CN21 cells

Immunofluorescence staining of HEK293 cells was used to assess the impact of rapsyn on cell surface AChR distribution. In the absence of rapsyn, AChR distribution showed a mainly linear staining with some small clusters on the cell membrane in both HEK293-γ and HEK293-ε, whereas the co-transfection of cells with rapsyn cDNA was associated with evidence of AChR aggregation appearing as

larger clusters on the cell surface (Figure 4-2). The effect of rapsyn on the cell surface distribution of fetal and adult AChRs was also assessed by comparison of muscle cells co-transfected with and without rapsyn cDNA (these cells do not express endogenous rapsyn (Vogt et al., 2008)). Immunofluorescence staining of TE671/CN21 cells also revealed increased AChR aggregation upon rapsyn cDNA co-transfection (Figure 4.3). The level of AChR aggregation, however, was lower compared to rapsyn-induced AChR aggregation in HEK293 cells, probably due to lower AChR expression levels in TE671/CN21 cells. After increasing AChR expression levels in TE671/CN21 cells by additional transfection with cDNA of the corresponding AChR isoform subunits (TE671 + fetal AChRs and CN21 + adult AChRs, respectively) the level of AChR aggregation also increased and helped to distinguish cells with and without rapsyn visually (Figure 4-4). As a result of the heterogeneity and small size of the AChR aggregates ranging around 0.5 μm, their quantification by Fiji macro analysis was not feasible in both HEK293 and TE671/CN21 cells.

4.4 Influence of rapsyn on AChR surface expression

Previous data using ^{125}I-BTX for AChR radiolabelling reported that rapsyn was associated with reduced AChR degradation rates and an increase of the metabolic stability of AChRs on the surface of transfected COS cells and cultured myotubes (Wang et al., 1999b). In this project, the impact of rapsyn on AChR surface expression was tested by the measurement of peak current amplitudes in whole-cell patch clamp experiments expecting these to be higher in cells expressing rapsyn.

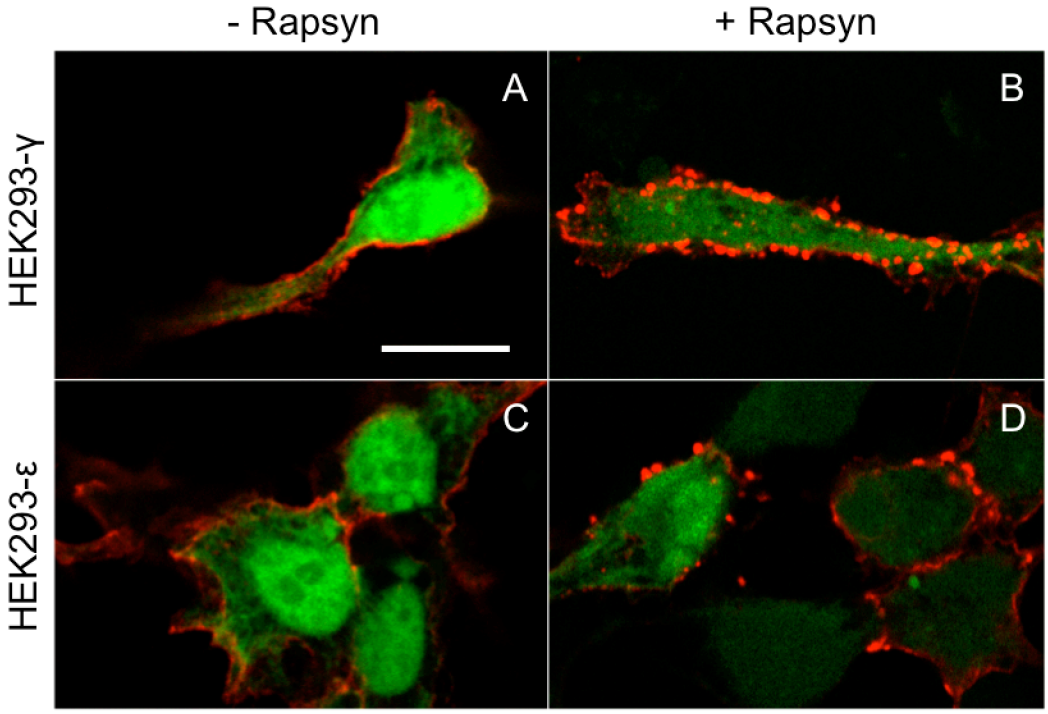


Figure 4-2 Effect of rapsyn on surface AChR expression and distribution in HEK293 cells

In both fetal (A, B) and adult (C, D) AChRs expressed in HEK293 cells, the co-transfection with rapsyn cDNA resulted in a change of AChR distribution (red staining, AF594) from a more linear peripheral staining (with only few AChR aggregates) (A, C) to receptor aggregation on the cell surface (B, D). The mean size of the AChR aggregates ranged between 0.5-1 µm. The use of a bicistronic plasmid (pIRES-RAPSN-EGFP) enabled the simultaneous expression of both rapsyn and EGFP from the same construct. Magnification: 60x, Scale bar = 10 µm.

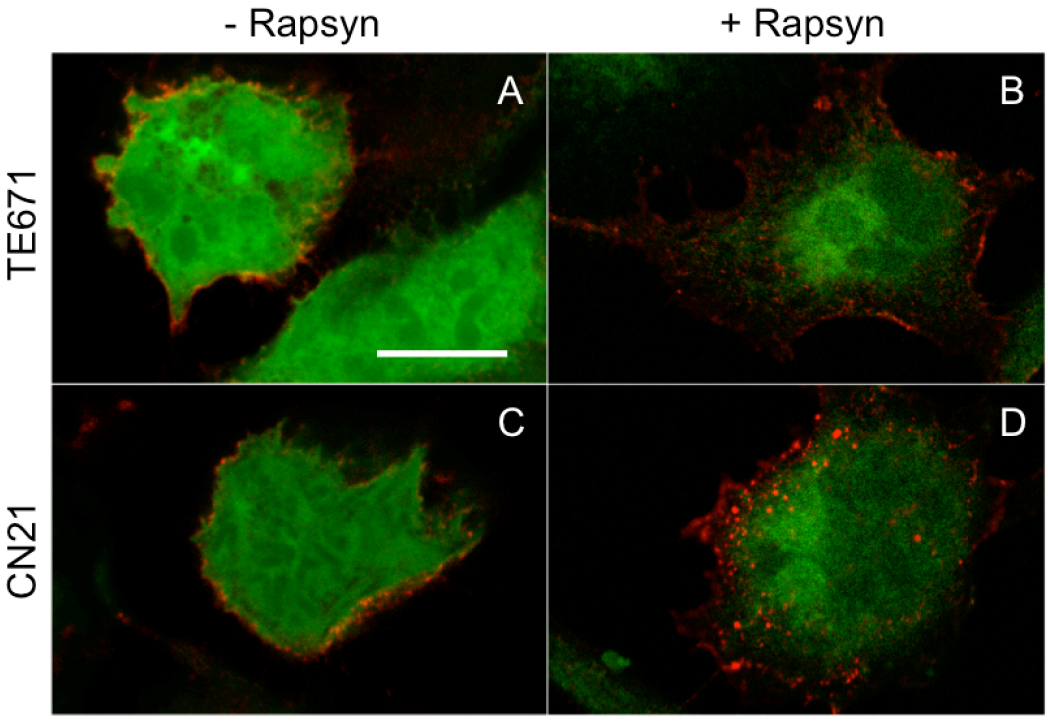


Figure 4-3 Effect of rapsyn on surface AChR expression and distribution in TE671/CN21 cells

The transfection of both TE671 (A, B) and CN21 cells (C, D) with rapsyn cDNA was associated with improved AChR aggregation on the cell surface (B, D). Magnification: 60x, Scale bar = 10 μm.

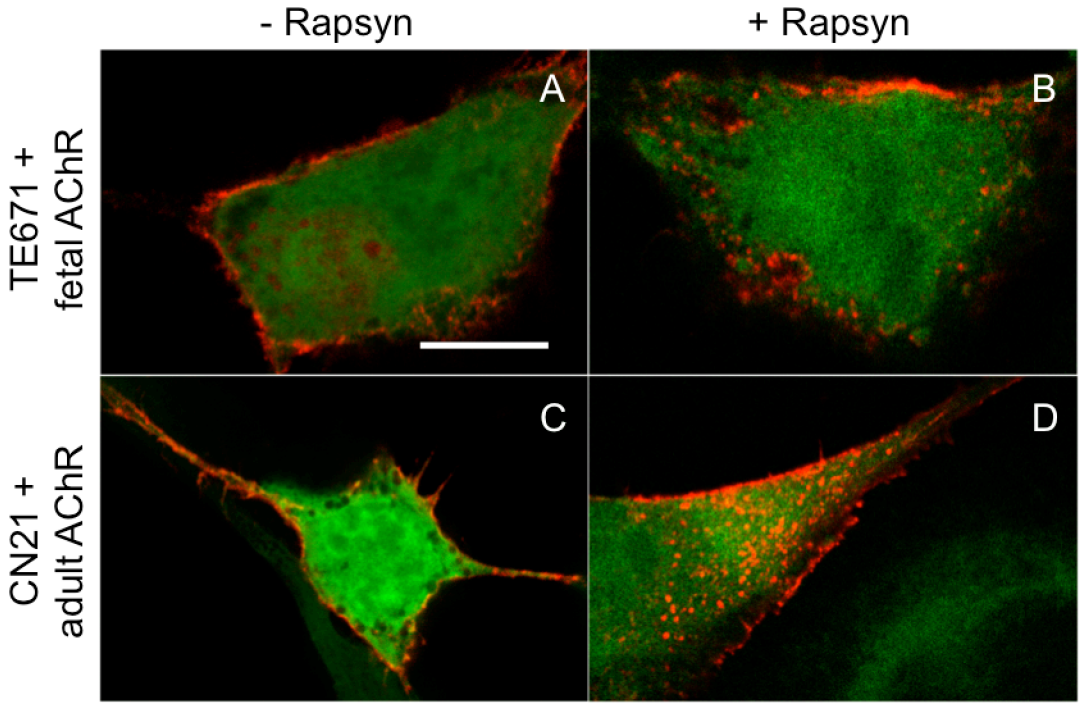


Figure 4-4 Effect of rapsyn on surface AChR expression and distribution in TE671/CN21 cells after co-transfection with fetal and adult AChR subunit cDNA

After the transfection of TE671 cells (A, B) with fetal AChR subunits and CN21 cells (C, D) with adult AChR subunits, AChR aggregation was clearer to visualise upon rapsyn co-transfection (B, D). Magnification: 60x, Scale bar = 10 μm.

4.4.1 Estimation of AChR surface expression by the measurement of peak current amplitudes

Peak current amplitudes were measured in HEK293-γ and HEK293-ε co-transfected with pEGFP-N1 coding for EGFP or pIRES2-RAPSN-EGFP allowing the simultaneous but separate expression of rapsyn and EGFP. In HEK293-γ cells, peak current amplitudes were significantly higher when co-transfected with pIRES2-RAPSN-EGFP (–23.2±2.9 nA with rapsyn (n=15) and –8.6±1.8 nA without rapsyn (n=10), p=0.0009). In HEK293-ε cells, peak current amplitudes were also higher when co-transfected with pIRES2-RAPSN-EGFP but the difference was not significant (–30.5±4.2 nA with rapsyn (n=15) and –19.2±2.3 nA without rapsyn (n=10), p=0.0505) (Figure 4-5). Very high current amplitudes (especially in cells with rapsyn), however, were associated with high SR errors that could not be fully compensated and, thus, had to be excluded from the analysis. This resulted in underestimation of the mean peak current amplitudes especially in HEK293-ε cells co-transfected with pIRES2-RAPSN-EGFP.

4.4.2 Estimation of AChR surface expression using a cell-surface ^{125}I-BTX binding assay

One obvious reason for higher peak current amplitudes in cells co-transfected with pIRES2-RAPSN-EGFP is that rapsyn stabilised AChRs and increased AChR surface expression. This was further analysed using a cell-surface ^{125}I-BTX binding assay on HEK293T cells. Surprisingly, there was no significant difference in ^{125}I-BTX binding between cells co-transfected with pIRES2-RAPSN-EGFP and pEGFP-N1

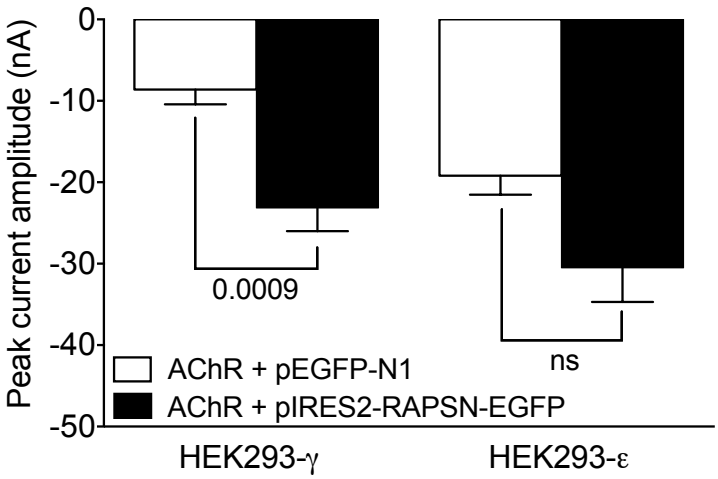


Figure 4-5 Impact of rapsyn on peak current amplitudes in HEK293-γ and HEK293-ε

In both HEK293-γ and HEK293-ε cells, peak current amplitudes were compared between cells co-transfected with pEGFP-N1 (coding for EGFP) and pIRES2-RAPSN-EGFP (coding for rapsyn and EGFP). The expression of rapsyn was associated with higher peak current amplitudes. HEK293-γ and HEK293-ε cells derived from different cell cultures. A direct comparison of peak current amplitudes between fetal and adult AChRs is thus limited by the cell culture-inherent variation of AChR surface expression levels (see Chapter 3-7). Unpaired t-test.

suggesting similar AChR expression levels with and without rapsyn. In HEK293T-γ, ^{125}I-BTX binding was 52697±10731 cpm without rapsyn and 42086±7628 cpm with rapsyn (n=5, ns), and in HEK293T-ε, ^{125}I-BTX binding was 57705±11827 cpm without rapsyn and 31848±8166 cpm with rapsyn (n=5, ns) (Figure 4-6). These results were in contrast to the patch clamp experiments with higher peak current amplitudes recorded in cells expressing rapsyn. One potential explanation for this discrepancy was that rapsyn modified AChR function and increased the electric charge entering the cell, e.g. by increasing AChR conductance. This would have resulted in higher peak current amplitudes. However, differences in the transfection efficiency of both plasmids with fewer transfected cells using pIRES2-RAPSN-EGFP could also have biased the results when the population is assessed by radiolabelling. It would thus be helpful to evaluate AChR surface expression in individual cells, which would require fluorescence-activated cell scanning (FACS) analysis, rather than in a cohort of cells as performed by the ^{125}I-BTX binding assay.

4.4.3 Estimation of AChR surface expression using FACS

AChR surface expression in individual HEK293 cells was analysed using FACS in order to test whether rapsyn was associated with increased AChR surface expression as suggested by the higher peak current amplitudes. The fluorescence intensities of AF594 immunolabelled AChRs and EGFP in individual HEK293-γ and HEK293-ε cells were measured. The comparison between cells co-transfected with pEGFP-N1 and pIRES2-RAPSN-EGFP revealed no clear difference in maximum AF594 fluorescence intensities suggesting similar AChR surface expression in cells with and

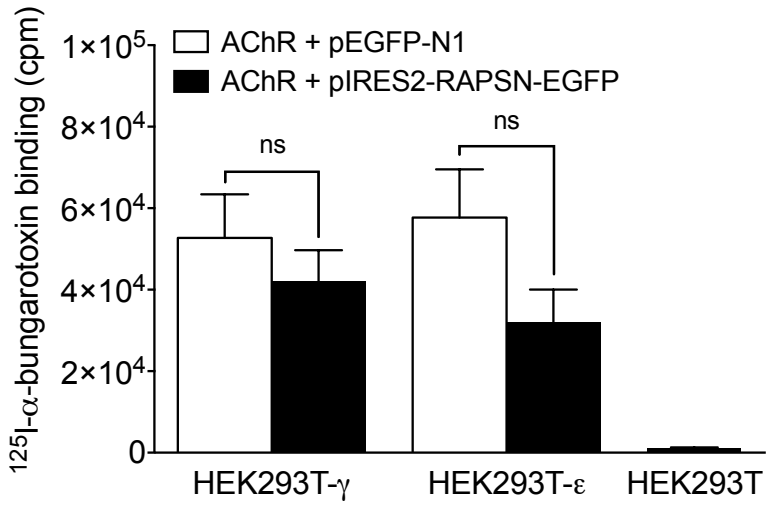


Figure 4-6 Estimation of AChR surface expression in HEK293T-γ and HEK293T-ε using a cell-surface ^{125}I-BTX binding assay
In both HEK293T-γ (A) and HEK293T-ε (B), rapsyn had no significant effect on AChR surface expression. Unpaired t-test.

without rapsyn (Figure 4-7), which was in line with the cell-surface ^{125}I-BTX binding assay and in contrast to the patch clamp experiments with higher peak current amplitudes in cells expressing rapsyn. Only in HEK293-γ, the mean AF594 fluorescence intensity was significantly higher in cells expressing rapsyn compared to cells without rapsyn, but the difference was not high enough to explain the difference in peak current amplitudes (the mean AF594 fluorescence intensity was 3616±333 in cells with rapsyn and 2091±195 in cells without rapsyn [n=3, p=0.0168]). In HEK293-ε, the mean AF594 fluorescence intensity was 4189±371 in cells with rapsyn and 3649±252 in cells without rapsyn (n=3, ns) (Figure 4-8). One explanation for the discrepancy between higher peak current amplitudes and similar AF594 fluorescence intensities in cells co-transfected with rapsyn might have derived from the selective approach to choose cells in patch clamp experiments. Cells were chosen and patched according to the fluorescence intensity of EGFP under the microscope with a preference for the least green cells. The FACS analysis shows that cells with low EGFP fluorescence intensities were associated with higher AF594 fluorescence intensities when co-transfected with rapsyn, suggesting higher AChR surface expression at low EGFP levels (Figure 4-9, 4-10). Thus, by patching faintly green cells there was a higher likelihood to record high peak current amplitudes in cells co-transfected with pIRES2-RAPSN-EGFP than in cells co-transfected with pEGFP-N1. However, an increase of AChR conductance by rapsyn as another explanation for the higher peak current amplitudes in cells co-transfected by pIRES2-RAPSN-EGFP cannot be ruled out.

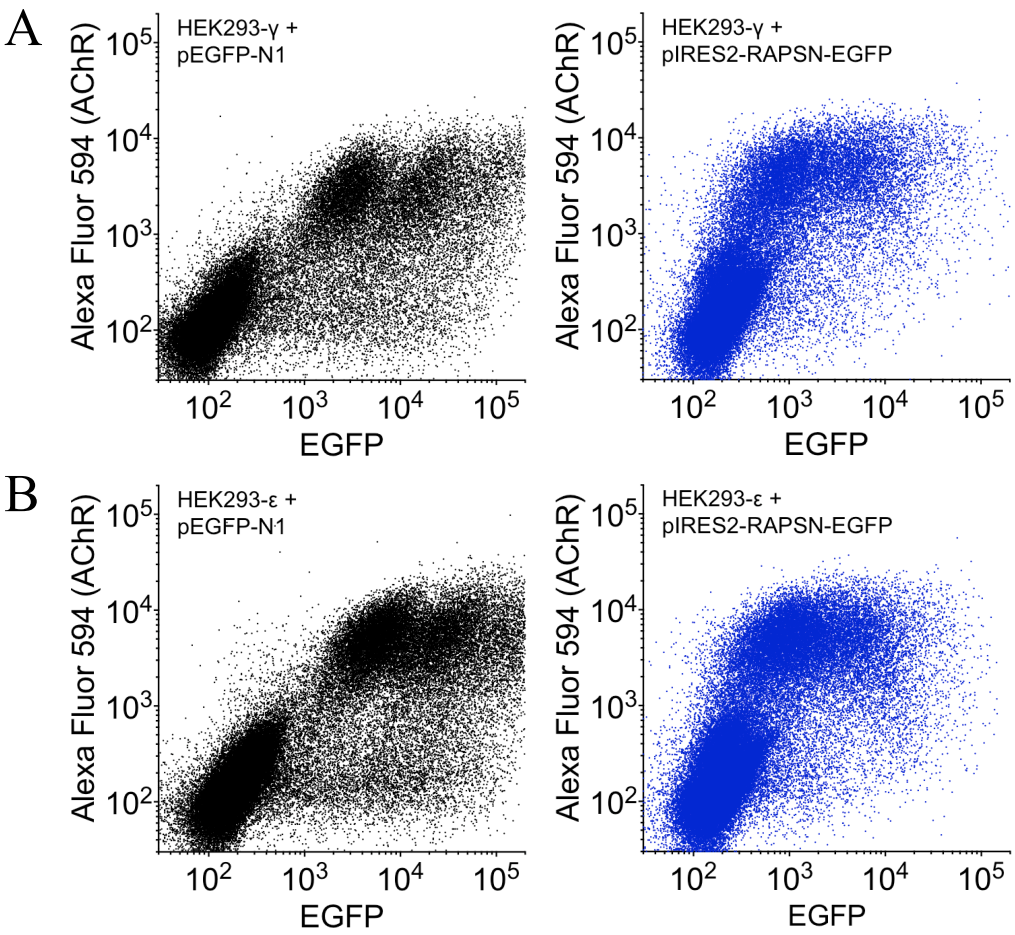


Figure 4-7 Estimation of AChR surface expression in HEK293-γ and HEK293-ε using FACS

In both HEK293-γ (A) and HEK293-ε (B), the influence of rapsyn on AChR surface expression was assessed by fluorescence intensity measurements of AF594 immunolabelled AChRs and EGFP. AChR surface expression was analysed between cells co-transfected with either pEGFP-N1 coding for EGFP (black scatterplots) or with pIRES2-RAPSN-EGFP coding for rapsyn and EGFP (blue scatterplots). Each dot represents a single cell with corresponding EGFP (x-axis) and AF594 (y-axis) fluorescence intensities. Maximum AF594 fluorescence intensities were similar between both cells with and without rapsyn, but maximum EGFP fluorescence intensities were lower in cells with rapsyn.

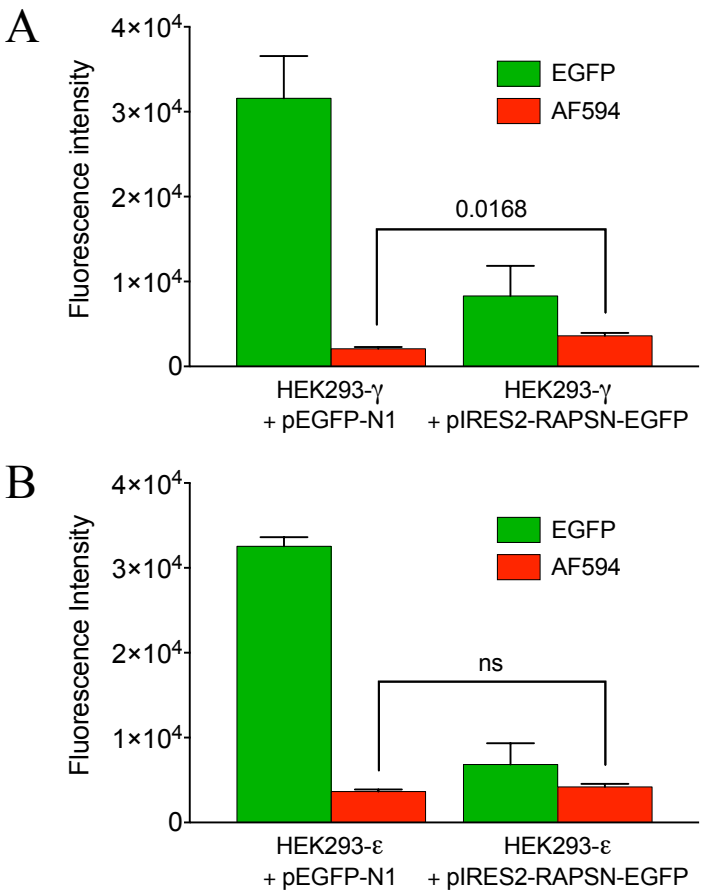


Figure 4-8 Mean EGFP and AF594 fluorescence intensities in HEK293-γ and HEK293-ε co-transfected with pEGFP-N1 and pIRES2-RAPSN-EGFP

In both HEK293-γ (A) and HEK293-ε (B), EGFP fluorescence intensities were clearly reduced in cells co-transfected with pIRES2-RAPSN-EGFP with only marginally increased AF594 fluorescence intensity levels (although the difference was significant in HEK293-γ). The results are the means of three experiments with 80000-100000 cells measured and averaged per experiment. The difference in EGFP fluorescence intensities between both groups may have resulted from a lower transfection efficiency of the pIRES2-RAPSN-EGFP vector. Alternatively, the IRES-dependent translation of EGFP (located downstream to RAPSN) could have been lower compared to the translation of RAPSN. In fact, there is evidence in the literature for a significantly lower IRES-dependent second gene expression in comparison with first gene expression (Mizuguchi et al., 2000). Unpaired t-test.

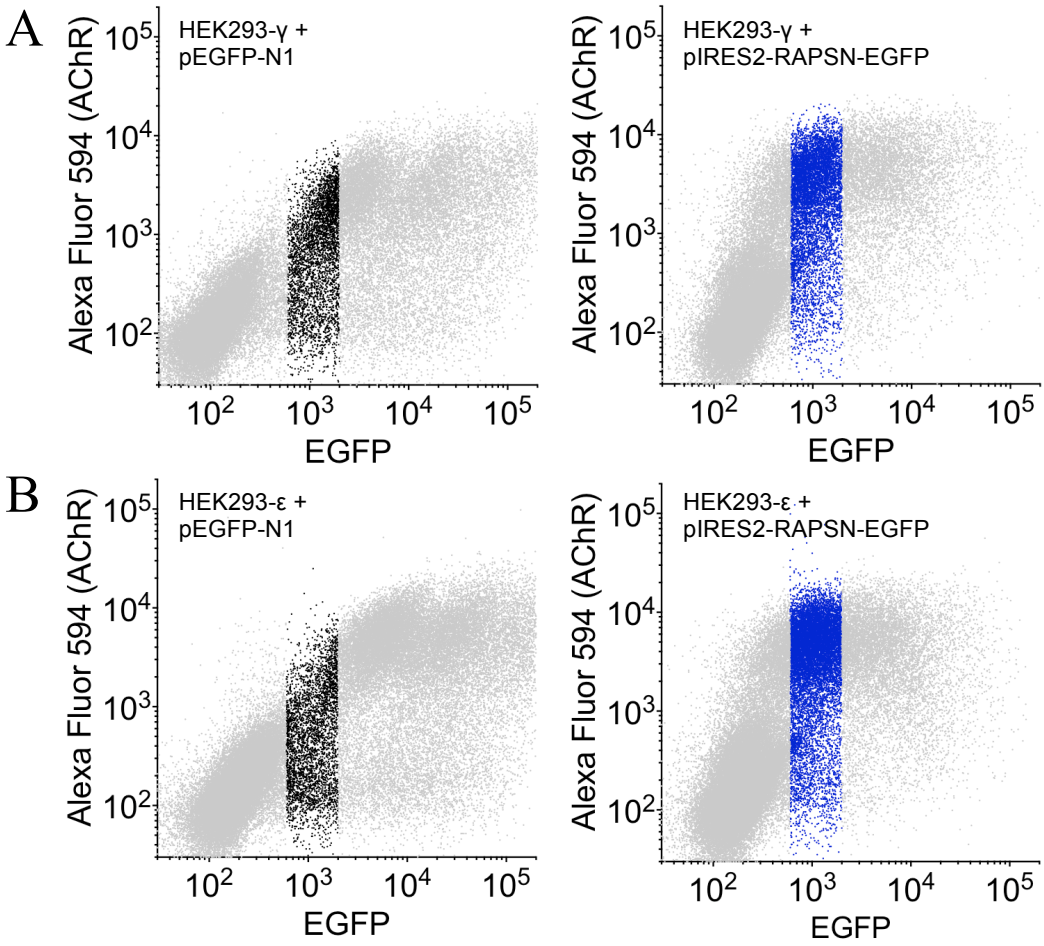


Figure 4-9 Estimation of AChR surface expression in HEK293-γ and HEK293-ε with low EGFP fluorescence intensities using FACS

FACS data were re-analysed including only the least green HEK293-γ (A) and HEK293-ε cells (B) with EGFP fluorescence intensities between 600-2000 (to better correlate AChR surface expression with peak current amplitudes in whole-cell patch clamp experiments). Cells with EGFP fluorescence intensities <600 were considered as untransfected and would not have been patched in patch clamp experiments. AChR surface expression was analysed between cells co-transfected with either pEGFP-N1 coding for EGPF (black scatterplots) or with pIRES2-RAPSN-EGFP coding for rapsyn and EGFP (blue scatterplots). Each dot represents a single cell with corresponding EGFP (x-axis) and AF594 (y-axis) fluorescence intensities. Maximum AF594 fluorescence intensities were higher in cells co-transfected with rapsyn.

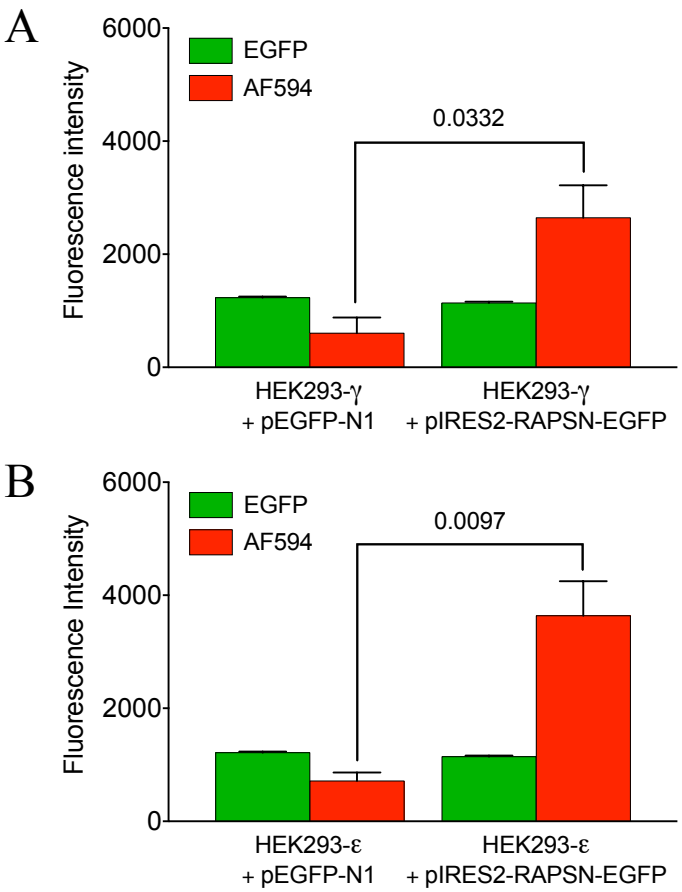


Figure 4-10 Comparison of AF594 fluorescence intensities in HEK293-γ and HEK293-ε with low EGFP fluorescence intensities
In both HEK293-γ (A) and HEK293-ε (B), AF594 fluorescence intensity levels were significantly higher when co-transfected with pIRES2-RAPSN-EGFP. The analysis only included cells with EGFP fluorescence intensities between 600-2000. Unpaired t-test.

4.5 The impact of rapsyn on AChR desensitisation and recovery from desensitisation

Whole-cell patch clamp experiments were performed to test the effect of rapsyn on desensitisation and recovery from desensitisation in fetal and adult AChRs. A muscle (TE671/CN21) and a non-muscle (HEK293) cell line were used to account for cell-specific differences in the expression profile of intracellular factors that could affect the function of rapsyn, of the AChR or the interaction between both.

4.5.1 The acetylcholine application protocol

The ACh application protocol included ten sweeps of 25 s duration, each of which consisted of two consecutive ACh pulses. A "desensitising" pulse of 3 s duration was followed by a 50 ms "test" pulse. The interval between pulses increased with each sweep from 300 ms to 7 s until full recovery from desensitisation (Figure 3-1). The extracellular solution contained (in mM): NaCl 150, KCl 2.8, HEPES 10, $MgCl_2$ 2, $CaCl_2$ 2 and glucose 10 with pH adjusted to 7.4 using NaOH. The pipette solution contained (in mM): NaCl 4, KCl 144, HEPES 10, $MgCl_2$ 2, Mg-ATP 2 and EGTA 10 with pH adjusted to 7.2 using KOH (Table 3-1).

4.5.2 The impact of rapsyn on AChR desensitisation and recovery from desensitisation in TE671/CN21 cells

Rapsyn had no effect on current decay time constants in either fetal or adult AChRs expressed in TE671 and CN21 cells, respectively. Mean current decay time constants were 646±56 ms without rapsyn (n=10) and 600±73 ms with rapsyn (n=10) in TE671

cells, and 464±61 ms without rapsyn (n=10) and 627±80 ms with rapsyn (n=10) in CN21 cells (Figure 4-11). Recovery from desensitisation, by contrast, was significantly faster in AChRs expressed in TE671 and CN21 cells co-transfected with rapsyn cDNA. Mean recovery time constants were 2289±234 ms without rapsyn (n=10) and 1368±85 ms with rapsyn (n=10) in TE671 cells (p=0.0016), and 1584±128 ms without rapsyn (n=10) and 1014±89 ms with rapsyn (n=10) in CN21 cells (p=0.0018) (Figure 4-12). Recovery ratio plots could be fitted best by a single exponential in both groups.

4.5.3 The impact of rapsyn on AChR desensitisation and recovery from desensitisation in HEK293 cells

In contrast to TE671/CN21 cells, the co-transfection of HEK293 cells with rapsyn cDNA resulted in slower current decay time constants in both fetal and adult AChRs. Mean current decay time constants were 312±43 ms without rapsyn (n=20) and 518±68 ms with rapsyn (n=20) in HEK293-γ cells (p=0.0128), and 251±38 ms without rapsyn (n=20) and 353±32 ms with rapsyn (n=20) in HEK293-ε cells (p=0.0450) (Figure 4-13). Facilitation of recovery from desensitisation, by contrast, could only be observed in HEK293 cells expressing fetal AChRs. Mean recovery time constants were 2002±174 ms without rapsyn (n=20) and 1161±137 ms with rapsyn (n=20) in HEK293-γ cells (p=0.0005). Rapsyn had no effect on AChR recovery kinetics in HEK293-ε (mean recovery time constants were 1176±74 ms without rapsyn [n=20] and 1014±84 ms with rapsyn [n=20], ns) (Figure 4-14).

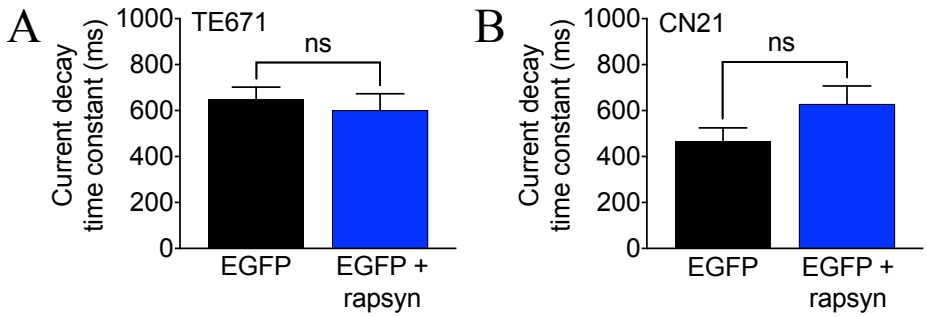


Figure 4-11 The effect of rapsyn on current decay time constants in AChRs expressed in TE671 and CN21 cells

Rapsyn does not affect AChR current decay time constants in TE671 (A) and CN21 cells (B). Cells were transfected with pEGFP-N1 (black bars) for EGFP expression or with pIRES2-RAPSN-EGFP for simultaneous expression of rapsyn and EGFP (blue bars). Unpaired t-test.

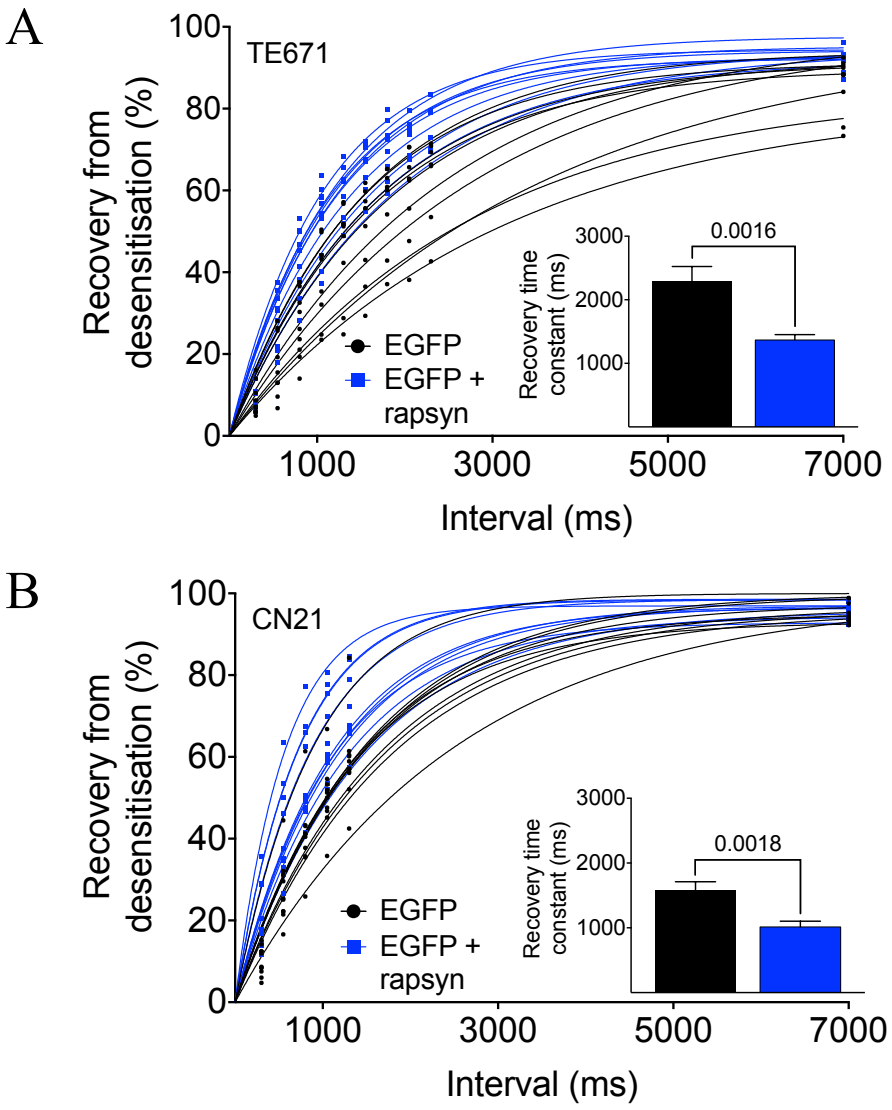


Figure 4-12 The effect of rapsyn on recovery time constants in AChRs expressed in TE671 and CN21 cells

Rapsyn facilitates AChR recovery from desensitisation in both TE671 (A) and CN21 cells (B). Cells were transfected with pEGFP-N1 (black curves/bars) for EGFP expression or with pIRES2-RAPSN-EGFP for simultaneous expression of rapsyn and EGFP (blue curves/bars). Unpaired t-test.

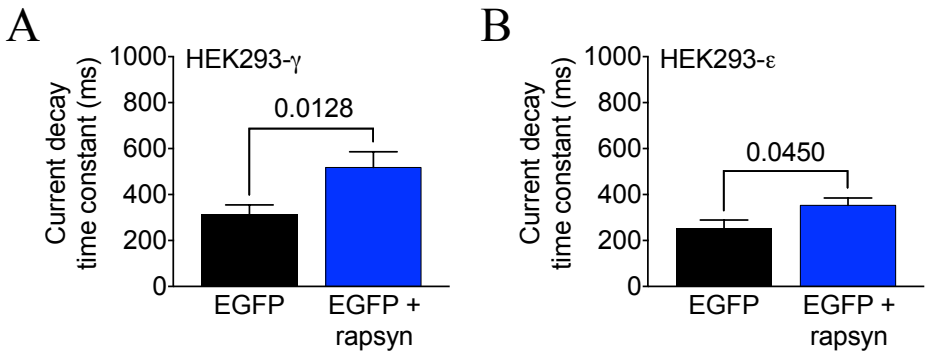


Figure 4-13 The effect of rapsyn on current decay time constants in AChRs expressed in HEK293-γ and HEK293-ε cells

Rapsyn prolongs AChR current decay time constants in HEK293-γ (A) and HEK293-ε cells (B). Cells were transfected with pEGFP-N1 (black bars) for EGFP expression or with pIRES2-RAPSN-EGFP for simultaneous expression of rapsyn and EGFP (blue bars). Unpaired t-test.

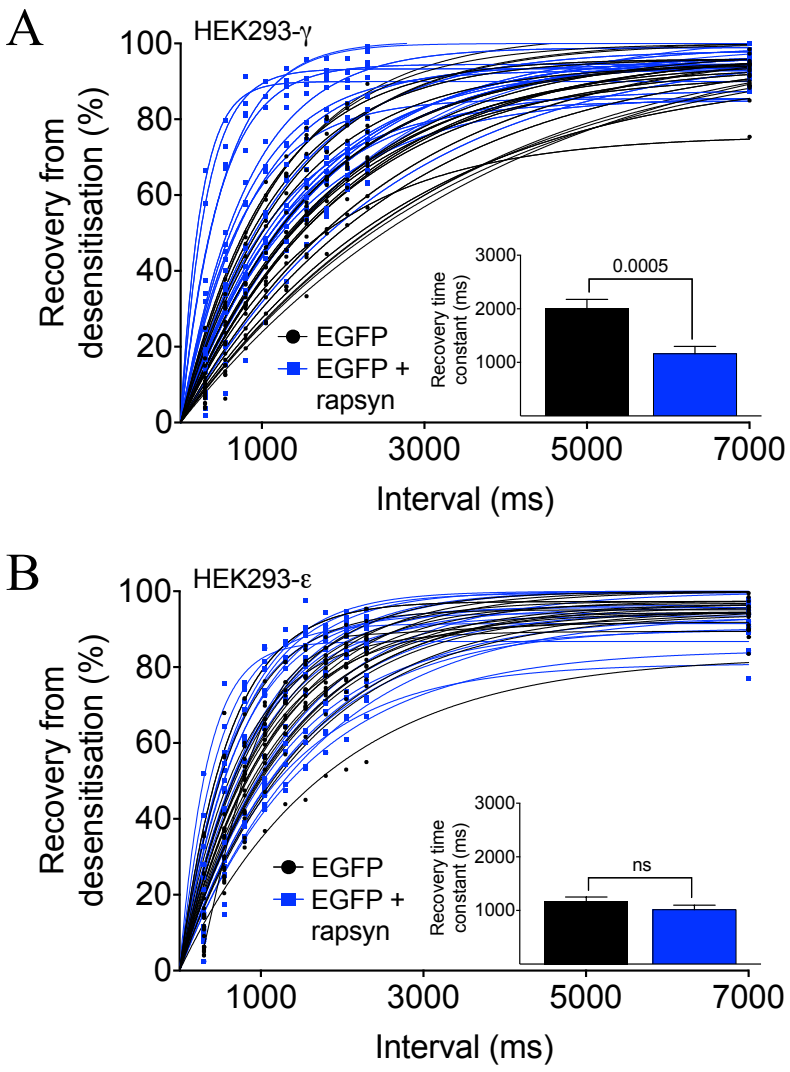


Figure 4-14 The effect of rapsyn on recovery time constants in AChRs expressed in HEK293-γ and HEK293-ε cells

Rapsyn facilitates AChR recovery from desensitisation in HEK293-γ (A) but not in HEK293-ε cells (B). Experiments were performed using two different cell cultures in HEK293-γ and HEK293-ε. Cells were transfected with pEGFP-N1 (black curves/bars) for EGFP expression or with pIRES2-RAPSN-EGFP for simultaneous expression of rapsyn and EGFP (blue curves/bars). Unpaired t-test.

4.6 Rapsyn can facilitate recovery kinetics in an AChR mutant that prevents receptor clustering in C2C12 myotubes

Facilitation of AChR recovery kinetics by rapsyn could be mediated by the interaction of rapsyn with individual subunits of the receptor or depend on AChR clustering. To try to distinguish these possibilities, we took advantage of a naturally occurring CMS mutation (p.δArg375His, from here on referred to as δR375H), located in the M3-M4 cytoplasmic loop of the δ-subunit.

4.6.1 The δR375H prevents AChR clustering in C2C12 myotubes

These experiments were performed by Dr. Wei Liu. The impact of the δR375H mutation on AChR clustering was analysed in C2C12 myotubes expressing fetal AChRs after knocking-out the CHRND gene that codes for the AChR δ-subunit ($C2C12_{\delta KO}$) and transfecting $C2C12_{\delta KO}$ with either δWT ($C2C12_{\delta WT}$) or δR375H cDNA ($C2C12_{\delta R375H}$). Agrin was applied in order to compare AChR clustering between $C2C12_{\delta WT}$ and $C2C12_{\delta R375H}$. The presence of the δR375H was associated with markedly reduced AChR cluster numbers comparable to those found in $C2C12_{\delta KO}$ (Figure 4-15). Mean cluster numbers were 75.3±10.5 per vision field in $C2C12_{\delta WT}$ (n=3) and 4.4±1.2 per vision field in $C2C12_{\delta R375H}$ (n=3) (p=0.0026). In $C2C12_{\delta KO}$, the mean cluster number per vision field was 3.2±2.1 (n=3) (Figure 4-16A). The size of AChR clusters remained unaffected in $C2C12_{\delta R375H}$. The mean cluster size was 10.1±2.0 μm^2 in $C2C12_{\delta WT}$ (n=3) and 7.0±1.9 μm^2 in $C2C12_{\delta R375H}$ (ns) (Figure 4-16B).

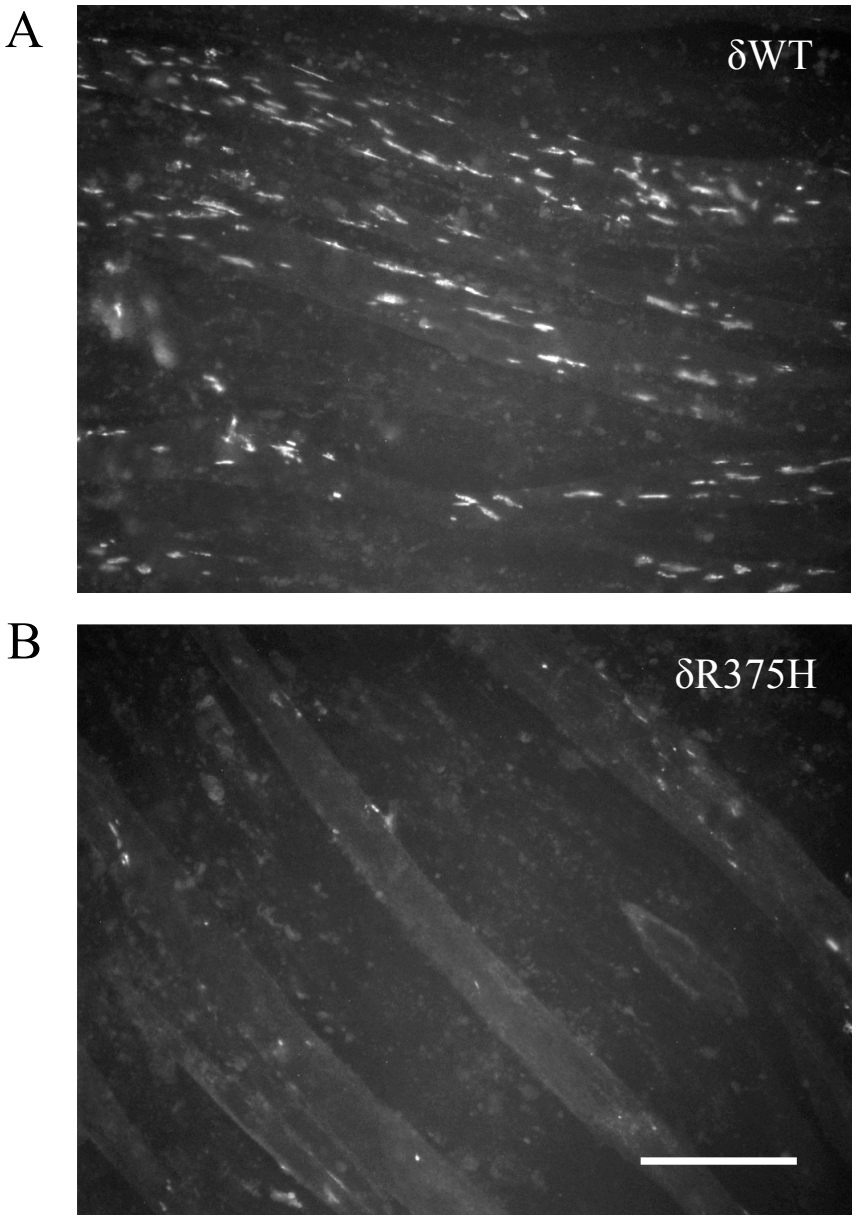


Figure 4-15 The δR375H mutation prevents agrin stimulated clustering of AChRs in C2C12 myotubes

Comparison of C2C12 myotubes expressing wild-type fetal AChRs (A) or fetal AChRs bearing the δR375H mutation (B). The mutation was associated with the failure of the receptors to cluster upon agrin stimulation. Scale bar = 100 μm. Images were taken by Dr. Wei Liu.

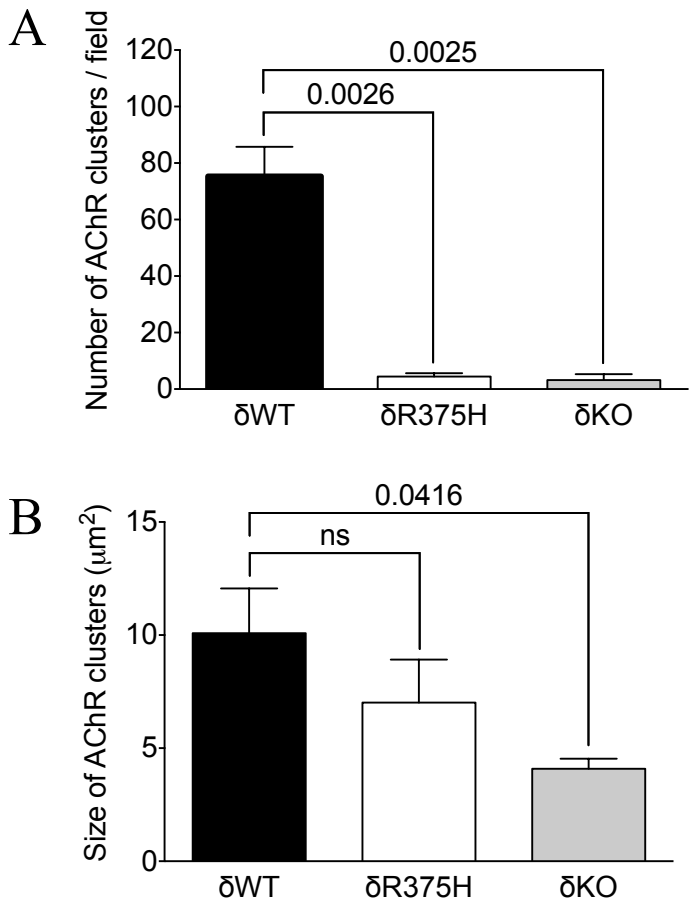


Figure 4-16 The δR375H mutation prevents agrin stimulated clustering of AChRs in C2C12 myotubes

Comparison of AChR clustering in C2C12 myotubes expressing wild-type fetal AChRs or fetal AChRs bearing the δR375H mutation. The mutation was associated with the failure of the receptors to cluster upon agrin stimulation (A). The size of remaining AChR clusters, however, was not significantly reduced in $C2C12_{\delta R375H}$ compared to $C2C12_{\delta WT}$ (B). Only AChR clusters ≥2.5 μm^2 were accepted in the analysis. Unpaired t-test. Experiments were performed by Dr. Wei Liu.

4.6.2 Rapsyn does not affect current decay but facilitates recovery kinetics in fetal $AChR_{\delta R375H}$

The functional impact of rapsyn was then tested on HEK293 cells expressing fetal AChRs including either the WT- (HEK293-$\gamma_{\delta WT}$) or mutant δ-subunit (HEK293-$\gamma_{\delta R375H}$). Fetal AChRs were chosen in order to be able to correlate the results with findings in C2C12 myotubes, which also express fetal AChRs. Current decay time constants were longer in HEK293-$\gamma_{\delta WT}$ when co-transfected with rapsyn (330±38 ms without rapsyn and 479±37 ms with rapsyn, p=0.0110), but in HEK293-$\gamma_{\delta R375H}$ current decay was not affected by rapsyn (354±42 ms without rapsyn and 407±35 ms with rapsyn, ns) (Figure 4-17). Surprisingly, recovery time constants were shorter in both HEK293-$\gamma_{\delta WT}$ and HEK293-$\gamma_{\delta R375H}$ when co-transfected with rapsyn cDNA. In HEK293-$\gamma_{\delta WT}$, mean recovery time constants were 1799±176 ms without rapsyn (n=10) and 1037±132 ms with rapsyn (n=10) (p=0.0028) (Figure 4-18A), and in HEK293-$\gamma_{\delta R375H}$, mean recovery time constants were 1541±95 ms without rapsyn (n=10) and 1085±129 ms with rapsyn (n=10) (n=0.0107) (Figure 4-18B).

4.6.3 Rapsyn colocalises with $AChR_{\delta R375H}$ in HEK293-γ cells

AChR clustering in C2C12 myotubes was tested after agrin stimulation and revealed the inability of $AChR_{\delta R375H}$ to cluster. This could have been due to the inability of rapsyn to bind to AChRs bearing the δR375H mutation and induce clustering, or rapsyn still bound to AChRs but the δR375H mutation prevented AChR clustering. Concluding from the functional data with facilitation of recovery kinetics in $AChR_{\delta R375H}$ expressed in HEK293-γ cells, it was likely that rapsyn still interacted

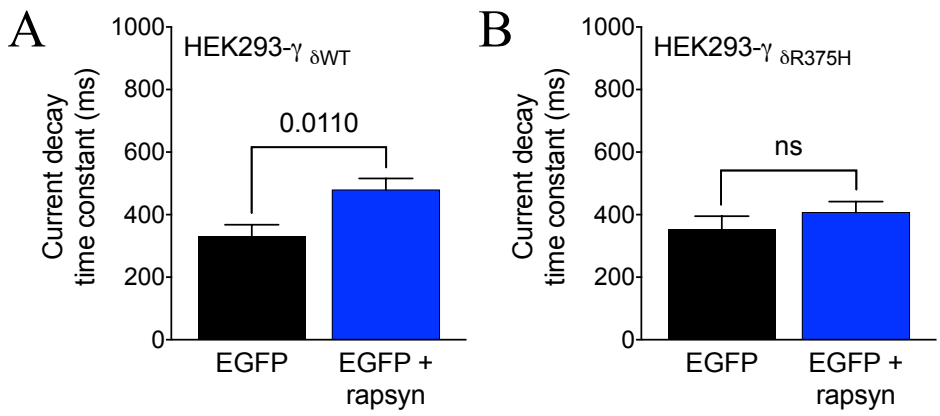


Figure 4-17 The effect of rapsyn on current decay time constants in AChRs expressed in HEK293-γ cells bearing the wild-type or mutant δ-subunit

Rapsyn prolongs AChR current decay time constants in HEK293-$\gamma_{\delta WT}$ (A) but not in HEK293-$\gamma_{\delta R375H}$ (B). Cells were transfected with pEGFP-N1 (black bars) for EGFP expression or with pIRES2-RAPSN-EGFP for simultaneous expression of rapsyn and EGFP (blue bars). Unpaired t-test.

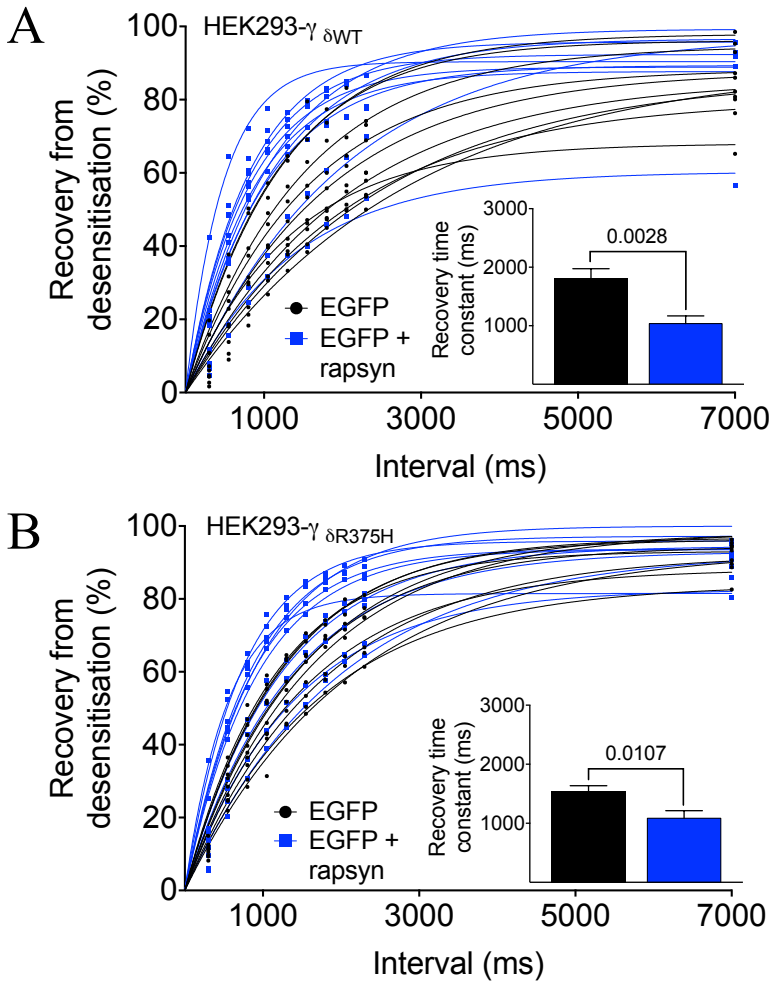


Figure 4-18 Rapsyn facilitates recovery from desensitisation in mutant AChRs bearing the δR375H mutation

Recovery from desensitisation is facilitated by rapsyn in both HEK293-γ $_{\delta WT}$ (A) and in HEK293-γ $_{\delta R375H}$ (B). Cells were transfected with pEGFP-N1 (black curves/bars) for EGFP expression or with pIRES2-RAPSN-EGFP for simultaneous expression of rapsyn and EGFP (blue curves/bars). Unpaired t-test.

with $AChR_{\delta R375H}$. The potential interaction of rapsyn with $AChR_{\delta R375H}$ was further assessed by immunofluorescence staining of HEK293-γ cells co-transfected with pEGFP-N1-RAPSN coding for rapsyn tagged to EGFP.

In HEK293-γ cells, EGFP-tagged rapsyn colocalised with both $AChR_{\delta WT}$ and $AChR_{\delta R375H}$ and AChR aggregates were also found in both $AChR_{\delta WT}$ and $AChR_{\delta R375H}$, although AChR aggregation was less consistent in $AChR_{\delta R375H}$ (Figure 4-19). These findings suggest that rapsyn still interacts with AChRs bearing the δR375H mutation, the presence of which was shown to prevent AChR clustering in C2C12 myotubes. The interaction between rapsyn and AChR subunits could thus be sufficient to enable facilitation of recovery kinetics in fetal $AChR_{\delta R375H}$. Desensitisation, by contrast, could be regulated by another mechanism involving the δR375 residue and might thus not be affected by rapsyn in $AChR_{\delta R375H}$.

4.7 Discussion

This chapter aimed to assess several aspects of the functional relationship between rapsyn and AChRs. Rapsyn is one of the few proteins directly interacting with the AChR (Maimone and Merlie, 1993; Ramarao and Cohen, 1998; Huebsch and Maimone, 2003). Only three other proteins including Src-family kinases (Fuhrer and Hall, 1996), the tumour suppressor protein adenomatous polyposis coli (Wang et al., 2003) and caveolin-3 (Hezel et al., 2010) have been described to bind directly to AChRs and regulate clustering (Jones et al., 2010). No previous studies have investigated the functional effect of a direct interaction of AChRs with other proteins.

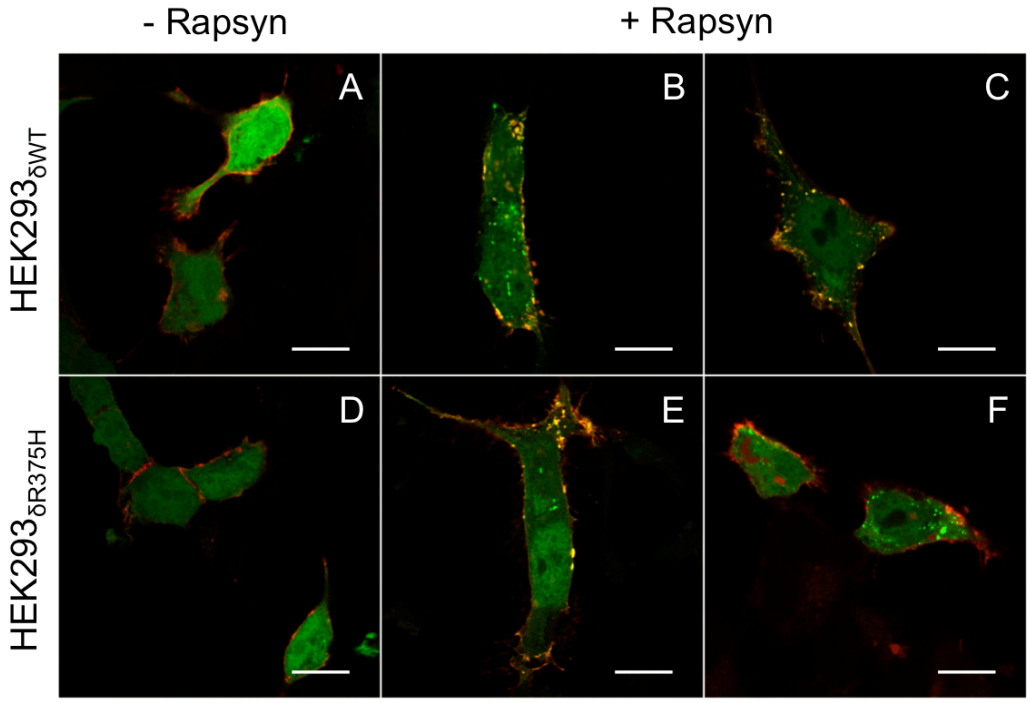


Figure 4-19 The effect of rapsyn on the surface distribution of $AChR_{\delta WT}$ and $AChR_{\delta R375H}$ expressed in HEK293-γ cells

HEK293 cells were transfected with fetal AChR $_{\delta WT}$ (A-C) or fetal $AChR_{\delta R375H}$ (D-F) subunits and either pEGFP-N1 for EGFP expression (A, D) or pEGFP-N1-RAPSN for the expression of EGFP-tagged rapsyn (B, C, E, F). EGFP-tagged rapsyn was used to determine the colocalisation of rapsyn with AChRs. The co-transfection with rapsyn cDNA resulted in a change of AChR distribution (red staining, AF594) from a linear peripheral staining (A, D) to receptor aggregation appearing as small clusters on the surface of HEK293-γ $_{\delta WT}$ (B, C) and of HEK293-γ $_{\delta R375H}$ (E, F). In HEK293-γ $_{\delta R375H}$, however, receptor aggregation was inconsistent despite the co-localisation of rapsyn with $AChR_{\delta R375H}$ showing a more linear peripheral staining in many cells (F). Magnification: 40x, Scale bar = 10 μm.

4.7.1 The impact of rapsyn on AChR distribution on the cell surface

AChR clustering is an essential characteristic of the normal NMJ. Previous studies reported that the co-transfection of heterologous cell lines with cDNA coding for AChR subunits together with rapsyn is sufficient for AChR aggregation (Cossins et al., 2006; Leite et al., 2008). The ability of rapsyn to aggregate AChRs was confirmed in this project by using HEK293 and TE671/CN21 cells. The AChR aggregates were smaller and differed obviously from the large clusters in C2C12 myotubes and the pretzel-shaped array of branches that is characteristic for AChR clusters in muscle cells. AChR aggregation in HEK293 cells and AChR clustering in C2C12 myotubes might thus represent different structural modifications of AChR surface expression. This is supported by experiments based on the δR375H mutation. In HEK293 cells, the failure of $AChR_{\delta R375H}$ to aggregate was not as clearly defined as the failure of $AChR_{\delta R375H}$ to cluster in C2C12 myotubes.

Whole-cell patch clamp experiments revealed higher peak current amplitudes in cells co-transfected with rapsyn, which could be explained by rapsyn decreasing the AChR degradation rate on the cell surface as suggested before (Wang et al., 1999b). In this project, there was no evidence for higher AChR surface expression associated with rapsyn co-transfection using a ^{125}I-BTX binding assay or FACS. The higher peak current amplitudes in cells expressing rapsyn may have resulted from the selective approach to choose cells in patch clamp experiments with a preference for faintly green cells and the use of two vectors with different EGFP expression levels. The impact of rapsyn on AChR conductance, however, remains an intriguing explanation for the increased peak current amplitudes.

4.7.2 The effect of rapsyn on AChR function

An unexpected finding in this project was that rapsyn co-transfection into muscle cells facilitated recovery kinetics of both fetal and adult AChRs. In HEK293 cells, rapsyn facilitated recovery kinetics of fetal AChRs only, and in contrast to TE671/CN21 cells current decay time constants of both fetal and adult AChRs were significantly slower when co-transfected with rapsyn. It can thus be concluded that rapsyn affects fetal and adult AChR function differently depending on intracellular factors, the expression of which might vary between muscle and non-muscle cells. The modulation of AChR function by intracellular factors is well established in literature (Huganir et al., 1986; Middleton et al., 1986; Hopfield et al., 1988; Paradiso and Brehm, 1998), and, as discussed above, differences in posttranslational AChR modification or the interaction of AChRs with other proteins differently expressed in both cell lines could have contributed to the observed variations between TE671/CN21 and HEK293 cells. Alternatively, different membrane lipid compositions between muscle and non-muscle cells could have affected AChR function differently in both cell lines. There is a structural relationship between AChRs and the surrounding lipids, the composition of which was shown to be involved in the modulation of AChR function (Barrantes, 2010; Baenziger et al., 2015; Unwin, 2017). Especially anionic lipids and cholesterol in the cell membrane are crucial for proper AChR function, the absence of which was associated with AChR transition into an uncoupled conformation, which is able to bind agonist but does not undergo a conformational change into the open state (daCosta et al., 2013). AChR isoform specific effects of the lipid composition on desensitisation and recovery from desensitisation have not been examined so far.

To further assess the underlying mechanism for the facilitation of AChR recovery kinetics by rapsyn, experiments were performed on cells expressing the δR375H mutation, a naturally occurring CMS mutation located in the M3-M4 cytoplasmic domain of the δ-subunit close to the phosphorylation site at Y369. This mutation was shown to prevent agrin-dependent AChR clustering in C2C12 myotubes, but when transfected into HEK293 cells, AChRs bearing the δ-mutation still colocalised with rapsyn and were able to form aggregates. In whole-cell patch clamp experiments, rapsyn facilitated recovery kinetics of δ-mutant AChRs suggesting that facilitation of recovery kinetics by rapsyn does not necessarily depend on receptor clustering as usually found in C2C12 myotubes but on the interaction of the AChRs with rapsyn. However, these findings were limited by the obvious differences in AChR aggregation/clustering between HEK293 cells and myotubes, which could have compromised the results. AChR aggregates on HEK293 cells and AChR clusters on C2C12 myotubes are likely to be structurally different, and the δR375H mutation might only affect the structure of the branched clusters that are typical for C2C12 myotubes. Due to their ability to form proper AChR clusters, C2C12 myotubes might thus qualify as a better model to experiment on aspects of NMJ function, but their utilisation for measurements of recovery from desensitisation by whole-cell patch clamping is associated with various methodological problems due to the large cell size and large current amplitudes (Traynelis, 1998; Fu et al., 2011). Moreover, the study of mutant AChRs or proteins involved in AChR clustering is limited by the endogenous expression of the wild-type form of the proteins in C2C12 myotubes.

Chapter 5

Inhibition of AChR function by myasthenia gravis sera

5.1 Introduction

Myasthenia gravis is an autoimmune disorder of the NMJ leading to weakness and increased fatigability. Autoantibodies (Abs) directed against the AChR can be detected in about 80% of cases. They are found to be polyclonal IgG binding to different extracellular epitopes of the receptor (Tzartos et al., 1998; Vincent, 2002). The pathological effect depends on the IgG subclass and on the interaction of the antibodies with the specific AChR epitopes, and act via the following mechanisms:

i) AChR antibodies are typically of the IgG1, and variably IgG3, subclasses that activate complement and lead to lysis of the postsynaptic membrane. This results in a simplification of postsynaptic folds and is associated with a loss of AChRs, various molecules involved in AChR clustering and VGSCs that generate the action potential (Ruff and Lennon, 2008).

ii) Antibodies binding to the main immunogenic region on each of the two α-subunits (Tzartos et al., 1982; Tzartos et al., 1998) increase the degradation rate by AChR cross-linking (Drachman et al., 1978).

iii) Antibodies against the ACh-binding site are characterised by their ability to block the binding of ^{125}I-BTX to AChRs and their potential inhibition of AChR function (Lang et al., 1988; Burges et al., 1990; Bufler et al., 1996b). Not all sera that inhibit ^{125}I-BTX binding block the activation of AChRs by ACh. Those that do inhibit AChR function are rare and their symptomatic contribution remains uncertain (Drachman et al., 1982; Vernet-der Garabedian et al., 1986; Lennon and Griesmann, 1989).

iv) Other antibodies binding to the extracellular domain of the γ-subunit specific to fetal AChRs can inhibit fetal AChR function and be a cause of AMC (Vincent et al., 1995; Riemersma et al., 1996).

Using electrophysiological methods, some of the sera from patients without AChR antibodies in routine diagnostic assays have also been shown to inhibit AChR function (Yamamoto et al., 1991; Barrett-Jolley et al., 1994; Plested et al., 2002; Spreadbury et al., 2005), and it was hypothesised that other circulating factors directly affect AChR function. Some of those sera were identified retrospectively to contain antibodies binding only to AChRs that are clustered on a cell surface (i.e. clustered AChR-Ab) (Leite et al., 2008) or to MuSK (Hoch et al., 2001), which could perhaps have mediated the observed effects. However, most studies identify a proportion of patients whose sera lack any of those antibodies.

5.2 Aims

In the process of reinvestigating previous findings and relating them to the presence of various antibodies, this chapter aimed a comprehensive functional analysis of the effects of sera with AChR-, clustered AChR- or MuSK-Abs, or of sera from SNMG patients without any of those antibodies. Experiments were performed first on unclustered and then on clustered AChRs using CN21 cells in order to asses the effect of rapsyn on current inhibition by MG sera. The proportion of sera in each MG subgroup inhibiting AChR currents was determined and the inhibition of AChR function by the different MG antibodies was electrophysiologically characterised.

5.3 The acetylcholine application protocol

For these experiments, the ACh application protocol consisted of a series of five sweeps (I to V) with two consecutive ACh pulses in each sweep (a "desensitising" pulse of 3 s duration was followed by a "test" pulse of 50 ms duration). The interval between both pulses increased for 250 ms with each sweep (Figure 5-1A). Peak current amplitudes, desensitisation and recovery from desensitisation were analysed as described in the Materials and methods section (Chapter 2.8.5). In each cell, the ACh application protocol was repeated three times corresponding to three trials: i) a "control trial", in which the cell was perfused with extracellular solution only, ii) a "test trial", in which the cell was perfused with extracellular solution in the presence of serum and iii) a "wash-out trial", in which the cell was again perfused with extracellular solution only (Figure 5-1B). Extracellular solution contained (in mM): NaCl 150, KCl 2.8, HEPES 10, $MgCl_2$ 2, $CaCl_2$ 2 and glucose 10 with pH adjusted

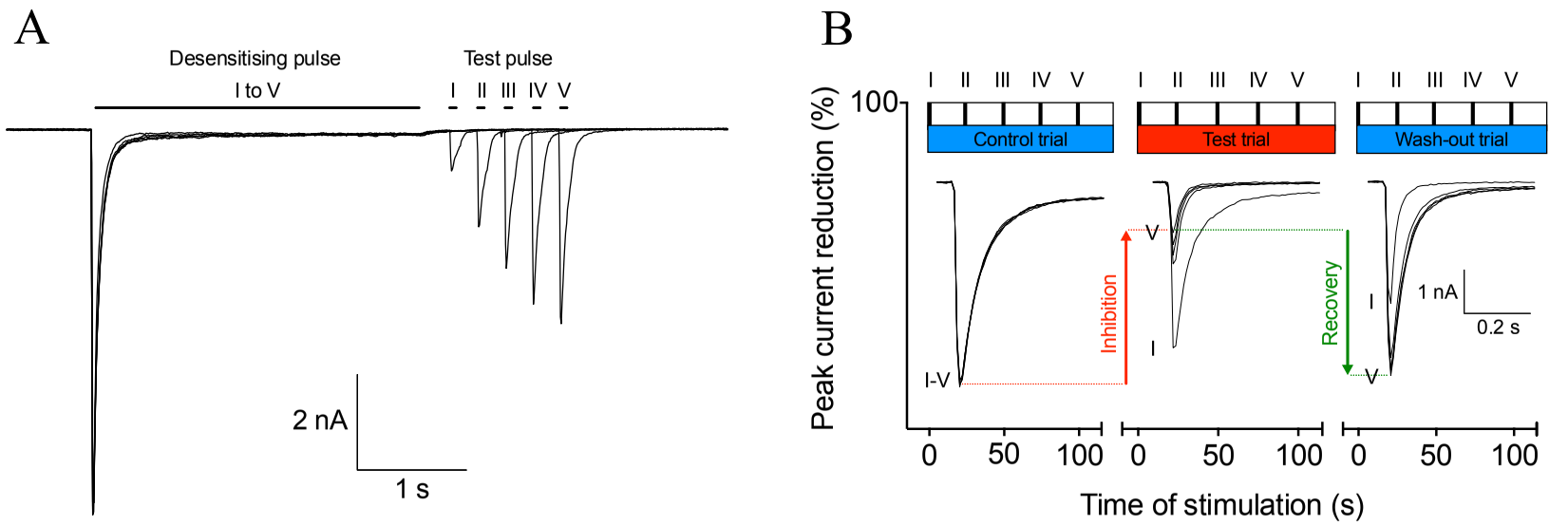


Figure 5-1 Acetylcholine application protocol to test inhibition of AChR currents by MG sera
(A) The ACh application protocol consisted of five sweeps (I to V), each of which included two consecutive pulses of 1 mM ACh: a desensitising pulse of 3 s duration was followed by a test pulse of 50 ms duration, with the interval between both pulses increasing for 250 ms with each sweep. (B) The ACh application protocol was repeated three times on each cell according to three trials: a control trial (i.e. perfusion of cells with extracellular solution only, left blue bar), a test trial (i.e. perfusion of cells with extracellular solution in the presence of serum, red bar) and a wash-out trial (i.e. perfusion of cells again with extracellular solution only, right blue bar). The inlaid current traces display the desensitising pulses of the five sweeps in each trial and show current inhibition by fluoxetine, an open-channel blocker of the AChR. Current inhibition by MG sera was defined by the change of peak current amplitudes of desensitising pulses in the test trial as compared to the control trial (i.e. the difference between stimulation V of the test trial and stimulation V of the control trial, red arrow). Current recovery was defined by the change of peak current amplitudes in the wash-out trial as compared to the test trial (i.e. the difference between stimulation V of the wash-out and stimulation V of the test trial, green arrow).

to 7.4 using NaOH. The pipette solution contained (in mM): NaCl 4, KCl 144, HEPES 10, $MgCl_2$ 2, Mg-ATP 2 and EGTA 10 with pH adjusted to 7.2 using KOH (Table 3-1).

5.4 Serum samples

Serum samples were obtained from MG patients diagnosed by clinical, electromyographic or serological criteria. SNMG patients were included only if the Tensilon test and/or the repetitive stimulation test was positive. All samples were screened for autoantibodies using RIA (testing for AChR-Ab) and cell based assays (CBA, testing for clustered AChR-, MuSK- and LRP4-Ab). According to the antibody status, all sera were grouped into AChR-Ab positive sera (i.e. RIA-positive, n=6), clustered AChR-Ab positive sera (i.e. RIA-negative and CBA-positive, n=5), MuSK-Ab positive sera (i.e. CBA-positive, n=5) and SNMG sera (i.e. CBA-negative for AChR-, MuSK- and LRP4-Abs, n=5). Sera of mothers with infants born with AMC were screened using RIA (n=3). The results were compared to healthy controls (HC, n=5) including three males and two females aged between 33 and 50 years.

5.5 Testing of the effect of MG sera on AChR peak current amplitudes, desensitisation and recovery from desensitisation

AChR current inhibition by MG sera was defined by the change of peak current amplitudes of desensitising pulses in the test trial compared to the control trial (after normalisation of peak current amplitudes in the three trials to the peak current amplitude of stimulation I in the control trial, the difference between stimulation V

of the test trial and stimulation V of the control trial was calculated in per cent, red arrow in Figure 5-1B). The reversibility of AChR current inhibition was defined by the change of current amplitudes in the wash-out trial as compared to the test trial (calculated as the difference between stimulation V of the wash-out trial and stimulation V of the test trial in per cent, green arrow in Figure 5-1B). The effect of MG sera on desensitisation and recovery from desensitisation was also analysed in order to determine their contribution to AChR current inhibition by MG sera. Desensitisation was assessed by the calculation of current decay time constants of desensitising pulses in all three trials (see Materials and methods, Chapter 2.8.5). The effect of MG sera on AChR desensitisation was defined by the difference of current decay time constants between stimulation V of the test trial and stimulation V of the control trial in per cent (after normalisation to the current decay time constant in stimulation I of the control trial). The effect of MG sera on AChR recovery from desensitisation was calculated by the difference of recovery time constants between the test trial and the control trial in ms. The effect of MG sera was compared to the effect of sera from HC, and any current reduction higher than three standard deviations from HC mean values was considered to denote a serum that inhibited AChR function. Each serum was tested on at least three different cells.

5.6 The effect of control agents on AChR whole-cell currents

Experiments with extracellular solution in all three trials were performed to reveal an influence of the perfusion system on current recordings. Different agents (serum, drug or toxin) at specific concentrations were first used as controls in order to assess the suitability and specificity of the setup for detecting inhibition of AChR function.

The open-channel blocker fluoxetine (Garcia-Colunga et al., 1997; Deflorio et al., 2014) and the competitive antagonist α-bungarotoxin (BTX) (Frazier et al., 1998; Vincent et al., 1998) provided positive controls (at a concentration of 10 μM and 50 nM, respectively) in order to evaluate the sensitivity of the experimental setup to detect fast current inhibition. HC sera (diluted 1:20) and albumin as the main protein of human serum (at a concentration of 2.25g/l) were tested as negative controls. Salbutamol that has been demonstrated to be an effective treatment in various CMS (Burke et al., 2013; Rodriguez Cruz et al., 2015b), as discussed earlier in Chapter 3, was also tested. In earlier studies using carbachol-induced $^{22}Na^{+}$ flux to measure AChR function, salbutamol was reported to inhibit AChR function, but the maximal effect was seen at about 20 minutes and tended to diminish at about 30 minutes (Li et al., 1996). In this project, the fast effect of salbutamol (at a concentration of 10 μM) on AChR function was measured. Agent-specific effects on AChR function were determined by comparisons of all control agents with extracellular solution.

5.6.1 The effect of control agents on AChR peak current amplitudes

Fluoxetine and BTX significantly reduced peak current amplitudes (–66.1±0.7% [n=3, $p<0.0001$] and –65.0±11.8% [n=3, $p<0.0001$], respectively, compared to –5.1±1.7% [n=8] using extracellular solution). HC serum (–8.8±1.2%, n=5, ns), albumin (–8.7±5.1%, n=3, ns) and salbutamol (–9.1±2.3%, n=3, ns) had no effect on AChR currents (Figure 5-2). Current inhibition by fluoxetine was reversible, whereas current inhibition by BTX was irreversible during the wash-out trial (Figure 5-2A).

5.6.2 The effect of control agents on AChR desensitisation

Desensitisation was assessed by the calculation of current decay time constants, which varied markedly between different agents (Figure 5-3A). The application of fluoxetine was associated with a significantly shorter mean current decay time constant as expected from an open channel blocker (Deflorio et al., 2014). The mean current decay time constant in the test-trial was –77.5±5.9% shorter than in the control trial using fluoxetine (n=3), compared to –14.3±9.7% using extracellular solution (n=8), p=0.0043. HC sera (17.5±18.7%, n=5, ns), albumin (22.0±5.6%, n=3, ns), salbutamol (9.8±3.9%, n=3, ns) and BTX (–10.0±21.8%, n=3, ns), by contrast, were not associated with a significant change of current decay time constants (Figure 5-3B).

5.6.3 The effect of control agents on AChR recovery from desensitisation

Similar to current decay time constants, recovery from desensitisation varied markedly between different agents (Figure 5-4A). Only fluoxetine was associated with significantly longer recovery time constants. The mean recovery time constant in the test-trial was 37.3±20.9% longer than in the control trial using fluoxetine (n=3), compared to –4.3±6.5% using extracellular solution (n=8) (p=0.0283). HC sera (–6.9±4.6%, n=5, ns), albumin (25.4±22.3%, n=3, ns), salbutamol (21.5±30.6%, n=3, ns) and BTX (–30.3±13.5%, n=3, ns), by contrast, were not associated with a significant change of recovery time constants (Figure 5-4B).

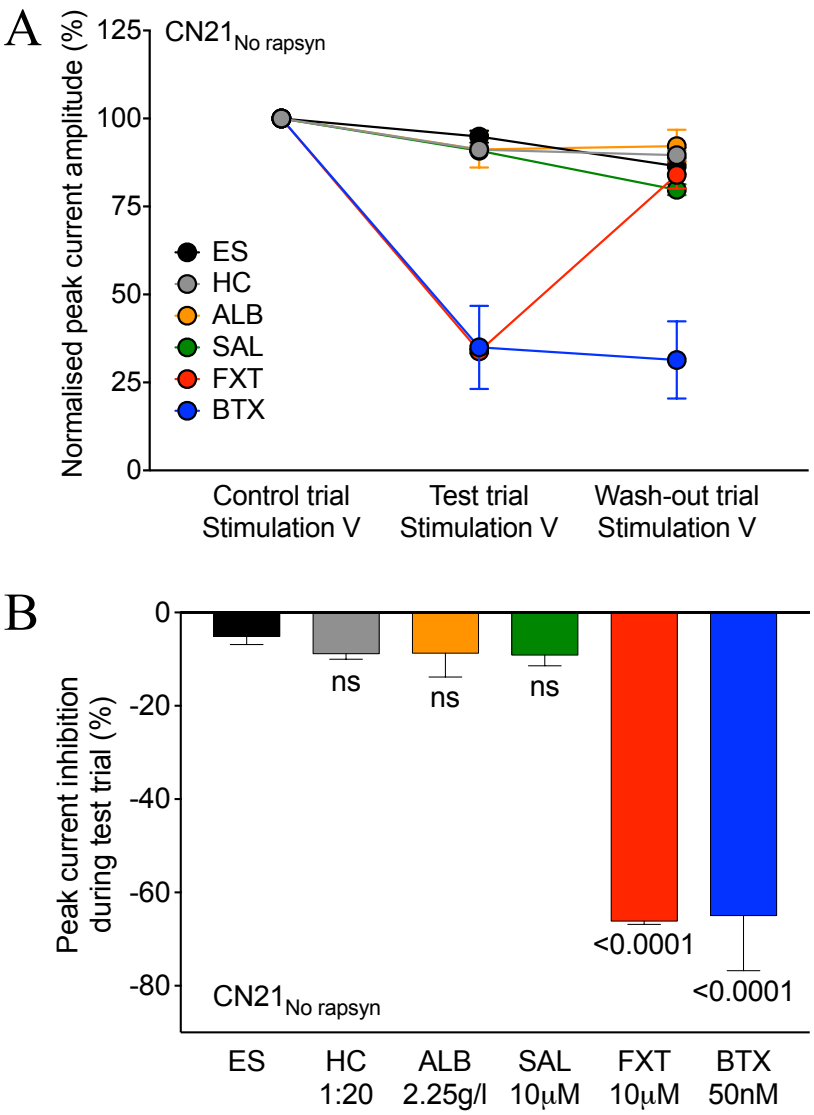


Figure 5-2 The effect of control agents on AChR whole-cell currents
The effect of different control agents on AChR whole-cell currents was tested in CN21 cells predominantly expressing adult AChRs. The mean current amplitudes of the different control agents in the test and wash-out trial normalised to the control trial are displayed in (A). Only fluoxetine and BTX significantly reduced AChR peak current amplitudes compared to extracellular solution, whereas HC serum, albumin and salbutamol had not effect on AChR current amplitudes (B). Current inhibition by fluoxetine was reversible, whereas current inhibition by BTX was irreversible (A). Each agent was tested on at least three different cells. Unpaired t-test.
ES, extracellular solution; HC, healthy control sera; FXT, fluoxetine; BTX, α-bungarotoxin; ALB, albumin; SAL, salbutamol.

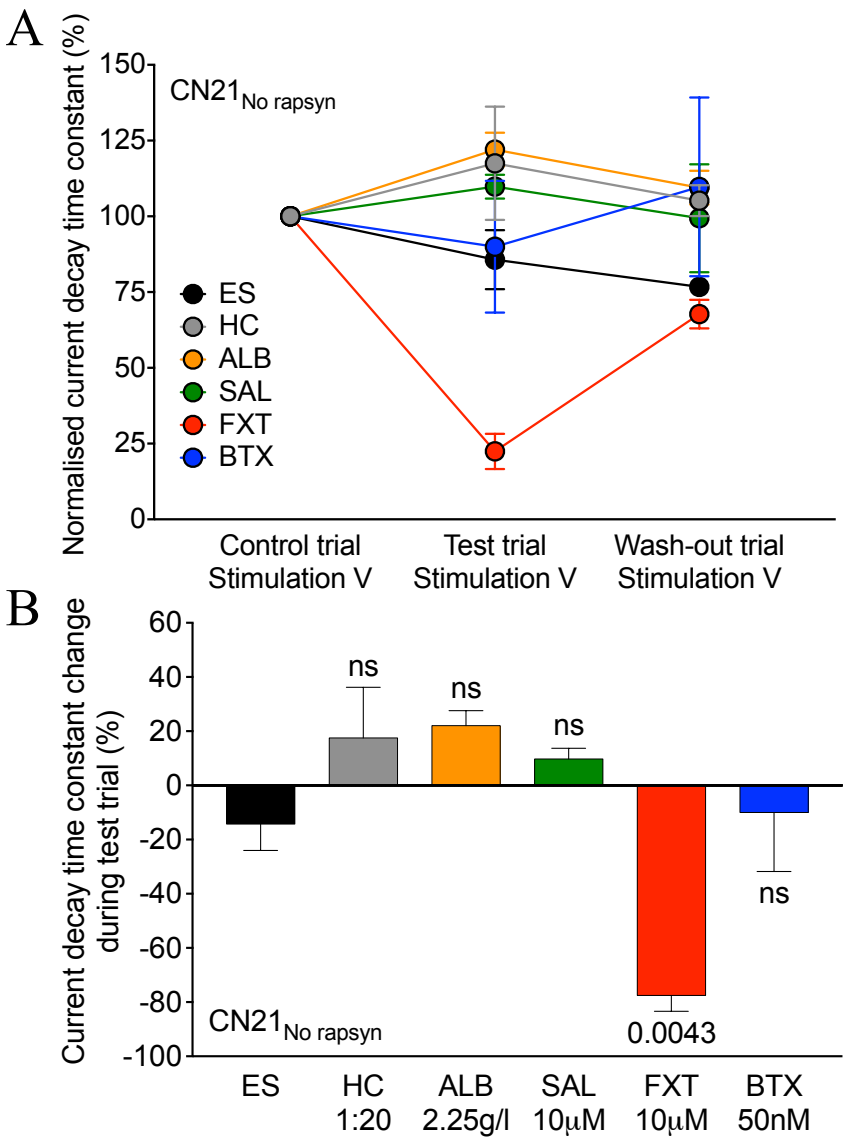


Figure 5-3 The effect of control agents on AChR desensitisation
Current decay time constants were derived by fitting one or two exponential components to the current decay phase of desensitising pulses applied to CN21 cells. The effect of control agents on current decay time constants and their reversibility are displayed in (A). Only fluoxetine was associated with significantly shorter current decay time constants compared to experiments obtained by perfusion with extracellular solution (B). Current decay time constants varied markedly between groups but also between cells within a group. Each agent was tested on at least three different cells. Unpaired t-test.
ES, extracellular solution; HC, healthy control sera; FXT, fluoxetine; BTX, α-bungarotoxin; ALB, albumin; SAL, salbutamol.

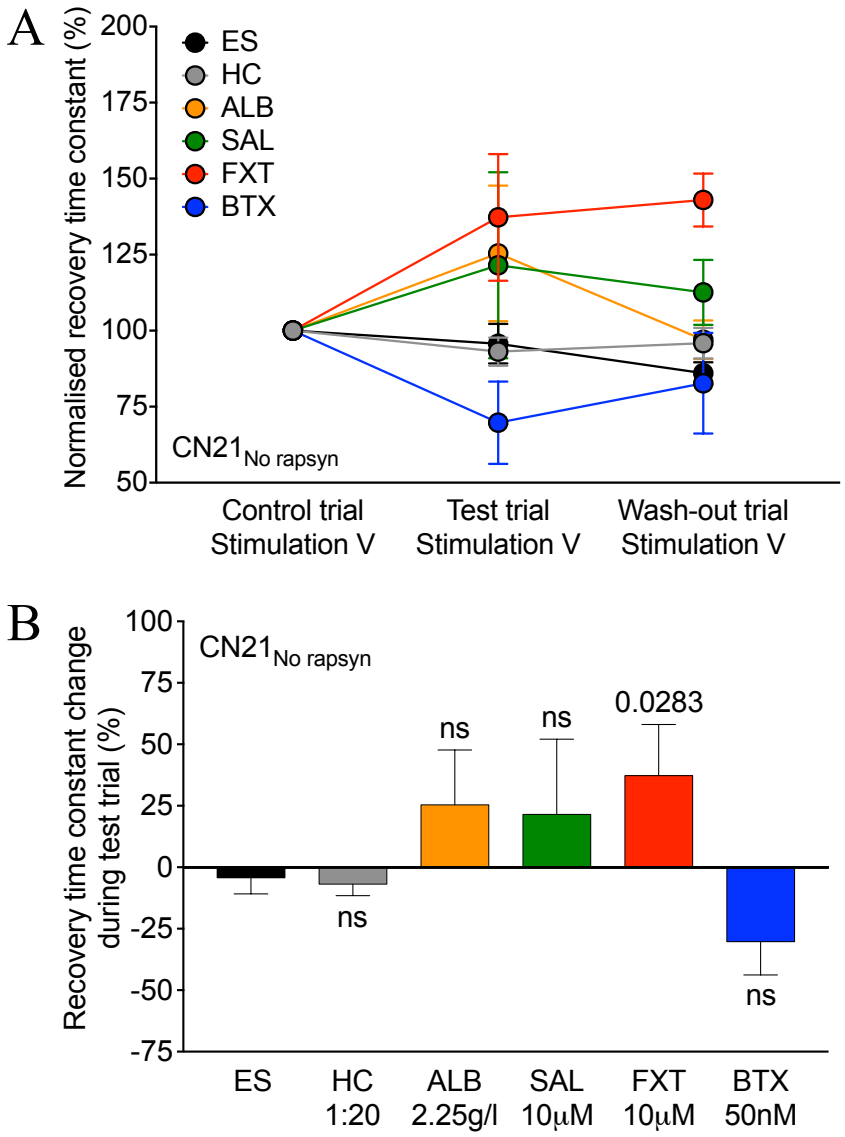


Figure 5-4 The effect of control agents on AChR recovery from desensitisation

Recovery time constants in the test and wash-out trial normalised to the control trial are displayed in (A). The change of recovery from desensitisation during the perfusion with control agents was calculated as the difference between recovery time constants in the test and control trial. Only fluoxetine was associated with significantly longer recovery time constants (B). Recovery time constants varied markedly between groups but also between cells within a group. Each agent was tested on at least three different cells. Experiments were performed on CN21 cells. Unpaired t-test.

ES, extracellular solution; HC, healthy control sera; FXT, fluoxetine; BTX, α-bungarotoxin; ALB, albumin; SAL, salbutamol.

5.7 AMC sera inhibit fetal AChR function only

CN21 cells without rapsyn (predominantly expressing unclustered adult AChRs) and TE671 cells with and without rapsyn (expressing clustered and unclustered fetal AChRs, respectively) were used to confirm and further analyse the effect of AMC sera on AChR whole-cell currents. Adult AChR current inhibition by AMC sera was similar to that of HC serum in CN21 cells (mean current inhibition of –3.8±5.8% in HC serum [n=3 cells] and –4.5±1.3% in AMC1 [n=3 cells, ns], –2.3±3.3% in AMC2 [n=3 cells, ns] and –11.9±4.2% in AMC3 [n=3 cells, ns]). Fetal AChR currents, by contrast, were significantly inhibited by 3/3 AMC sera in TE671 cells with rapsyn (mean current inhibition of –6.5±1.5% in HC serum [n=3 cells] and –22.2±3.0% in AMC1 [n=5 cells, p=0.0086], –88.9±4.1% in AMC2 [n=3 cells, p<0.0001] and –80.6±13.3% in AMC3 [n=3 cells, p=0.0052]), and by 2/3 AMC sera in TE671 cells without rapsyn (mean current inhibition of –5.7±3.7% in HC serum [n=3 cells] and –18.3±8.6% in AMC1 [n=5 cells, ns], –77.0±4.9% in AMC2 [n=3 cells, p=0.0003] and –73.3±12.9% in AMC3 [n=3 cells, p=0.0072]) (Figure 5-5A). Current inhibition was similar between unclustered and clustered fetal AChRs (–49.3±10.2% and –56.3±10.5%, respectively; ns) (Figure 5-5B) and irreversible during the wash-out trial (Figure 5-5C).

5.8 AChR current inhibition by MG sera depends on receptor clustering

Finally, having established the appropriateness of the methodology to show differences in direct current inhibition and in desensitisation characteristics between different substances, MG sera were tested on CN21 cells expressing unclustered

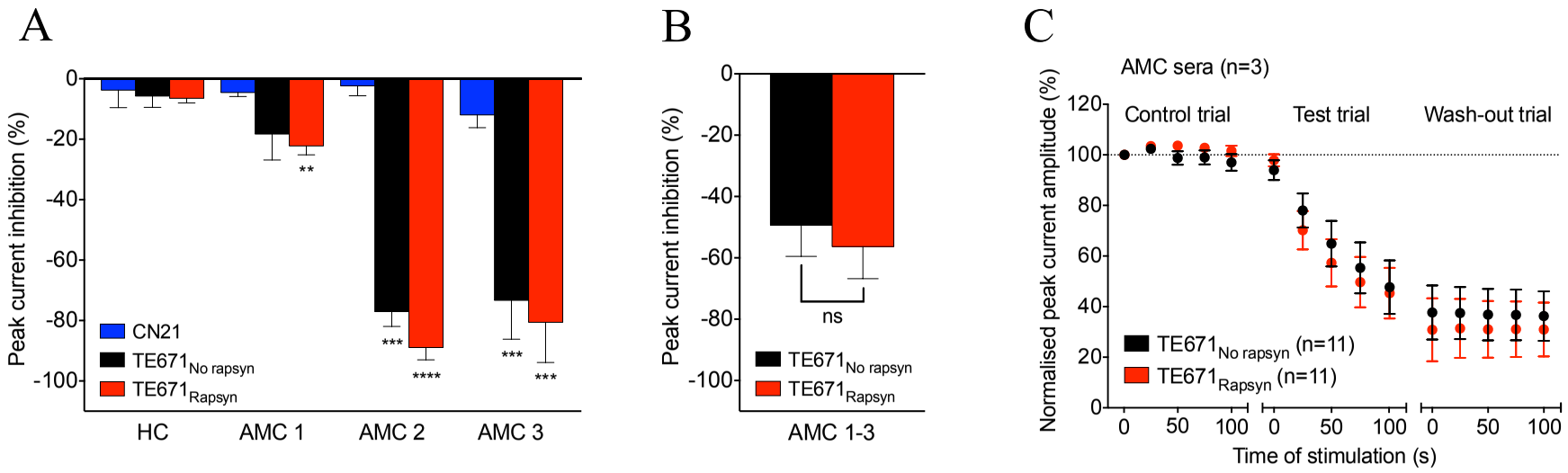


Figure 5-5 Fetal and adult AChR current inhibition by AMC sera

The effect of three AMC sera on fetal and adult AChR function was tested and compared to the effect of serum from a HC. AChR whole-cell currents were inhibited by 2/3 AMC sera in TE671 cells without rapsyn and by 3/3 AMC sera in TE671 cells with rapsyn (A). By contrast, no effect could be observed using CN21 cells predominantly expressing unclustered adult AChRs. Whole-cell current inhibition was similar between TE671 cells with (AMC1-3, n=11 cells) and without rapsyn (AMC1-3, n=11 cells) (B, C). Current inhibition was irreversible during the wash-out trial (C). Sera were diluted 1:20 in extracellular solution. Unpaired t-test.

AChRs and on CN21 cells co-transfected with rapsyn to enable receptor clustering. These cells, therefore, expressed adult AChRs in both unclustered and clustered forms. The mean inhibition of whole-cell currents by five HC sera was –8.8±2.7% in unclustered AChRs and –8.0±4.1% in clustered AChRs (mean±SD). Any whole-cell current inhibition higher than three standard deviations from HC mean values by MG sera was considered to denote significant current inhibition. Unclustered AChR currents were inhibited by 2/6 AChR-Ab positive sera, by 1/5 clustered AChR-Ab positive serum, by 1/5 MuSK-Ab positive serum and by 2/5 SNMG sera (Figure 5-6A). The effect on clustered AChRs was more specific. Clustered AChR currents were inhibited by none of the MuSK-Ab positive or SNMG sera (in which the lack of Abs directed against AChRs was confirmed by CBAs performed by Dr. Akiko Nagaishi) but by 2/6 AChR-Ab positive sera (one of which also inhibited unclustered AChR currents) and by 4/5 clustered AChR-Ab positive sera (one of which also inhibited unclustered AChR currents) (Figure 5-6B and 5-7). In clustered AChR-Ab positive sera inhibiting AChR currents (n=4 sera), the effect on clustered AChRs was stronger compared to unclustered AChRs (–30.3±3.9% in CN21 cells with rapsyn and –15.3±4.4% in CN21 cells without rapsyn, p=0.0174), whereas the effect of AChR-Ab positive sera inhibiting AChR currents (n=3 sera) was similar when tested on unclustered and clustered AChRs (–18.8±3.7% in CN21 cells with rapsyn and –19.1±4.2% in CN21 cells without rapsyn, ns) (Figure 5-8). Current inhibition was not fully reversible upon wash-out of sera. Desensitisation and recovery from desensitisation were not significantly different between MG sera that inhibited AChR function and HC sera.

Since typical AChR-Abs and clustered AChR-Abs can both bind to clustered

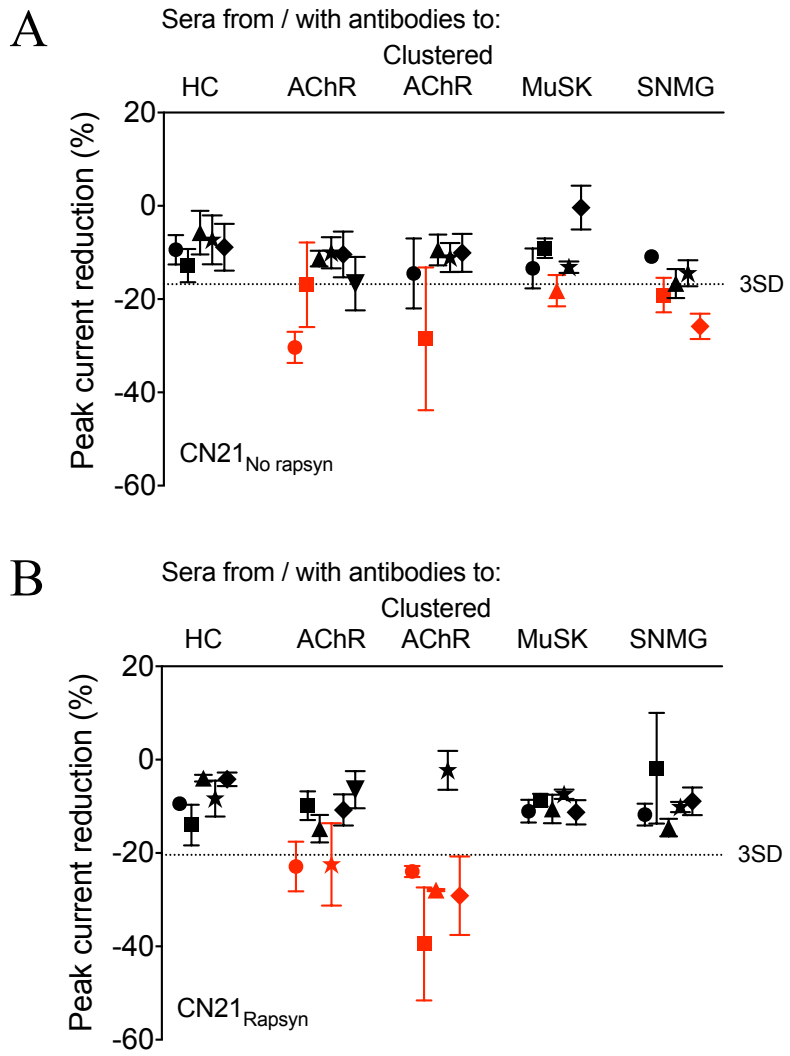


Figure 5-6 AChR whole-cell current inhibition by different MG sera
A total of twenty-six different sera were tested (five healthy control sera, six AChR-Ab positive sera, five clustered AChR-Ab positive sera, five MuSK-Ab positive sera and five SNMG sera). Individual sera tested on at least three CN21 cells expressing unclustered (A) and clustered AChRs (B) are characterised by the same symbols. The effect on clustered AChRs was more specific with sera only in the AChR-Ab and clustered AChR-Ab group inhibiting clustered AChR currents. Each symbol in (A) and (B) represents the mean±SEM of at least three experiments on different CN21 cells. Red symbols denote sera with current inhibition >3 SD of the mean current inhibition exhibited by the five healthy control sera. Sera were diluted 1:20 in extracellular solution.

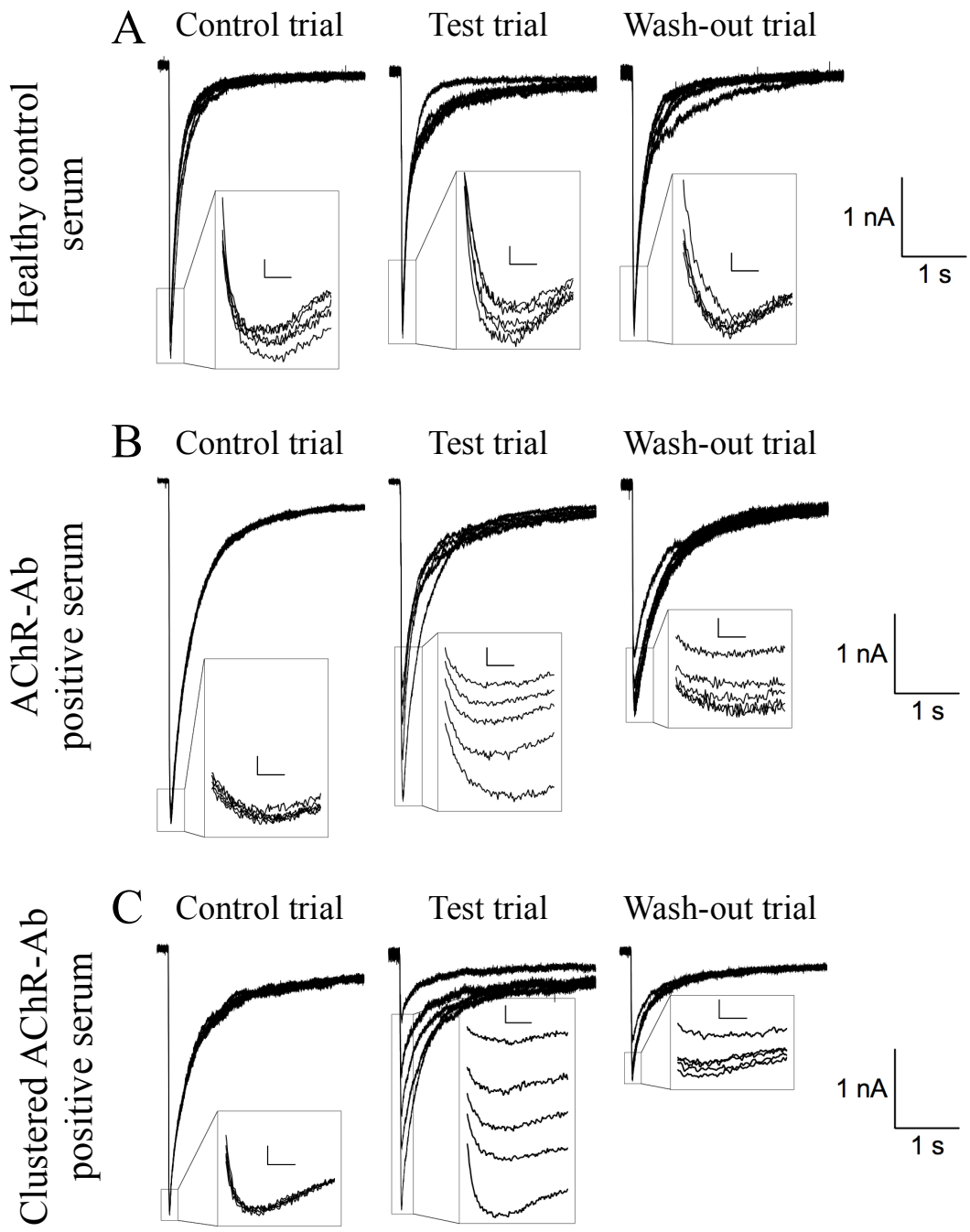


Figure 5-7 The effect of three sera on AChR whole-cell currents
The recordings were made during the desensitising ACh pulse of the five sweeps in each trial, and the effect of a HC serum (A), an AChR-Ab positive serum (B) and a clustered AChR-Ab positive serum (C) was assessed during the test trial in CN21 cells co-transfected with rapsyn. The inlaid traces display the corresponding peak current region of each sweep on an expanded time base (scale bar = 10 ms, 200 pA). Current inhibition was –9.9% by the HC serum, –38.6% by the AChR-Ab positive serum and –74.3% by the clustered AChR-Ab positive serum.

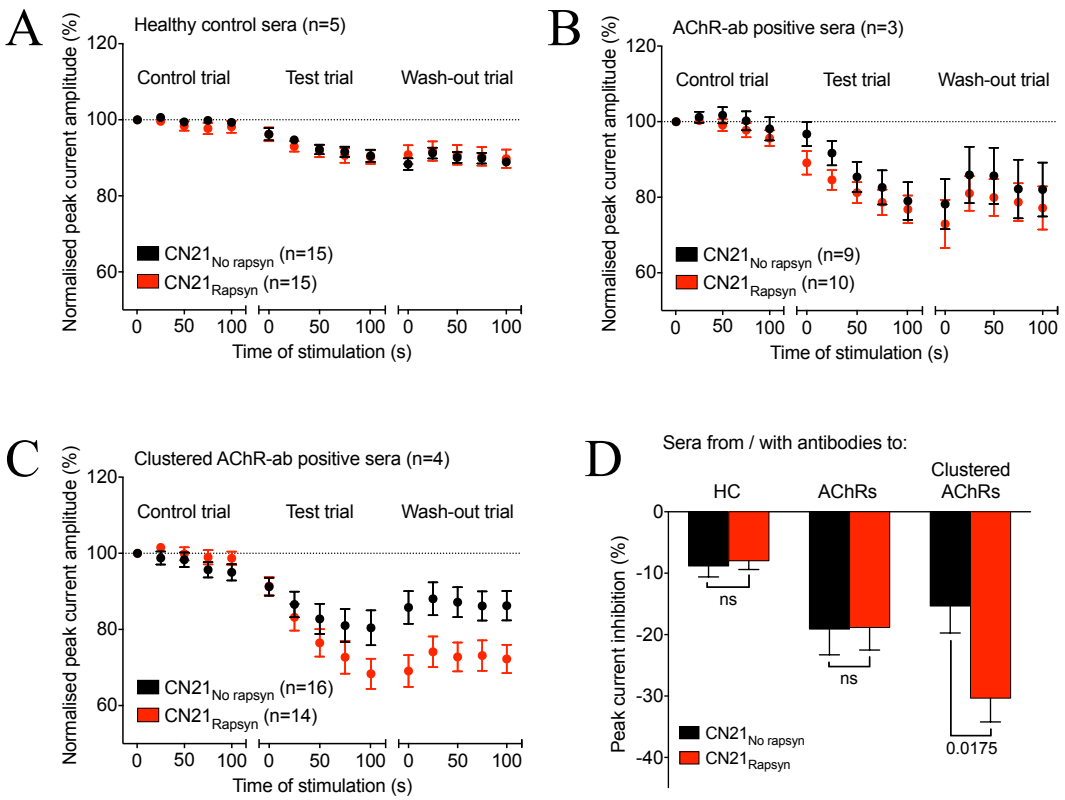


Figure 5-8 AChR current inhibition by AChR-Ab and clustered AChR-Ab positive sera in dependence of receptor clustering

In HC sera (5 sera tested on 15 cells), there was no difference between mean current amplitudes in unclustered and clustered AChRs (A). 3/6 sera in the AChR-Ab group (B) and 4/5 sera in the clustered AChR-Ab group inhibited unclustered and/or clustered AChR currents. In the AChR-Ab group, current inhibition of unclustered (n=9) and clustered AChRs (n=10) was similar but clustered AChR-Ab positive sera inhibited clustered AChR currents significantly stronger compared to unclustered AChRs (n=16 CN21 cells without rapsyn and n=14 cells with rapsyn) (D). Only sera inhibiting unclustered and/or clustered AChR currents were considered in B-D. Unpaired t-test.

AChRs, the results from the two subtypes were pooled. The results showed that 6/11 AChR-Ab positive sera (2 AChR-Ab positive and 4 clustered AChR-Ab positive sera) inhibited function of clustered AChRs compared with only 3/11 on unclustered AChRs. AChR antibodies thus more often inhibited AChRs when they were clustered, although the difference was not significant (p=0.3870, Fisher's exact test).

5.9 Discussion

This chapter was aimed to evaluate the fast effects of different MG sera on AChR function. A total of twenty-four MG sera covering the whole disease spectrum were tested on both cells expressing unclustered and clustered AChRs. The use of clustered AChRs in a functional assay on the effect of MG sera is novel and seems crucial taking into account the subset of antibodies binding only to AChRs that are clustered on a cell surface (Leite et al., 2008).

5.9.1 The effect of AChR-Ab and clustered AChR-Ab positive sera on AChR function

It is well established in literature that AChR-Ab positive sera as well as monoclonal antibodies directed against the ACh binding site of the receptor (i.e. the WF6 mAb specifically binding to the α-subunit (Fels et al., 1986)) can inhibit AChR function (Burges et al., 1990; Bufler et al., 1996b; Riemersma et al., 1996; Bufler et al., 1998; Krampfl et al., 2002). Antibodies directed against other extracellular AChR epitopes (i.e. the WF20 mAb binding distant from the ACh binding site), by contrast, have not been associated with current inhibition (Bufler et al., 1996b). Together, these

findings suggest competitive antagonism as a likely mechanism underlying AChR current inhibition by MG sera. This is further supported by experiments, in which current inhibition by IgG purified from AChR-Ab positive MG patients correlated to the block mediated by α-bungarotoxin (Jahn et al., 2000). In both, the effect was reversible but proceeded to irreversible inhibition of AChR function with time (i.e. after two minutes incubation). This corresponds well with the data in this chapter revealing irreversible current inhibition by AChR-Ab and clustered AChR-Ab positive sera after 125 seconds incubation. It was hypothesised that the binding of specific antibodies to AChRs might proceed in several stages from low-affinity reversible inhibition to higher-affinity irreversible inhibition of AChR function (Jahn et al., 2000), which could be mediated by conformational changes of the AChR induced by the antibodies (such as desensitisation). The effect of MG sera on desensitisation was evaluated by analyses of current decay time constants in this project revealing no significant difference between MG and HC sera, but experiments on more sera and cells might be necessary to increase the statistical power in order to reveal more subtle modifications of desensitisation.

5.9.2 The effect of AMC sera on AChR function

Sera from mothers of affected infants with AMC have been shown to be specific to the fetal AChR isoform and to block its function after an incubation time of 40 minutes (Riemersma et al., 1996). In this project, current inhibition of the fetal AChR isoform by AMC sera was more extensive than for other MG sera and occurred within seconds. The effect was irreversible and current decay was not altered. These results confirm the earlier studies and demonstrate how fast the

binding of these highly specific antibodies is to their antigenic targets on the fetal AChR.

5.9.3 Clinical relevance of current inhibition by AChR-Ab and clustered AChR-Ab positive sera

The pathogenic effect of clustered AChR antibodies was previously reported to be mediated by IgG1 that activate complement, which was shown to occur on the surface of clustered AChR-expressing cells and to some extent after passive transfer of the antibodies to mice (Jacob et al., 2012). Potential inhibitory effects of these antibodies were not explored. Here, it was found that the majority of clustered AChR-Ab positive sera (4/5) inhibited AChR function, and more than the typical AChR antibodies. The observation of fast AChR current inhibition in AChR-Ab positive sera may help to understand some clinical phenomena in MG patients, such as the rapid fluctuations of muscle weakness and the rapid recovery of muscle strength after therapeutic plasma exchange (Gilhus and Verschuuren, 2015).

5.9.4 The effect of AChR-Ab negative MG sera on AChR function

In SNMG and MuSK-Ab positive sera, the lack of AChR antibodies was confirmed by both RIAs and CBAs. Only a few AChR-Ab negative MG sera were found to inhibit AChR function (1/5 MuSK-Ab positive and 2/5 SNMG sera, overall 3/10). The effect was irreversible after 125 seconds incubation and current decay time constants were not significantly different compared to HC sera. These sera may have

contained AChR antibodies that were not identified appropriately by any of the routine techniques (RIA and CBAs).

Inhibition of AChR function by SNMG plasma was reported before by the host laboratory and others (Yamamoto et al., 1991; Barrett-Jolley et al., 1994; Bufler et al., 1998; Plested et al., 2002; Spreadbury et al., 2005). The effect was initially shown to co-purify with the non-IgG fraction (Spreadbury et al., 2005) and the IgM fraction (Yamamoto et al., 1991; Plested et al., 2002), respectively. Based on the observation that SNMG plasma acts on channels protected within cell-attached patches, it was hypothesised that SNMG plasma may induce AChR phosphorylation and indirectly inhibit AChR function (Plested et al., 2002). An indirect mechanism was also suggested by another study showing that AChR whole-cell current inhibition was rescued by EGTA in the pipette solution (Barrett-Jolley et al., 1994). A more recent study, by contrast, failed to show an influence of different second messenger inhibitors on AChR current inhibition by SNMG plasma, and it was concluded that AChR current inhibition is mediated directly by antibodies present in SNMG sera (Spreadbury et al., 2005). The same plasma as well as other samples used in those studies, however, turned out to contain antibodies directed against clustered AChRs when tested retrospectively using CBAs, which complicates the interpretation of those results. Only few, if any, of the original samples studied in these publications are still available.

In this project, current inhibition by MG sera without AChR antibodies could not be observed in cells expressing clustered AChRs, which was established by the co-transfection of cells with rapsyn cDNA (as coded by pIRES2-RAPSN-EGFP). It remains unclear how the interaction between rapsyn and AChRs with consequent

AChR clustering can prevent current inhibition by the few MG sera without detectable AChR antibodies. One explanation could be that other circulating factors present in those sera inhibit AChR currents by their interaction with AChR epitopes available for binding only when the receptors are unclustered. Clustering of the receptors could then block the access of circulating factors to the epitopes and prevent inhibition of AChR function. However, the biological significance of current inhibition of unclustered AChRs may be limited because AChRs are usually clustered at the NMJ. The use of cells expressing clustered AChRs could thus help to improve the sensitivity as well as the specificity of functional assays on MG sera in future studies.

Chapter 6

Functional characterisation of the αL251R mutation found in a patient with congenital myasthenic syndrome

---

6.1 Introduction

The mutation was found in a female patient, now 14-year-old, with predominant bilateral fatigable ptosis and restriction of upgaze and lateral gaze in both eyes. She had no obvious muscle weakness in the upper and lower limbs and could walk for about forty minutes but would start to fatigue thereafter. Chewing or swallowing difficulties were not present. As an infant, her facial expression was reduced and feeding difficulties, dribbling and mild motor delay was reported. A muscle MRI was normal and a muscle biopsy showed mild myopathic changes but was non-diagnostic. Electromyography showed decrement, jitter and block suggesting a disorder of neuromuscular transmission. Mutations were excluded for most CMS genes (including CHRNB1, CHRNE, CHRND, DOK7, RAPSN, DPAGT1, GFPT1) but a single heterozygous de-novo mutation (not present in either mother or father) predicted to be pathogenic was identified in CHRNA1 (c.812T>G, p.αLeu251Arg, from here on referred to as αL251R).

The αL251 residue lies within the second transmembrane (M2) domain at the 9' position of the muscle AChR (L9') and is highly conserved across species and paralogues (Lester, 1992). (The 9' position corresponds to the consensus numbering

system of Miller, in which position 1' refers to the cytoplasmic end of the M2 domain (Miller, 1989). This consensus numbering system is used for comparisons with other Cys-loop ligand-gated ion channels in this chapter). The L9' occupies a kink in each of the five AChR subunits pointing into the closed channel (Unwin, 1995). Upon receptor activation, the M2 transmembrane domains rotate so that the L9' residues no longer occlude the conduction pathway (Miyazawa et al., 2003). In α_7 neuronal AChRs, the substitution of L9' by both polar and hydrophobic amino acids was shown to result in slower desensitisation kinetics and increased sensitivity to agonist, but only substitutions with polar amino acids were also associated with a change of inward rectification, which is characteristic for neuronal AChRs, into a linear I-V relationship (Revah et al., 1991). These findings are supported by studies on muscle AChRs, reporting that substitutions of L9' by the polar amino acids serine (Labarca et al., 1995) or threonine (Filatov and White, 1995) in each of the five subunits slow desensitisation and independently increase sensitivity to ACh. The substitution of L9' by charged amino acids has not been examined so far.

6.2 Aims

The aim of this chapter was to reveal the pathomechanism of CMS with the underlying αL251R mutation. Surface expression of mutant AChRs was analysed using HEK293 cells, and single-channel and whole-cell patch clamp experiments were performed to assess the functional impact of the αL251R mutation. All results were compared to wild-type adult AChRs.

6.3 Transfection of HEK293 cells for the expression of wild-type and mutant AChRs

Human muscle AChR αWT-, β-, δ- and ε-subunit cDNA in a ratio of 2:1:1:1 were transfected into HEK293 cells for wild-type adult AChR expression (referred to as $AChR_{\alpha WT}$, Figure 6-1A), αL251R-, β-, δ- and ε-subunit cDNA in a ratio of 2:1:1:1 was used for mutant AChR expression (referred to as $AChR_{\alpha L251R}$, Figure 6-1B) and αWT-, αL251R-, β-, δ- and ε-subunit cDNA in a ratio of 1:1:1:1:1 was used to express a mixture of AChRs with two αWT-subunits, with two αL251R-subunits and with one αWT- and one αL251R-subunit (Figure 6-1) (referred to as $HEK293_{\alpha WT/\alpha L251R_Mix}$ emphasising the expression of AChRs with a mixed range of subunit stoichiometries. Correspondingly, $HEK293_{\alpha WT}$ referred to HEK293 cells expressing $AChR_{\alpha WT}$ only, and $HEK293_{\alpha L251R}$ referred to HEK293 cells expressing $AChR_{\alpha L251R}$ only). The expression of both αWT- and αL251R-subunits in HEK293 cells represented the in vivo AChR expression in the heterozygous status with a mixed range of subunit stoichiometries. Theoretically, this would result in the expression of 25% $AChR_{\alpha WT/\alpha WT}$, 25% $AChR_{\alpha WT/\alpha L251R}$, 25% $AChR_{\alpha L251R/\alpha WT}$ and 25% $AChR_{\alpha L251R/\alpha L251R}$ in individual cells (Figure 6-1). These fractions, however, can vary if the surface expression of AChRs bearing the αL251R mutation is reduced.

6.4 The acetylcholine application protocol

Peak currents and desensitisation were measured by the application of desensitising pulses (see Materials and methods, Chapter 2.8.5). Deactivation was assessed by the analysis of the current decay phase at the end of the desensitising

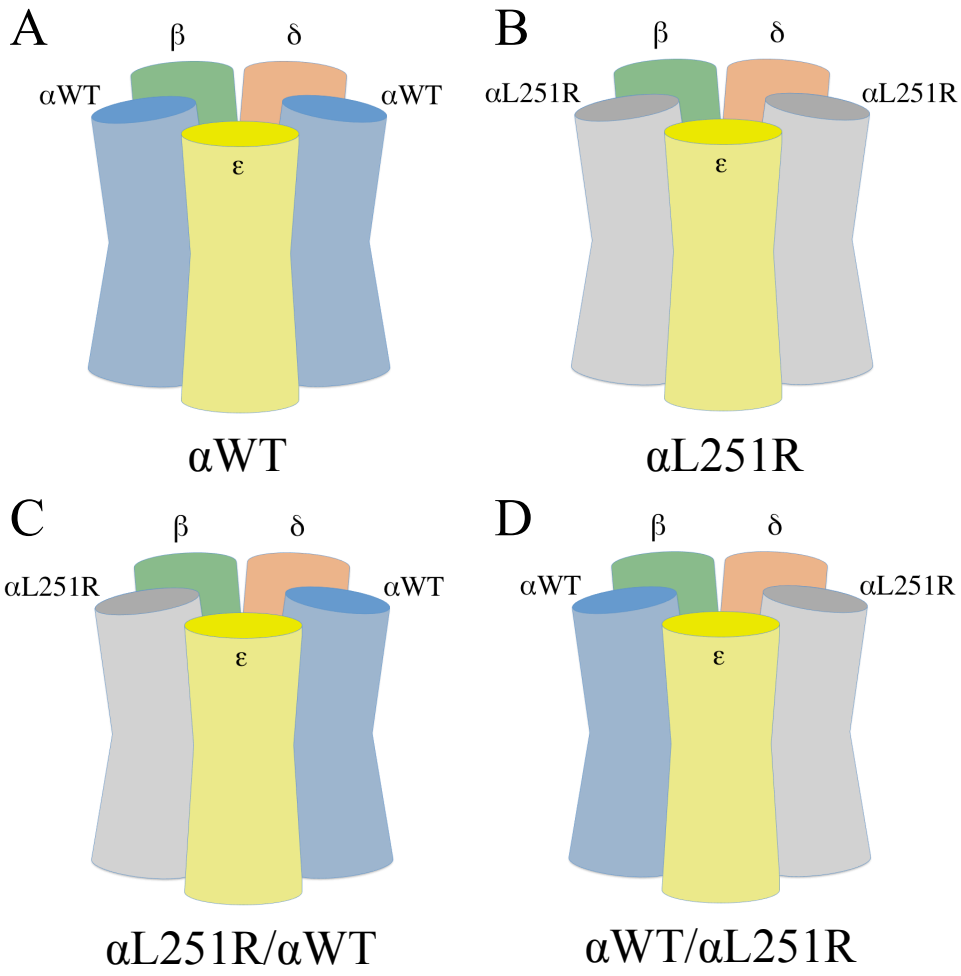


Figure 6-1 Different AChR subunit stoichiometries resulting from the heterozygous αL251R status of the CMS patient
Due to the heterozygous status of the CMS patient, a mixed range of subunit stoichiometries in AChRs can be expected including wild-type AChRs (i.e. αWT, A), mutant AChRs bearing the L251R mutation in both α-subunits (i.e. αL251R, B) and mutant AChRs bearing the L251R mutation in only one α-subunit (αL251R/αWT and αWT/αL251R in C and D, respectively). All four AChR stoichiometries are expected to be present in the patient (referred to as αWT/αL251R$_{Mix}$). αWT-, αL251R-, β-, δ- and ε-subunits are coloured blue, grey, green, orange and yellow, respectively.

pulse, when ACh application was stopped, and could be fitted with one single exponential (Figure 6-2A). All recordings were made at a holding potential of −60 mV.

The application protocol for the I-V curves contained 11 sweeps of 10 s duration with the holding potential ranging from –100 mV to +100 mV by 20 mV steps (Figure 6-2B). AChR stimulation in each sweep was performed by the application of 1 mM ACh for 50 ms. The rectification index (RI) was calculated as the peak current at positive holding potentials divided by the peak current at corresponding negative holding potentials. A RI < 1 indicates inward rectification, a RI = 1 indicates a linear I-V relationship and a RI > 1 indicates outward rectification. Extracellular solution contained (in mM): NaCl 150, KCl 2.8, HEPES 10, $MgCl_2$ 2, $CaCl_2$ 2 and glucose 10 with pH adjusted to 7.4 using NaOH. The pipette solution contained (in mM): NaCl 4, KCl 144, HEPES 10, $MgCl_2$ 2, Mg-ATP 2 and EGTA 10 with pH adjusted to 7.2 using KOH (Table 3-1). Data from experiments that tested different concentrations of chloride or sodium were corrected for liquid junction potentials using pClamp 10.

6.5 Surface expression of mutant AChRs is reduced

The impact of the αL251R mutation on receptor surface expression was tested by transfection of cDNAs encoding the corresponding AChR subunits into HEK293T cells and counting AChR-binding of radioactive ^{125}I-BTX. Surface expression of $HEK293T_{\alpha WT/\alpha L251R_Mix}$ was robust at 72.7% of $HEK293T_{\alpha WT}$ (42706±8196 cpm in $HEK293_{\alpha WT/\alpha L251R_Mix}$ [n=5] and 58751±7548 cpm in $HEK293T_{\alpha WT}$ [n=5], ns), whereas surface expression of $HEK293T_{\alpha L251R}$ was depressed at 29.0% of

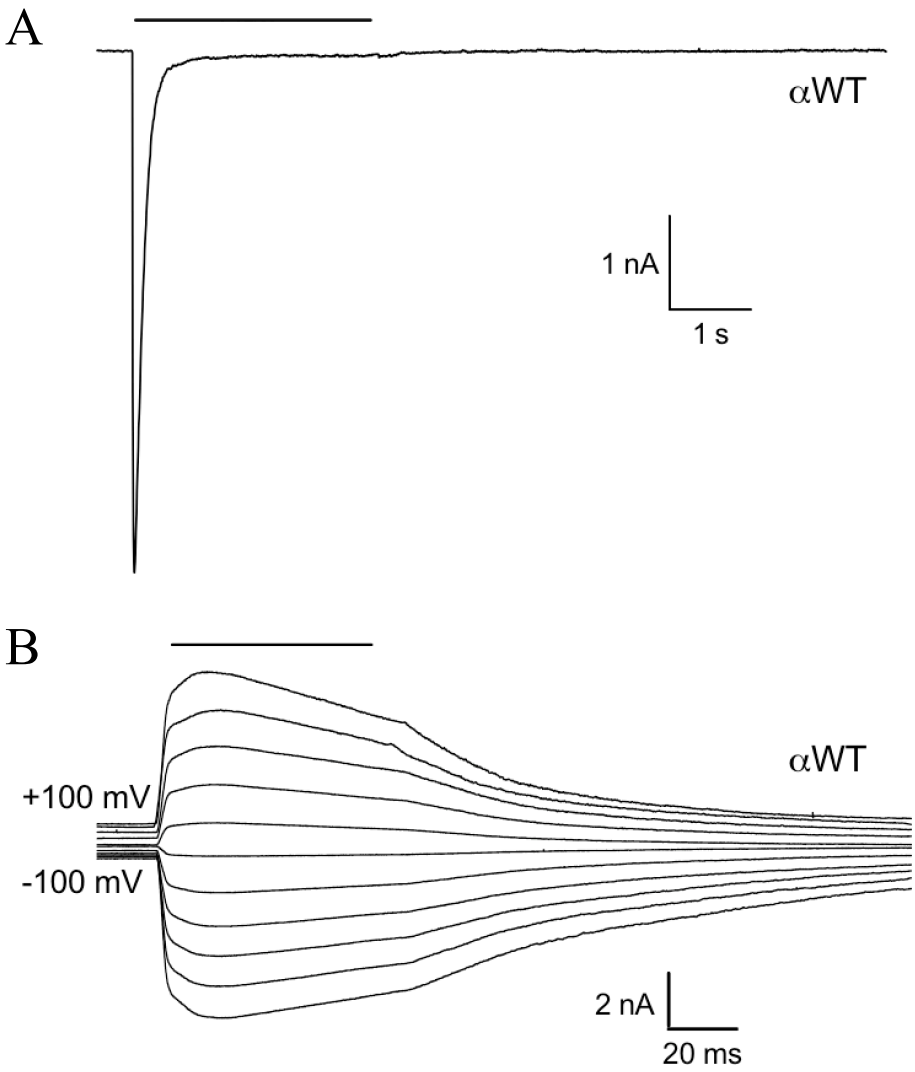


Figure 6-2 Acetylcholine application protocols
Both traces were recorded from HEK293 cells expressing adult AChRs. (A) Peak current and desensitisation were assessed during the application of a 3 s ACh pulse (bar in A), whereas deactivation was measured at the end of the pulse, when the AChR current returned to the baseline as a result of ACh wash-out. (B) The I-V relationship was determined by the application of 50 ms ACh pulses (bar in B) at different holding potentials ranging from –100 mV to +100 mV by 20 mV steps.

HEK293T$_{\alpha WT}$ (17064±2876 cpm in HEK293T$_{\alpha L251R}$ [n=5] and 58751±7548 cpm in HEK293T$_{\alpha WT}$ [n=5], p=0.0009) (Figure 6-3). The background level of radioactivity measured in untransfected HEK293T cells was 892±39 cpm (n=5).

6.6 No single-channel currents can be recorded in AChR$_{\alpha L251R}$

The functional consequences of the αL251R mutation were first assessed by the analysis of burst duration of AChR$_{\alpha L251R}$ expressed in HEK293 cells. Performing recordings at low (100 nM) and high (30 μM) ACh concentrations and at various holding potentials ranging between –100 mV to +80 mV, no channel activity could be detected (5 transfections and 50 patches tested) (Figure 6-4). Although surface expression levels of AChR$_{\alpha L251R}$ were reduced, the lack of any corresponding channel activity has not been seen previously in the host laboratory.

6.7 Whole-cell current amplitude, desensitisation and deactivation are altered in AChR$_{\alpha L251R}$

Whole-cell patch clamp experiments were performed to further evaluate the functional consequences of the αL251R mutation. In AChR$_{\alpha WT}$, current traces displayed a fast rise and a peak followed by an exponential current decay with almost complete desensitisation after a 3 s pulse of 1 mM ACh (Figure 6-5A). In AChR$_{\alpha L251R}$, current architecture was changed in many aspects (Figure 6-5C). Current amplitudes were significantly reduced in AChR$_{\alpha L251R}$ (n=18) compared to AChR$_{\alpha WT}$ (n=26) (mean peak current amplitude of –12.11±2.22 nA in AChR$_{\alpha WT}$ and

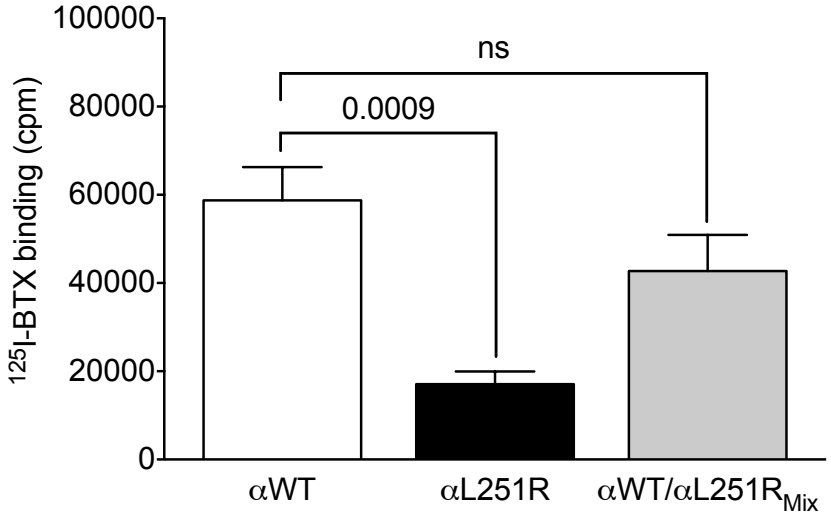


Figure 6-3 The influence of the αL251R mutation on AChR surface expression
The ^{125}I-BTX binding assay was used to assess AChR surface expression. The bars show final results with the background level of radioactivity already subtracted from the cell-surface ^{125}I-BTX activity in transfected HEK293T cells. Unpaired t-test.

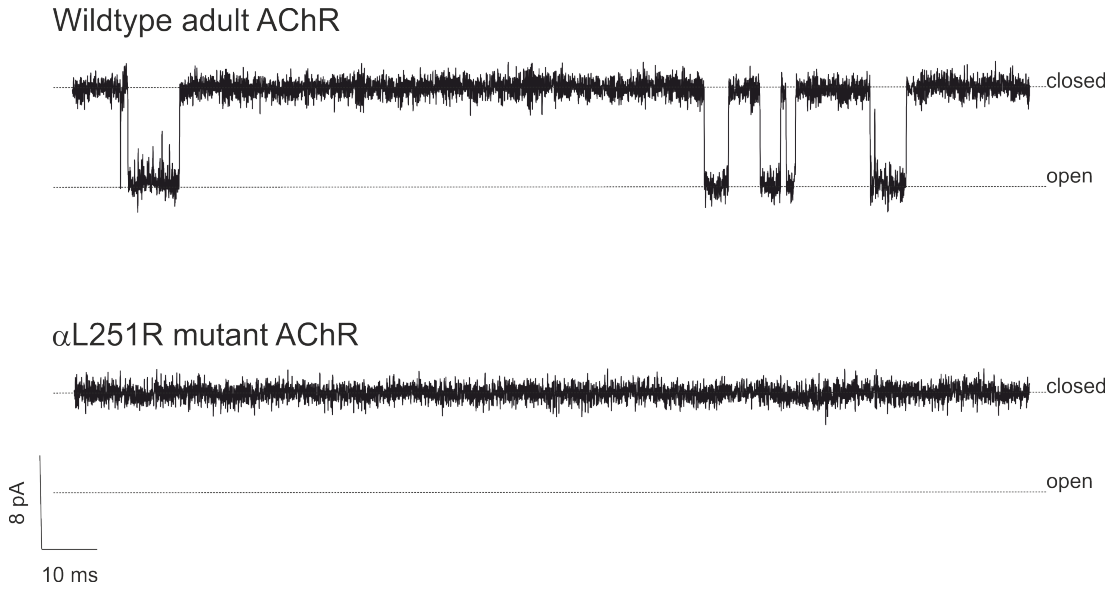


Figure 6-4 Single channel recordings of wild-type and mutant AChRs
Cell-attached patch clamp configuration. Current traces were recorded with the pipette potential at +80 mV and 100nM ACh. No single-channel currents could be recorded in AChR$_{\alpha L251R}$.

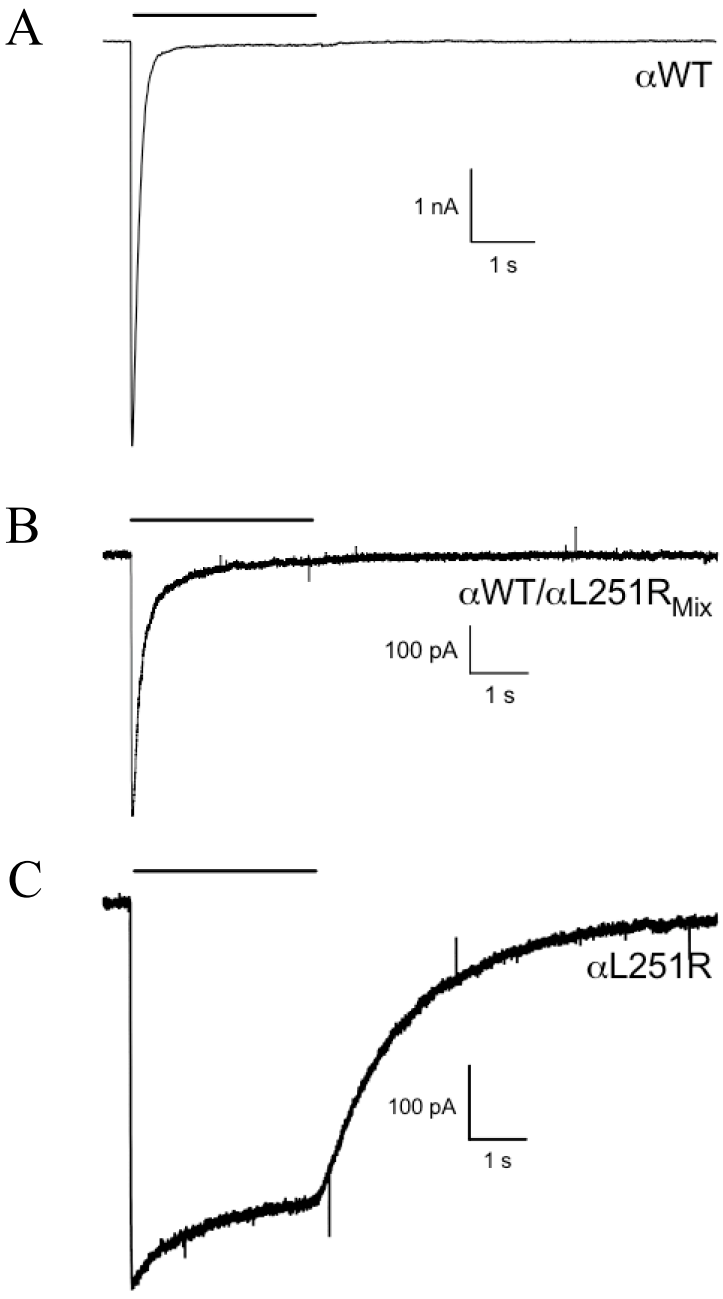


Figure 6-5 Current characteristics of wild-type and mutant AChRs expressed in HEK293 cells
Compared to HEK293$_{\alpha WT}$ (A), current amplitudes were lower in HEK293$_{\alpha WT/\alpha L251R_Mix}$ (B) and HEK293$_{\alpha L251R}$ (C). Desensitisation and deactivation were markedly slower in HEK293$_{\alpha L251R}$ compared to HEK293$_{\alpha WT}$ and HEK293$_{\alpha WT/\alpha L251R_Mix}$.

–0.36±0.05 nA in $AChR_{\alpha L251R}$, p<0.0001) (Figure 6-6A). The current rose to a plateau and remained stable during ACh application (mean fractional current decay of 95.4±1.0% in $AChR_{\alpha WT}$ and 15.3±1.7% in $AChR_{\alpha L251R}$, p<0.0001) (Figure 6-6B). Receptor deactivation defined as current decay during ACh wash-out at the end of receptor stimulation when remaining open receptors return to the closed state was slower in $AChR_{\alpha L251R}$ compared to $AChR_{\alpha WT}$ (mean deactivation time constant of 76±13 ms in $AChR_{\alpha WT}$ and 2169±256 ms in $AChR_{\alpha L251R}$, p<0.0001) (Figure 6-6C).

In $HEK293_{\alpha WT/\alpha L251R_Mix}$, the co-transfection of αWT- and αL251R-subunits revealed functional features of both $AChR_{\alpha WT}$ and $AChR_{\alpha L251R}$. Current amplitudes were significantly reduced in $HEK293_{\alpha WT/\alpha L251R_Mix}$ compared to $HEK293_{\alpha WT}$ (mean peak current amplitude of –12.11±2.21 nA in $HEK293_{\alpha WT}$ and –4.38±1.42 nA in $HEK293_{\alpha WT/\alpha L251R_Mix}$, p=0.0060) (Figure 6-6A). Current decay was similar between $HEK293_{\alpha WT/\alpha L251R_Mix}$ and $HEK293_{\alpha WT}$ (mean fractional current decay of 90.8±2.9% in $HEK293_{\alpha WT/\alpha L251R_Mix}$ and 95.4±1.0% in $HEK293_{\alpha WT}$, ns) (Figure 6-6B), but deactivation was significantly slower (mean deactivation time constant of 148±23 ms in $HEK293_{\alpha WT/\alpha L251R_Mix}$ and 76±13 ms in $HEK293_{\alpha WT}$, p=0.0097) (Figure 6-6C).

6.8 In $HEK293_{\alpha L251R}$, the mutation is associated with a change of rectification from linear to outward

The comparison of the current-voltage (I-V) relationship between $HEK293_{\alpha WT}$, $HEK293_{\alpha L251R}$ and $HEK293_{\alpha WT/\alpha L251R_Mix}$ revealed further functional aspects of the mutation. Whereas the I-V relationship was linear in $HEK293_{\alpha WT}$ and $HEK293_{\alpha WT/\alpha L251R_Mix}$ with a RI close to 1, there was a strong outward rectification

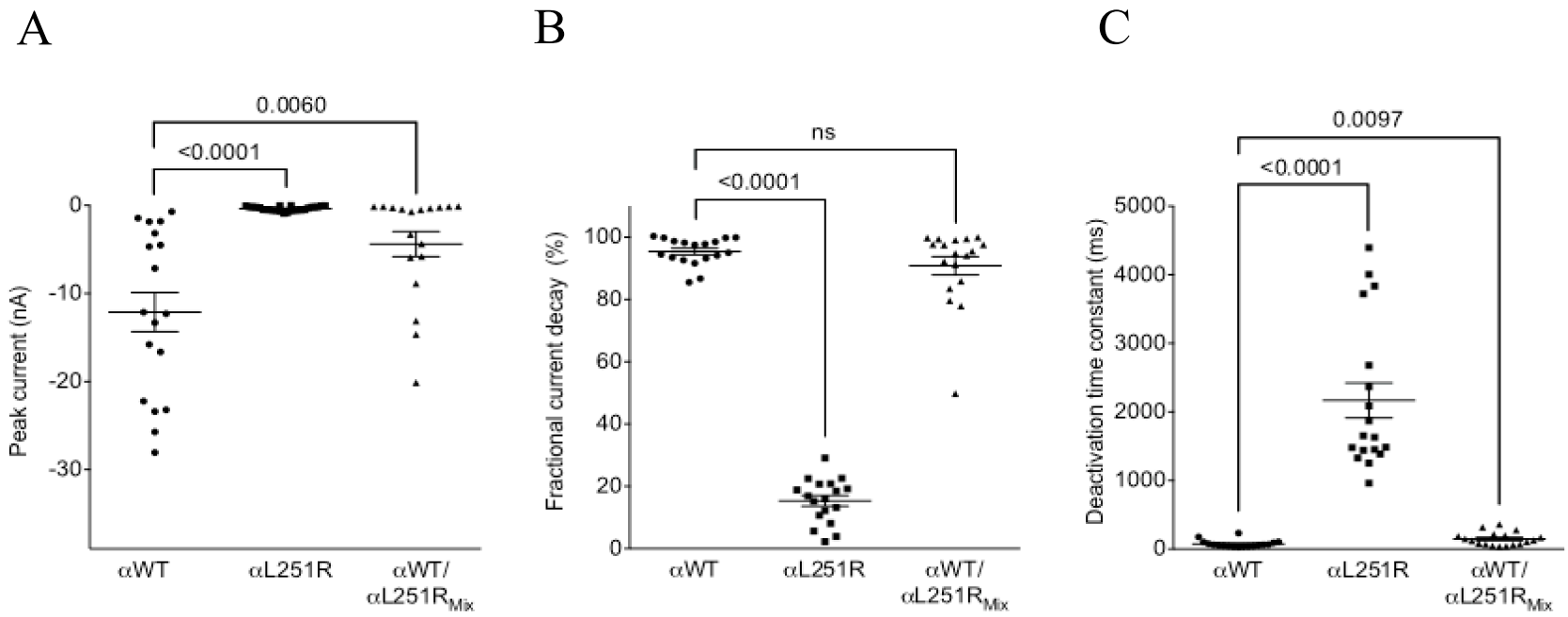


Figure 6-6 Peak currents, desensitisation and deactivation in HEK293$_{\alpha WT}$, HEK293$_{\alpha L251R}$ and HEK293$_{\alpha WT/\alpha L251R_Mix}$
The αL251R mutation was associated with reduced peak currents (A) and with slower desensitisation (B) and deactivation (C). Unpaired t-test.

observed at positive potentials in HEK293$_{\alpha L251R}$ with an increasing RI up to 4.7±0.7 at ±100 mV (Figure 6-7). There was no shift of the reversal potential.

6.9 In AChR$_{\alpha L251R}$, current characteristics are not chloride-dependent at a holding potential of –60 mV

The whole-cell current reduction in AChR$_{\alpha L251R}$ to less than 3% of AChR$_{\alpha WT}$ was not simply explained by the reduced surface expression, which was still 29% in AChR$_{\alpha L251R}$ compared to AChR$_{\alpha WT}$. A functional defect of mutant AChRs, therefore, was likely. Although reversal potential was not altered in AChR$_{\alpha L251R}$, the change of the linear I-V relationship in AChR$_{\alpha WT}$ into outward rectification in AChR$_{\alpha L251R}$ was indicative of a modification of AChR conductance or ion selectivity. Whole-cell patch clamp experiments with altered Cl^- concentrations were thus performed to further elucidate the underlying pathomechanism and to unmask a potential Cl^- dependence of current characteristics in AChR$_{\alpha L251R}$.

After substitution of intra- or extracellular Cl^- by SO_4^{2-} to a residual Cl^- concentration of 10 mM (Table 6-1 and 6-2), peak current amplitudes, desensitisation and deactivation were measured, and, for both AChR$_{\alpha WT}$ and AChR$_{\alpha L251R}$, compared between experiments at low intracellular Cl^- concentration (10 mM Cl^-_{IN}) and low extracellular Cl^- concentration (10 mM Cl^-_{EX}). All measurements were performed at a holding potential of –60 mV.

No significant difference could be detected between 10 mM Cl^-_{IN} and 10 mM Cl^-_{EX} in both AChR$_{\alpha WT}$ and AChR$_{\alpha L251R}$ as to peak current amplitudes (Figure 6-8A), desensitisation (Figure 6-8B) and deactivation (Figure 6-8C), indicating that current changes associated with the αL251R mutation were Cl^--independent at –60 mV.

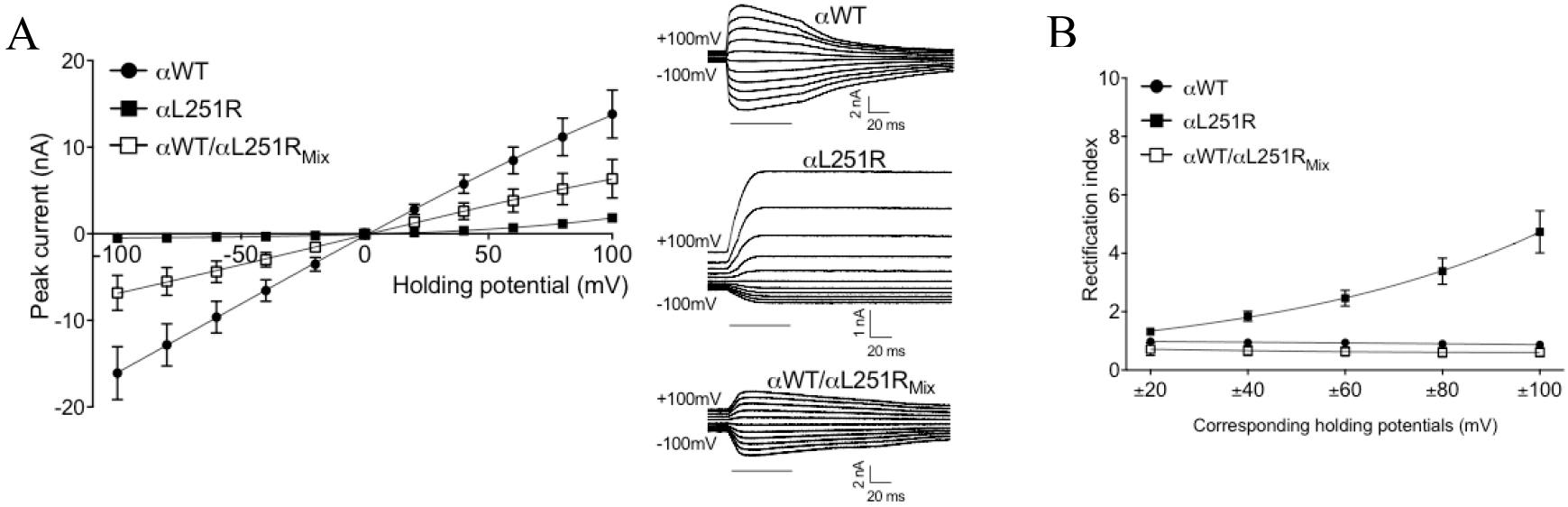


Figure 6-7 The I-V relationship in HEK293$_{\alpha WT}$, HEK293$_{\alpha L251R}$ and HEK293$_{\alpha WT/\alpha L251R_Mix}$
The αL251R mutation was associated with a change of the linear I-V relationship into outward rectification in HEK293$_{\alpha L251R}$ (A) with a RI >1 at several holding potentials (B).

Table 6-1 Extracellular and pipette solution composition for the substitution of intracellular Cl^- by SO_4^{-2} to a final Cl^- concentration of 10 mM (i.e. 10 mM Cl^-_{IN})

	Extracellular solution (mM)	Pipette solution (mM)
NaCl	150	-
Na_2SO_4	-	2
KCl	2.8	10
K_2SO_4	-	67
HEPES	10	10
$MgCl_2$	2	-
$MgSO_4$	-	2
$CaCl_2$	2	-
$CaCl_2$	-	-
Glucose	10	-
Mg-ATP	-	2
EGTA	-	10
pH	7.4	7.2

Table 6-2 Extracellular and pipette solution composition for the substitution of extracellular Cl^- by SO_4^{-2} to a final Cl^- concentration of 10 mM (i.e. 10 mM Cl^-_{EX})

	Extracellular solution (mM)	Pipette solution (mM)
NaCl	10	4
Na_2SO_4	70	
KCl	-	144
K_2SO_4	1.4	-
HEPES	10	10
$MgCl_2$	-	2
$MgSO_4$	2	-
$CaCl_2$	-	-
$CaSO_4$	2	-
Glucose	10	
Mg-ATP	-	2
EGTA		10
pH	7.4	7.2

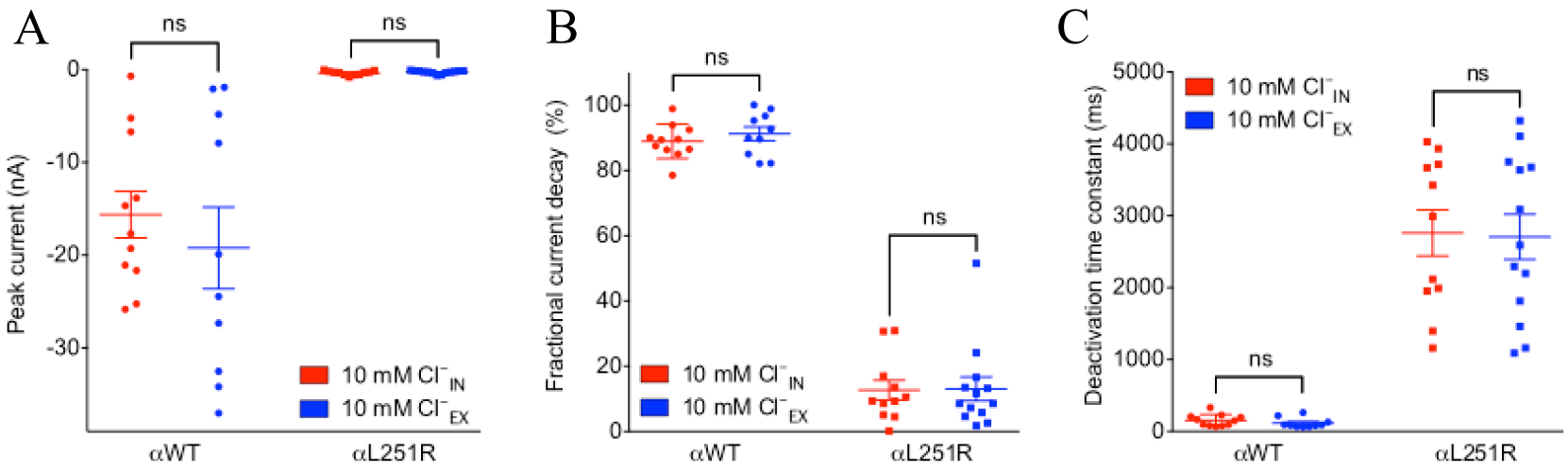


Figure 6-8 Peak currents, desensitisation and deactivation in $AChR_{\alpha WT}$ and $AChR_{\alpha L251R}$ after substitution of intracellular or extracellular Cl^- by SO_4^{2-}

In both $AChR_{\alpha WT}$ and $AChR_{\alpha L251R}$, peak current amplitudes (A), desensitisation (B) and deactivation (C) did not significantly differ between experiments at 10 mM Cl^-_{IN} and 10 mM Cl^-_{EX}. Unpaired t-test.

6.10 In AChR$_{\alpha L251R}$, the mutation is associated with a conversion from cationic to anionic selectivity at positive holding potentials

To further elucidate the underlying mechanism of the observed current rectification in AChR$_{\alpha L251R}$, the I-V relationship was analysed after substitution of intra- or extracellular Cl^- by SO_4^{2-} to a residual Cl^- concentration of 10 mM. In AChR$_{\alpha WT}$, Cl^- substitution had no effect on current rectification and reversal potential (Figure 6-9). In AChR$_{\alpha L251R}$, by contrast, the reduction of intracellular Cl^- concentration was associated with increased current amplitudes at positive holding potentials (Figure 6-10A) with the RI increasing to 8.0±1.1 at ±100 mV. Correspondingly, the reduction of extracellular Cl^- concentration reduced current amplitudes at positive holding potentials with a rectification index of 2.6±0.4 at ±100 mV (one-way ANOVA: $F_{(2,36)}$=1.7, p=0.0004) (Figure 6-10B). Reversal potential was not shifted indicating no significant Cl^- conductance at negative holding potentials up to 0 mV.

Single-channel experiments were repeated under conditions associated with higher whole-cell currents (i.e. at 10 mM Cl^-_{IN} and positive membrane potentials up to +80 mV), but there was still a lack of single-channel activity in AChR$_{\alpha L251R}$.

6.11 In AChR$_{\alpha L251R}$, sodium conductance is severely reduced but prevails at negative holding potentials

To explore charge selectivity of AChR$_{\alpha L251R}$ at negative holding potentials further, whole-cell patch clamp experiments were performed after the substitution of NaCl by glucose to a residual concentration of 20 mM in the extracellular solution (Table 6-3). This resulted in a shift of the reversal potential towards negative voltages in

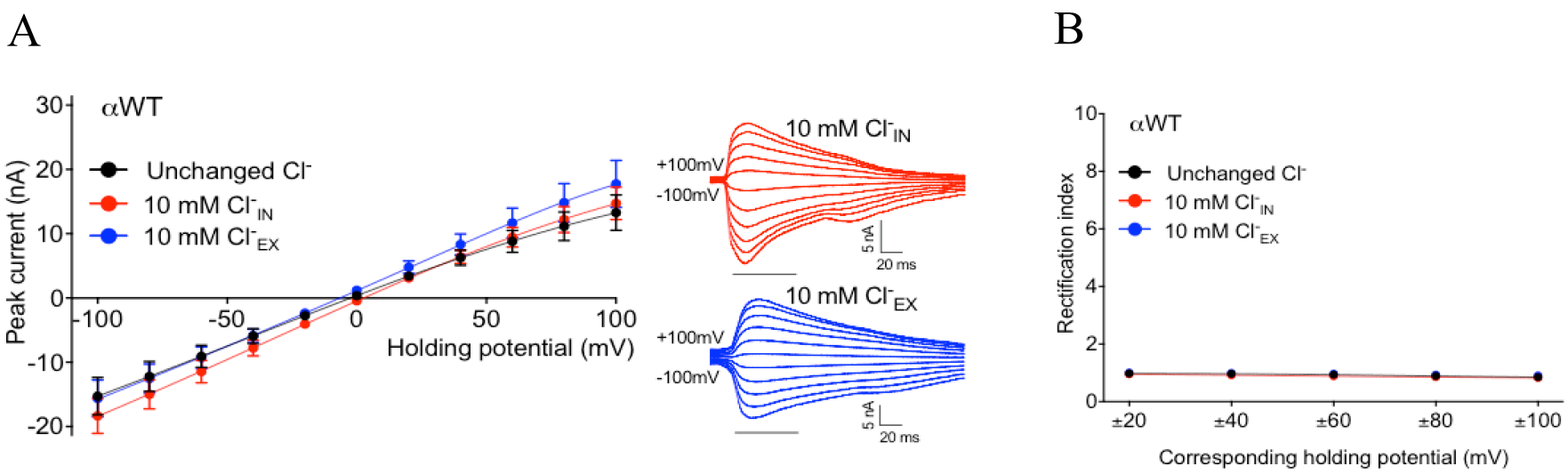


Figure 6-9 The I-V relationship in $AChR_{\alpha WT}$ was independent of the intracellular and extracellular Cl^- concentration
In $AChR_{\alpha WT}$, the I-V relationship was independent of the intracellular or extracellular Cl^- concentration (A), with a RI around 1 in all groups with different Cl^- gradients (B). This was indicative of an insignificant Cl^- conductance in $AChR_{\alpha WT}$.

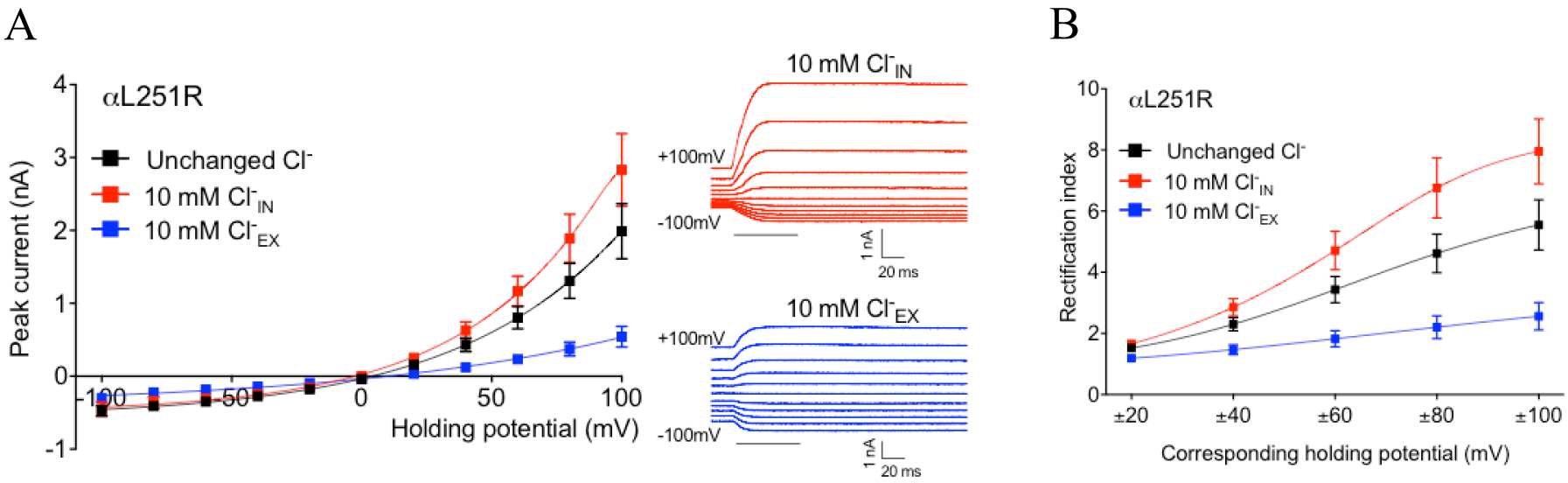


Figure 6-10 The I-V relationship in $AChR_{\alpha L251R}$ in dependence of the intracellular and extracellular Cl^- concentration
In $AChR_{\alpha L251R}$, the I-V relationship was independent of the intracellular or extracellular Cl^- concentration at negative holding potentials, but was strongly chloride-dependent at positive holding potentials (A), when current amplitudes increased at a reduced intracellular Cl^- concentration and decreased at a reduced extracellular Cl^- concentration, indicating a significant Cl^- conductance in $AChR_{\alpha L251R}$ at positive holding potentials only. The RI displayed a sigmoidal relationship in all groups with differing Cl^- gradients (B).

Table 6-3 Extracellular and pipette solution composition for the substitution of extracellular NaCl by glucose to a final NaCl concentration of 20 mM

	Extracellular solution (mM)	Pipette solution (mM)
NaCl	20	4
KCl	2.8	144
HEPES	10	10
$MgCl_2$	2	2
$CaCl_2$	2	-
Glucose	260	-
Mg-ATP	-	2
EGTA	-	10
pH	7.4	7.2

$AChR_{\alpha L251R}$ following the equilibrium potential of potassium (mean reversal potential of –28.3±4.8 mV at 20 mM extracellular NaCl [n=10] compared to 4.3±3.7 mV at 150 mM extracellular NaCl [n=16], $p<0.0001$), and was very similar to the shift observed in $AChR_{\alpha WT}$ (mean reversal potential of –28.3±4.8 mV in $AChR_{\alpha L251R}$ at 20 mM NaCl [n=10] compared to –32.0±1.3 mV in $AChR_{\alpha WT}$ at 20 mM NaCl [n=10], ns) (Figure 6-11). This is indicative of insignificant chloride permeability at negative holding potentials in $AChR_{\alpha L251R}$.

6.12 Discussion

This chapter evaluates the impact of the αL251R mutation (L9'R) found in a CMS patient on AChR function. The L9' residue lies at the approximate midpoint of the M2 transmembrane domain and occupies a kink in each of the five AChR subunits pointing into the closed channel (Unwin, 1995). Together with V13', the L9' creates the narrowest part of the hydrophobic girdle around the pore introducing an energetic barrier to ion permeation across the lipid bilayer (Beckstein, 2001; Miyazawa et al., 2003). The pore is too constricting for ions to pass through while retaining their hydration shell. The dehydration barrier cannot be overcome in the absence of polar residues that could substitute for water (Miyazawa et al., 2003). Upon receptor activation, the M2 transmembrane domains rotate so that the L9' residues no longer occlude the conduction pathway (Miyazawa et al., 2003). The pore widens, and once a critical radius is exceeded, hydration of the pore removes the energetic barrier and allows ions to pass through (Beckstein, 2001).

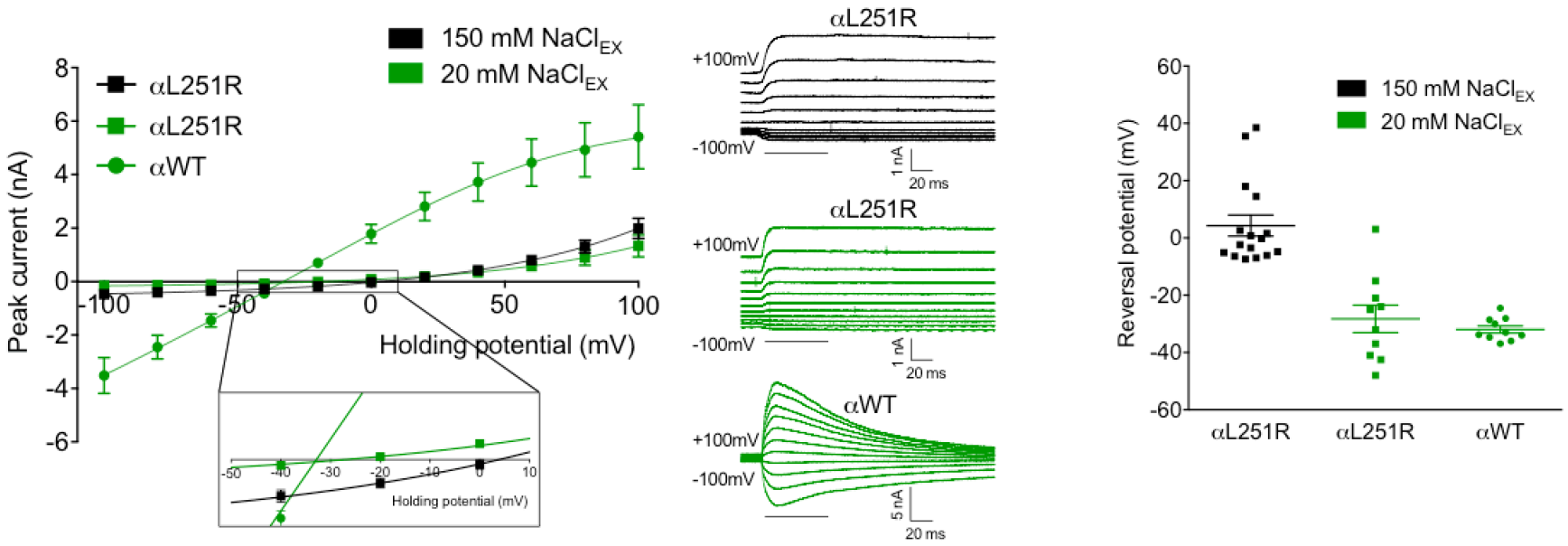


Figure 6-11 The I-V relationship in AChR$_{αWT}$ and AChR$_{αL251R}$ after substitution of extracellular NaCl by glucose
In AChR$_{αWT}$, the substitution of extracellular NaCl by glucose to a residual concentration of 20 mM resulted in a shift of the reversal potential towards negative voltages following the equilibrium potential of potassium. In AChR$_{αL251R}$, the shift of the reversal potential upon substitution of extracellular NaCl by glucose also followed the equilibrium potential of potassium towards negative voltages, indicating a predominant permeability of AChR$_{αL251R}$ for sodium and potassium at negative holding potentials very similar to AChR$_{αWT}$. Any significant Cl^- conductance would have resulted in a shift of the reversal potential towards positive voltages following the equilibrium potential of chloride.

6.12.1 Unravelling the pathomechanism of the αL251R mutation by whole-cell patch clamp experiments

In this project, the substitution of αL9' by the positively charged amino acid arginine altered AChR function in many aspects and also reduced AChR surface expression. Whole-cell currents were profoundly reduced and desensitisation and deactivation time constants were prolonged. Single-channel currents could not be detected, probably due to impaired channel conductance together with reduced surface expression of $AChR_{\alpha L251R}$. These findings are consistent with studies on α_7 neuronal AChRs, in which the substitution of L9' by both polar and hydrophobic amino acids was shown to result in slower desensitisation kinetics and increased sensitivity to agonist, and substitutions with polar amino acids were also associated with a change of the inward rectification, which is characteristic for neuronal AChRs, into a linear I-V relationship (Revah et al., 1991) (Figure 6-12). Other studies on muscle AChRs reported that substitutions of L9' by the hydrophilic amino acids serine (Labarca et al., 1995) or threonine (Filatov and White, 1995) in each of the five subunits slow desensitisation and increase sensitivity to ACh (Figure 6-12). Although deactivation was not examined in those studies, its prolongation in this project could have resulted from increased affinity of $AChR_{\alpha L251R}$ to ACh as reported before (Revah et al., 1991; Filatov and White, 1995; Labarca et al., 1995). The substitution of L9' by charged amino acids has not been examined so far.

An unexpected observation in this project was the change of the I-V relationship into outward rectification, which was found to derive from a voltage-dependent conversion of ion selectivity from cationic to anionic. The conductance of $AChR_{\alpha L251R}$ for chloride was high at positive membrane potentials but declined

Type	Sequence		Selectivity	Characteristics	Reference
	M1-M2	M2			
m-AChR αWT	G–EK	MTLSISVLLSLTVFL	C		
m-AChR αL251R	G–EK	MTLSISVLRSLTVFL	A	Upon depolarisation	
m-AChR αL251S	G–EK	MTLSISVLSSLTVFL	–	Slow desensitisation, high ACh-affinity	Labarca et al., 1995
m-AChR αL251T	G–EK	MTLSISVLTSLTVFL	–	Slow desensitisation, high ACh-affinity	Filatov and White, 1995
$5HT_{3A}R$ WT	G–ER	VSFKITLLLGYSVFL	C		
$5HT_{3A}R$ 1	GPAR	VSFKITLLLGYSTFL	A	Slow desensitisation, high 5HT-affinity	Gunthorpe and Lummis, 2001
GlyR WT	APAR	VGLGITTVLTMTTQS	A		
$GlyR_1$	A–ER	VGLGITTVLTMTVQS	C	Reduced conductance	Keramidas et al., 2000
n-AChR α7WT	G–EK	ISLGITVLLSLTVFM	C		
n-AChR α7-1	GPAK	ISLGITVLLSLTTFM	A		Galzi et al., 1992, Corringer et al., 1999
n-AChR α7-2	GPEK	ISLGITVLLSLTVFM	–	Not functional	Galzi et al., 1992, Corringer et al., 1999
n-AChR α7-3	GPAK	ISLGITVLLSLTVFM	–	Not functional	Galzi et al., 1992, Corringer et al., 1999
n-AChR α7-4	GPEK	ISLGITVLLSLTTFM	–	Not functional	Galzi et al., 1992, Corringer et al., 1999
n-AChR α7-5	G–AK	ISLGITVLLSLTTFM	C		Galzi et al., 1992, Corringer et al., 1999
n-AChR α7-6	G–AK	ISLGITVLLSLTVFM	C		Galzi et al., 1992, Corringer et al., 1999
n-AChR α7-7	G–EK	ISLGITVLLSLTTFM	C		Galzi et al., 1992, Corringer et al., 1999
n-AChR α7-8	GPAK	ISLGITVLTSLTVFM	A		Corringer et al., 1999
n-AChR α7-9	G–EK	ISLGITVLFSLTVFM	–	Slow desensitisation, high ACh-affinity	Revah et al., 1991
n-AChR α7-10	G–EK	ISLGITVLVSLTVFM	–	Slow desensitisation, high ACh-affinity	Revah et al., 1991
n-AChR α7-11	G–EK	ISLGITVLSSLTVFM	–	Slow desensitisation, high ACh-affinity, linear I-V relationship	Revah et al., 1991
n-AChR α7-12	G–EK	ISLGITVLTSLTVFM	–	Slow desensitisation, high ACh-affinity, linear I-V relationship	Revah et al., 1991

Figure 6-12 Mutations of the charge selectivity filter in Cys-loop ligand-gated ion channels published in the literature
mAChR: muscle-type AChR, $5HT_{3A}R$: 5-hydroxytryptamine$_3$ receptor, GlyR: glycine receptor, nAChR: neuronal AChR, C: cationic, A: anionic.

progressively as the membrane was hyperpolarised. Instead, whole-cell currents, although markedly reduced, were found to be carried by sodium at negative membrane potentials. Among nicotinic acetylcholine receptors, only muscle AChRs display a linear I-V relationship (Imoto et al., 1988), while neuronal AChRs are characterised by inward rectification (Forster and Bertrand, 1995). Mechanisms postulated to underlie inward rectification in neuronal AChRs include a combination of block by intracellular magnesium or polyamines and voltage-dependent mechanisms intrinsic to the receptor (Mathie et al., 1990; Sands and Barish, 1992; Haghighi and Cooper, 1998).

Conversion of ion selectivity was reported before in α_7 neuronal AChRs (Galzi et al., 1992; Corringer et al., 1999), in 5-hydroxytryptamine$_3$ receptors (Gunthorpe and Lummis, 2001) and in glycine receptors (Keramidas et al., 2000), but those studies found a minimum number of three mutations to be necessary for successful transformation. In α_7 neuronal AChRs, the conversion of ion selectivity required the insertion of proline at the cytoplasmic end of the M2 helix (i.e. G236_E237insP) along with E237A and V251T (Galzi et al., 1992; Corringer et al., 1999) or L247T (Corringer et al., 1999) (corresponding to the substitution of leucine at the 9' position). The insertion of proline, either alone or together with E237A or V251T, however, yielded non-functional receptors. And in the absence of G236_E237insP, the E237A and V251T mutations were fully compatible with cationic receptors, either when introduced alone or together (Galzi et al., 1992; Corringer et al., 1999) (summarised in Figure 6-12). It was hypothesised that conversion of ion selectivity in α_7 neuronal AChRs is not based on alterations of the M2 helix configuration, but rather due to a local structural reorganisation in the

vicinity of the proline insertion (Corringer et al., 1999). Data presented in this chapter provide first evidence that conversion of ion selectivity does not exclusively depend on the insertion of proline at G236_E237insP as suggested before (Corringer et al., 1999). Further studies are needed to elucidate the underlying mechanism for the conversion of ion selectivity associated with the αL251R mutation. One explanation could be that the charged arginines within the pore could have acted as sensors of membrane potential affecting channel conformation and, consequently, the conductance for chloride. However, electrophysiological studies performed in this project cannot completely exclude other pathomechanisms. Alternatively, chloride concentration changes could have influenced the gating mechanism and cation permeability. Low intracellular chloride concentrations could have resulted in increased sodium permeability of $AChR_{\alpha L251R}$ in a voltage-dependent manner resulting in increased sodium outflow at positive membrane potentials. A similar mechanism with modification of channel gating by intracellular chloride was already reported for glycine and GABA receptors (Moroni et al., 2011). In $AChR_{\alpha L251R}$, membrane potential and the chloride gradient across the ion channel could have modified the conformation of the channel pore containing the charged arginine residues, which, as a result, could have affected sodium permeability.

6.12.2 Data from computational modelling reveals the introduction of an energetic reward for chloride by both arginine residues

In collaboration with the Structural Bioinformatics and Computational Biochemistry Unit at the Department of Biochemistry, University of Oxford, the underlying mechanism of the conversion of ion selectivity in mutant AChRs was analysed

further by computational modelling. Umbrella sampling molecular dynamics simulations revealed that the substitution of L9' by arginine in both α-subunits in $AChR_{\alpha L251R}$ leads to a constriction of the channel pore to approximately 60% of $AChR_{\alpha WT}$, a diameter that requires ions to desolvate in order to permeate the pore. Ion desolvation is associated with an energetic penalty that can be compensated for by the favourable electrostatic interaction of both arginines with chloride in $AChR_{\alpha L251R}$. Due to the positive charge of sodium, by contrast, the energetic penalty of desolvation cannot be accounted for by interaction with both arginines resulting in an impairment of sodium permeability (Figure 6-13 and 6-14). However, even at positive membrane potentials, when $AChR_{\alpha L251R}$ conductance for chloride was high, whole-cell current amplitudes were still reduced compared to $AChR_{\alpha WT}$. This might be due to the strong interaction between chloride and both arginines, which, despite the energetic penalty of desolvation, results in an energetic reward for chloride with increasing dwell times at the position of both arginines (Figure 6-14). An energetic well in the permeation pathway would be expected to slow down passage of ions and may have contributed to a lower conductance than would be predicted on the basis of diameter alone. AChRs with one αWT- and one αL251R-subunit (i.e. $AChR_{\alpha WT/\alpha L251R}$ and $AChR_{\alpha L251R/\alpha WT}$) are likely to be impermeable for both Na^+ and Cl^- with energy barrier heights for Na^+ close to that at $AChR_{\alpha L251R}$ and for Cl^- close to that at $AChR_{\alpha WT}$ (Figure 6-13A, B).

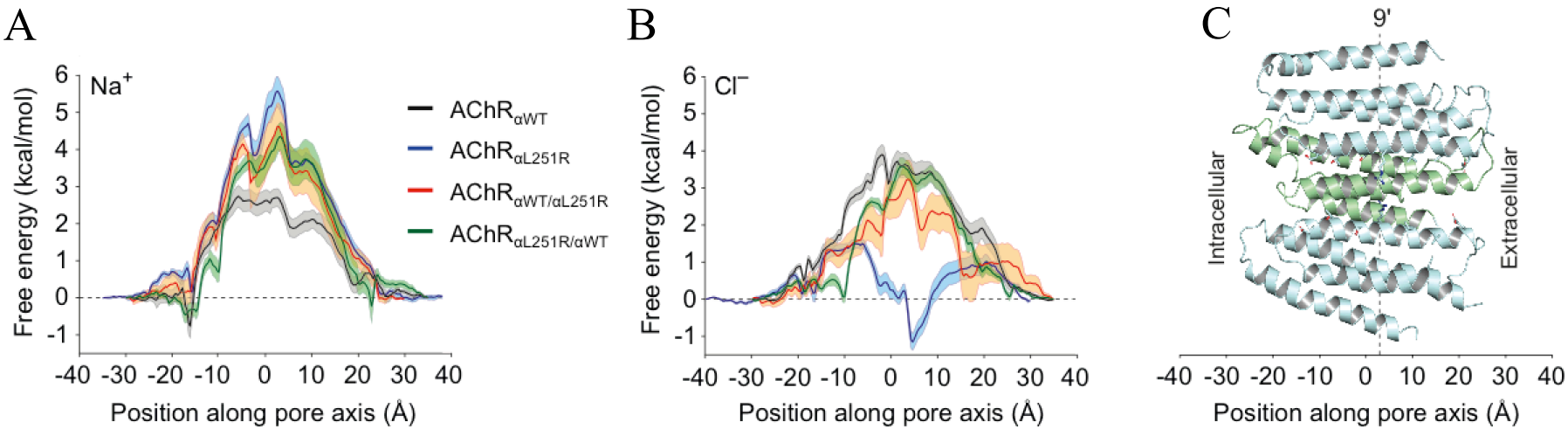


Figure 6-13 Analysis of Na^+ and Cl^- passage through the transmembrane pore in wild-type and mutant AChRs by calculations of the potential of mean force profiles

Potential of mean force (PMF) profiles for Na^+ (A) and Cl^- (B) ions in $AChR_{\alpha WT}$ (black), $AChR_{\alpha L251R}$ (blue), $AChR_{\alpha WT/\alpha L251R}$ (red) and $AChR_{\alpha L251R/\alpha WT}$ (green). (C) View on side of $AChR_{\alpha L251R}$ model within the same coordinate space as the PMF profiles in (A) and (B). Residues at key positions are indicated in stick representation. The β, δ and γ/ε-subunits have been removed for clarity. All barrier heights for sodium at mutant channels were higher than for chloride at $AChR_{\alpha WT}$, indicative of reduced sodium permeability of $AChR_{\alpha L251R}$. Both $AChR_{\alpha WT/\alpha L251R}$ and $AChR_{\alpha L251R/\alpha WT}$ possessed similar (within error) PMF profiles with chloride barrier heights greater than that for sodium at $AChR_{\alpha WT}$ and lower than that for chloride at $AChR_{\alpha WT}$. It is thus likely that these values represent non-conductive states. The most pronounced effect occurred for chloride at $AChR_{\alpha L251R}$ revealing a reduction in barrier height to 1.5 kcal/mol (around z = –8Å) as well as the introduction of an energetic well around z = 5Å of –1.15 kcal/mol. This, together with the increase in barrier height to 5.57 kcal/mol for sodium is indicative for strongly chloride selective permeation. Error bars are one standard deviation of the mean. Data were obtained by Max Epstein and Prof. Philip Biggin, Department of Biochemistry, University of Oxford.

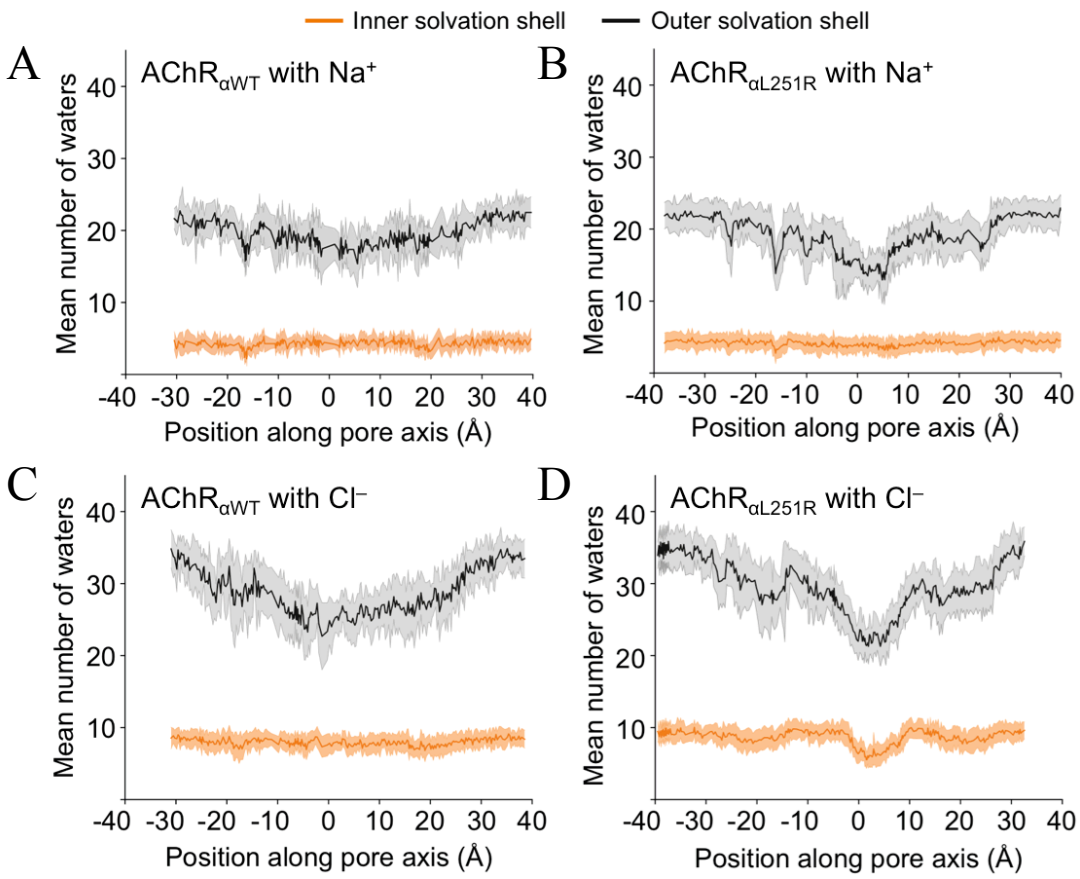


Figure 6-14 Solvation shells of Na^+ and Cl^- ions as a function of their position along the reaction coordinate

Sodium is never desolvated from its inner solvation shell and only minor perturbations are observed in the outer solvation shell in both AChR$_{\alpha WT}$ and AChR$_{\alpha L251R}$ (A and B). Thus, the lack of Na^+ permeation observed reflects repulsion of the solvated Na^+. In contrast, Cl^- is observed to be desolvated around the L251R residue (at the 9' position around 3Å (z) in the reaction coordinate) in AChR$_{\alpha L251R}$ but not in AChR$_{\alpha WT}$. More substantial deformation of the outer solvation shell is also observed. The energetic penalty incurred through this desolvation is accounted for by the favourable electrostatic interactions of both arginine residues with chloride, in which they act as surrogate water molecules chelating the probe ion. Error bars are one standard deviation of the mean. Data were obtained by Max Epstein and Prof. Philip Biggin, Department of Biochemistry, University of Oxford.

6.12.3 Pathophysiological implications of CMS due to the αL251R mutation

With the $AChR_{\alpha L251R}$, $AChR_{\alpha WT/\alpha L251R}$ and $AChR_{\alpha L251R/\alpha WT}$ representing non-conductive states for Na^+, only $AChR_{\alpha WT}$ accounting for around 25% of normal AChR numbers remain to be functionally active in the CMS patient who was heterozygous for the mutation. A reduction of AChR numbers to around 25% of normal is likely to be borderline with respect to compromising the safety margin for neuromuscular transmission (Webster et al., 2004). This would be compatible with the mild phenotype of the patient. The conversion of ion selectivity from cationic to anionic in $AChR_{\alpha L251R}$ could add a detrimental impact on endplate potentials or action potentials at the NMJ. Upon activation by ACh, the inhibitory current carried by chloride influx in $AChR_{\alpha L251R}$ could antagonise the endplate potential during depolarisation mediated by the remaining $AChR_{\alpha WT}$. The threshold potential necessary for the generation of an action potential in muscle cells, however, ranges around –50 mV (Wood and Slater, 1995), which is far below the membrane potential when $AChR_{\alpha L251R}$ became permeable for chloride. Only in situations of increased (compensatory) vesicle release (Molenaar et al., 1979; Cull-Candy et al., 1980; Plomp et al., 1995) or high input resistance, it could be possible that the postsynaptic membrane is depolarised close to a potential region, at which chloride may be able to pass through $AChR_{\alpha L251R}$. Action potentials also cause depolarisations up to 30-40 mV (Wood and Slater, 1995) and may therefore induce inhibitory currents in $AChR_{\alpha L251R}$, which could accelerate the decline phase and contribute to early termination of action potentials limiting their propagation.

Chapter 7

Concluding remarks and future directions

The aim of this thesis was to examine AChR function under various conditions to understand better NMJ physiology and the mechanisms underlying different myasthenic disorders, in which AChR function is compromised. The whole-cell application of the patch clamp method and a fast perfusion system were used on different cell lines in order to assess the effect of rapsyn, MG sera and CMS mutations on AChR function. In Chapter 3, it was demonstrated that recovery from desensitisation is faster in the adult AChR isoform and depends on the isoform specific M3-M4 cytoplasmic loop. In Chapter 4, it was shown that rapsyn facilitates recovery from desensitisation in both fetal and adult AChRs in muscle cells. The effect of MG sera on AChR function was tested in Chapter 5. Fast current inhibition was observed with a proportion of sera with antibodies directed against AChRs, and the co-transfection of CN21 cells with rapsyn increased the sensitivity for sera inhibiting AChR currents. And finally, the impact of the new CHRNA1 mutation L251R on receptor function was examined in Chapter 6, revealing a novel mechanism for the conversion of AChR ion selectivity from cationic to anionic. The relevance of these findings will be outlined in the following sections, together with ideas for future experiments to gain further insight into AChR function in both physiological and pathological conditions.

Desensitisation in fetal and adult AChRs has been characterised before with

varying time constants between studies ranging from tens of milliseconds (Paradiso and Brehm, 1998; Jahn et al., 2001; Krampfl et al., 2002) to several seconds (Hopfield et al., 1988; Wagoner and Pallotta, 1988). Different agonist application methods and agonist concentrations, and the use of different applications of the patch clamp technique could have contributed to the range of observations reported. In this thesis, desensitisation and recovery from desensitisation were analysed using constant ACh concentrations and a fast perfusion system, and the whole-cell patch clamp method was applied in order to measure AChR function in a physiological intracellular environment; this is an important consideration given the reported effects of phosphorylation of the M3-M4 loop on desensitisation and recovery form desensitisation (Huganir et al., 1986; Hopfield et al., 1988; Hoffman et al., 1994; Paradiso and Brehm, 1998). In experiments performed on muscle and non-muscle cells, recovery from desensitisation was faster in adult compared to fetal AChRs. This is a novel finding that might help to understand better different aspects of NMJ development and function, although the physiological significance of desensitisation and recovery from desensitisation at the NMJ remains controversial in the literature (Giniatullin et al., 2005). Desensitisation is a slow process compared to the lifetime of ACh in the synaptic cleft (Smart and McCammon, 1998; Jahn et al., 2001; Krampfl et al., 2002), and might thus not have a significant impact on shaping endplate currents. Motor neuron firing rates higher than 40 Hz, however, have been shown to overcome the catalytic AChE capacity and increase the lifetime of ACh in the synaptic cleft sufficiently to desensitise AChRs at the frog NMJ (Magleby and Pallotta, 1981). In mice and rats, motor neuron firing rates are low at birth but increase from about the second postnatal week (Vrbova et al., 1985; Personius and

Balice-Gordon, 2001), which coincides with the developmental switch from fetal to adult AChRs (Sakmann and Brenner, 1978). The presence of adult AChRs associated with faster recovery from desensitisation could facilitate the robust and reproducible high-frequent neuromuscular transmission in the adult. However, this has not been confirmed on NMJ preparations so far. The utilisation of animal models such as the transgenic mouse model constitutively expressing the human γ-subunit in an ε-subunit knock-out background (Cossins et al., 2004) could help to further elucidate the role of adult AChRs for neuromuscular transmission. And more work will also be required to define more closely the molecular region in the ε-subunit that determines fast recovery from desensitisation in the adult AChR. In experiments using chimeric AChRs with exchanged M3-M4 domains between the γ- and ε-subunit, the isoform specific differences in recovery time constants were determined to depend on the isoform specific M3-M4 cytoplasmic loop. The application of salbutamol, a β_2-agonist that increases intracellular cAMP and activates PKA, facilitated recovery from desensitisation in the adult AChR only. It is thus likely that the PKA consensus site present in the ε-M3-M4 loop but not in the γ-M3-M4 loop plays a key role for fast recovery from desensitisation in the adult AChR, but this needs to be tested by using more specific agents (i.e. PKA activators or inhibitors) or other chimeric AChRs with mutations of the PKA consensus site.

The effect of rapsyn on AChR function was assessed in the next chapter. Rapsyn is one of the few proteins directly interacting with the cytoplasmic loops of AChR subunits (Maimone and Merlie, 1993; Maimone and Enigk, 1999; Huebsch and Maimone, 2003) and required for AChR clustering at the NMJ. Modification of AChR function by rapsyn could reveal novel insights into the pathomechanism of

various myasthenic syndromes, in which AChR clustering is often impaired.

Analysis of AChR function is usually performed in heterologous expression systems without native or transfected rapsyn. In this thesis, rapsyn co-transfected into muscle cells facilitated recovery from desensitisation in both fetal and adult AChRs with unaffected current decay time constants. In HEK293 cells, rapsyn facilitated recovery from desensitisation in fetal AChR only, and in contrast to TE671/CN21 cells, prolonged current decay time constants in both fetal and adult AChRs. The modulation of AChR function by intracellular factors (Huganir et al., 1986; Middleton et al., 1986; Hopfield et al., 1988; Paradiso and Brehm, 1998) or by lipids (Barrantes, 2010; Baenziger et al., 2015; Unwin, 2017) is well established in the literature, and differences in those factors between TE671/CN21 cells and HEK293 cells could have contributed to the differential effect of rapsyn in the two cell lines. Further characterisation of the mechanisms and factors required for AChR modification is crucial to improve the interpretation of studies on AChR function and for the understanding of NMJ biology in health and disease.

Rapsyn also facilitated recovery from desensitisation in HEK293 cells with AChRs harbouring the δR375H mutation, which was shown to prevent AChR clustering in C2C12 myotubes. In HEK293 cells, however, AChR aggregation into clusters could still be observed in the presence of the δR375H mutation, which could have contributed to the facilitation of AChR recovery kinetics in HEK293 cells. The small dot-shaped AChR aggregates in HEK293 cells were smaller and appeared as rudimentary forms of the AChR clusters in myotubes and might thus represent different structural modifications of the AChR surface distribution. One potential explanation for the variations of AChR aggregation or clustering between both cell

lines is the lack of the molecular machinery in HEK293 cells that is required for proper AChR clustering. Future studies need to elucidate the ultrastructural basis of the AChR aggregates in HEK293 cells and the underlying molecular interactions. MuSK, LRP4 and Dok7 as crucial components of the molecular machinery required for AChR clustering could be co-transfected into HEK293 cells in order to assess their impact on AChR aggregation.

The facilitation of AChR recovery kinetics by rapsyn is of physiological as well as clinical relevance. Together with the developmental switch from fetal to adult AChRs, the interaction of rapsyn with AChR subunits could provide an adaptation to increasing motor neuron firing rates after birth reported in mice and rats (Vrbova et al., 1985; Personius and Balice-Gordon, 2001). By facilitation of recovery kinetics rapsyn could help to ensure the robust and reproducible high-frequent neuromuscular transmission in adult muscle.

Rapsyn-induced clustering of AChRs is the result of a highly regulated pathway at the NMJ initiated by nerve-released agrin, interacting with LRP4 and stimulating MuSK and Dok7 phosphorylation, which then leads eventually to rapsyn and AChR clusters. CMS with underlying mutations in AChRs, rapsyn or Dok7 are associated variably with extraocular muscle weakness. Extraocular muscles have exceptionally high motor neuron firing frequencies in the range of several hundred Hz (Yu Wai Man et al., 2005), which, therefore, could rely on fast AChR recovery rates for efficient neuromuscular transmission. In patients with null mutations of the CHRNE gene (coding for the ε-subunit) (Ealing et al., 2002; Engel et al., 2015), neuromuscular transmission has to depend on the fetal AChR, and one major symptomatic feature for these patients is ophthalmoplegia, possibly due to

desensitisation of the fetal AChR. Rapsyn-induced clustering of the fetal form and its effect on recovery from desensitisation could be crucial in allowing a number of these patients to have some, albeit impaired, extraocular muscle function. Moreover, various autoimmune and genetic myasthenic syndromes including MuSK-MG (Hoch et al., 2001) and CMS with underlying Dok7 and rapsyn mutations (Beeson et al., 2006; Cossins et al., 2006) are associated with an impairment of AChR clustering resulting in postsynaptic receptor dissipation and reduction of AChR densities. In some of these disorders, however, the prolongation of recovery from desensitisation as a result of the failure to recruit rapsyn could further impair the reproducible high-frequent neuromuscular transmission and contribute to weakness and increased fatigability in affected patients. Further study of the role of rapsyn and its interaction with the AChR could help in understanding better the pathophysiology of these very heterogeneous and interesting synaptic disorders.

Another part of this thesis dealt with the role of rapsyn for AChR current inhibition by various MG sera. The pathological effect of AChR antibodies depends on the IgG subclass (Cetin and Vincent, 2018) and on the interaction of the antibodies with specific AChR epitopes (Tzartos et al., 1998). AChR current inhibition as one of the pathological effects was reported to be confined to AChR antibodies directed against the ACh-binding site (Burges et al., 1990; Bufler et al., 1996a; Riemersma et al., 1996; Bufler et al., 1998) with competitive antagonism as a likely mechanism underlying current inhibition. There are also reports on sera from SNMG patients that were shown to inhibit AChR currents (Yamamoto et al., 1991; Barrett-Jolley et al., 1994; Plested et al., 2002; Spreadbury et al., 2005), and it was hypothesised that circulating factors other than IgG affect AChR function

(Spreadbury et al., 2005). Indirect mechanisms including AChR phosphorylation by intracellular factors (Barrett-Jolley et al., 1994; Plested et al., 2002) as well as a direct block (Spreadbury et al., 2005) have been discussed to underlie AChR current inhibition by SNMG sera. The exact mechanism, however, could not be elucidated so far.

In this work, the application of cells co-transfected with rapsyn was considered to be important because AChRs are usually clustered at the NMJ. The physiological and clinical significance of current inhibition by MG sera in unclustered AChRs only may thus be limited. Current inhibition by AChR-Ab and clustered AChR-Ab positive sera, by contrast, was observed in both unclustered and clustered AChRs or in clustered AChRs only, which therefore is more likely to denote a physiologically and clinically relevant effect. However, current inhibition could not be detected in all MG samples used in this project, possibly due to the clinical heterogeneity of the patients and the variety of therapies used, including steroids, other immunosuppressive agents or thymectomy. Due to the lack of detailed clinical information at the time of blood sampling it was not feasible to correlate electrophysiological findings with clinical status, which could help to further elucidate the significance of current inhibition in unclustered and clustered AChRs. Samples from untreated, severely affected MG patients with high antibody titres should ideally be used for electrophysiological studies on AChR function, but this is difficult to accomplish considering that MG is a relatively rare disorder and effective treatment can generally be established in the early disease course in most patients. It is thus difficult to collect samples that meet the requirements mentioned above.

The last part of this thesis evaluated the functional impact of the novel

αL251R mutation found in a CMS patient and provides evidence for the conversion of AChR ion selectivity resulting from a single amino acid substitution. Charge selectivity is essential for physiological receptor function and forms the basis for excitatory and inhibitory ligand-gated ion channels. Mutations associated with reversed charge selectivity thus give rise to transmembrane potentials that are physiologically detrimental. The first evidence for a transformation of a cation selective into an anion selective ligand-gated ion channel derived from experiments on chimeric α_7 neuronal AChRs with substituted homologous residues from the glycine receptor (Galzi et al., 1992). A minimum number of two substitutions (E237A and V251T) and the insertion of a proline residue between positions G236 and E237 were necessary for successful transformation. The conversion of ion selectivity due to the αL251R mutation is associated with the transformation of the AChR from an excitatory into an inhibitory channel, which could have a detrimental impact on endplate or action potentials at the NMJ. Further studies are needed to elucidate the physiological impact of the αL251R mutation on neuromuscular transmission under more physiological conditions. Direct measurements of MEPPs and EPPs in animal models or muscle specimen from patients could help to further elucidate the underlying pathomechanism.

The findings of this thesis present novel insights into various physiological aspects of NMJ function and into disease mechanisms in myasthenic syndromes, and may also have implications outside the NMJ. First, recovery from desensitisation is shown to be faster in the adult AChR isoform, the expression of which at late gestation in humans or after birth in mice could help to facilitate the high-frequent neuromuscular transmission in adult muscle. Second, rapsyn interacting with AChRs

is reported to facilitate recovery from desensitisation in both fetal and adult AChRs. This finding could be of particular interest for other molecules at the postsynaptic NMJ region directly interacting with the AChR (Fuhrer and Hall, 1996; Wang et al., 2003; Hezel et al., 2010), which could also have an effect on AChR function. Moreover, the observation of a novel regulatory mechanism of AChR function by rapsyn could have implications for other ligand gated ion channels at synapses of the central nervous system such as the glycine receptor that is clustered through interaction with the intracellular protein gephyrin (Levi et al., 2004; Patrizio et al., 2017). Third, AChR current inhibition by MG sera is shown to be enhanced upon AChR clustering, and because AChRs are usually clustered at the NMJ, the application of cells expressing clustered AChRs in future studies on the effect of MG sera could help to identify physiologically and clinically relevant effects and identify more pathogenic sera. Finally, the description of voltage-dependent conversion of AChR ion selectivity from cationic to anionic by a single amino acid substitution denotes a novel mechanism and could be of clinical relevance for CMS patients.

Bibliography

Aaij C, Borst P (1972) The gel electrophoresis of DNA. Biochim Biophys Acta 269:192-200.

Adams DJ, Dwyer TM, Hille B (1980) The permeability of endplate channels to monovalent and divalent metal cations. J Gen Physiol 75:493-510.

Albuquerque EX, Barnard EA, Porter CW, Warnick JE (1974) The density of acetylcholine receptors and their sensitivity in the postsynaptic membrane of muscle endplates. Proc Natl Acad Sci U S A 71:2818-2822.

Albuquerque EX, Pereira EF, Alkondon M, Rogers SW (2009) Mammalian nicotinic acetylcholine receptors: from structure to function. Physiol Rev 89:73-120.

Asher O, Kues WA, Witzemann V, Tzartos SJ, Fuchs S, Souroujon MC (1993) Increased gene expression of acetylcholine receptor and myogenic factors in passively transferred experimental autoimmune myasthenia gravis. J Immunol 151:6442-6450.

Auerbach A, Akk G (1998) Desensitization of mouse nicotinic acetylcholine receptor channels. A two-gate mechanism. J Gen Physiol 112:181-197.

Baenziger JE, Henault CM, Therien JP, Sun J (2015) Nicotinic acetylcholine receptor-lipid interactions: Mechanistic insight and biological function. Biochim Biophys Acta 1848:1806-1817.

Barnard EA, Dolly JO, Porter CW, Albuquerque EX (1975) The acetylcholine receptor and the ionic conductance modulation system of skeletal muscle. Exp Neurol 48:1-28.

Barrantes FJ (2010) Cholesterol effects on nicotinic acetylcholine receptor: cellular aspects. Subcell Biochem 51:467-487.

Barrett-Jolley R, Byrne N, Vincent A, Newsom-Davis J (1994) Plasma from patients with seronegative myasthenia gravis inhibit nAChR responses in the TE671/RD cell line. Pflugers Arch 428:492-498.

Bartoli M, Ramarao MK, Cohen JB (2001) Interactions of the rapsyn RING-H2 domain with dystroglycan. J Biol Chem 276:24911-24917.

Beckstein O, Biggin PC, Sansom MSP (2001) A hydrophobic gating mechanism for nanopores. J Phys Chem B 105:12902-12905.

Beeson D, Brydson M, Betty M, Jeremiah S, Povey S, Vincent A, Newsom-Davis J (1993) Primary structure of the human muscle acetylcholine receptor. cDNA cloning of the gamma and epsilon subunits. Eur J Biochem 215:229-238.

Beeson D, Amar M, Bermudez I, Vincent A, Newsom-Davis J (1996) Stable functional expression of the adult subtype of human muscle acetylcholine receptor following transfection of the human rhabdomyosarcoma cell line TE671 with cDNA encoding the epsilon subunit. Neuroscience letters 207:57-60.

Beeson D, Higuchi O, Palace J, Cossins J, Spearman H, Maxwell S, Newsom-Davis J, Burke G, Fawcett P, Motomura M, Muller JS, Lochmuller H, Slater C, Vincent A, Yamanashi Y (2006) Dok-7 mutations underlie a neuromuscular junction synaptopathy. Science 313:1975-1978.

Berg DK, Kelly RB, Sargent PB, Williamson P, Hall ZW (1972) Binding of -bungarotoxin to acetylcholine receptors in mammalian muscle (snake venom-denervated muscle-neonatal muscle-rat diaphragm-SDS-polyacrylamide gel electrophoresis). Proc Natl Acad Sci U S A 69:147-151.

Bernard C (1856) Physiological analysis of the muscle and nerve properties by means of curare. CR Acad Sci 43:825-829.

Betz H, Changeux JP (1979) Regulation of muscle acetylcholine receptor synthesis in vitro by cyclic nucleotide derivatives. Nature 278:749-752.

Borges LS, Yechikhov S, Lee YI, Rudell JB, Friese MB, Burden SJ, Ferns MJ (2008) Identification of a motif in the acetylcholine receptor beta subunit whose phosphorylation regulates rapsyn association and postsynaptic receptor localization. J Neurosci 28:11468-11476.

Bourne Y, Talley TT, Hansen SB, Taylor P, Marchot P (2005) Crystal structure of a Cbtx-AChBP complex reveals essential interactions between snake alpha-neurotoxins and nicotinic receptors. EMBO J 24:1512-1522.

Boyd ND (1987) Two distinct kinetic phases of desensitization of acetylcholine receptors of clonal rat PC12 cells. J Physiol 389:45-67.

Braithwaite AW, Harris AJ (1979) Neural influence on acetylcholine receptor clusters in embryonic development of skeletal muscles. Nature 279:549-551.

Brejc K, van Dijk WJ, Klaassen RV, Schuurmans M, van Der Oost J, Smit AB, Sixma TK (2001) Crystal structure of an ACh-binding protein reveals the ligand-binding domain of nicotinic receptors. Nature 411:269-276.

Brenner HR, Witzemann V, Sakmann B (1990) Imprinting of acetylcholine receptor messenger RNA accumulation in mammalian neuromuscular synapses. Nature 344:544-547.

Brett RS, Dilger JP, Adams PR, Lancaster B (1986) A method for the rapid exchange of solutions bathing excised membrane patches. Biophys J 50:987-992.

Bufler J, Wilhelm R, Parnas H, Franke C, Dudel J (1996a) Open channel and competitive block of the embryonic form of the nicotinic receptor of mouse myotubes by (+)-tubocurarine. J Physiol 495 (Pt 1):83-95.

Bufler J, Pitz R, Czep M, Wick M, Franke C (1998) Purified IgG from seropositive and seronegative patients with mysasthenia gravis reversibly blocks currents through nicotinic acetylcholine receptor channels. Ann Neurol 43:458-464.

Bufler J, Kahlert S, Tzartos S, Toyka KV, Maelicke A, Franke C (1996b) Activation and blockade of mouse muscle nicotinic channels by antibodies directed against the binding site of the acetylcholine receptor. J Physiol 492 (Pt 1):107-114.

Burden SJ, Huijbers MG, Remedio L (2018) Fundamental molecules and mechanisms for forming and maintaining neuromuscular synapses. Int J Mol Sci 19.

Burges J, Wray DW, Pizzighella S, Hall Z, Vincent A (1990) A myasthenia gravis plasma immunoglobulin reduces miniature endplate potentials at human endplates in vitro. Muscle Nerve 13:407-413.

Burke G, Hiscock A, Klein A, Niks EH, Main M, Manzur AY, Ng J, de Vile C, Muntoni F, Beeson D, Robb S (2013) Salbutamol benefits children with

congenital myasthenic syndrome due to DOK7 mutations. Neuromuscular disorders: NMD 23:170-175.

Celie PH, Klaassen RV, van Rossum-Fikkert SE, van Elk R, van Nierop P, Smit AB, Sixma TK (2005a) Crystal structure of acetylcholine-binding protein from Bulinus truncatus reveals the conserved structural scaffold and sites of variation in nicotinic acetylcholine receptors. J Biol Chem 280:26457-26466.

Celie PH, Kasheverov IE, Mordvintsev DY, Hogg RC, van Nierop P, van Elk R, van Rossum-Fikkert SE, Zhmak MN, Bertrand D, Tsetlin V, Sixma TK, Smit AB (2005b) Crystal structure of nicotinic acetylcholine receptor homolog AChBP in complex with an alpha-conotoxin PnIA variant. Nat Struct Mol Biol 12:582-588.

Cetin H, Vincent A (2018) Pathogenic mechanisms and clinical correlations in autoimmune myasthenic syndromes. Semin Neurol 38:344-354.

Chang CC, Chen TF, Chuang ST (1973) Influence of chronic neostigmine treatment on the number of acetylcholine receptors and the release of acetylcholine from the rat diaphragm. J Physiol 230:613-618.

Changeux JP, Galzi JL, Devillers-Thiery A, Bertrand D (1992) The functional architecture of the acetylcholine nicotinic receptor explored by affinity labelling and site-directed mutagenesis. Q Rev Biophys 25:395-432.

Changeux JP, Kasai M, Huchet M, Meunier JC (1970) Extraction from electric tissue of gymnotus of a protein presenting several typical properties characteristic of the physiological receptor of acetylcholine. C R Acad Sci 270D:2864-2867.

Chen F, Qian L, Yang ZH, Huang Y, Ngo ST, Ruan NJ, Wang J, Schneider C, Noakes PG, Ding YQ, Mei L, Luo ZG (2007) Rapsyn interaction with calpain stabilizes AChR clusters at the neuromuscular junction. Neuron 55:247-260.

Chesnut TJ (1983) Two-component desensitization at the neuromuscular junction of the frog. J Physiol 336:229-241.

Cole RN, Reddel SW, Gervasio OL, Phillips WD (2008) Anti-MuSK patient antibodies disrupt the mouse neuromuscular junction. Ann Neurol 63:782-789.

Cole RN, Ghazanfari N, Ngo ST, Gervasio OL, Reddel SW, Phillips WD (2010) Patient autoantibodies deplete postsynaptic muscle-specific kinase leading to disassembly of the ACh receptor scaffold and myasthenia gravis in mice. J Physiol 588:3217-3229.

Colquhoun D, Hawkes AG (1977) Relaxation and fluctuations of membrane currents that flow through drug-operated channels. Proc R Soc Lond B Biol Sci 199:231-262.

Colquhoun D, Ogden DC (1988) Activation of ion channels in the frog end-plate by high concentrations of acetylcholine. J Physiol 395:131-159.

Colquhoun D, Hawkes A (1995) The principles of the stochastic interpretation of ion-channel mechanisms. Single-Channel Recording, 2nd ed B Sakmann and E Neher, editors Springer Press, New York 397-482.

Corringer PJ, Bertrand S, Bohler S, Edelstein SJ, Changeux JP, Bertrand D (1998) Critical elements determining diversity in agonist binding and desensitization of neuronal nicotinic acetylcholine receptors. J Neurosci 18:648-657.

Corringer PJ, Galzi JL, Eisele JL, Bertrand S, Changeux JP, Bertrand D (1995) Identification of a new component of the agonist binding site of the nicotinic alpha 7 homooligomeric receptor. J Biol Chem 270:11749-11752.

Corringer PJ, Bertrand S, Galzi JL, Devillers-Thiery A, Changeux JP, Bertrand D (1999) Mutational analysis of the charge selectivity filter of the alpha7 nicotinic acetylcholine receptor. Neuron 22:831-843.

Corry B (2006) An energy-efficient gating mechanism in the acetylcholine receptor channel suggested by molecular and Brownian dynamics. Biophys J 90:799-810.

Cortes-Vicente E, Gallardo E, Martinez MA, Diaz-Manera J, Querol L, Rojas-Garcia R, Illa I (2016) Clinical characteristics of patients with double-seronegative myasthenia gravis and antibodies to cortactin. JAMA neurology 73:1099-1104.

Cossins J, Webster R, Maxwell S, Burke G, Vincent A, Beeson D (2004) A mouse model of AChR deficiency syndrome with a phenotype reflecting the human condition. Human molecular genetics 13:2947-2957.

Cossins J, Burke G, Maxwell S, Spearman H, Man S, Kuks J, Vincent A, Palace J, Fuhrer C, Beeson D (2006) Diverse molecular mechanisms involved in AChR deficiency due to rapsyn mutations. Brain 129:2773-2783.

Cossins J, Belaya K, Zoltowska K, Koneczny I, Maxwell S, Jacobson L, Leite MI, Waters P, Vincent A, Beeson D (2012) The search for new antigenic targets in myasthenia gravis. Ann N Y Acad Sci 1275:123-128.

Cousin MT (2013) History of anaesthesia: who discovered the neuromuscular junction? The opposing views of Claude Bernard and Alfred Vulpian. Eur J Anaesthesiol 30:1-4.

Croxen R, Newland C, Beeson D, Oosterhuis H, Chauplannaz G, Vincent A, Newsom-Davis J (1997) Mutations in different functional domains of the human muscle acetylcholine receptor alpha subunit in patients with the slow-channel congenital myasthenic syndrome. Human molecular genetics 6:767-774.

Croxen R, Young C, Slater C, Haslam S, Brydson M, Vincent A, Beeson D (2001) End-plate gamma- and epsilon-subunit mRNA levels in AChR deficiency syndrome due to epsilon-subunit null mutations. Brain 124:1362-1372.

Cull-Candy SG, Miledi R, Trautmann A, Uchitel OD (1980) On the release of transmitter at normal, myasthenia gravis and myasthenic syndrome affected human end-plates. J Physiol 299:621-638.

Cymes GD, Grosman C (2016) Identifying the elusive link between amino acid sequence and charge selectivity in pentameric ligand-gated ion channels. Proc Natl Acad Sci U S A.

daCosta CJ, Dey L, Therien JP, Baenziger JE (2013) A distinct mechanism for activating uncoupled nicotinic acetylcholine receptors. Nat Chem Biol 9:701-707.

Dale HH, Feldberg W, Vogt M (1936) Release of acetylcholine at voluntary motor nerve endings. J Physiol 86:353-380.

de Meel RH, Lipka AF, van Zwet EW, Niks EH, Verschuuren JJ (2015) Prognostic factors for exacerbations and emergency treatments in myasthenia gravis. J Neuroimmunol 282:123-125.

Deflorio C, Catalano M, Fucile S, Limatola C, Grassi F (2014) Fluoxetine prevents acetylcholine-induced excitotoxicity blocking human endplate acetylcholine receptor. Muscle Nerve 49:90-97.

Del Castillo J, Katz B (1957) Interaction at end-plate receptors between different choline derivatives. Proc R Soc Lond B Biol Sci 146:369-381.

Dennis M, Giraudat J, Kotzyba-Hibert F, Goeldner M, Hirth C, Chang JY, Lazure C, Chretien M, Changeux JP (1988) Amino acids of the Torpedo marmorata acetylcholine receptor alpha subunit labeled by a photoaffinity ligand for the acetylcholine binding site. Biochemistry 27:2346-2357.

Devic P, Petiot P, Simonet T, Stojkovic T, Delmont E, Franques J, Magot A, Vial C, Lagrange E, Nicot AS, Risson V, Eymard B, Schaeffer L (2014) Antibodies to clustered acetylcholine receptor: expanding the phenotype. European journal of neurology: the official journal of the European Federation of Neurological Societies 21:130-134.

Devillers-Thiery A, Giraudat J, Bentaboulet M, Changeux JP (1983) Complete mRNA coding sequence of the acetylcholine binding alpha-subunit of Torpedo marmorata acetylcholine receptor: a model for the transmembrane organization of the polypeptide chain. Proc Natl Acad Sci U S A 80:2067-2071.

Dilger JP, Liu Y (1992) Desensitization of acetylcholine receptors in BC3H-1 cells. Pflugers Arch 420:479-485.

Drachman DB, Adams RN, Josifek LF, Self SG (1982) Functional activities of autoantibodies to acetylcholine receptors and the clinical severity of myasthenia gravis. N Engl J Med 307:769-775.

Drachman DB, Angus CW, Adams RN, Michelson JD, Hoffman GJ (1978) Myasthenic antibodies cross-link acetylcholine receptors to accelerate degradation. N Engl J Med 298:1116-1122.

Ealing J, Webster R, Brownlow S, Abdelgany A, Oosterhuis H, Muntoni F, Vaux DJ, Vincent A, Beeson D (2002) Mutations in congenital myasthenic syndromes reveal an epsilon subunit C-terminal cysteine, C470, crucial for maturation and surface expression of adult AChR. Human molecular genetics 11:3087-3096.

Elenes S, Auerbach A (2002) Desensitization of diliganded mouse muscle nicotinic acetylcholine receptor channels. J Physiol 541:367-383.

Elenes S, Ni Y, Cymes GD, Grosman C (2006) Desensitization contributes to the synaptic response of gain-of-function mutants of the muscle nicotinic receptor. J Gen Physiol 128:615-627.

Engel AG, Lambert EH, Santa T (1973) Study of long-term anticholinesterase therapy. Effects on neuromuscular transmission and on motor end-plate fine structure. Neurology 23:1273-1281.

Engel AG, Lambert EH, Gomez MR (1977) A new myasthenic syndrome with end-plate acetylcholinesterase deficiency, small nerve terminals, and reduced acetylcholine release. Ann Neurol 1:315-330.

Engel AG, Shen XM, Selcen D, Sine SM (2015) Congenital myasthenic syndromes: pathogenesis, diagnosis, and treatment. Lancet Neurol 14:461.

Engel AG, Lambert EH, Mulder DM, Torres CF, Sahashi K, Bertorini TE, Whitaker JN (1982) A newly recognized congenital myasthenic syndrome attributed to a prolonged open time of the acetylcholine-induced ion channel. Ann Neurol 11:553-569.

Engel AG, Ohno K, Milone M, Wang HL, Nakano S, Bouzat C, Pruitt JN, 2nd, Hutchinson DO, Brengman JM, Bren N, Sieb JP, Sine SM (1996) New mutations in acetylcholine receptor subunit genes reveal heterogeneity in the slow-channel congenital myasthenic syndrome. Human molecular genetics 5:1217-1227.

Erb W (1879) Zur casuistik der bulbaeren Laehmungen. Arch Psychiatr Nervenkr 9:336-350.

Fatt P, Katz B (1951) An analysis of the end-plate potential recorded with an intracellular electrode. J Physiol 115:320-370.

Fatt P, Katz B (1952) Spontaneous subthreshold activity at motor nerve endings. J Physiol 117:109-128.

Feldberg W, Gaddum JH (1934) The chemical transmitter at synapses in a sympathetic ganglion. J Physiol 81:305-319.

Fels G, Plumer-Wilk R, Schreiber M, Maelicke A (1986) A monoclonal antibody interfering with binding and response of the acetylcholine receptor. J Biol Chem 261:15746-15754.

Feltz A, Trautmann A (1982) Desensitization at the frog neuromuscular junction: a biphasic process. J Physiol 322:257-272.

Fertuck HC, Salpeter MM (1976) Quantitation of junctional and extrajunctional acetylcholine receptors by electron microscope autoradiography after 125I-

alpha-bungarotoxin binding at mouse neuromuscular junctions. J Cell Biol 69:144-58.

Fiekers JF, Spannbauer PM, Scubon-Mulieri B, Parsons RL (1980) Voltage dependence of desensitization. Influence of calcium and activation kinetics. J Gen Physiol 75:511-529.

Filatov GN, White MM (1995) The role of conserved leucines in the M2 domain of the acetylcholine receptor in channel gating. Mol Pharmacol 48:379-384.

Fontaine B, Klarsfeld A, Changeux JP (1987) Calcitonin gene-related peptide and muscle activity regulate acetylcholine receptor alpha-subunit mRNA levels by distinct intracellular pathways. J Cell Biol 105:1337-1342.

Forster I, Bertrand D (1995) Inward rectification of neuronal nicotinic acetylcholine receptors investigated by using the homomeric alpha 7 receptor. Proc Biol Sci 260:139-148.

Frail DE, McLaughlin LL, Mudd J, Merlie JP (1988) Identification of the mouse muscle 43,000-dalton acetylcholine receptor-associated protein (RAPsyn) by cDNA cloning. J Biol Chem 263:15602-15607.

Franke C, Hatt H, Parnas H, Dudel J (1992) Recovery from the rapid desensitization of nicotinic acetylcholine receptor channels on mouse muscle. Neuroscience letters 140:169-172.

Franke C, Parnas H, Hovav G, Dudel J (1993) A molecular scheme for the reaction between acetylcholine and nicotinic channels. Biophys J 64:339-356.

Frazier CJ, Buhler AV, Weiner JL, Dunwiddie TV (1998) Synaptic potentials mediated via alpha-bungarotoxin-sensitive nicotinic acetylcholine receptors in rat hippocampal interneurons. J Neurosci 18:8228-8235.

Friese MB, Blagden CS, Burden SJ (2007) Synaptic differentiation is defective in mice lacking acetylcholine receptor beta-subunit tyrosine phosphorylation. Development 134:4167-4176.

Fu Y, Struyk A, Markin V, Cannon S (2011) Gating behaviour of sodium currents in adult mouse muscle recorded with an improved two-electrode voltage clamp. J Physiol 589:525-546.

Fucile S, Sucapane A, Grassi F, Eusebi F, Engel AG (2006) The human adult subtype ACh receptor channel has high Ca2+ permeability and predisposes to endplate Ca2+ overloading. J Physiol 573:35-43.

Fuhrer C, Hall ZW (1996) Functional interaction of Src family kinases with the acetylcholine receptor in C2 myotubes. J Biol Chem 271:32474-32481.

Gallardo E, Martinez-Hernandez E, Titulaer MJ, Huijbers MG, Martinez MA, Ramos A, Querol L, Diaz-Manera J, Rojas-Garcia R, Hayworth CR, Verschuuren JJ, Balice-Gordon R, Dalmau J, Illa I (2014) Cortactin autoantibodies in myasthenia gravis. Autoimmun Rev 13:1003-1007.

Galzi JL, Revah F, Black D, Goeldner M, Hirth C, Changeux JP (1990) Identification of a novel amino acid alpha-tyrosine 93 within the cholinergic ligands-binding sites of the acetylcholine receptor by photoaffinity labeling. Additional evidence for a three-loop model of the cholinergic ligands-binding sites. J Biol Chem 265:10430-10437.

Galzi JL, Devillers-Thiery A, Hussy N, Bertrand S, Changeux JP, Bertrand D (1992) Mutations in the channel domain of a neuronal nicotinic receptor convert ion selectivity from cationic to anionic. Nature 359:500-505.

Gao F, Bren N, Burghardt TP, Hansen S, Henchman RH, Taylor P, McCammon JA, Sine SM (2005) Agonist-mediated conformational changes in acetylcholine-binding protein revealed by simulation and intrinsic tryptophan fluorescence. J Biol Chem 280:8443-8451.

Garcia-Colunga J, Awad JN, Miledi R (1997) Blockage of muscle and neuronal nicotinic acetylcholine receptors by fluoxetine (Prozac). Proc Natl Acad Sci U S A 94:2041-2044.

Gasperi C, Melms A, Schoser B, Zhang Y, Meltoranta J, Risson V, Schaeffer L, Schalke B, Kroger S (2014) Anti-agrin autoantibodies in myasthenia gravis. Neurology 82:1976-1983.

Gentet LJ, Stuart GJ, Clements JD (2000) Direct measurement of specific membrane capacitance in neurons. Biophys J 79:314-320.

Gilhus NE, Verschuuren JJ (2015) Myasthenia gravis: subgroup classification and therapeutic strategies. Lancet Neurol 14:1023-1036.

Giniatullin R, Nistri A, Yakel JL (2005) Desensitization of nicotinic ACh receptors: shaping cholinergic signaling. Trends in neurosciences 28:371-378.

Giniatullin RA, Khazipov RN, Vyskocil F (1993) A correlation between quantal content and decay time of endplate currents in frog muscles with intact cholinesterase. J Physiol 466:95-103.

Giniatullin RA, Talantova M, Vyskocil F (1997) Desensitization shortens the high-quantal-content endplate current time course in frog muscle with intact cholinesterase. J Physiol 502 (Pt 3):641-648.

Goldflam S (1893) Ueber einen scheinbar heilbaren bulbaerparalytischen Symptomencomplex mit Betheiligung der Extremitaeten. Dtsch Z Nervenheilk 4:312-352.

Grutter T, Changeux JP (2001) Nicotinic receptors in wonderland. Trends Biochem Sci 26:459-463.

Grutter T, de Carvalho LP, Dufresne V, Taly A, Changeux JP (2006) Identification of two critical residues within the Cys-loop sequence that determine fast-gating kinetics in a pentameric ligand-gated ion channel. J Mol Neurosci 30:63-64.

Grutter T, de Carvalho LP, Dufresne V, Taly A, Edelstein SJ, Changeux JP (2005) Molecular tuning of fast gating in pentameric ligand-gated ion channels. Proc Natl Acad Sci U S A 102:18207-18212.

Gu Y, Hall ZW (1988) Immunological evidence for a change in subunits of the acetylcholine receptor in developing and denervated rat muscle. Neuron 1:117-125.

Gunthorpe MJ, Lummis SC (2001) Conversion of the ion selectivity of the 5-HT(3a) receptor from cationic to anionic reveals a conserved feature of the ligand-gated ion channel superfamily. J Biol Chem 276:10977-10983.

Guyon T, Levasseur P, Truffault F, Cottin C, Gaud C, Berrih-Aknin S (1994) Regulation of acetylcholine receptor alpha subunit variants in human myasthenia gravis. Quantification of steady-state levels of messenger RNA in muscle biopsy using the polymerase chain reaction. J Clin Invest 94:16-24.

Guyon T, Wakkach A, Poea S, Mouly V, Klingel-Schmitt I, Levasseur P, Beeson D, Asher O, Tzartos S, Berrih-Aknin S (1998) Regulation of acetylcholine

receptor gene expression in human myasthenia gravis muscles. Evidences for a compensatory mechanism triggered by receptor loss. J Clin Invest 102:249-263.

Haghighi AP, Cooper E (1998) Neuronal nicotinic acetylcholine receptors are blocked by intracellular spermine in a voltage-dependent manner. J Neurosci 18:4050-4062.

Hansen SB, Sulzenbacher G, Huxford T, Marchot P, Taylor P, Bourne Y (2005) Structures of Aplysia AChBP complexes with nicotinic agonists and antagonists reveal distinctive binding interfaces and conformations. EMBO J 24:3635-3646.

Harpole TJ, Grosman C (2014) Side-chain conformation at the selectivity filter shapes the permeation free-energy landscape of an ion channel. Proc Natl Acad Sci U S A 111:E3196-3205.

Hesselmans LF, Jennekens FG, Van den Oord CJ, Veldman H, Vincent A (1993) Development of innervation of skeletal muscle fibers in man: relation to acetylcholine receptors. The Anatomical record 236:553-562.

Hezel M, de Groat WC, Galbiati F (2010) Caveolin-3 promotes nicotinic acetylcholine receptor clustering and regulates neuromuscular junction activity. Mol Biol Cell 21:302-310.

Higuchi O, Hamuro J, Motomura M, Yamanashi Y (2011) Autoantibodies to low-density lipoprotein receptor-related protein 4 in myasthenia gravis. Ann Neurol 69:418-422.

Hoch W, Ferns M, Campanelli JT, Hall ZW, Scheller RH (1993) Developmental regulation of highly active alternatively spliced forms of agrin. Neuron 11:479-490.

Hoch W, McConville J, Helms S, Newsom-Davis J, Melms A, Vincent A (2001) Auto-antibodies to the receptor tyrosine kinase MuSK in patients with myasthenia gravis without acetylcholine receptor antibodies. Nat Med 7:365-368.

Hoffman PW, Ravindran A, Huganir RL (1994) Role of phosphorylation in desensitization of acetylcholine receptors expressed in Xenopus oocytes. J Neurosci 14:4185-4195.

Hopfield JF, Tank DW, Greengard P, Huganir RL (1988) Functional modulation of the nicotinic acetylcholine receptor by tyrosine phosphorylation. Nature 336:677-680.

Horn R, Marty A (1988) Muscarinic activation of ionic currents measured by a new whole-cell recording method. J Gen Physiol 92:145-159.

Hu J, Han J, Li H, Zhang X, Liu LL, Chen F, Zeng B (2018) Human embryonic kidney 293 cells: A vehicle for biopharmaceutical manufacturing, structural biology, and electrophysiology. Cells Tissues Organs 205:1-8.

Huda S, Waters P, Woodhall M, Leite MI, Jacobson L, De Rosa A, Maestri M, Ricciardi R, Heckmann JM, Maniaol A, Evoli A, Cossins J, Hilton-Jones D, Vincent A (2017) IgG-specific cell-based assay detects potentially pathogenic MuSK-Abs in seronegative MG. Neurol Neuroimmunol Neuroinflamm 4:e357.

Hucho F, Changeux JP (1973) Molecular weight and quaternary structure of the cholinergic receptor protein extracted by detergents from Electrophorus electricus electric tissue. FEBS Lett 38:11-15.

Huebsch KA, Maimone MM (2003) Rapsyn-mediated clustering of acetylcholine receptor subunits requires the major cytoplasmic loop of the receptor subunits. J Neurobiol 54:486-501.

Huganir RL, Delcour AH, Greengard P, Hess GP (1986) Phosphorylation of the nicotinic acetylcholine receptor regulates its rate of desensitization. Nature 321:774-776.

Huh KH, Fuhrer C (2002) Clustering of nicotinic acetylcholine receptors: from the neuromuscular junction to interneuronal synapses. Mol Neurobiol 25:79-112.

Huijbers MG, Querol LA, Niks EH, Plomp JJ, van der Maarel SM, Graus F, Dalmau J, Illa I, Verschuuren JJ (2015) The expanding field of IgG4-mediated neurological autoimmune disorders. European journal of neurology : the official journal of the European Federation of Neurological Societies 22:1151-1161.

Huijbers MG, Zhang W, Klooster R, Niks EH, Friese MB, Straasheijm KR, Thijssen PE, Vrolijk H, Plomp JJ, Vogels P, Losen M, Van der Maarel SM, Burden SJ, Verschuuren JJ (2013) MuSK IgG4 autoantibodies cause myasthenia gravis by inhibiting binding between MuSK and Lrp4. Proc Natl Acad Sci U S A 110:20783-20788.

Imoto K, Busch C, Sakmann B, Mishina M, Konno T, Nakai J, Bujo H, Mori Y, Fukuda K, Numa S (1988) Rings of negatively charged amino acids

determine the acetylcholine receptor channel conductance. Nature 335:645-648.

Ito M, Matsuo Y, Nishikawa K (1997) Prediction of protein secondary structure using the 3D-1D compatibility algorithm. Comput Appl Biosci 13:415-424.

Ivanov I, Cheng X, Sine SM, McCammon JA (2007) Barriers to ion translocation in cationic and anionic receptors from the Cys-loop family. J Am Chem Soc 129:8217-8224.

Jacob S, Viegas S, Leite MI, Webster R, Cossins J, Kennett R, Hilton-Jones D, Morgan BP, Vincent A (2012) Presence and pathogenic relevance of antibodies to clustered acetylcholine receptor in ocular and generalized myasthenia gravis. Arch Neurol 69:994-1001.

Jacobson L, Beeson D, Tzartos S, Vincent A (1999) Monoclonal antibodies raised against human acetylcholine receptor bind to all five subunits of the fetal isoform. J Neuroimmunol 98:112-120.

Jahn K, Franke C, Bufler J (2000) Mechanism of block of nicotinic acetylcholine receptor channels by purified IgG from seropositive patients with myasthenia gravis. Neurology 54:474-479.

Jahn K, Mohammadi B, Krampfl K, Abicht A, Lochmuller H, Bufler J (2001) Deactivation and desensitization of mouse embryonic- and adult-type nicotinic receptor channel currents. Neuroscience letters 307:89-92.

Jolly F (1895) Ueber myasthenia gravis pseudoparalytica. Berl Klin Wochenschr 32:1-7.

Jones AK, Buckingham SD, Sattelle DB (2010) Proteins interacting with nicotinic acetylcholine receptors: expanding functional and therapeutic horizons. Trends Pharmacol Sci 31:455-462.

Karlin A, Cox RN, Dipaola M, Holtzman E, Kao PN, Lobel P, Wang L, Yodh N (1986) Functional domains of the nicotinic acetylcholine receptor. Ann N Y Acad Sci 463:53-69.

Katz B, Thesleff S (1957) A study of the desensitization produced by acetylcholine at the motor end-plate. J Physiol 138:63-80.

Katz B, Miledi R (1965) Release of acetylcholine from a nerve terminal by electric pulses of variable strength and duration. Nature 207:1097-1098.

Kawakami Y, Ito M, Hirayama M, Sahashi K, Ohkawara B, Masuda A, Nishida H, Mabuchi N, Engel AG, Ohno K (2011) Anti-MuSK autoantibodies block binding of collagen Q to MuSK. Neurology 77:1819-1826.

Kawanami S, Tsuji R, Oda K (1984) Enzyme-linked immunosorbent assay for antibody against the nicotinic acetylcholine receptor in human myasthenia gravis. Ann Neurol 15:195-200.

Keramidas A, Lynch JW (2013) An outline of desensitization in pentameric ligand-gated ion channel receptors. Cell Mol Life Sci 70:1241-1253.

Keramidas A, Moorhouse AJ, French CR, Schofield PR, Barry PH (2000) M2 pore mutations convert the glycine receptor channel from being anion- to cation-selective. Biophys J 79:247-259.

Kerty E, Elsais A, Argov Z, Evoli A, Gilhus NE (2014) EFNS/ENS Guidelines for the treatment of ocular myasthenia. European journal of neurology : the

official journal of the European Federation of Neurological Societies 21:687-693.

Klarsfeld A, Changeux JP (1985) Activity regulates the levels of acetylcholine receptor alpha-subunit mRNA in cultured chicken myotubes. Proc Natl Acad Sci U S A 82:4558-4562.

Kleinle J, Vogt K, Luscher HR, Muller L, Senn W, Wyler K, Streit J (1996) Transmitter concentration profiles in the synaptic cleft: an analytical model of release and diffusion. Biophys J 71:2413-2426.

Klooster R, Plomp JJ, Huijbers MG, Niks EH, Straasheijm KR, Detmers FJ, Hermans PW, Sleijpen K, Verrips A, Losen M, Martinez-Martinez P, De Baets MH, van der Maarel SM, Verschuuren JJ (2012) Muscle-specific kinase myasthenia gravis IgG4 autoantibodies cause severe neuromuscular junction dysfunction in mice. Brain 135:1081-1101.

Koneczny I, Cossins J, Waters P, Beeson D, Vincent A (2013) MuSK myasthenia gravis IgG4 disrupts the interaction of LRP4 with MuSK but both IgG4 and IgG1-3 can disperse preformed agrin-independent AChR clusters. PLoS One 8:e80695.

Koneczny I, Stevens JA, De Rosa A, Huda S, Huijbers MG, Saxena A, Maestri M, Lazaridis K, Zisimopoulou P, Tzartos S, Verschuuren J, van der Maarel SM, van Damme P, De Baets MH, Molenaar PC, Vincent A, Ricciardi R, Martinez-Martinez P, Losen M (2017) IgG4 autoantibodies against muscle-specific kinase undergo Fab-arm exchange in myasthenia gravis patients. J Autoimmun 77:104-115.

Kouvatsos N, Giastas P, Chroni-Tzartou D, Poulopoulou C, Tzartos SJ (2016) Crystal structure of a human neuronal nAChR extracellular domain in pentameric assembly: Ligand-bound alpha2 homopentamer. Proc Natl Acad Sci U S A 113:9635-9640.

Krampfl K, Jahn K, Cordes AL, Dengler R, Bufler J (2002) Analysis of a slow desensitized state of recombinant adult-type nicotinic acetylcholine receptor channels. The European journal of neuroscience 16:652-658.

Kurosawa N, Owada E, Kato A, Bando K, Ito K, Kurosawa S (1993) Serum concentration and cardiovascular effects of salbutamol after oral and rectal administration in healthy volunteers. J Clin Pharm Ther 18:103-108.

Labarca C, Nowak MW, Zhang H, Tang L, Deshpande P, Lester HA (1995) Channel gating governed symmetrically by conserved leucine residues in the M2 domain of nicotinic receptors. Nature 376:514-516.

Lang B, Richardson G, Rees J, Vincent A, Newsom-Davis J (1988) Plasma from myasthenia gravis patients reduces acetylcholine receptor agonist-induced Na+ flux into TE671 cell line. J Neuroimmunol 19:141-148.

Langley JN (1905) On the reaction of cells and of nerve-endings to certain poisons, chiefly as regards the reaction of striated muscle to nicotine and to curari. J Physiol 33:374-413.

Le Novere N, Corringer PJ, Changeux JP (1999) Improved secondary structure predictions for a nicotinic receptor subunit: incorporation of solvent accessibility and experimental data into a two-dimensional representation. Biophys J 76:2329-2345.

Lee WY, Sine SM (2005) Principal pathway coupling agonist binding to channel gating in nicotinic receptors. Nature 438:243-247.

Lee Y, Rudell J, Ferns M (2009) Rapsyn interacts with the muscle acetylcholine receptor via alpha-helical domains in the alpha, beta, and epsilon subunit intracellular loops. Neuroscience 163:222-232.

Lee Y, Rudell J, Yechikhov S, Taylor R, Swope S, Ferns M (2008) Rapsyn carboxyl terminal domains mediate muscle specific kinase-induced phosphorylation of the muscle acetylcholine receptor. Neuroscience 153:997-1007.

Leite MI, Waters P, Vincent A (2010) Diagnostic use of autoantibodies in myasthenia gravis. Autoimmunity 43:371-379.

Leite MI, Jacob S, Viegas S, Cossins J, Clover L, Morgan BP, Beeson D, Willcox N, Vincent A (2008) IgG1 antibodies to acetylcholine receptors in 'seronegative' myasthenia gravis. Brain 131:1940-1952.

Lennon VA, Griesmann GE (1989) Evidence against acetylcholine receptor having a main immunogenic region as target for autoantibodies in myasthenia gravis. Neurology 39:1069-1076.

Lester HA (1992) The permeation pathway of neurotransmitter-gated ion channels. Annu Rev Biophys Biomol Struct 21:267-292.

Levi S, Logan SM, Tovar KR, Craig AM (2004) Gephyrin is critical for glycine receptor clustering but not for the formation of functional GABAergic synapses in hippocampal neurons. J Neurosci 24:207-217.

Li L, Cao Y, Wu H, Ye X, Zhu Z, Xing G, Shen C, Barik A, Zhang B, Xie X, Zhi W, Gan L, Su H, Xiong WC, Mei L (2016) Enzymatic Activity of the Scaffold Protein Rapsyn for Synapse Formation. Neuron 92:1007-1019.

Li Z, Forester N, Vincent A (1996) Modulation of acetylcholine receptor function in TE671 (rhabdomyosarcoma) cells by non-AChR ligands: possible relevance to seronegative myasthenia gravis. J Neuroimmunol 64:179-183.

Lindstrom JM, Seybold ME, Lennon VA, Whittingham S, Duane DD (1976) Antibody to acetylcholine receptor in myasthenia gravis. Prevalence, clinical correlates, and diagnostic value. Neurology 26:1054-1059.

Liu Y, Dilger JP (1991) Opening rate of acetylcholine receptor channels. Biophys J 60:424-432.

Loewi O (1921) Über humorale Übertragbarkeit der Herznervenwirkung. Pflugers Arch 189:239-242.

Lynch GS, Ryall JG (2008) Role of beta-adrenoceptor signaling in skeletal muscle: implications for muscle wasting and disease. Physiol Rev 88:729-767.

MacLennan C, Beeson D, Buijs AM, Vincent A, Newsom-Davis J (1997) Acetylcholine receptor expression in human extraocular muscles and their susceptibility to myasthenia gravis. Ann Neurol 41:423-431.

Maconochie DJ, Steinbach JH (1998) The channel opening rate of adult- and fetal-type mouse muscle nicotinic receptors activated by acetylcholine. J Physiol 506 (Pt 1):53-72.

Magazanik LG, Vyskocil F (1970) Dependence of acetylcholine desensitization on the membrane potential of frog muscle fibre and on the ionic changes in the medium. J Physiol 210:507-518.

Magazanik LG, Vyskocil F (1975) The effect of temperature on desensitization kinetics at the post-synaptic membrane of the frog muscle fibre. J Physiol 249:285-300.

Magleby KL, Pallotta BS (1981) A study of desensitization of acetylcholine receptors using nerve-released transmitter in the frog. J Physiol 316:225-250.

Maimone MM, Merlie JP (1993) Interaction of the 43 kd postsynaptic protein with all subunits of the muscle nicotinic acetylcholine receptor. Neuron 11:53-66.

Maimone MM, Enigk RE (1999) The intracellular domain of the nicotinic acetylcholine receptor alpha subunit mediates its coclustering with rapsyn. Mol Cell Neurosci 14:340-354.

Martin AR (1994) Amplification of neuromuscular transmission by postjunctional folds. Proc Biol Sci 258:321-326.

Mathie A, Colquhoun D, Cull-Candy SG (1990) Rectification of currents activated by nicotinic acetylcholine receptors in rat sympathetic ganglion neurones. J Physiol 427:625-655.

Matsui N, Nakane S, Nakagawa Y, Kondo K, Mitsui T, Matsumoto T, Arisawa K, Kaji R (2009) Increasing incidence of elderly onset patients with myasthenia gravis in a local area of Japan. J Neurol Neurosurg Psychiatry 80:1168-1171.

Matthews-Bellinger J, Salpeter MM (1978) Distribution of acetylcholine receptors at frog neuromuscular junctions with a discussion of some physiological implications. J Physiol 279:197-213.

Matthews-Bellinger JA, Salpeter MM (1983) Fine structural distribution of acetylcholine receptors at developing mouse neuromuscular junctions. J Neurosci 3:644-657.

Meyers JA, Sanchez D, Elwell LP, Falkow S (1976) Simple agarose gel electrophoretic method for the identification and characterization of plasmid deoxyribonucleic acid. J Bacteriol 127:1529-1537.

Middleton P, Jaramillo F, Schuetze SM (1986) Forskolin increases the rate of acetylcholine receptor desensitization at rat soleus endplates. Proc Natl Acad Sci U S A 83:4967-4971.

Miledi R, Molinoff P, Potter LT (1971) Isolation of the cholinergic receptor protein of Torpedo electric tissue. Nature 229:554-557.

Miledi R, Molenaar PC, Polak RL (1978) Alpha-bungarotoxin enhances transmitter "released" at the neuromuscular junction. Nature 272:641-643.

Miller C (1989) Genetic manipulation of ion channels: a new approach to structure and mechanism. Neuron 2:1195-1205.

Miller PS, Aricescu AR (2014) Crystal structure of a human GABAA receptor. Nature 512:270-275.

Mishina M, Takai T, Imoto K, Noda M, Takahashi T, Numa S, Methfessel C, Sakmann B (1986) Molecular distinction between fetal and adult forms of muscle acetylcholine receptor. Nature 321:406-411.

Miyazawa A, Fujiyoshi Y, Stowell M, Unwin N (1999) Nicotinic acetylcholine receptor at 4.6 A resolution: transverse tunnels in the channel wall. J Mol Biol 288:765-786.

Miyazawa A, Fujiyoshi Y, Unwin N (2003) Structure and gating mechanism of the acetylcholine receptor pore. Nature 423:949-955.

Mizuguchi H, Xu Z, Ishii-Watabe A, Uchida E, Hayakawa T (2000) IRES-dependent second gene expression is significantly lower than cap-dependent first gene expression in a bicistronic vector. Mol Ther 1:376-382.

Mohamed AS, Swope SL (1999) Phosphorylation and cytoskeletal anchoring of the acetylcholine receptor by Src class protein-tyrosine kinases. Activation by rapsyn. J Biol Chem 274:20529-20539.

Molenaar PC, Newsom-Davis J, Polak RL, Vincent A (1981) Choline acetyltransferase in skeletal muscle from patients with myasthenia gravis. J Neurochem 37:1081-1088.

Molenaar PC, Polak RL, Miledi R, Alema S, Vincent A, Newsom-Davis J (1979) Acetylcholine in intercostal muscle from myasthenia gravis patients and in rat diaphragm after blockade of acetylcholine receptors. Progress in brain research 49:449-458.

Morales-Perez CL, Noviello CM, Hibbs RE (2016) X-ray structure of the human alpha4beta2 nicotinic receptor. Nature 538:411-415.

Mori S, Yamada S, Kubo S, Chen J, Matsuda S, Shudou M, Maruyama N, Shigemoto K (2012) Divalent and monovalent autoantibodies cause dysfunction of MuSK by distinct mechanisms in a rabbit model of myasthenia gravis. J Neuroimmunol 244:1-7.

Moroni M, Biro I, Giugliano M, Vijayan R, Biggin PC, Beato M, Sivilotti LG (2011) Chloride ions in the pore of glycine and GABA channels shape the time course and voltage dependence of agonist currents. J Neurosci 31:14095-14106.

Morsch M, Reddel SW, Ghazanfari N, Toyka KV, Phillips WD (2012) Muscle specific kinase autoantibodies cause synaptic failure through progressive wastage of postsynaptic acetylcholine receptors. Exp Neurol 237:286-295.

Nayak TK, Bruhova I, Chakraborty S, Gupta S, Zheng W, Auerbach A (2014) Functional differences between neurotransmitter binding sites of muscle acetylcholine receptors. Proc Natl Acad Sci U S A 111:17660-17665.

Neher E, Sakmann B (1976) Single-channel currents recorded from membrane of denervated frog muscle fibres. Nature 260:799-802.

Nemecz A, Prevost MS, Menny A, Corringer PJ (2016) Emerging molecular mechanisms of signal transduction in pentameric ligand-gated ion channels. Neuron 90:452-470.

Ochoa EL, Chattopadhyay A, McNamee MG (1989) Desensitization of the nicotinic acetylcholine receptor: molecular mechanisms and effect of modulators. Cellular and molecular neurobiology 9:141-178.

Ohno K, Hutchinson DO, Milone M, Brengman JM, Bouzat C, Sine SM, Engel AG (1995) Congenital myasthenic syndrome caused by prolonged acetylcholine receptor channel openings due to a mutation in the M2 domain of the epsilon subunit. Proc Natl Acad Sci U S A 92:758-762.

Ohno K, Wang HL, Milone M, Bren N, Brengman JM, Nakano S, Quiram P, Pruitt JN, Sine SM, Engel AG (1996) Congenital myasthenic syndrome caused by decreased agonist binding affinity due to a mutation in the acetylcholine receptor epsilon subunit. Neuron 17:157-170.

Paradiso K, Brehm P (1998) Long-term desensitization of nicotinic acetylcholine receptors is regulated via protein kinase A-mediated phosphorylation. J Neurosci 18:9227-9237.

Patrick J, Lindstrom J (1973) Autoimmune response to acetylcholine receptor. Science 180:871-872.

Patrizio A, Renner M, Pizzarelli R, Triller A, Specht CG (2017) Alpha subunit-dependent glycine receptor clustering and regulation of synaptic receptor numbers. Sci Rep 7:10899.

Pear WS, Nolan GP, Scott ML, Baltimore D (1993) Production of high-titer helper-free retroviruses by transient transfection. Proc Natl Acad Sci U S A 90:8392-8396.

Personius KE, Balice-Gordon RJ (2001) Loss of correlated motor neuron activity during synaptic competition at developing neuromuscular synapses. Neuron 31:395-408.

Pevzner A, Schoser B, Peters K, Cosma NC, Karakatsani A, Schalke B, Melms A, Kroger S (2012) Anti-LRP4 autoantibodies in AChR- and MuSK-antibody-negative myasthenia gravis. J Neurol 259:427-435.

Plested CP, Tang T, Spreadbury I, Littleton ET, Kishore U, Vincent A (2002) AChR phosphorylation and indirect inhibition of AChR function in seronegative MG. Neurology 59:1682-1688.

Plomp JJ, Van Kempen GT, De Baets MB, Graus YM, Kuks JB, Molenaar PC (1995) Acetylcholine release in myasthenia gravis: regulation at single end-plate level. Ann Neurol 37:627-636.

Ponce A, Castillo A, Hinojosa L, Martinez-Rendon J, Cereijido M (2018) The expression of endogenous voltage-gated potassium channels in HEK293 cells is affected by culture conditions. Physiol Rep 6:e13663.

Purohit Y, Grosman C (2006) Block of muscle nicotinic receptors by choline suggests that the activation and desensitization gates act as distinct molecular entities. J Gen Physiol 127:703-717.

Quick MW, Lester RA (2002) Desensitization of neuronal nicotinic receptors. J Neurobiol 53:457-478.

Ramarao MK, Cohen JB (1998) Mechanism of nicotinic acetylcholine receptor cluster formation by rapsyn. Proc Natl Acad Sci U S A 95:4007-4012.

Ramarao MK, Bianchetta MJ, Lanken J, Cohen JB (2001) Role of rapsyn tetratricopeptide repeat and coiled-coil domains in self-association and nicotinic acetylcholine receptor clustering. J Biol Chem 276:7475-7483.

Revah F, Bertrand D, Galzi JL, Devillers-Thiery A, Mulle C, Hussy N, Bertrand S, Ballivet M, Changeux JP (1991) Mutations in the channel domain alter desensitization of a neuronal nicotinic receptor. Nature 353:846-849.

Riemersma S, Vincent A, Beeson D, Newland C, Hawke S, Vernet-der Garabedian B, Eymard B, Newsom-Davis J (1996) Association of arthrogryposis multiplex congenita with maternal antibodies inhibiting fetal acetylcholine receptor function. J Clin Invest 98:2358-2363.

Rivner MH, Liu S, Quarles B, Fleenor B, Shen C, Pan J, Mei L (2017) Agrin and low-density lipoprotein-related receptor protein 4 antibodies in amyotrophic lateral sclerosis patients. Muscle Nerve 55:430-432.

Rodriguez Cruz PM, Palace J, Beeson D (2018) The neuromuscular junction and wide heterogeneity of congenital myasthenic syndromes. Int J Mol Sci 19.

Rodriguez Cruz PM, Huda S, Lopez-Ruiz P, Vincent A (2015a) Use of cell-based assays in myasthenia gravis and other antibody-mediated diseases. Exp Neurol 270:66-71.

Rodriguez Cruz PM, Palace J, Ramjattan H, Jayawant S, Robb SA, Beeson D (2015b) Salbutamol and ephedrine in the treatment of severe AChR deficiency syndromes. Neurology 85:1043-1047.

Rodriguez Cruz PM, Al-Hajjar M, Huda S, Jacobson L, Woodhall M, Jayawant S, Buckley C, Hilton-Jones D, Beeson D, Vincent A, Leite MI, Palace J (2015c) Clinical features and diagnostic usefulness of antibodies to clustered acetylcholine receptors in the diagnosis of seronegative myasthenia gravis. JAMA neurology 72:642-649.

Rudell JB, Ferns MJ (2013) Regulation of muscle acetylcholine receptor turnover by beta subunit tyrosine phosphorylation. Dev Neurobiol 73:399-410.

Ruff RL (2011) Endplate contributions to the safety factor for neuromuscular transmission. Muscle Nerve 44:854-861.

Ruff RL, Lennon VA (2008) How myasthenia gravis alters the safety factor for neuromuscular transmission. J Neuroimmunol 201-202:13-20.

Ruzzier F, Scuka M (1986) The effect of repetitive neuromuscular activity on the sensitivity of acetylcholine receptors. Pflugers Arch 406:99-103.

Sakmann B, Brenner HR (1978) Change in synaptic channel gating during neuromuscular development. Nature 276:401-402.

Sakmann B, Patlak J, Neher E (1980) Single acetylcholine-activated channels show burst-kinetics in presence of desensitizing concentrations of agonist. Nature 286:71-73.

Sands SB, Barish ME (1992) Neuronal nicotinic acetylcholine receptor currents in phaeochromocytoma (PC12) cells: dual mechanisms of rectification. J Physiol 447:467-487.

Shen C, Lu Y, Zhang B, Figueiredo D, Bean J, Jung J, Wu H, Barik A, Yin DM, Xiong WC, Mei L (2013) Antibodies against low-density lipoprotein receptor-related protein 4 induce myasthenia gravis. J Clin Invest 123:5190-5202.

Shen XM, Brengman JM, Sine SM, Engel AG (2012a) Myasthenic syndrome AChRalpha C-loop mutant disrupts initiation of channel gating. J Clin Invest 122:2613-2621.

Shen XM, Fukuda T, Ohno K, Sine SM, Engel AG (2008) Congenital myasthenia-related AChR delta subunit mutation interferes with intersubunit communication essential for channel gating. J Clin Invest 118:1867-1876.

Shen XM, Brengman JM, Edvardson S, Sine SM, Engel AG (2012b) Highly fatal fast-channel syndrome caused by AChR epsilon subunit mutation at the agonist binding site. Neurology 79:449-454.

Shen XM, Ohno K, Tsujino A, Brengman JM, Gingold M, Sine SM, Engel AG (2003) Mutation causing severe myasthenia reveals functional asymmetry of AChR signature cystine loops in agonist binding and gating. J Clin Invest 111:497-505.

Shiraishi H, Motomura M, Yoshimura T, Fukudome T, Fukuda T, Nakao Y, Tsujihata M, Vincent A, Eguchi K (2005) Acetylcholine receptors loss and postsynaptic damage in MuSK antibody-positive myasthenia gravis. Ann Neurol 57:289-293.

Simasko SM, Soares JR, Weiland GA (1986) Two components of carbamylcholine-induced loss of nicotinic acetylcholine receptor function in the neuronal cell line PC12. Mol Pharmacol 30:6-12.

Sine SM (2012) End-plate acetylcholine receptor: structure, mechanism, pharmacology, and disease. Physiol Rev 92:1189-1234.

Sine SM, Engel AG (2006) Recent advances in Cys-loop receptor structure and function. Nature 440:448-455.

Sine SM, Wang HL, Hansen S, Taylor P (2010) On the origin of ion selectivity in the Cys-loop receptor family. J Mol Neurosci 40:70-76.

Slater CR, Lyons PR, Walls TJ, Fawcett PR, Young C (1992) Structure and function of neuromuscular junctions in the vastus lateralis of man. A motor point biopsy study of two groups of patients. Brain 115 (Pt 2):451-478.

Smart JL, McCammon JA (1998) Analysis of synaptic transmission in the neuromuscular junction using a continuum finite element model. Biophys J 75:1679-1688.

Smit AB, Syed NI, Schaap D, van Minnen J, Klumperman J, Kits KS, Lodder H, van der Schors RC, van Elk R, Sorgedrager B, Brejc K, Sixma TK, Geraerts WP (2001) A glia-derived acetylcholine-binding protein that modulates synaptic transmission. Nature 411:261-268.

Smit AB, Celie PH, Kasheverov IE, Mordvintsev DY, van Nierop P, Bertrand D, Tsetlin V, Sixma TK (2006) Acetylcholine-binding proteins: functional and structural homologs of nicotinic acetylcholine receptors. J Mol Neurosci 30:9-10.

Song C, Corry B (2009) Role of acetylcholine receptor domains in ion selectivity. Biochim Biophys Acta 1788:1466-1473.

Spreadbury I, Kishore U, Beeson D, Vincent A (2005) Inhibition of acetylcholine receptor function by seronegative myasthenia gravis non-IgG factor correlates with desensitisation. J Neuroimmunol 162:149-156.

Stratton MR, Darling J, Pilkington GJ, Lantos PL, Reeves BR, Cooper CS (1989) Characterization of the human cell line TE671. Carcinogenesis 10:899-905.

Sukhorukov VL, Arnold WM, Zimmermann U (1993) Hypotonically induced changes in the plasma membrane of cultured mammalian cells. J Membr Biol 132:27-40.

Tintignac LA, Brenner HR, Ruegg MA (2015) Mechanisms regulating neuromuscular junction development and function and causes of muscle wasting. Physiol Rev 95:809-852.

Traynelis SF (1998) Software-based correction of single compartment series resistance errors. J Neurosci Methods 86:25-34.

Tzartos JS, Zisimopoulou P, Rentzos M, Karandreas N, Zouvelou V, Evangelakou P, Tsonis A, Thomaidis T, Lauria G, Andreetta F, Mantegazza R, Tzartos SJ (2014) LRP4 antibodies in serum and CSF from amyotrophic lateral sclerosis patients. Ann Clin Transl Neurol 1:80-87.

Tzartos SJ, Seybold ME, Lindstrom JM (1982) Specificities of antibodies to acetylcholine receptors in sera from myasthenia gravis patients measured by monoclonal antibodies. Proc Natl Acad Sci U S A 79:188-192.

Tzartos SJ, Barkas T, Cung MT, Mamalaki A, Marraud M, Orlewski P, Papanastasiou D, Sakarellos C, Sakarellos-Daitsiotis M, Tsantili P, Tsikaris V (1998) Anatomy of the antigenic structure of a large membrane

autoantigen, the muscle-type nicotinic acetylcholine receptor. Immunol Rev 163:89-120.

Ulens C, Hogg RC, Celie PH, Bertrand D, Tsetlin V, Smit AB, Sixma TK (2006) Structural determinants of selective alpha-conotoxin binding to a nicotinic acetylcholine receptor homolog AChBP. Proc Natl Acad Sci U S A 103:3615-3620.

Unwin N (1995) Acetylcholine receptor channel imaged in the open state. Nature 373:37-43.

Unwin N (1998) The nicotinic acetylcholine receptor of the Torpedo electric ray. J Struct Biol 121:181-190.

Unwin N (2003) Structure and action of the nicotinic acetylcholine receptor explored by electron microscopy. FEBS Lett 555:91-95.

Unwin N (2005) Refined structure of the nicotinic acetylcholine receptor at 4A resolution. J Mol Biol 346:967-989.

Unwin N (2017) Segregation of lipids near acetylcholine-receptor channels imaged by cryo-EM. IUCrJ 4:393-399.

Unwin N, Fujiyoshi Y (2012) Gating movement of acetylcholine receptor caught by plunge-freezing. J Mol Biol 422:617-634.

Unwin N, Toyoshima C, Kubalek E (1988) Arrangement of the acetylcholine receptor subunits in the resting and desensitized states, determined by cryoelectron microscopy of crystallized Torpedo postsynaptic membranes. J Cell Biol 107:1123-1138.

Unwin N, Miyazawa A, Li J, Fujiyoshi Y (2002) Activation of the nicotinic acetylcholine receptor involves a switch in conformation of the alpha subunits. J Mol Biol 319:1165-1176.

Vernet-der Garabedian B, Morel E, Bach JF (1986) Heterogeneity of antibodies directed against the alpha-bungarotoxin binding site on human acetylcholine receptor and severity of myasthenia gravis. J Neuroimmunol 12:65-74.

Verschuuren JJ, Huijbers MG, Plomp JJ, Niks EH, Molenaar PC, Martinez-Martinez P, Gomez AM, De Baets MH, Losen M (2013) Pathophysiology of myasthenia gravis with antibodies to the acetylcholine receptor, muscle-specific kinase and low-density lipoprotein receptor-related protein 4. Autoimmun Rev 12:918-923.

Viegas S, Jacobson L, Waters P, Cossins J, Jacob S, Leite MI, Webster R, Vincent A (2012) Passive and active immunization models of MuSK-Ab positive myasthenia: electrophysiological evidence for pre and postsynaptic defects. Exp Neurol 234:506-512.

Villarroel A, Sakmann B (1996) Calcium permeability increase of endplate channels in rat muscle during postnatal development. J Physiol 496 (Pt 2):331-338.

Vincent A (2002) Unravelling the pathogenesis of myasthenia gravis. Nat Rev Immunol 2:797-804.

Vincent A, Newsom-Davis J (1985) Acetylcholine receptor antibody as a diagnostic test for myasthenia gravis: results in 153 validated cases and 2967 diagnostic assays. J Neurol Neurosurg Psychiatry 48:1246-1252.

Vincent A, Jacobson L, Curran L (1998) Alpha-bungarotoxin binding to human muscle acetylcholine receptor: measurement of affinity, delineation of AChR

subunit residues crucial to binding, and protection of AChR function by synthetic peptides. Neurochem Int 32:427-433.

Vincent A, Cull-Candy SG, Newsom-Davis J, Trautmann A, Molenaar PC, Polak RL (1981) Congenital myasthenia: end-plate acetylcholine receptors and electrophysiology in five cases. Muscle Nerve 4:306-318.

Vincent A, Newland C, Brueton L, Beeson D, Riemersma S, Huson SM, Newsom-Davis J (1995) Arthrogryposis multiplex congenita with maternal autoantibodies specific for a fetal antigen. Lancet 346:24-25.

Vincent A, Huda S, Cao M, Cetin H, Koneczny I, Rodriguez-Cruz P, Jacobson L, Viegas S, Jacob S, Woodhall M, Nagaishi A, Maniaol A, Damato V, Leite MI, Cossins J, Webster R, Palace J, Beeson D (2018) Serological and experimental studies in different forms of myasthenia gravis. Ann N Y Acad Sci 1413:143-153.

Vogt J, Harrison BJ, Spearman H, Cossins J, Vermeer S, ten Cate LN, Morgan NV, Beeson D, Maher ER (2008) Mutation analysis of CHRNA1, CHRNB1, CHRND, and RAPSN genes in multiple pterygium syndrome/fetal akinesia patients. Am J Hum Genet 82:222-227.

Vrbova G, Navarrete R, Lowrie M (1985) Matching of muscle properties and motoneurone firing patterns during early stages of development. The Journal of experimental biology 115:113-123.

Vulpian A (1866) Leçons sur la physiologie générale et comparée du systéme nerveux. Paris, France: Doin:207-210.

Wagoner PK, Pallotta BS (1988) Modulation of acetylcholine receptor desensitization by forskolin is independent of cAMP. Science 240:1655-1657.

Wallace BG, Qu Z, Huganir RL (1991) Agrin induces phosphorylation of the nicotinic acetylcholine receptor. Neuron 6:869-878.

Walsh RM, Jr., Roh SH, Gharpure A, Morales-Perez CL, Teng J, Hibbs RE (2018) Structural principles of distinct assemblies of the human alpha4beta2 nicotinic receptor. Nature 557:261-265.

Wang HL, Milone M, Ohno K, Shen XM, Tsujino A, Batocchi AP, Tonali P, Brengman J, Engel AG, Sine SM (1999a) Acetylcholine receptor M3 domain: stereochemical and volume contributions to channel gating. Nature neuroscience 2:226-233.

Wang J, Jing Z, Zhang L, Zhou G, Braun J, Yao Y, Wang ZZ (2003) Regulation of acetylcholine receptor clustering by the tumor suppressor APC. Nature neuroscience 6:1017-1018.

Wang Q, Lynch JW (2011) Activation and desensitization induce distinct conformational changes at the extracellular-transmembrane domain interface of the glycine receptor. J Biol Chem 286:38814-38824.

Wang ZZ, Mathias A, Gautam M, Hall ZW (1999b) Metabolic stabilization of muscle nicotinic acetylcholine receptor by rapsyn. J Neurosci 19:1998-2007.

Webster R, Brydson M, Croxen R, Newsom-Davis J, Vincent A, Beeson D (2004) Mutation in the AChR ion channel gate underlies a fast channel congenital myasthenic syndrome. Neurology 62:1090-1096.

Webster R, Maxwell S, Spearman H, Tai K, Beckstein O, Sansom M, Beeson D (2012) A novel congenital myasthenic syndrome due to decreased acetylcholine receptor ion-channel conductance. Brain 135:1070-1080.

Whiting PJ, Vincent A, Schluep M, Newsom-Davis J (1986) Monoclonal antibodies that distinguish between normal and denervated human acetylcholine receptor. J Neuroimmunol 11:223-235.

Willis T (1672) De Anima Brutorum. Oxonii Theatro Sheldoniano, Oxford:404-407.

Wilson G, Karlin A (2001) Acetylcholine receptor channel structure in the resting, open, and desensitized states probed with the substituted-cysteine-accessibility method. Proc Natl Acad Sci U S A 98:1241-1248.

Wood SJ, Slater CR (1995) Action potential generation in rat slow- and fast-twitch muscles. J Physiol 486 (Pt 2):401-410.

Wu H, Lu Y, Shen C, Patel N, Gan L, Xiong WC, Mei L (2012) Distinct roles of muscle and motoneuron LRP4 in neuromuscular junction formation. Neuron 75:94-107.

Yamamoto T, Vincent A, Ciulla TA, Lang B, Johnston I, Newsom-Davis J (1991) Seronegative myasthenia gravis: a plasma factor inhibiting agonist-induced acetylcholine receptor function copurifies with IgM. Ann Neurol 30:550-557.

Yamodo IH, Chiara DC, Cohen JB, Miller KW (2010) Conformational changes in the nicotinic acetylcholine receptor during gating and desensitization. Biochemistry 49:156-165.

Yu Wai Man CY, Chinnery PF, Griffiths PG (2005) Extraocular muscles have fundamentally distinct properties that make them selectively vulnerable to certain disorders. Neuromuscular disorders: NMD 15:17-23.

Yumoto N, Kim N, Burden SJ (2012) Lrp4 is a retrograde signal for presynaptic differentiation at neuromuscular synapses. Nature 489:438-442.

Zeytuni N, Zarivach R (2012) Structural and functional discussion of the tetra-trico-peptide repeat, a protein interaction module. Structure 20:397-405.

Zhang B, Shen C, Bealmear B, Ragheb S, Xiong WC, Lewis RA, Lisak RP, Mei L (2014) Autoantibodies to agrin in myasthenia gravis patients. PLoS One 9:e91816.

Zhang B, Tzartos JS, Belimezi M, Ragheb S, Bealmear B, Lewis RA, Xiong WC, Lisak RP, Tzartos SJ, Mei L (2012) Autoantibodies to lipoprotein-related protein 4 in patients with double-seronegative myasthenia gravis. Arch Neurol 69:445-451.

Zhang W, Coldefy AS, Hubbard SR, Burden SJ (2011) Agrin binds to the N-terminal region of Lrp4 protein and stimulates association between Lrp4 and the first immunoglobulin-like domain in muscle-specific kinase (MuSK). J Biol Chem 286:40624-40630.

Zisimopoulou P, Brenner T, Trakas N, Tzartos SJ (2013) Serological diagnostics in myasthenia gravis based on novel assays and recently identified antigens. Autoimmun Rev 12:924-930.

Zisimopoulou P et al. (2014) A comprehensive analysis of the epidemiology and clinical characteristics of anti-LRP4 in myasthenia gravis. J Autoimmun 52:139-145.

Zong Y, Jin R (2013) Structural mechanisms of the agrin-LRP4-MuSK signaling pathway in neuromuscular junction differentiation. Cell Mol Life Sci 70:3077-3088.

Zuber B, Unwin N (2013) Structure and superorganization of acetylcholine receptor-rapsyn complexes. Proc Natl Acad Sci U S A 110:10622-10627.